Spring 2021

Stability of Low Crested and Submerged Breakwaters: A Reanalysis and Model Development

Christopher P. Burgess
Old Dominion University, cburgess@ceacsolutions.com

STABILITY OF LOW CRESTED AND SUBMERGED BREAKWATERS: REANALYSIS, PHYSICAL MODEL AND MODEL DEVELOPMENT

by

Christopher P. Burgess

Ph.D. February 2016, University of the West Indies

A Thesis Submitted to the Faculty of

Old Dominion University in Partial Fulfilment of the

Requirements for the Degree of

MASTER OF SCIENCE

CIVIL ENGINEERING

OLD DOMINION UNIVERSITY

May 2021

Approved by:

Ma Gangfeng (Director)

Navid Tahvildari (member)

Jaewan Yoon (member)

Proquest

ABSTRACT

STABILITY OF LOW CRESTED AND SUBMERGED BREAKWATERS: REANALYSIS, PHYSICAL MODEL AND MODEL DEVELOPMENT

Christopher P. Burgess

Old Dominion University, 2021

Director: Dr. Gangfeng Ma

Low-crested and submerged structures (LCS) play an integral part in the stabilization of shorelines for recreational purposes, yet there are a plethora of empirical models and gaps in the understanding of their stability and damage progression. The objectives were: i) to evaluate the present formulae, ii) explore variable importance, iii) formulate a stability model, iv) extend the current datasets and v) explore a new model for LCS. The literature points to an increasing understanding of the initiation of damage of LCS and recent exploration of the shear stress-induced erosion (van Rijn, 2019). Assessment of two existing models (Kramer, 2006 and Van der Meer and Daemen, 1994) points to reliability in predicting initiation of damage but limitations in skill in modelling progression of damage, for Re >40,000. Two analytical models (and two variations) developed herein point to difficulty (skill) in predicting damage initiation (progression) and the benefit of removing transmitted wave energy. A scale model testing programme added 124 new data points and confirms the importance of relative crest height, increased relative vulnerability of the seaward slope and crest and damage progression. Exploration of several improvements in the model was useful in deriving an LCS model that predicted damage similar to the pooled data and offered insights into the importance of i) seaward slope erosion, ii) drag and lift forces, and iii) Shield's stress relation to relative depth and stone size, Re and gradation. Importantly, damage progression is likely to be non-linear. The model is likely to be conservative and best applied for S<10. A comparative assessment to Van der Meer and Daemen model suggests that it predicts marginally lower (higher) damage for limited (extended) number of waves (in damage progression). A simplified "Rule of Thumb" suggest a relationship similar to Burcharth et al., 2006 and Pilarczyk, 2003 models.

Keywords: Low crested, breakwater, damage progression, physical modelling, variable analysis, climate-resilient

DEDICATION

This dissertation is dedicated to my family and those in furtherance of the Truth.

ACKNOWLEDGEMENTS

I gratefully acknowledge the efforts and skills of Dr. Gangfeng Ma in sharing a foundation for understanding coastal structures, hydrodynamics and processes, along with Dr. Navid Tahvildari. I also acknowledge Dr. Jaewan Yoon who skilfully shared his insights and tools in variable assessment and model development.

The author gratefully acknowledges the data provided by Dr. Morten Bech Kramer of Aalborg University, Aalborg, Denmark.

All tests were conducted in CEAC Solutions Co. Ltd. facility and the author acknowledge the efforts by all the persons involved in the testing.

NOMENCLATURE

Symbol	Unit	Meaning
A	m^2	Area of cross-section or stones
C_L		Lift coefficient
C_D		Drag coefficient
D_{n50}	m	Nominal rock diameter
D_{85} and D_{15}	m	85% finer and 15% finer rock diameter
e	m	Erosion depth
F_D	N	Drag force
F_L	N	Lift force
$F_{\tau b}$	N	Shear stress induced force
g	m/s^2	Gravitational acceleration
h	m	Depth of water at toe
h_c	m	Height of crest from toe elevations
H_s	m	Significant wave height
H_b	m	Breaking wave height
$H_{2\%}$	m	2% wave height
H_{so}	m	Significant wave height in deep water
K		Stability coefficient in Hudson formulae
KC		Keulegan Carpenter coefficient
$K_{h/Dn50}$		Parameter for water depth to stone size in Shield's reduction (r)
K_{Re}		Parameter for Reynold's in Shield's reduction (r)
$K_{D85:D15}$		Parameter for stone size D_{85} to D_{15} ratio in Shield's reduction (r)
K_t		Wave height transmission coefficient
L	m	Wave length
Ma	kg	Mass of armor stone
Mw	kg	Mass of water in pore
n		Porosity of armour stones

N_{rm}		Number of moving rocks
N_s		Stability number
N_{s*}		Spectral stability number
N_w		Number of waves
P		Notional porosity of breakwater
q_r	$m^3/s.m$	Flow of stone
q_b	kg/s.m	Mass flux flow of stone
r		Van Rijn Shield parameter reduction factor
R_c	m	freeboard
Re		Reynolds Number
s_{op}		Deepwater wave steepness
S		Damage ($A_{erosion}/A_{Dn50}$)
T_m	Seconds	Mean wave period at toe of structure
T_p	Seconds	Peak wave period at toe of structure
T_{po}	Seconds	Peak wave period in deep water
u_m	m/s	Particle velocity
Va	m^3	Volume of armor stone
Y	m	Width of erosion area
Φ	degrees	Angle of repose of armor stone
α	Degrees	Angle to horizontal of slope
ξ		Iribarren number
θ		Shield's parameter
ρ_a	kg/m^3	Density of armor stone
ρ_w	kg/m^3	Density of water
τ	N/m^2	Shear stress
μ		Morrison's Friction factor
ν	m^2/s	Kinematic viscosity of water
κ		Ratio of breaking wave height to depth
Δ		Specific density of armor relative to water

Table of Contents

FIGURES

TABLES

1 INTRODUCTION

1.1 Background

Infrastructure and recreational sectors have put added pressures on the stability, form and performance of shorelines. Additionally, climate change perturbations have put added stress on the stability of shorelines with increased wave energy and water levels. There are several instances where low-crested structures (LCS) have been used to address these needs. A reliable understanding of LCS stability and performance is therefore crucial to meet these needs and challenges.

Coastal defense and shoreline stabilization needs are addressed with a combination of several forms of coastal structures that function in different ways. These include i) groins that interrupt sediment flow, ii) breakwaters and revetments that protect erodible material by reducing wave energy reaching the shoreline, and iii) beach nourishment for adding material to the longshore and cross-shore processes and planform. Breakwaters and LCS are usually a part of beach stabilization, and enhancement projects and a combination of aesthetics and economic factors usually drive these projects to select LCS in a number of instances.

Breakwaters in beach stabilization projects are usually categorized as emergent, low-crested structures (LCS) or submerged. LCS and submerged structures are more applicable to beach and shoreline stabilization than the former for several reasons. Emergent structures are usually placed in deeper water, where the height of the structures above the seafloor results in higher volumes per unit length. Both the construction and maintenance costs of these structures can be prohibitive. LCS and submerged breakwaters can reduce wave transmission to desirable levels to enhance shoreline stability and planform. The reduced overall height of the structures results in lower life cycle cost costs per unit length. LCS and submerged structures have fewer aesthetic impacts on recreational projects than emergent structures, and even partial emergence at low tides is usually tolerable for end-users. Additionally, LCS can trigger early wave breaking and minimize water quality impacts by avoiding circulation issues. Presently, LCS and submerged structures are designed with semi-empirical formulae for emergent structures in non-depth limited water wave conditions or with guidance from laboratory studies on the initiation of damage. However, these structures are often placed nearshore in shallow depth, where they often experience breaking wave conditions. Additionally, at this time, there is no means of estimating the lifetime evolution of the structural condition based on its wave climate exposure and they are often designed for resisting the initiation of damage condition. This situation can lead to overly conservative designs or progressive damage due to a limited understanding of the stability of these structures over the life cycle.

1.2 Aims and Objectives

The aim of this study was to evaluate the current knowledge and advance the understanding of stability and progression of damage to LCS in shallow water and depth limited wave conditions. This study was limited to the trunk of the structures as a whole and not the performance of the head and spatial variations in the stability of the front, crest and back slopes of the truck. The premise is advanced that a better understanding of damage progression will aid in more economical structural design, over the design life of these structures, in a climate change regime.

The objectives were as follows:

1. **To evaluate the present formulae for the initiation of damage and damage levels.** Some models have provided quantification of the reliability of predictions. Additionally, the comparison of the performance of the existing models does not exist. The hypothesis is that a formula exists that reliably predicts damage and offers the potential for further development.
2. **To identify important variables that explained the initiation and progression of damage in shallow water and depth-limited conditions.** Current formulae for LCS and submerged structures focused on the initiation of damage and damage level but did not explore damage progression. The hypothesis is that additional variables are important to describe damage progression. If so, then this will form a basis for the inclusion of these variables in LCS models.
3. **To formulate a model that explains the stability and damage of LCS.** There are concerns that the existing models do not explain the progression of damage and the most vulnerable section of the structures. The hypothesis is that a new model can explain the damage data and that a new model can better explain the damage data than the best assessed existing model.
4. **To extend the dataset of stability and damage of LCS and submerged structures.** There are concerns about the amount, variability and quality of existing data in the variables of importance. Therefore, the current dataset does not allow for the reliable formulation of models for explaining the damage. By extending the available data, the hypothesis is that the adequacy of the sample of variables will be improved.
5. **To explore model development of a new LCS formula considering both variables of importance and the extended dataset.** Existing models do not consider damage progression, structure geometry and wave characteristics in nearshore and breaking wave conditions. The hypothesis is that a new formula can better describe damage initiation and progression than the existing formulae. Such a model would improve the understanding of these structures and form a basis for future work.

1.3 Scope and Outline

This study focused on LCS and submerged structures in shallow water and breaking wave conditions. Chapter 2, a review of the current design formulae, damage evaluation, wave interactions and experimental conditions. Chapter 3 presents methodologies for exploring the various objectives for the data screening, model assessment, experiments and model development. Existing models and data are examined, and the best existing model for further comparison and most important variables is identified. Chapter 4 explored the theoretical basis and initial performance of the models on the current stability and damage data. Chapter 5 presents the data collection program and model development for a new LCS stability formula. Finally, Chapter 6 summarizes the findings and offers recommendations for future research.

2 LITERATURE REVIEW

2.1 Empirical Formulae

2.1.1 Rubble mound structures

There have been several developments in understanding the structural response of rubble mounds since CERC (1984). CERC presented the Hudson formulae (Equation 2.1) that related stability to wave height, geometric and material properties. Burcharth and Hughes (2002) showed the derivation of Hudson formulae from the Morrison equation of wave-generated (drag, lift and inertial) forces and underlines that the Hudson formulae account for the fundamental processes involved in the stability or initiation and progression of damage. The Van der Meer formulae (Equation 2.2, Equation 2.3 and Equation 2.4) represents an advancement that accounted for additional important sea-state, structural and combined parameters, such as wave steepness and the number of waves (N_w). This model was supported by earlier work by Thompson and Shuttler (1975), who showed the dependence of damage on the number of waves (N_w). This study plans to build on this body of work.

Monochromatic wave studies and the "zero-damage" assumption in the Hudson approach are not practical in the design context. Burcharth and Hughes (2002) noted that precautions were necessary for using findings from previous formulae developed on monochromatic waves versus irregular waves. Van der Meer (1988) pointed out that damage progression is a stochastic process, and the parameters estimated are simply averages with uncertainties with the 6.2 (1.0) parameter for plunging (surging) waves had a standard deviation of 1.0 (0.08). This statistical approach accounts for variability in natural materials and other factors in the scale model. Unfortunately, several past experiments have not explored these parameters (Powell and Allsop, 1985). Both irregular waves and damage progression will be considered in the data collection, experimental design and model development.

Equation 2.1. Hudson formulae for rubble stability

$$N_s = \frac{H_s}{\Delta . D_{n50} . K . Cot(\alpha)}$$

Equation 2.2. Van der Meer formulae for rubble mound stability for plunging waves conditions, $\zeta m < \zeta cr$

$$N_s = 6.2 . S^{0.2} . P^{0.18} . N_w^{-0.1} . {\xi_m}^{-0.5}$$

Equation 2.3 Van der Meer formulae for rubble mound stability for surging waves conditions, $\zeta m > \zeta cr$

$$N_s = 1.0 . S^{0.2} . P^{-0.13} . N_w^{-0.1} . [Cot(\alpha)]^{0.5} . {\xi_m}^{P}$$

Equation 2.4. The transition from plunging to surging waves

$$\xi_{cr} = \left[6.2.P^{0.31}\sqrt{tan(\alpha)}\right]^{\frac{1}{P+0.5}}$$

Accounting for all wave characteristics does not necessarily significantly improve model performance given typical scale model data scatter. Van Gent's (2003) model (Equation 2.5) that is a simplified version of Van der Meer's removed wave steepness and wave height ratios ($H_{2\%}/H_s$), performed equally well. Model development should reward goodness of fit and the least number of parameters.

Equation 2.5. Van Gent (2003) formulae for the stability of rubble mound structure

$$\frac{S}{\sqrt{N_w}} = \left(0.57.\frac{H_s}{\Delta D_{n50}}.\sqrt{tan(\alpha)}.\frac{1}{1+{D_{n50core}}/{D_{n50}}}\right)^5$$

2.1.2 Low crested and submerged breakwater

Wave energy is transmitted over low-crested and submerged breakwaters (LCS). The Hudson formulae derived primarily on emergent structures in a deeper condition have several drawbacks related to LCS. Namely, i) it will result in larger armor size due to the presupposition that most of the energy is discharged on the front face and ii) wave steepness and period were not considered. Powell and Allsop showed that damage to the rear (front) increases with increasing (decreasing) wave period. Also, damage to the rear of the structure was more dependent on the dimensionless freeboard than the structural number (N_s). A point also confirmed by Gilver (1986), who pointed out that damage to the rear (front) occurred with $h_c/h < 0.6$ (>0.7). Powell and Allsop hypothesized that although the spectral Stability Number (N_s*) did not account for all the uncertainties in model development, it was unlikely that the Stability Number derived from no overtopping cases would apply to overtopped structures. Also, the effects of wave period and steepness were significant. In Powell and Allsop's formulation (Equation 2.6), the number of waves (Nw) is not accounted for and represents a drawback. Exploring a range of hc/h ratio below and above 0.6, wave characteristics, and the number of waves may help understand submerged structures.

Equation 2.6. Powell and Allsop (1985) submerged breakwater armor stability. Coefficients A and B vary for Rc, Powell and Allsop (1985)

$$\frac{\Delta}{N_a} = A.e^{(B.N_{s*})}, where\ N_{s*} = \frac{H_s^{\frac{2}{3}}L^{\frac{1}{3}}}{\Delta.D_{n50}}$$

Increasing submergence increases stability. Van der Meer (1988) found that the mass required increased by a factor of 8 for non-overtopped structures compared to overtopped for the same damage. An adjustment (Equation 2.7) was proposed by Van der Meer to account for this observation and summarizes

the importance of a better understanding of submerged structures' stability. An alternative model by Van der Meer and Daemen (1994) focused on LCS and provided insight into the stochastic nature of parameter 2.1 in Equation 2.8. This model offers the possibility of estimating damage for various wave and material conditions. However, both structural geometry and duration are not considered in the model. LCS have not had the research focus as emergent structures. For example, only 31 tests were conducted on LCS versus 700 on emergent structures were undertaken in Van der Meer's study. Filling this gap in the body of LCS datasets will be the focus of this study.

Equation 2.7. Adjustment for the stability of LCS from Van der Meer (1988)

$$N_{s\ low-crested} = \frac{H_s}{\Delta.\mathrm{D}_{n50}}\left(1.25 - 0.25\frac{R_c}{H_s}\right)$$

Equation 2.8. Stability of LCS from Van der Meer and Daemen (1994)

$$\frac{h_c}{h} = (2.1 + 0.1S)e^{(-0.14.Ns*)}, where\ Ns* = \frac{H_S}{\Delta.D_{n50}}.s_{0p}^{-1/3}$$

Burcharth et al. (2005), Kramer (2006), and Vidal (2007) LCS studies focused on the initiation of damage or "no damage." Their premise includes i) LCS are frequently overtopped in exposed shallow water conditions, ii) LCS experience the design wave conditions head-on frequently, iii) damage is likely to progress quickly. See Equation 2.9 and Equation 2.10. Kramer's experiments focused on shallow water and depth-limited conditions. They only estimated the threshold for "initiation of damage" that equates to a particular wave height for a specific size and material property and does not estimate damage across various geometry, duration (N_w) or wave characteristics. While there are instances that justify exploring "zero damage," a better understanding of damage progression can inform design life considerations.

Equation 2.9. Stability formulae for LCS from Burcharth et al. (2005) and Kramer (2006)

$$\frac{H_S}{\Delta.\mathrm{D}_{n50}} = 0.06\left(\frac{R_c}{D_{n50}}\right)^2 - 0.23\frac{R_c}{D_{n50}} + 1.36, -3 < Rc/D_{n50} < 2$$

Equation 2.10. Stability of LCS from Vidal et al. (2007) with parameters in Table 2.1.

$$\frac{H_s}{\Delta.\mathrm{D}_{n50}} = C\left(\frac{R_c}{D_{n50}}\right)^2 + B\frac{R_c}{D_{n50}} + A, -2.01Rc/D_{n50} < 2.41$$

Table 2.1. Coefficients A, B and C for Vidal et al. (2007)

Sector	*A*	*B*	*C*
Front slope and front head	1.831	-0.2450	0.0119
Crest	1.652	0.0182	0.1590
Back slope	2.575	-0.5400	0.1150
Back head	1.681	-0.4740	0.1050

Simplified design rules have evolved from LCS studies that are based on "zero damage." For example, Burcharth et al. (2005) and Kramer (2006) suggested $D_{n50}/h_c>0.29$. the result in shallow water is a structure without a core. Such design configurations are typical as well of more economical cross-sections and warrant further investigations.

2.2 Damage evaluation and estimation

Several approaches have evolved to estimate damage in LCS flume studies (Campos et al. 2020). The most commonly used method applies the Modified Broderick formula (Equation 2.11). This method equates the number of displaced stones (test width and porosity) to damage. Alternately, it can be applied by measuring the average cross-section erosion area (Ae) for a width (w) to the nominal diameter (D_{n50}). Its most straightforward application relies on observations of displaced stones and does not consider settlement, erosion, and reshaping that could have long-term effects on performance.

Equation 2.11. Modified Broderick formulae for estimation of damage, from the measurement of erosion

$$S = \frac{A_e}{{D_{n50}}^2} = \frac{N.D_{n50}}{(1-n).Y} = \frac{\left(\frac{V_e.(1-n)}{{D_{n50}}^3}\right).D_{n50}}{(1-n).Y} = \frac{V_e}{Y.{D_{n50}}^2}$$

A second family of recent work relies on a more precise measurement of erosion and proposes equating vertical distance to erosion (z) to erosion depths (e) for slope angle (α) to the traditional damage number (S). Hofland et al. (2011) explored Melby and Kobayashi's (1998) formulation of the dimensionless damage (E) using digital stereoscopic pairs and found potential robustness in the estimate of the damage. They defined the application to the various states of damage (i.e., initiation, E=0.2 to 0.3, intermediate damage, E= 0.5 to 0.6 to failure, E= 1.5 to 1.6) and various layer thicknesses (i.e., 2D or greater). See Equation 2.12.

Equation 2.12. Relationship between dimensionless damage number (E) over a moving average of mD_{50} to damage number (S).

$$E = \frac{\overline{(z_o - z)}_w.Cos(\alpha)}{D_{50}} = \frac{e}{D_{50}} \xrightarrow{for\ width\ (w)} S = \frac{\int_{e_w>0} e_w\,.\,dx}{D_{50}}$$

Equation 2.13. Dimensionless erosion depth E_{2D} using maximum erosion for average profile

$$E_{2D} = \frac{Max(\langle e_w \rangle)}{D_{50}}$$

There are advantages to the dimensionless damage number (E) over the traditional damage number (S). E can be related to erosion depth relative to the filter layer (typically $2D_{50}$) whereas S cannot. Precise measurement techniques allow for the estimation of E (<0.3) equivalent to S<2 (initiation of damage). This allows for a wider body of test results, whereas Broderick defined S=2 as the lowest level of damage that can reliably be detected. Additionally, the location of the scatter typically seen in test results can be partially addressed by averaging the maximum erosion observed (e_{max}) over the width of the test section for the slope length (x) (Hofland et al., 2017). This leads to another variation, E_{2D} that focuses on the maximum depth of erosion over the cross-section. This method has an advantage because it can directly be related to the armor layer's vulnerability for the erosion of 2 stone diameters ($2D_{50}$). See Equation 2.13. Variations in E_{2D} with sampling width have shown that variations decrease with increasing sampling. A minimum recommended sampling width of ~25 Dn50 is recommended (de Almeida et al., 2019).

Several methods are used for the measurement of damage, including i) mechanical profiling, ii) laser scanning, iii) photogrammetry iv) visual counting of displaced stones (Todd et al. 2016). Both laser scanning and photogrammetry have found recent use in rubble mound scale modeling. These methods are proven to have high accuracies (<4% error) in estimating erosion depth and damage. Photogrammetry has been proven to be effective and cheaper to implement. However, there are concerns with refraction between the water-air interface (Porter et al., 2014). Several techniques have been investigated to reduce refraction effects, including i) images parallel to the refraction plane, ii) numerical algorithms, and iii) underwater photography. Agrawal et al. (2012) showed that a multi-layer system (such as water-air in flume models) could be approximated with multi-point calibration and a single-layer system. Calibration points underwater are therefore required for photogrammetry to be effective. Alternately, draining of the flume after runs to survey post-Nw surface is required.

2.3 Damage initiation versus progression

LCS research on damage has focused on damage initiation and the stochastic nature of armor stone movement. Van Rijn (2019) investigated the initiation of motion of coarse material in currents and waves and bed load transport of armor stones, albeit with a limited data set. His investigation concluded that that the Shield's parameter could predict the stability of rock sizes and bed load transport. There are similar conclusions from Farhadzadeh et al. (2009) in which the prediction of erosion was accurately predicted but variability in the results across several structural configurations. This aspect of rubble mound

structures is promising but developing at this time and emphasis will be placed on better understanding of the prediction of initial versus progression using the Shield mobility approach.

An understanding of damage progression is critical in understanding the long-term performance of rubble mound structures. Kobayashi et al. (2003) demonstrated the importance of rock size and layer thickness versus rock placement in the long-term survival of rubble mound structures. Cover thickness to the core can be reduced by over 40 to 50% in 100 years of simulation and underlines the importance of understanding damage progression. For this reason, a series of more extended tests will be done to understand this aspect of performance better.

Damage progression in the structure's design life has been investigated in a disjointed manner from stability and could give rise to inconsistencies between the tests. Questions arise in the different forms of damage progression and the applicability from differing test conditions and structural configurations (shallow water versus limited depth conditions). Most experiments appear to use between 1,000 and 3,000 waves. For example, Van der Meer (2001) used up to 3,000 waves and assumed a square root function for estimating damage progression to the usual design guidelines are for 7,500 waves to duplicate the typical number of waves in a storm (Kobayashi, 2015). However, Burcharth et al. (2005) showed that the square root function that reliably described damage progression in emergent structures did not apply to low crested structures. Similarly, Melby (1999) showed that damage progression in long-duration series approximates $N_w^{1/4}$ functions rather than the square root. Investigations are necessary to co-jointly examine stability and damage progression for longer durations and the form of the function.

2.4 Wave current and force Interaction with LCS

Rational design and understanding of armor stones' stability require knowledge of wave force from currents and pressures that oscillate and are not steady or uni-directional. Such an understanding could aid in developing a model that could predict damage progression from i) no damage, ii) incipient motion, iii) minor damage, to iv) major damage. An understanding of no damage and minor damage can only lead to overly conservative designs or under prediction of damage with damage progression.

Wave steepness and vertical wave forces are very important. Melby and Kobayashi (1997) showed that the velocities outside the armor were higher (-0.2 to 0.6 m/s) and more important than inside the armor (-0.1 to 0.1 m/s) and suggested this should be the focus. Additionally, for the dominant incipient motion, that: i) maximum velocities increased with wave steepness and reduced with relative depth to toe. In other words, the higher velocities were closer to the upper parts of the LCS, and ii) that maximum vertical velocities with projections outside of the face of the structure occurred at the steep wave front. They summarized that the stability was due to the balance of vertical weight and fluid forces. Additionally, when a convective form of the forces is considered, it reduces to a relationship of similar form to the

Shield's parameter Equation 2.14. Further laboratory measurements of incipient motion confirmed the relationship and imply that armor stone stability is linked to fluid forces and is particularly vulnerable to vertical wave forces from steep wave fronts.

Equation 2.14. Stability criterion (LHS) for incipient motion and stability number. With Cd and Dm modified by the respective empirical convection coefficients Ka and Kc, respectively.

$$\frac{v_c^2}{D_n.g.\Delta} = (C'_D + C'_m)^{-1} \xrightarrow{yields} N_s = \frac{H_c}{D_n.\Delta} = \frac{g.H_c}{v_c}.(C'_D + C'_m)^{-1}$$

Researchers have found that drag, lift, and inertia varies with Reynolds number and Kuelegan and Carpenter number (KC). Generally, for Ks<16 (Kc>16) Cd = 0 (Ci = 0) (Zhang et al. 2015). Zhang et al. also showed that the higher the angle of repose (ϕ), the higher the stability and Shield's parameter for incipient motion. For example, when ϕ=30˚ then θc=0.045 and when ϕ=45˚ then θc=0.073. In other words, stability is a function of rock roughness, and incipient motion occurs below unity. Additionally, drag decreased with Re >10,000 such that Cd = 0.4 to 0.6 for 1,000<Re<100,000 but decreased in more turbulent conditions (Re>100,000) to approximately 0.3.

Drag is generally a function of both Reynolds Number and roughness (Asai et al., 1998) (Figure 2.1). The range of likely Re ($2.2x10^4$<Re<$5.4x10^4$) suggests that Cd could take on values of between 0.25 to 0.5, depending on the stones' roughness. Attempts to formulate relationships between drag and Reynolds Number across a range of Re have been without much usefulness (Garde and Sethuraman, 1969). A relationship of 0.58 x Cd = Cl was suggested. Likewise, Norton and Holmes (1993) noted that there was not much guidance on lift and chose a Cl of 0.15 in their experiments.

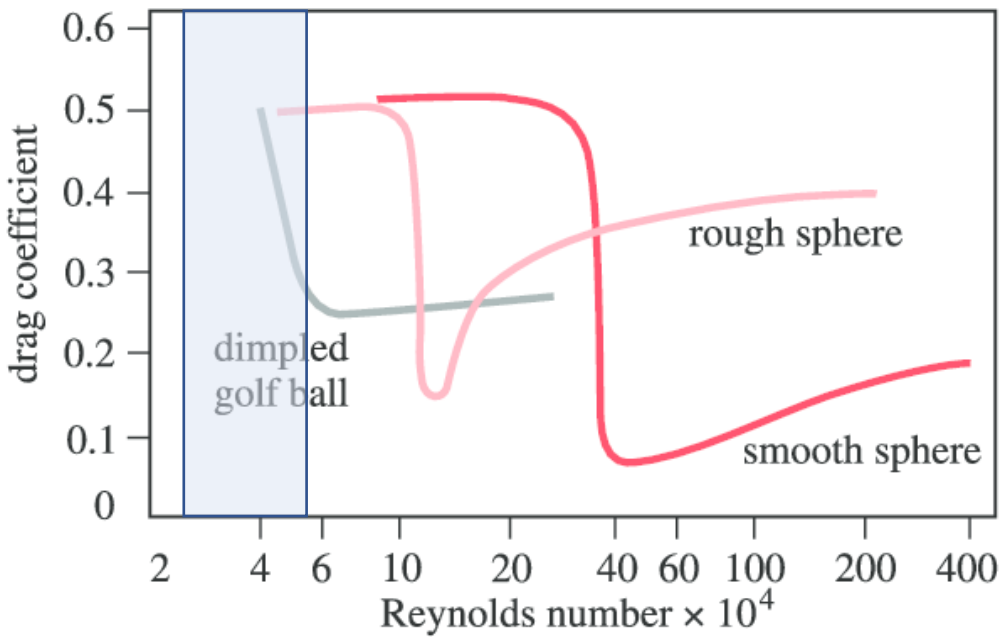

Figure 2.1Relationship between drag coefficient (Cd) and roughness and Reynolds Number from Asai et al. 1998.

Additional concerns with lift are thought to vary considerably with material protrusion and flow conditions in the irregular or oscillatory conditions associated with the wave. Lift and drag are thought to cease when the stone is close to the bed (not protruding or rather mostly protected). This is not the case for a stone on the crest or forward edge of an LCS. Conversely, a stone on a bed will experience both a quasi-stationary lift and an irregular lift (Vithana, 2013)). This situation leads to a need to consider the maximum lift. Torum (1994) derived Cl of 0.1 to 0 (0 to -0.1) for KC<50 (>50) and Cd of 0.1 to 0.8 for KC 30 to 90 (Figure 2.2). The results underline that the relationships between stability and wave-induced forces are not constant but are dependent on both material properties and fluid flow conditions, more accurately represented by the Reynolds Number. Also, that simple relationships between drag and Re and lift and drag may not be easily possible.

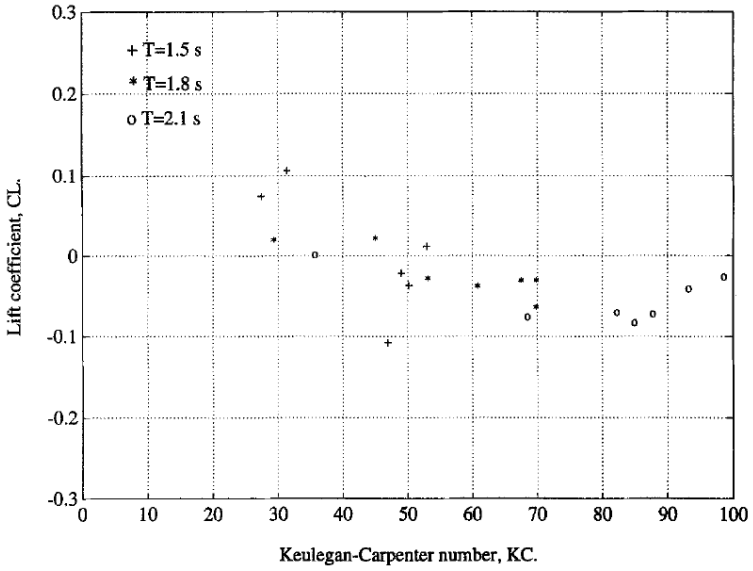

FIG. 14. Lift Coefficient C_L versus Keulegan-Carpenter Number

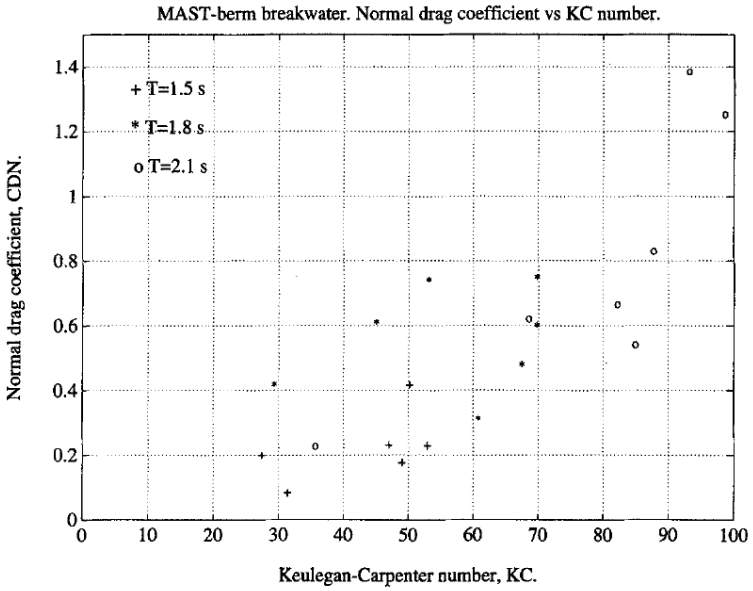

FIG. 15. Drag Coefficient C_{DN} versus Keulegan-Carpenter Number

Figure 2.2. derived lift and drag coefficients with KC number from Torum (1994)

Analytical and laboratory studies have shown that wave forces and internal pore pressures are maximized at the crest's leading-edge during breaking wave conditions. Also, velocity can be represented by the characteristic shallow water equations (Losada et al., 2005 and Garcia et al., 2004). Similarly, Neves et al.'s (2016) study of velocities and pressures on smooth and rough impermeable and rough permeable structures concluded that the highest dynamic velocities and pressures were found on the upper seaward

slope and crown. These findings are different from the usual formulation of considering forces on a typical armor stone unit on the front face (Sila, 2004).

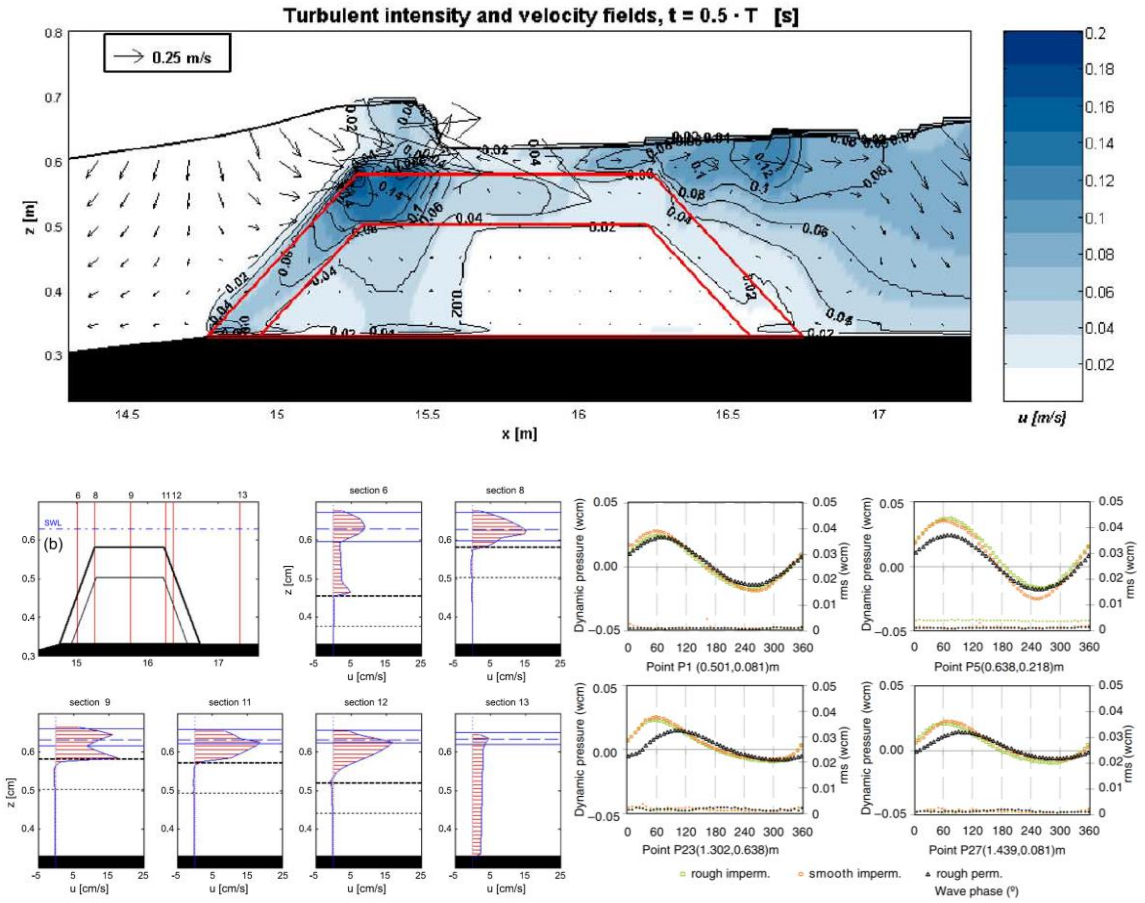

Figure 2.3Velocity distribution for breaking waves on an LCS from Losada et al. (2005, figure 5) (top) and Garcia et al. (2004) measurements and simulations (bottom left) and Neves et al. (2005) (bottom right)

2.5 Experimental Conditions

2.5.1 Wave parameters

Description of wave height is a concern for shallow water low-crested and submerged breakwaters. Hs described by the Rayleigh distribution usually describe wave characteristics. However, the highest waves break in shallow water, and the Rayleigh distribution can accurately describe the spectrum. Other characteristic ways of describing the truncated distribution may become necessary, such as $H_{2\%}$ or $H_{1/10}$ as

noted by Van der Meer (1995), who opted for the $H_{2\%}$ for shallow water conditions. Similarly, local wave steepness (s_p) may also be more relevant than deep-water steepness (s_{op}). These concepts will be tested in the review and assessment of the models on existing data in a Principal Component Analysis (PCA) exercise.

2.5.2 Scale Effects

Viscosity effects in scale model experiments have been a concern. In several tests, Thompson and Shuttler (1975) determined that a range of 7,000 to 40,000 had no scale effects. Similarly, Van der Meer (1988) noted that his experiments were done at Reynold's Number (Re) (Equation 2.15) of 40,000 to 80,000, albeit that several authors had suggested no scale effects would occur at a range of 10,000 to 40,000. Large scale versus small-scale test verified that no scale effects occurred at values of 40,000. Jensen and Klinting (1983), using a theoretical approach, reasoned that if 1% error was accepted that a range of Re>6,000 was acceptable, albeit that this was comparable to Martin et al. (2002) suggested range of >10,000 but much less than Dai and Kamel (1963) range of > 30,000. The main difference is that the higher recommendations for Re to avoid scale effects consider a core of finer material in which there is flow. For example, in Shimada et al. (1987), a range >40,000 was determined because of the core. This study was limited to homogenous LCS and used a Re criterion of >10,000. Previous studies were screened with this criterion.

Despite the foregone, some concerns required further understanding of scaling accuracy for breaking waves on armor stone structures. Tirindelli and Lamberti (2004) reason that the impulsive (pulsating) forces from the initial (secondary) impact of breakers on the armors could not be (could be) accurately scaled using Froude or Cauchy scaling. This was due to the compressibility of entrained air in a short time in impulsive impacts. A point also reinforced by Martin et al. (2002). Therefore, our study will have to bear this in mind for LCS in shallow conditions that will experience breakers. For this reason, we follow the general guidelines of Wolton et al. (2007), who suggested if the Reynolds number is in the same range as the prototype, then the Froude scaling can be used.

Equation 2.15. Reynold's number for armor stone layer used by several authors

$$Re = \frac{\sqrt{g.H_s}.D_{n50}}{\nu}$$

2.6 Summary

Understanding the stability and response of rubble mound structures from the Hudson equation has evolved to include a deeper understanding of the roll of sea state, wave type, and the number of waves.

LCS presents several challenges in better understanding wave steepness, and the role of the relative crest elevation in the hc/h ratio was underlined by Van der Meer and Daemen (1994). Notwithstanding, there has been limited focus on LCS in the literature. Recent studies (Kramer, 2006) have unfortunately focused on the initiation of damage rather than damage progression and simplified "rules of thumb."

Evaluation and measurement of damage have evolved from simple cross-section profiling measurements to more detailed erosion depth measurements using photogrammetry and lasers. These improvements allow for better estimates of structural vulnerability.

The shear stress-induced flow of armor stones has found increased presence in LCS research. It shows the potential to explain the evolution of damage with a modified Shield's parameter formulation (Rijn, 2019). Several challenges are evident in the literature, including the limited number of waves (<3000) and disjointed approach in considering stability separate from damage progression. It is our opinion that Shield's stress formulation offers promise in bridging this gap in the understanding of LCS.

The relationships between stability and erosion from wave-induced forces (drag, lift and shear stress) and stabilizing internal friction and gravity are documented in the literature. Variations with several hydraulic variables, including Re and KC, offer insight into the variabilities involved. The importance of the increased vulnerability at the leading edge of LCS has been underlined in several studies.

Notwithstanding the foregone, scale model testing challenges have occurred and should be avoided by ensuring similitude at a suitable minimum Re (>10,000).

3 ASSESSMENT OF EXISTING DATA AND MODELS

3.1 Method

3.1.1 Scalability, Porosity, LCS and Outliers

Several data filtering requirements were applied to ensure scalability. These included: homogeneity, head-on truck investigations and only LCS ($hc/h<1.25$) that met $Re>10,000$ were accepted from the stability datasets. Only homogenous ($P=0.6$) or 2-layer structures ($P=0.45$) were assessed because of the subjective quality of the notional porosity for scenarios with fine cores and the implications for using a higher Re criterion of 30,000. This was to ensure that the results apply to prototype scale structures and resulted in filtering out a lot of the available data from the DELFT dataset.

3.1.2 Assessment and Variable Selection

Both the Van der Meer and Daemen (VdM) (1994) model for stability and Kramer's (2006) model for initiation of damage were assessed. Model performance and repeatability for each formula were assessed on: i) the dataset with which the models were each developed and; ii) other datasets. Performance was assessed by determining the following:

1. Bias and repeatability (variance) of the VdM model on DEFLT and AU datasets.
2. Proportions of positive predictions using k-proportions test was used to assess Kramer's and Van der Meer's and Daemen's models on both the AU and DELFT datasets
3. VdM model predictions of damage are similar to the data (Null hypothesis, H_o) and therefore reliable for practical use under similar conditions. The alternative hypothesis is that VdM cannot produce predictions similar to the damage data (Alternative hypothesis, H_a) and would therefore require further development or qualifications of its limitations,
4. Analysis of variance techniques was used to assess model, variable treatment and block effects. Factorial design using multiple means was used in the variable analysis of both treatments and blocks to test the hypothesis that there is no relationship with damage. Variables and treatments of importance were further explored in model development. The hypotheses were: i) that no variable contributes significantly to explaining the damage and alternately that there is at least one variable contributing to the explanation of the damage. If there are important variables, these will be identified and compared to the model variables. And if not, then collinearity will be investigated. Ii)That there are no collinearity relationships amongst the variables. If there are, then these relationships will be flagged for further investigation.
    a. Blocking was explored using Randomized Complete Block. Duncan's Multi-Range Test of the variables of the model (treatment) and other variables (blocks) will be explored to gain deeper insight into the variables and range of conditions (blocks) that the model

might apply to. The hypothesis is that the means of the pairs are the same (Ho), and the Null hypothesis is the means are different (Ha).

b. In the event of Ha, the following hypothesis will be tested: VdM model is capable of predicting similar results to the data for some blocks (Ho) and, therefore, reliable for certain ranges of Re. The alternative hypothesis is that VdM cannot produce predictions similar to the data (Ha).

5. The importance of variables from the three available datasets (UC, AU and DELFT) was assessed using Principal component analysis (PCA) for both i) the variables of the best-assessed model (h_c/h, Hs, Δ, Dn50, s_{op}, and S,) and ii) potential variables (s_m N_w, P, $H_{2\%}$, ζ_{om}) identified in the literature. Importance was assessed in two stages. First, normality and the presence of outliers were tested at the 5% level. Non-normal variables were transformed with either a natural log function and in the case of wave steepness -1/3rd power function. Outliers were removed. The existing and potential variables were examined with PCA and screened only to include variables that were likely to be important with PCA. Kaiser-Meyer-Olkin (KMO) test was used to assess the suitability of the sample size and variables. Principal components that had eigen values greater than 0.8 and explained over 80% of the variance were used to identify significant variables taken to model development.
6. Akaike Information Criterion (AIC) and Bayesian Information Criterion (BIC) of both models on the DELFT and AU datasets. The Burnham and Anderson (2004) criteria for ΔAIC and Raftery (1999) criteria for ΔBIC were used to determine the models' level of support. The best-assessed model was considered for further development. Three scenarios were explored:
    a. Damage using Van der Meer and Daemen model on both DELFT and AU datasets
    b. Initiation of damage using
        i. Kramer model on both DELFT and AU datasets
        ii. Van der Meer and Daemen model on both DELFT and AU datasets, using S=2 as the threshold

3.2 Existing Data

Three datasets were identified and described herein from Kramer et al. (2002, 2006) and Van der Meer (1990).

3.2.1 Sources

Stability tests were carried out at the University of Cantabria in 2001 (UC 2001) on a homogeneous cross-section and had 16 data points available. Side slopes of 1:1.5 and non-depth limited wave conditions were used. Kramer (2006) raised concerns about the small stone sizes (4 grams) and the possibility of viscous

effects. We agree and estimate that the Re was <7000 for the range of wave heights ($H_{1/10}$ <0.09 meters). UC was found worthy of further inspection.

Kramer (2006) carried out over 69 tests at the Aalborg University in 2006. Thirty-six of the tests being head-on and with freeboards of 0.05 to -0.1 meters. A core of coarse material was used with 1:2 side slopes. Only 1,000 waves were typically used, and this represents a drawback in this test series. Damage was estimated by the Modified Broderick formulae that equates the number, size and porosity of stones to damage. Notwithstanding, this represents a viable dataset.

Van der Meer (1988) performed over 600 stability tests in the wave flume at Delft Hydraulics in 1988, including some on LCS. This dataset is the most comprehensive dataset with 652 tests and a range of h_c from 0.3 to 5.0 meters. Damage was estimated by a profile measuring technique and could have captured and equated setting to damage with loss in the cross-sectional area. The dataset was filtered to include $h_c/h<1.2$ and results not suspected of viscosity. The relative freeboard (h_c/h) of 0.75 is a significant drawback and represents a gap to be filled.

3.2.2 Comparison and filtering of available data

The existing datasets offer a unique opportunity to test repeatability, albeit that they have limitations. See a summary of datasets in Table 3.1. Froude scaling, duration (N_w) and wave conditions were some of the drawbacks. The UC 2001 was conducted with very small stones and up to 2,000 waves. The resulting R_e criterion was not met in all instances. AU2006 is the most current data set with numerous oblique runs. These are not relevant to this study and were omitted.

Notwithstanding, 50 of the test results met all criteria. DEFLT dataset was the most extensive, with 652 test results, with a majority of them on emergent structures. Forty-four of the tests were relevant to this study. Overall, 94 test results were available for model development and testing.

Table 3.1. Existing stability datasets from UCA (Vidal, 2001), AU (Kramer 2006) and Delft, (Van der Meer, 1990)

	UC 2001	AU 2006	DELFT 1988
Number of tests	16	69	652
Number of tests that met criteria (Re>6,000, hc/h<1.2, Rc/Dn50<2)	0	50	44
Dn50 (m)	0.012	0.0325	0.034 to 0.21
Structure height (m), hc	**0.25**	0.3	1.15 (some 0.3 to 7.0)
Crest width (m)	0.25		
Structure slope, Cot α	1:2	1:2	1:1.5 to 4
Foreshore slope, m	1:20		
Water depth (m), h	0.20 to 0.30 m	0.25 to 0.40 m	0.20 to 5.00 m
Freeboard (m), Rc	-0.05 to 0.05	-0.1 to 0.05	-0.1 to 2.0
Relative freeboard, hc/h	0.83 to 1.25	0.75 to 1.2	0.75 to 3.25
Type of breakwater	Homogenous	Two-layers, Homogenous	Homogenous, layered, impermeable
Materials, specific density	Crushed stone, 2.65	Crushed stone, 2.65	Crushed stone, 2.62
Hs(m)	0.022 to 0.074	0.034 to 0.246	0.04 to 1.18
Tm (seconds)	1.5 to 2.82	0.75 to 2.1	1.24 to 4.4
Duration, Nw	1059 to 2000	1000	1000 to 3000

3.3 Analysis and Results

3.3.1 Damage Progression and Initiation of Damage

Van der Meer and Daemen's model predicted damage reasonably well across both the DEFLT and AU datasets. Predictions cluster around the measurements in the DEFLT dataset. See Figure 3.1 a and b. However, there seems to be a trend for under (over) prediction for lower (higher) stability numbers greater than 8 (less than 8) on the AU dataset. Correlation coefficients and bias were determined to be 0.74 (0.76) and 3.4 (1.3) respectively on the DELFT (AU) dataset. There was better (worst) performance on the AU (DELFT) dataset with a lower (higher) standard deviation of the bias of 1.92 (6.06). See Figure 3.2 a and b that shows the wider scatter of the predictions on the DEFLT data versus the AU data. This is

likely to be due to the differences in the method of estimation of damage and the narrow range of damages in the AU dataset. AU (DELFT) dataset typically has lower (higher) damages with a maximum of 9.6 (46.4). There are also differences in how damage is estimated. DELFT used a profiling method to estimate damage (across ten cross-sections) that can mistakenly equate some settling to damage. Whereas AU used the definitive Modified Broderick that equates displaced stones to damage. Van der Meer and Daemen's model performed reasonably well with some concerns about the variation of performance across the range of stability numbers and how the damages were estimated.

Both Kramer and Van der Meer's models predicted the initiation of damage in equal proportions to the data at significant levels ($p>0.5$) for an initiation of damage $S= 0.5$ and 1. See Table 3.2. Kramer's model was consistent for the range of damage 0.5 to 2.0. See Kramer's (Figure 3.1c and d) and Van der Meer's model (Figure 3.1e and f) predictions versus data. There were several instances that the threshold for initiation of damage had been exceeded, and there was no significant damage in the AU dataset, i.e., false positives (Figure 3.1c). The performance of the models depended on the definition of initiation of damage and this trend was considered in model development.

Blocking revealed improved VdM performance with predictions of damage are similar to the data for $Re<40{,}000$. VdM predictions were not similar to all the damage data ($p < 5\%$) in Figure 3.3a and b, and that there is a general tendency to over predict damage. Cluster in the range of $S<3$ (Figure 3.2) suggested that triggers typical in this range of damage should be explored. Blocking by Re for the ranges $Re<40{,}000$ ($Re>40{,}000$) revealed that there is sufficient (insufficient) evidence that the VdM and measured damage (S) are similar (not similar) (Figure 3.4a and b). It is therefore recommended that the VdM model only be used For $Re <40{,}000$.

Both Kramer and Van der Meer and Daemen's model performances were indistinguishable based on the AIC and BIC model selection methods (Table 3.3). ΔAIC (~0.0) and ΔBIC (~-0.1) suggest support for both models. Van der Meer and Daemen's model was taken forward for model development, given its flexibility to predict both damage and the initiation of damage. In contrast, Kramer's model only predicts the initiation of damage.

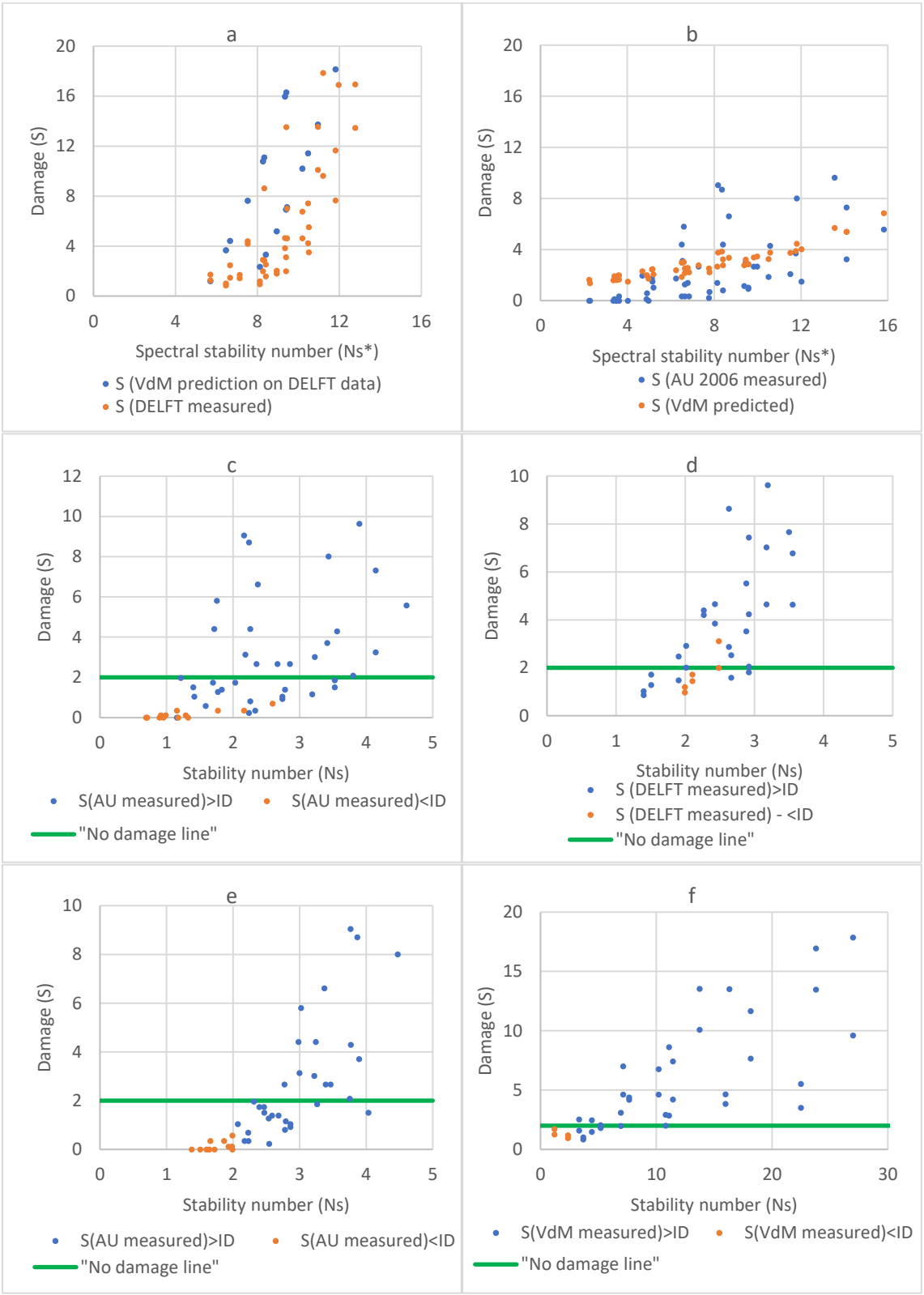

Figure 3.1. Damage prediction of: Van der Meer and Daemen (1994) model on DELFT (a) and AU (b) datasets (top row), Kramer (2006) on AU (c) and DELFT (d) datasets (middle row) and Van der Meer and Daemen (1994) on AU (e) and DELFT (f) datasets (bottom row).

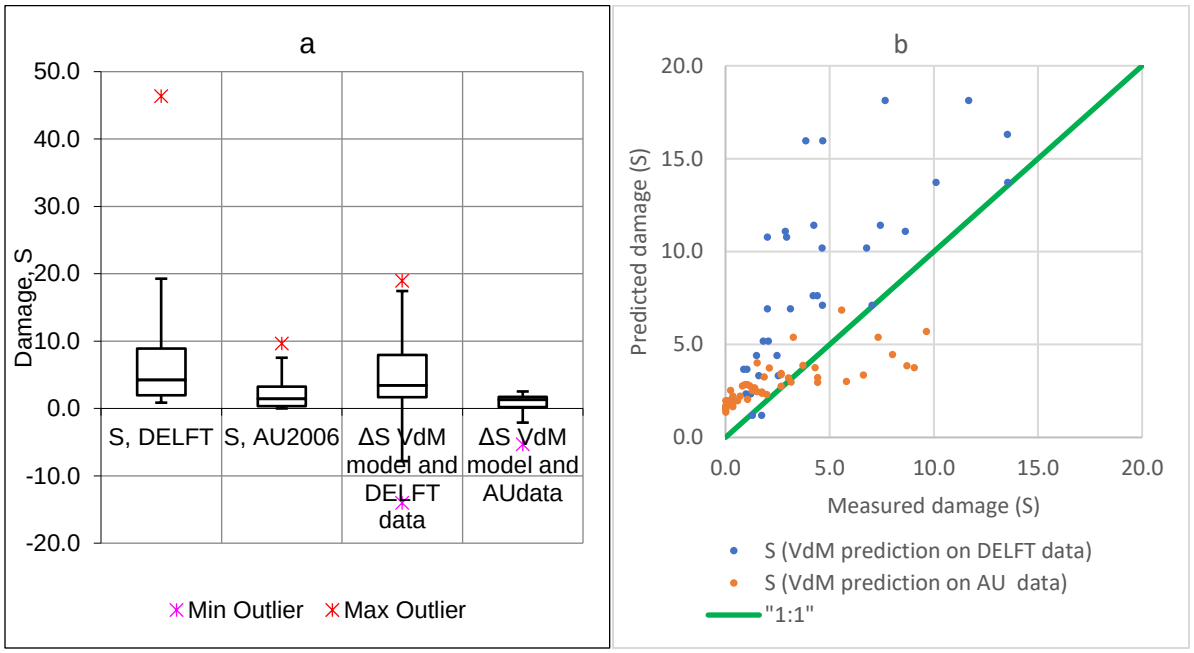

Figure 3.2. Summary of DELFT and AU damage datasets and model prediction biases from using DEFLT and AU data (a) and predicted versus measured damage for Van der Meer model on DELFT and AU data (b)

Table 3.2. k-proportions test of Kramer and VdM models to predict initiation of damage (S=2.0, 1.0 and 0.5) for AU and DELFT datasets.

	S = 2			**S = 1**			**S = 0.5**		
Contrast	Value	Critical value	Significant	Value	Critical value	Significant	Value	Critical value	Significant
|p(Kramer) - p(VdM)|	0.312	0.185	Yes	0.117	0.175	No	0.052	0.167	No
|p(Kramer) - p(S)|	0.026	0.195	No	0.065	0.181	No	0.065	0.165	No
|p(VdM) - p(S)|	0.286	0.186	Yes	0.052	0.170	No	0.013	0.158	No
Sample	Proportion	Groups		Proportion	Groups		Proportion	Groups	
S	0.442	A		0.727	A		0.792	A	
VdM	0.727		B	0.779	A		0.805	A	
Kramer	0.416	A		0.662	A		0.740	A	

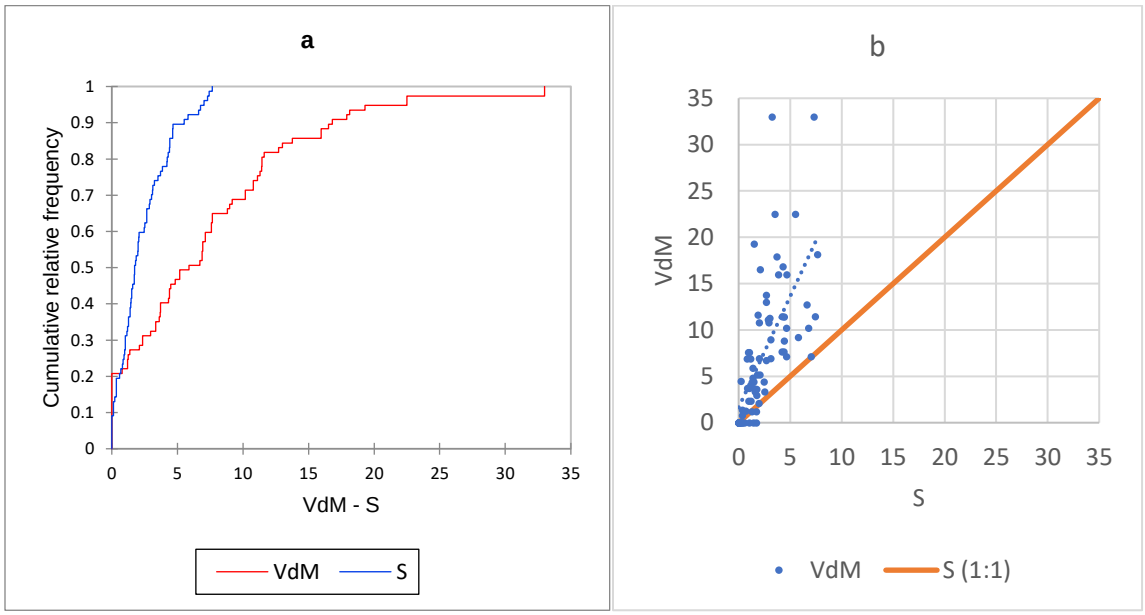

Figure 3.3. KS test of Vdm versus S (left) and scatter plot of (right) with 1:1 line

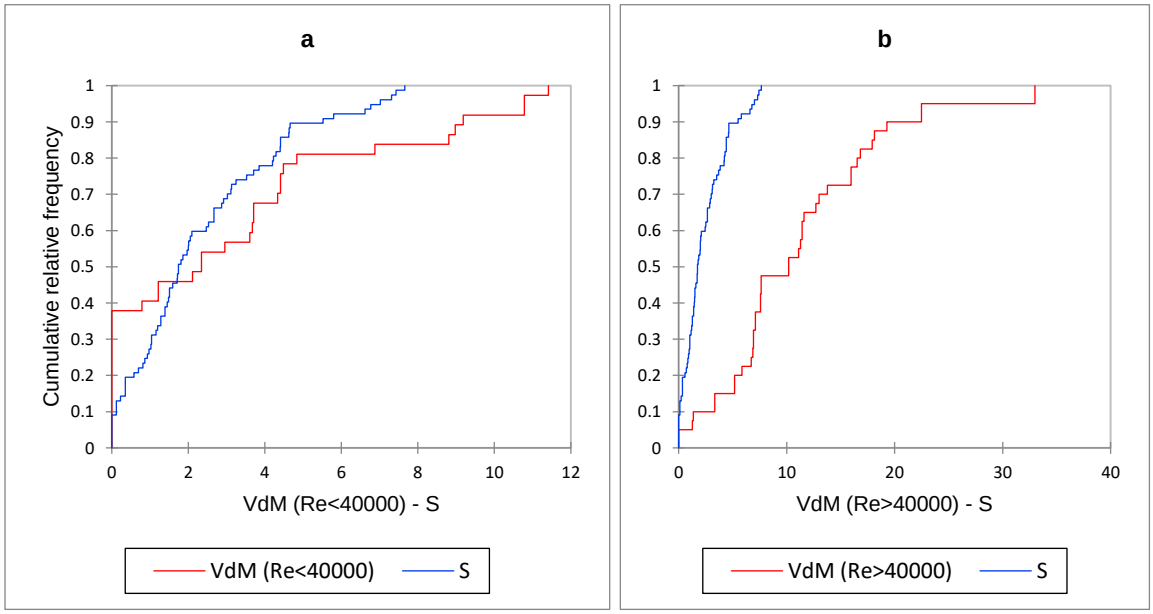

Figure 3.4 KS test of VdM versus S (a) and scatter plot of (b) with 1:1 line and KS test of Vdm versus S for Re<40,000 (a) and Re>40,000 (b)

Table 3.3. AIC and BIC model selection of Van der Meer and Daemen and Kramer models on DELFT and AU datasets.

	Van der Meer and Daemen		Kramer		Van der Meer and Daemen- Initiation of damage	
	Dataset		**Dataset**		**Dataset**	
Dataset	DELFT	AU	AU	DELFT	AU	DELFT
RMSE	1.3	0.76				
Number of data points, N	44	50	50	44	50	44
Likelihood, L	0.744	0.764	64%	81%	64%	86%
Number of parameters, K	6	6	5	5	5	5
Model selection method						
AIC	14.9	14.5	12.3	12.0	12.3	11.9
Δ AIC (relative to Kramer's model)	2.6	2.5			0.0	-0.1
BIC	23.3	24.0	20.5	19.3	20.5	19.2
Δ BIC (relative to Kramer's model)	2.8	4.7			0.0	-0.1

3.3.2 Variance, Means and Variable Importance

Data were filtered of outliers to remove outliers to retain the AU and DEFLT sources. The entire UC dataset and one outlier in the AU dataset were removed in the data preparation process. There was a preponderance of outliers in the UC dataset for D_{n50}, ξ_{om} and s_{om} and one point in the $H_{2\%}$ series in the AU dataset. The Iribarren number in the UC dataset suggest mostly surging condition in this dataset. In contrast, we are interested in shallow water and breaking wave conditions for LCS, which were therefore removed. Most variables were determined to be non-Gaussian distributed with $p<0.05$, except s_m ($p=0.077$).

Variance and blocking analysis underlined the importance of the formulated model's variables and provided insight into the design of the experimental program and model validation ($p<0.05$). The following was inferred:

1. Analysis at both the treatments ($H_{2\%}$, Kt, Ns, cot α, Nw, and Tm) and blocks (s_m, P, Laboratory, Re, Kc and ξ) revealed that it is highly likely that there is a relationship between at least one of

the variables and the damage (S) at significant levels (Table 3.4). Damage is therefore dependent on at least one of the variables.

2. Most of the treatments and blocks were confirmed as important. There is sufficient evidence that the treatments and blocks: Tm, Kt, $H_{2\%}$, Re, Nw, K_C and Cot α are not zero and providing significant input ($P<0.05$). Significantly, the central tendency for damage is maximized (minimized) for Kt-High Kt*Tm-Tm<2 (H2%-H2%<0.1*RE-Re<40000 and Nw-Nw<1000*KC-Kc<70). This is insightful as it suggests (confirms) high wave transmission and periods (a smaller number of waves, Re and less oscillatory forces) are more (less) damaging.
3. Other variables s_m, P, Laboratory and ξ are possibly not providing significant effects on the dependent variable (S) and are acting as fillers.

The importance of Kt, Re, Nw and Kc proved insightful and confirmed their usefulness in LCS model development. Additionally, there is insufficient evidence of the importance of Ns, s_m, laboratory and ξ effects and suggest that these variables can be simplified in model development.

Pairwise comparison of Means of the factorials (Table 3.5) underlined the importance of i) wave transmission (Kt), ii) Period (Tm), iii) Wave height (H2%), iv) Structure slope (cot α), v) Reynold's number (Re), vi) Number of waves (Nw) and vii) KC number. Significant differences in the means for damages were found for the following:

a. High (low) wave transmission (Kt) and short periods correlate with more (less) damage of 4 (1.3). This underlines the importance of considering increased wave transmission and short periods that can be more damaging.
b. Higher (lower) wave heights and flatter (steeper) slopes correlate with more (less) damage of 4.45 (1.4). Increased stability of steeper slopes was not expected and provided useful insight into the importance of LCS geometry
c. Higher (lower) wave heights and Re >40,000 (<40,000) resulted in greater (lower) damage with means of 4.45 (1.4). This underlines the importance of exploring more turbulent conditions with higher Re conditions wherein although wave energy increases (from 0.1 to 0.2 m), drag likely decreases from 0.5 to 0.25 and more than likely partially compensates with some added stability.
d. More waves and high drag conditions (Kc>70) correspond with greater damage. This underlines the importance of the number of waves and oscillatory forces.
e. High Kt (low Kt) of >0.8 (<0.1) resulted in higher (lower) damage with means of 3.9 (2.7).

In summary, a pairwise comparison of the means highlights the importance of the number of waves, wave transmission, period, height and structure slope in maximizing damage.

Table 3.4. Damage versus variable treatments and blocks analysis.

Source	DF	Sum of squares	Mean squares	F	Pr > F
Model	7	187.037	26.720	14.424	< **0.0001**
Error	69	127.815	1.852		
Corrected Total	76	314.852			

Model parameters (S):

Source	Value	Standard error	t	Pr > |t|	Lower bound (95%)	Upper bound (95%)
Tm-Tm<2	-1.616	0.661	-2.445	**0.017**	-2.934	-0.297
Kt-High Kt*Tm-Tm<2	2.725	0.474	5.749	< **0.0001**	1.779	3.670
H2%-0.1<H2%<0.2*cot a-Cot<1.61	-2.033	0.434	-4.686	< **0.0001**	-2.898	-1.167
H2%-0.1<H2%<0.2*RE-Re<40000	-1.991	0.270	-7.380	< **0.0001**	-2.529	-1.453
H2%-H2%<0.1*RE-Re<40000	-2.754	0.471	-5.845	< **0.0001**	-3.694	-1.814
Nw-Nw<1000*KC-70<Kc<110	-1.384	0.606	-2.282	**0.026**	-2.594	-0.174
Nw-Nw<1000*KC-Kc<70	-3.358	0.739	-4.543	< **0.0001**	-4.833	-1.883

Table 3.5. Damage versus Duncan's MRT pairwise comparison from factorial analysis

Category	LS means	Standard error	Lower (95%)	Upper (95%)	Groups		
Kt-High Kt*Tm-Tm<2	4.099	0.408	3.285	4.914	A		
Kt-High Kt*Tm-Tm>2	2.990	0.385	2.223	3.758	A		
Kt-Low Kt*Tm-Tm>2	2.990	0.385	2.223	3.758	A		
H2%-H2%>0.2*cot a-Cot<1.61	4.457	0.323	3.813	5.101	A		
H2%-H2%>0.2*cot a-Cot>1.61	4.457	0.323	3.813	5.101	A		
H2%-0.1<H2%<0.2*cot a-Cot>1.61	3.461	0.286	2.891	4.032		B	
H2%-H2%<0.1*cot a-Cot>1.61	1.703	0.456	0.792	2.613			C
H2%-0.1<H2%<0.2*cot a-Cot<1.61	1.428	0.239	0.952	1.905			C
H2%-H2%>0.2*RE-Re>40000	4.457	0.323	3.813	5.101	A		
H2%-0.1<H2%<0.2*RE-Re>40000	3.440	0.216	3.009	3.872		B	
H2%-H2%<0.1*RE-Re<40000	1.703	0.456	0.792	2.613			C
H2%-0.1<H2%<0.2*RE-Re<40000	1.449	0.185	1.079	1.819			C
Nw-Nw<1000*KC-Kc>110	3.812	0.401	3.012	4.612	A		
Nw-Nw>1000*KC-70<Kc<110	3.812	0.401	3.012	4.612	A		
Nw-Nw>1000*KC-Kc>110	3.812	0.401	3.012	4.612	A		

The PCA assessed the orientation and correlation of all existing variables (hc/h, Hs, Δ, Dn50 and sop) as important for explaining the data variance. There were concerns from the KMO test about the adequacy of the number of variables and sample size for all variables, particularly h_c/h, S and s_{op}. Care was taken in drawing inference on these variables and underlined the importance of additional experiments with more variability and additional variables to better explain the damage. The first three factors accounted for over 89% of the variance (Figure 3.5a). Orientation of the correlation between the variables and factors (Table 3.7) suggest:

1. increasing damage is correlated with Hs and decreasing h_c/h. This later point is not immediately intuitive but understandable. Increased overtopping implies increased wave energy being disposed of on the structure's rear rather than being transmitted over the structure.
2. Concerns about the usefulness of s_{op} (Figure 3.6a) that was mostly normal to the PC1 axis. The importance of this variable was assessed further.

Notwithstanding the foregone, all existing variables were taken forward for further analysis.

PCA of all existing and proposed variables (s_m, N_w, P, $H_{2\%}$, ξ_{om}, $s_m^{-1/3}$) provided more insight into the correlation direction of the variables than the previous analysis. There were repeated concerns from the

KMO test (Table 3.6) highlighted prioritizing improved sampling of the h_c/h and Hs variables with the lowest measures of 0.37 and 0.43, respectively. The 1st three PC explained over 86% of the variance (Figure 3.5b) with a strong correlation between the variables and factors. Several inferences were made, including:

1. Increasing damage with h, T_m, $H_{2\%}$, N_w, s_m and ξ_{om} are correlated with increasing damage.
2. There were concerns about the usefulness of Cotα, s_{op} and $s_{m,}$ with both being near normal to the damage in the correlation circle (Figure 3.6b). This required further assessment in the model development exercise.

Overall, there was strong support for the proposed variables, and these were carried to model development.

Table 3.6. Kaiser-Meyer-Olkin (KMO) measure of sampling adequacy for existing variables with variables with sampling concern (red).

Existing variables		Existing and proposed variables	
S	0.409	S	0.691
hc/h	0.405	hc/h	0.370
Hs	0.485	Hs	0.434
Δ	0.520	Δ	0.491
Dn50	0.520	Dn50	0.491
Sop	0.408	Sop	0.443
KMO	0.476	Sm	0.439
		Nw	0.922
		P	0.491
		$H_{2\%}$	0.434
		ξ_{om}	0.537
		$S_m^{-1/3}$	0.561
		KMO	0.493

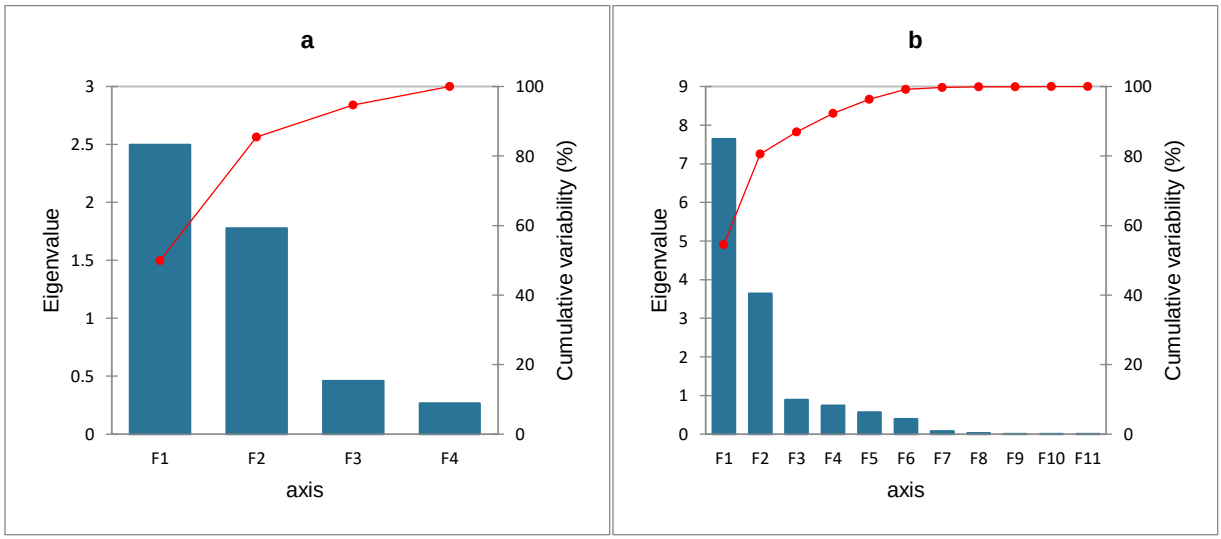

Figure 3.5. Scree plot of PCA for existing variables (a) and existing and proposed variables (b) showing Eigen values and cumulative variance explained.

Table 3.7. Correlation between variables and factors (high positive correlation red fill) and Squared cosine from PCA for existing variables

	Correlation			Square of cosines		
	F1	F2	F3	F1	F2	F3
hc/h	0.487	-0.743	0.353	0.237	**0.552**	0.125
Hs	-0.427	0.819	0.007	0.183	**0.671**	0.000
Δ	0.956	0.191	-0.217	**0.914**	0.036	0.047
Dn50	-0.956	-0.191	0.217	**0.914**	0.036	0.047
Sop	0.501	0.693	0.490	0.251	**0.481**	0.240
S	-0.431	0.252	0.144	**0.186**	0.064	0.021

Table 3.8 Correlation between variables and factors (high positive correlation red fill) and Squared cosine from PCA for existing and proposed variables

	Correlation			Square of cosines		
	F1	F2	F3	F1	F2	F3
hc/h	-0.353	-0.745	0.328	0.124	**0.555**	0.108
Hs	0.333	0.905	-0.059	0.111	**0.819**	0.004
Δ	-0.969	0.080	-0.133	**0.939**	0.006	0.018
Dn50	0.969	-0.080	0.133	**0.939**	0.006	0.018
Sop	-0.553	0.609	0.534	0.306	**0.371**	0.285
Sm	-0.474	0.787	0.373	0.225	**0.620**	0.139
Nw	0.620	-0.078	0.256	**0.385**	0.006	0.066
P	-0.969	0.080	-0.133	**0.939**	0.006	0.018
H2%	0.332	0.899	-0.068	0.110	**0.809**	0.005
ξom	0.949	-0.219	0.062	**0.901**	0.048	0.004
cot a	-0.969	0.080	-0.133	**0.939**	0.006	0.018
hc	0.674	-0.256	0.315	**0.454**	0.065	0.099
Tm	0.832	0.231	-0.331	**0.692**	0.053	0.110
h	0.761	0.518	-0.051	**0.579**	0.268	0.003
S	0.406	0.375	0.058	**0.165**	0.141	0.003

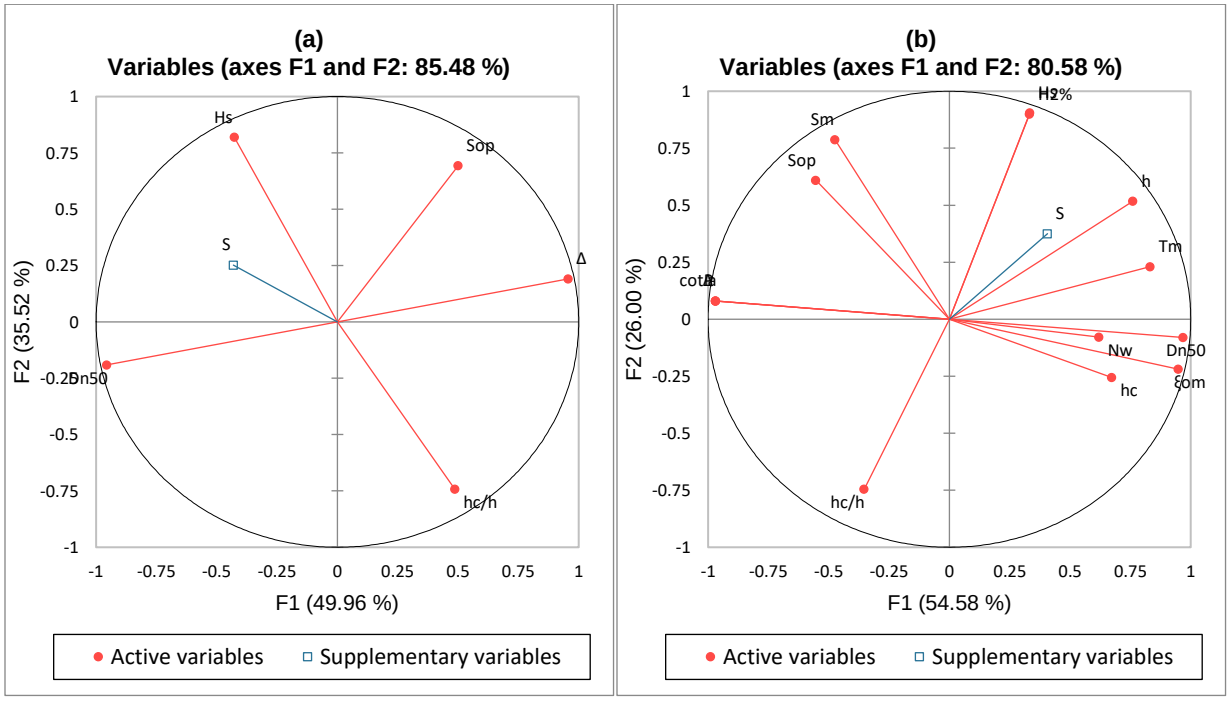

Figure 3.6. Correlation circle for existing variables in Kramer and VdM models (a) and existing and proposed variables (b) for 1st and 2nd PC. Supplementary variable (not used in the analysis) is shown for orientation purposes only.

3.4 Summary

LCS stability data exists from UC, AU and DEFLT datasets with over 737 points. There were differences in how the tests were conducted (method for estimation of damage, oblique waves and emergence), the hydraulic conditions (wave heights and Reynolds Number), and the resulting variables' range. The method for estimation of damage was a key factor, and the Modified Broderick equation was used herein as it is believed to be less subjective. The dataset was screened to 94 points and used in the evaluation of the performance of both Kramer and Van der Meer and Daemen stability models.

Van der Meer and Daemen's model (VdM) proved skilful in estimating damage progression and damage initiation. Damage progression was predicted with a moderately high correlation (0.74) across both the AU and DELFT datasets. There was a trend for under-prediction of damage with higher stability numbers. Notwithstanding, VdM predictions are not similar to the damage data, except for blocked data with Re <40,000. This suggested the limit of applicability of the VdM in very turbulent conditions needs to be explored. The need for a broader range of damage to better evaluate the model became apparent and was considered in the experimental design.

Kramer and Van der Meer and Daemen's models were not able to prediction initiation of damage in equal proportions to the data and their performances were indistinguishable. Improvement in this skill and defining uncertainty in the parameters was a focus of model development.

VdM empirical model was carried forward for further comparison in the model development process, albeit that this model does not consider the number of waves (Nw). The absence of critical variables of importance: damage estimate (S), wave steepness (s_{op}) and the number of waves (Nw), in Kramer's model precluded further detailed consideration.

Variance and blocking analysis and pairwise comparison of means underlined the importance of the formulated models' variables, particularly Tm, Kt, $H_{2\%}$, Re, Nw, K_C and Cot α. Significant differences of the means for damages highlight the need to investigate: i) higher (lower) wave heights and Re >40,000 (<40,000), ii) high Kt (low Kt) of >0.8 (<0.1) that resulted in higher (lower) damage and iii) surging and spilling (plunging) breaking wave types resulted in higher (lower) damage. PCA of both the existing variables in Van der Meer and Daemen model (S, h_c/h, H_s, Δ, D_{n50} and s_{op}) and proposed variables (s_m, N_w, P, $H_{2\%}$, ξ_{om}) suggest that all of the variables are of importance. However, there were concerns about the usefulness of Cot α , s_{op} and $s_{m,}$ and their importance was further assessed with the new dataset and in model development. Additionally, the KMO test highlighted the importance of increasing the sample size and range of variables, particularly for h_c/h and H_s. The design of the experimental data collection program considered these gaps.

4 THEORETICAL BASIS AND TESTING

4.1 Method

4.1.1 Procedure

Both friction (MF) and the stochastic Shield's process of bed transport models based on bed shear stress (BSS) were considered, and two stability equations for LCS were developed. The resolution of moments about the most vulnerable forward crest stone was the focus. The second class of models that removed transmitted wave energy was also developed, wherein the transmitted wave energy was removed (K_t). Both models were tested on existing flume damage data with parameter values from the literature.

Performance of the MF, BSS and VdM models were explored by comparing the predictions with the data. Development and performance were assessed progressively and by the following method:

1. MF, BSS and VdM were assessed against the data in two ways:
    a. Prediction of initiation of damage is defined as when the load (Ns) exceeds the capacity (MF, BSS or VdM) and results in S>2. The null hypothesis is that MF, BSS or VdM can predict damage initiation similar to the data using the k-proportion test at the 5% limits. If not, then
        i. the effects of calibration will be investigated. μ, Cd, Cl and r parameters were used in the calibration process with an optimization routine in Excel®. The null hypothesis is calibration improves the model performance, and MF or BSS can predict damage similar to the data. If not, then
            1. model development will be deemed as required. Removal of transmitted wave energy in the MFkt and BSSkt models was investigated with the null hypothesis that MFkt and BSSkt can predict initiation of damage. In the event of the alternative hypothesis, then the initiation of damage will be investigated using a damage progression formulation.
    b. Prediction of damage progression: The null hypothesis is that BSS or VdM can predict damage similar to the data. This was assessed using tests of similarity of distributions (KS) at the 5% limit. If not, then
        i. the effects of calibration will be investigated. Again, Cl and r parameters were used in the calibration process with an optimization routine in Excel® that minimized RMSE. The null hypothesis is calibration improves the model

performance, and MF or BSS predict damage similar to the data. If not, then model development will be deemed as required.

2. BSSkt performance of damage progression was assessed as follows:
    a. The null hypothesis is that removing transmitted wave energy improves the performance such that BSSkt can predict damage similar to the data (p>5%) and, therefore, reliable for practical use under similar conditions.
    b. If not, then the effects of treatment and block relationships gleaned from the multi-collinearity analysis will be investigated.
3. BSSkt model was further developed by converting favorable blocks to treatments based on multi-collinearity results. Variations in the coefficient of lift were investigated. The null hypothesis is that model performance improves by converting favorable blocks to variable treatments. The alterative hypothesis is that performance is not similar to the data.
    a. In the event of the null hypothesis, variations of the model for the lift will be investigated. The hypothesis is that parameters for the determination of lift from the literature can be optimized. The predictions of damage between the literature-based values are not similar to those determined by calibration herein. That calibration of the coefficient of lift model produces better results.
    b. In Alternative hypotheses, the model will be reverted to the most favorably assessed model and simplified.
4. The best assessed analytical model was simplified. The null hypothesis is that a simplified model can produce damage prediction similar to the data. In the event of the alternative hypothesis, the model will be reverted to the full form.
5. VdM Treatment and block relationships were explored to determine if there was a reliable range for the treatment or block wherein the predictions are similar to the data. If not, then the model will be deemed unreliable.

4.1.2 Parameters

Parameter values from the literature were used in the test as follows:

1. Friction factor (μ) of 0.4 from Muzutani et al (1993). A range of 0.35 to 0.45 was explored.
2. Cd of 0.4. A range of 0.25 to 0.5 was explored in order to determine the effects of either very rough and dimpled stones versus rough angular stones
3. Cl of 0.18 to 0.4 (0.35) respectively from Kobayashi and Otta (1987). It is noted that lift can be negative from Torum (1994).

4. Angle of response (ϕ) = 45˚. Froehlich (2011) noted 35˚ (rounded stones) and Van Rijn (1993) 45˚ degrees (angular stones). The stones were assumed angular with ϕ = 45˚
5. Reduction factor of 0.05 (Vithana, 2013, figure 2.8) to 1.0 (van Rijn, 2019). This factor of Critical Shield number for the incipient motion of rocks depends on the level of protrusion. There is a greater reduction in the critical Shield's number for more exposed (or protruded stone) than for level beds. We argue here that this value could be higher to account for the armoring effect resulting from LCS construction and note Vithana's observations that critical shear stress could vary between 0.01 to 0.1 depending on the level of protrusion etc. A broader range for this parameter, for calibration purposes, of between 0.01 to 2.0 is assigned until this parameter is better understood.

MF_{kt} and BSS_{kt} models that account for wave transmission and the removal of wave energy transmitted were explored. These models used the estimated Kt over LCS from Van der Meer and Daemen (1994) (Equation 4.1), wherein:

Equation 4.1. Model for Kt from Van deer Meer (1994)

$$K_t = 0.80\ for - 2.0 < \frac{h - hc}{H} < -1.13$$

$$K_t = 0.46 - 0.3.\frac{h - hc}{H}\ for - 1.13 < \frac{h - hc}{H} < 1.2$$

$$K_t = 0.10\ for\ 1.2 < \frac{h - hc}{H} < 2.0$$

A formulation for the lift that decreases with increasing KC number in keeping with the findings of Torum (1994) was also tested to see if BSS or BSSkt performance improved. An equation for Cl in the form of Equation 4.2 was tested. Additionally, another model wherein the coefficients to determined Cl from Kc was also tested.

Equation 4.2. The proposed equation for coefficient of lift from Torum (1994) data.

$$C_L = -0.00333.K_C + 0.2$$

4.1.3 Model development

Model development entailed testing the best evaluated existing and formulated stability models. AIC and similarity tests were used as assessment tools in the model development process. Model calibration entailed subjecting the proposed and existing model to an Artificial Neural network (ANN) to determine each model's best parameter values. Model performance was assessed incrementally on: i) new stability data ii) existing stability data and followed the previous procedure to determine repeatability.

4.2 Assumptions

The stable weight of armor stones is dependent on material properties, geometry and wave-induced forces. Initiated motion resulted from: i) tangential forces exceeding restoring or stabling forces resulting in sliding, ii) overturning moments on armor units exceeding restoring moments resulting in rolling or iii) uplifting when lift forces exceed stabilizing normal forces. Restoring forces include gravitational, buoyance and frictional forces. Several empirical models explain armor stone stability, and Hald and Burcharth (2001) presented 21 such equations. Analytical forms for LCS are explored here, with some empirical approximations.

The assumptive conditions for a model of forces, moments and stresses based on theoretical treatments and the findings of laboratory studies included:

1. The influence of wave forces and fluid velocity varies depending on the wave field and wave condition phase. In other words, the importance of inertia (drag) increases for Keulegan-Carpenter Number ($KC= u_m.T/D$)<10 (KC>20) (Mizutani et al. 1993). Inertial forces are typically minimal in LCS given the typical KC range being greater than 20 (Figure 4.1). Inertial forces were therefore neglected.
2. Most theoretical treatments and laboratory studies consider spherical armor units and neglect frictional forces. However, frictional effects might be significant for rough armor units that could be blocky or quadratic in form and are considered here. This will be considered in two ways: i) a group of models (MS) that consider drag in the Morrison type framework and ii) a group of models that consider the Shield's parameter type formulation (BSS).
3. Both normal and tangential forces can be maximized rather than maximizing one and finding the other's instantaneous value. Mizutani et al. (1993), showed where this occurs and represents the worst case. Likewise, both tangential and normal forces are important, particularly for the crest and, to a lesser extent, the slopes where the tangential component is more significant. Torum (1994) confirmed the latter point in laboratory investigations.
4. Wave forces and internal pore pressures are maximized at the leading edge of the crest, and velocity can be represented by the characteristic water velocity in shallow water, which is the focus of this study.
5. Two models were considered herein. The first is based on Morison-type forces of lift and drag (MF), and the second is based on bed shear stresses explained by the Shield parameter (BSS). There is a preference in the literature for the bed shear stress type model based on laboratory studies for LCS (Vidal et al. 1999).
    a. Model MF: Lift and drag forces are considered with opposing friction and gravitational forces, with the equivalent moments determined.

b. Model BSS: Bed-shear stress and lift on the armor unit's exposed surface are considered, and equivalent moments determined. Lift is considered herein because of observations in numerous studies that indicate that θ_{cr} has to be adjusted by a factor (r) of 0.3 to 0.6 to better account for boulders' mobility in waves and currents (van Rijn, 2019). This indicates that an additional mobilizing force was occurring at initiated mobility at velocities lower than the threshold. We reason that this is likely to be lift as drag is accounted for in the bed-shear stress formulation. The bed-shear stress results in an equivalent flow of armor units that are accounted for using the Shield's Number (θ) formulation (van Rijn, 2019). The flow was equated to equivalent damage (S) based on the number of waves (N_w). The energy of this flow was equated to an approximation of the available energy, that is, the incident energy, less reflected and transmitted. Here an empirical treatment of the reflected and transmitted energy is allowed.

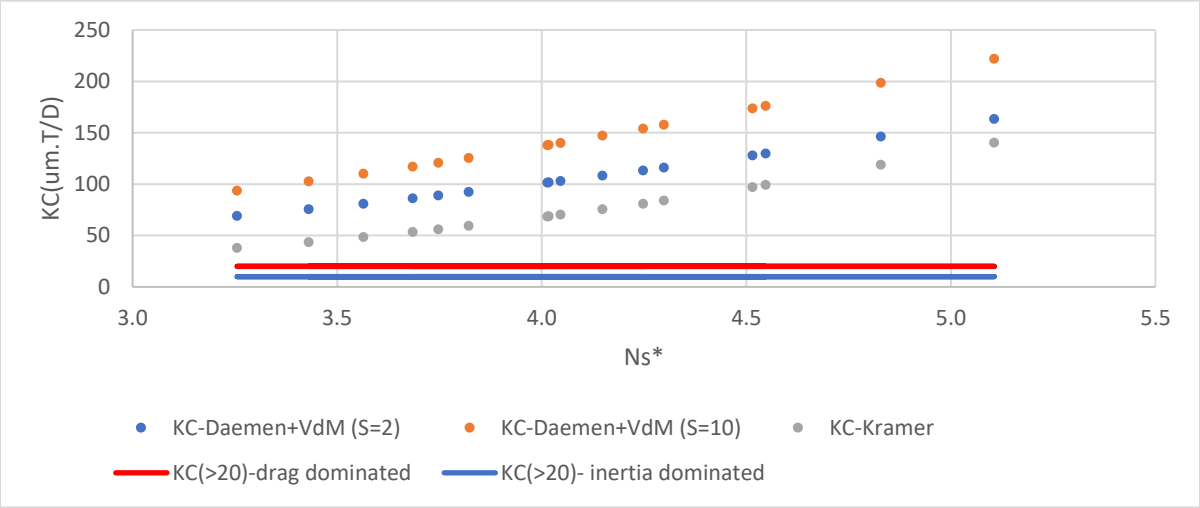

Figure 4.1. KC number for LCS structurers designed with D_{50} determined from Kramer (2004) (initiation of damage) and Daemen and Van der Meer (1994) at S = 2 and 10, for shallow water breaking wave conditions (κ=0.6).

4.3 Derivation

4.3.1 Friction and Bed Shear Stress Models

Moments are resolved for an armor unit with a nominal diameter (D), about point A (+anti-clockwise). Restoring buoyancy (W_s) that acts vertically and friction forces with friction coefficient (μ) that acts normal to the partially embedded slope angle from horizontal (α) are considered (Figure 4.2). Here, μ is known to lie between 0.4 to 0.6, with 0.6 being typical for rough angular particles (Sammis et al., 2011).

Destabilizing forces include lift (F_L) that acts normally to the slopes and tangentially acting drag (F_D) forces. Inertial forces are ignored for reasons previously stated. All forces are considered when maximum wave forces attempting to remove armor stone backward are also considered. It is noted that there is added exposure on the crest that increases lift and drag forces and bed-shear stress beyond the contemporary embedded scenario that only considers the exposed slope surface.

Equation 4.3. MF moments considering gravitational, friction, lift and drag forces.

$$\frac{D}{2}.g.D^3.(\rho_a-\rho_w)[1+\mu.Cos(\alpha)]-\frac{D}{2}.[F_L+F_D]=0$$

Equation 4.4. BSS moments considering gravitational, lift and bed-shear stress forces.

$$\frac{D}{2}.g.D^3.(\rho_a-\rho_w)-\frac{D}{2}.\left[F_L+F_{\tau_b}\right]=0$$

Force components, with added exposure on the crest and maximum horizontal velocity (u_m) are considered:

Equation 4.5. Lift force component on armor unit

$$F_L=\frac{\rho_w}{2}.C_L.\left(D.\left(1+Sin(\alpha)\right)\right)^2.{u_m}^2$$

Equation 4.6. Drag force component on armor unit

$$F_D=\frac{\rho_w}{2}.C_D.\left(D.Sin(\alpha)\right)^2.{u_m}^2$$

Equation 4.7. . Bed-shear stress force component on armor unit

$$F_{\tau_b}=\tau_b.D^2.\left(1+Sin(\alpha)\right)=\theta(\rho_a-\rho_w).g.D^3\left(1+Sin(\alpha)\right)$$

Inserting the terms for the forces into Equation 4.3 and Equation 4.4, multiplying by $2/(\rho_w .g.D^3)$

Equation 4.8. MF moments considering gravitational, friction, lift and drag forces.

$$D.\Delta.\left(1+\mu.Cos(\alpha)\right)-\frac{{u_m}^2}{2.g}.\left[C_L.\left(\left(1+Sin(\alpha)\right)\right)^2+C_D.\left(Sin(\alpha)\right)^2\right]=0$$

Equation 4.9. BSS moments considering gravitational, lift and bed-shear stress forces.

$$D.\Delta-\frac{{u_m}^2}{2.g}.C_L.\left(1+Sin(\alpha)\right)^2-D.\Delta.\theta.\left(1+Sin(\alpha)\right)=0$$

Solving for u_m^2 in Equation 4.8 and Equation 4.9:

Equation 4.10. Maximum velocity for MF considering gravitational, friction, lift and drag forces.

$$\frac{{u_m}^2}{D.\Delta} = 2.g.\frac{\left(1+\mu.Cos(\alpha)\right)}{C_L.\left(1+Sin(\alpha)\right)^2 + C_D.\left(Sin(\alpha)\right)^2}$$

Equation 4.11 Maximum velocity for BSS considering gravitational, lift and bed-shear stress forces.

$$\frac{{u_m}^2}{D.\Delta} = 2.g.\frac{1-\theta.\left(1+Sin(\alpha)\right)}{C_L.\left(1+Sin(\alpha)\right)^2}$$

Assuming: i) shallow water breaking wave conditions with horizontal velocity (u) at the toe approximating maximum tangential velocity to crest and ii) maximum particle velocity can be estimated from the shallow water breaking wave celerity ($c=\sqrt{(g.h_b)}$) and $H_b = h_b.\kappa$:

Equation 4.12. Maximum particle velocity at hc from linear wave theory

$$u \sim \sqrt{gh} \xrightarrow{breaking\ wave\ condition} \sqrt{g\frac{H_b}{\kappa}} \xrightarrow{squaring} {u_m}^2 = \frac{g.H}{\kappa}$$

Substituting u_m^2 and making Ns the subject for both the MF and BSS models:

Equation 4.13. Stability number for MF model

$$\frac{H}{D.\Delta} = N_s = 2.\kappa\frac{1+\mu.Cos(\alpha)}{\left[C_L.\left(1+Sin(\alpha)\right)^2 + C_D.\left(Sin(\alpha)\right)^2\right]}$$

Equation 4.14. Stability number for BSS model, with maximum particle velocity at hc and Shields parameter

$$\frac{H}{D.\Delta} = N_s = 2.\kappa.\frac{1-\theta.\left(1+Sin(\alpha)\right)}{C_L.\left(1+Sin(\alpha)\right)^2}$$

By definition, the number of moving rocks is related to the bed-load transport flow (q_b):

Equation 4.15. Relationship between number of moving stones and flow

$$N_{rm} = \frac{q_b}{\rho_a.D^3} = \frac{q_b}{\rho_a.D^3} = \frac{{kg}/{m.s}}{{kg.m3}/{m3}} = {\#}/{m.s}$$

Bed-load transport flow, q_b (with units kg/m.s) can be equated to damage (S). Note duration in terms of the number of waves (N_w), mean wave period (T_m) and the number of moving stones (N_{rm}) as follows, per unit rock width (D) in keeping with the definition of damage (S), thereby removing the length unit in N_{rm}:

Equation 4.16. Relationship between flow, damage (S), mean wave period (T_m) and number of waves (N_w) (van Rijn, 2019)

$$S \sim \Delta t.D.N_{rm}(unitless) = N_w.T_m.D.N_{rm} = N_w.T_m.D.\frac{q_b}{\rho_a.D^3} = \frac{N_w.T_m.q_b}{\rho_a.D^2} \xrightarrow{yields} q_b = \frac{S.D^2.\rho_a}{N_w.T_m}$$

Similarly, for bed load transport at low shear stress, van Rijn (2019) formulation suggest an average transport (versus an "excess" shear stress type model wherein stress above critical shear stress is considered):

Equation 4.17. Flow from Shields number (van Rijn, 2019)

$$q_b = 13.\rho_a.(g.\Delta)^{\frac{1}{2}}(D.\theta)^{\frac{3}{2}}$$

Equating flow (q_b) from damage (Equation 4.16) and stress (Equation 4.17), solving for θ, applying a reduction factor (r) and slope factor (K_α=Sin(ϕ+α)/Sinϕ) for up rushing flows and longitudinal slope (α) and internal friction or angle of repose (ϕ) (van Rijn, 2019):

Equation 4.18. Shields number from damage and flow

$$\vartheta = r.K_\alpha.\left[\frac{S.D^2.\rho_a}{N_w.T_m.13.\rho_a.(g.\Delta)^{\frac{1}{2}}.D^{\frac{3}{2}}}\right]^{\frac{2}{3}} = r.\left(\frac{Sin(\phi+\alpha)}{Sin(\phi)}\right).\left[\frac{S.D^{\frac{1}{2}}}{13.N_w.T_m.(g.\Delta)^{\frac{1}{2}}}\right]^{\frac{2}{3}}$$

Substituting into the equation for Ns for the BSS model:

Equation 4.19. Stability number for BSS model

$$\frac{H}{D.\Delta} = N_s = 2.\kappa.\frac{1 - r.\left(\frac{Sin(\phi+\alpha)}{Sin(\phi)}\right)\left[\frac{S.D^{\frac{1}{2}}}{13.N_w.T_m.(g.\Delta)^{\frac{1}{2}}}\right]^{\frac{2}{3}}.\left(1+Sin(\alpha)\right)}{C_L.\left(1+Sin(\alpha)\right)^2}$$

4.3.2 Removal of transmitted wave energy

An estimate of wave energy disposed on the structure is derived by removing the incident wave energy's transmitted energy (Equation 4.12). The amount of energy removed is wave transmission (K_t is wave transmission coefficient) over the crest of the LCS.

Equation 4.20. Estimate of incident energy

$$u_m{}^2 = \frac{g.H}{\kappa} \rightarrow H = \frac{u_m{}^2\kappa}{g} \xrightarrow{estimate\ of\ incident\ energy} E_i \propto \left(\frac{u_m{}^2\kappa}{g}\right)^2$$

Similarly, the energy disposed on the structure would be the incident less the transmitted:

Equation 4.21. Estimate of energy disposed on the structure

$$E_{structure} \propto \left(\frac{u_m{}^2\kappa}{g}\right)^2 - \left(\frac{u_m{}^2\kappa}{g}\right)^2.K_t{}^2 = \left(\frac{u_m{}^2\kappa}{g}\right)^2\left(1-K_t{}^2\right) \xrightarrow{deriving\ H} H = \frac{u_m{}^2\kappa}{g}\sqrt{\left(1-K_t{}^2\right)}$$

Equation 4.22. Stability number for MF_{kt} model with wave transmission removed.

$$\frac{H}{D.\Delta} = 2.\kappa.\sqrt{\left(1-{K_t}^2\right)}\frac{\left(1+\mu.Cos(\alpha)\right)}{C_L.\left(1+Sin(\alpha)\right)^2+C_D.\left(Sin(\alpha)\right)^2}$$

Equation 4.23. Stability number for BSS_{kt} model with wave transmission removed.

$$\frac{H}{D.\Delta} = 2.\kappa.\sqrt{\left(1-{K_t}^2\right)}\frac{1-r.\left(\frac{Sin(\phi+\alpha)}{Sin(\phi)}\right)\left[\frac{S.D^{\frac{1}{2}}}{13.N_w.T_m.(g.\Delta)^{\frac{1}{2}}}\right]^{\frac{2}{3}}.\left(1+Sin(\alpha)\right)}{C_L.\left(1+Sin(\alpha)\right)^2}$$

Making Ns the subject and solving for S:

Equation 4.24. Damage prediction from BSSkt model with transmitted wave energy removed.

$$S = \left[\frac{1-\frac{N_s}{2.\kappa.\sqrt{\left(1-{K_t}^2\right)}}\left(C_L.\left(1+Sin(\alpha)\right)^2\right)}{\left(1+Sin(\alpha)\right).r.\left(\frac{Sin(\phi+\alpha)}{Sin(\phi)}\right)}\right]^{3/2}.\frac{13.N_w.T_m.(g.\Delta)^{\frac{1}{2}}}{D^{\frac{1}{2}}}$$

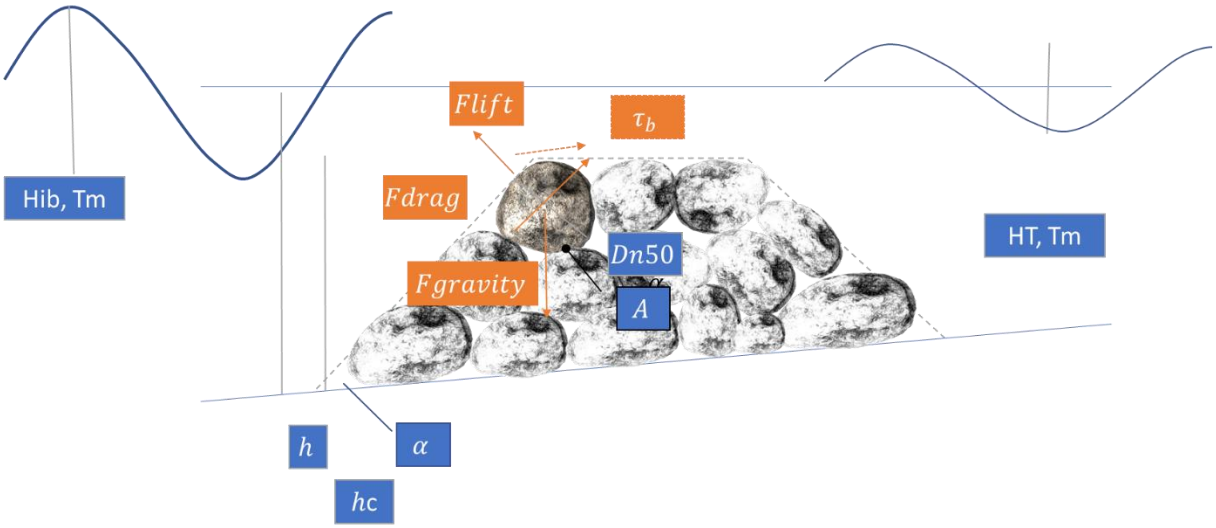

Figure 4.2. The concept for MF and BSS models

4.4 Results and Discussion

4.4.1 Initiation of Damage

MF, BSS and VdM models could not accurately predict the initiation of damage ($p<0.0001$) in equal proportions to the observed damage, using the k-proportions tests. For example, VdM predicted the initiation of damage 76%, whereas MF and BSS accuracies were 78% and 72%, respectively (Table 4.1). Visual inspection of the predictions (Figure 4.3a) suggests that MF and VdM have a general tendency to cluster around an MF:Ns and VdM:Ns value of 1 for sharp increases in damage. This makes physical sense as damage should increase when the load exceeds capacity. Further improvement with calibration was recommended.

Calibration improved the performance of BSS to an accuracy of 84% that was greater than the accuracy of the VdM of 76%. Notwithstanding, all three models could not accurately predict the initiation of damage at significant levels ($p<0.0001$). Visual inspection (Figure 4.3b) suggests that a sharp increase in predicted damage by all three models around MF:Ns, BSS:Ns and VdM:Ns less than 1 (i.e., when capacity is less than load). Calibration resulted in a decrease in all parameter values. The reduction of r to a value of 0.18 from 1 is closer to the value of 0.4 suggested by Van Rijn (2019). Further improvement by the removal of transmitted wave energy was explored.

Removal of transmitted wave energy improved the MFkt performance from 72 to 82%. Albeit that both MFkt and BSSkt were not able to predict initiation of damage reliably in equal proportions ($p<0.0001$) (Table 4.2). MF_{kt} and BSS_{kt} had better predictive capabilities (82% versus 76%) than VdM and suggested that the analytical framework offers potential for understanding the stability of LCS. See Figure 4.3c. Shield stress reduction parameter had the most significant effect after being reduced from 0.18 to 0.05, and provided more remarkable predictive ability. Attention was turned to modeling initiation of damage by calibration of "progressive damage" models, given the difficulty in accurately predicting the discrete nature of "initiation of damage."

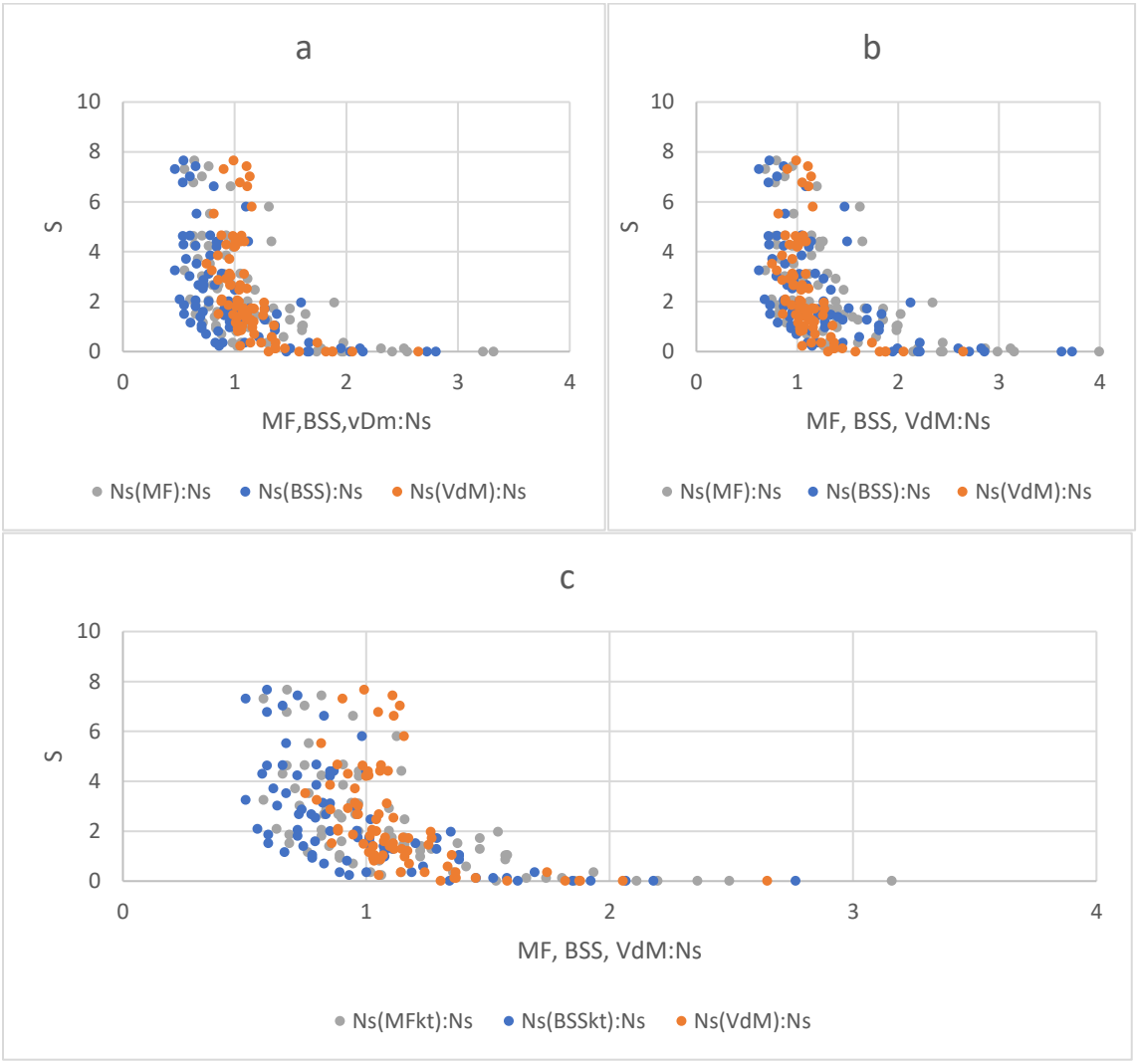

Figure 4.3. Damage (S) versus ratio of MF, BSS, VdM:Ns data (a), calibrated models (b) and MFkt and BSSkt:Ns data (c).

Table 4.1. Parameter estimates for MF and BSS models pre and post-calibration and with transmitted wave energy removed MFkt and BSSkt for initiation of damage experiment.

	μ	Cd	Cl	r
Original values	0.40	0.40	0.35	1.00
MF/BSS Calibrated values	0.39	0.47	0.26	0.17
MFkt/BSSkt Calibrated values	0.38	0.41	0.31	1.5

Table 4.2. k-proportions test for initiation damage for MF and BSS and MSkt and BSSkt models

Sample	Proportion	Groups		Sample	Proportion	Groups	
MF	0.724	A		VdM	0.763	A	
VdM	0.763	A		MFkt	0.816	A	
BSS	0.829	A		BSSkt	0.816	A	
S	1.000		B	S	1.000		B

4.4.2 Damage Progression

Both BSS and VdM were unable to predict damage similar to the data at significant levels for both: i) the model that used the previously calibrated parameters and ii) uncalibrated models (Figure 4.4a and b) using original parameter values. The VdM being a calibrated model, suggested exploring various blocks from the variance and means analysis. Damage was generally over (under)-predicted by VdM (BSS). Calibration for the BSS model was explored.

Calibration improved the BSS performance such that the predictions were similar to the damage data (Figure 4.4c and d). A bias of 3.4 or “excess” damage was determined and possibly due to a higher reduction parameter (r) in the BSS formulation (Table 4.3). The value of the r parameter was irrational and suggested that a better understanding of this parameter is needed. Further improvement was sought by removing wave energy that is transmitted past the LCS.

Removal of transmitted wave energy in the BSSkt model and calibration improved the performance of the BSSkt such that the predictions were similar ($p=0.105$) to the damage data (Figure 4.4e and f). Bias was reduced from 3.4 to 1.8 of “excess” damage. In other words, the BSSkt marginally under-predicted

damage, rather than over-predict in the BSS model. There were marginal changes in the calibrated parameters (Table 4.3). This suggests that the removal of transmitted wave energy improves the understanding of the stability of LCS. Further improvement was sought by removing wave energy that is transmitted past the LCS.

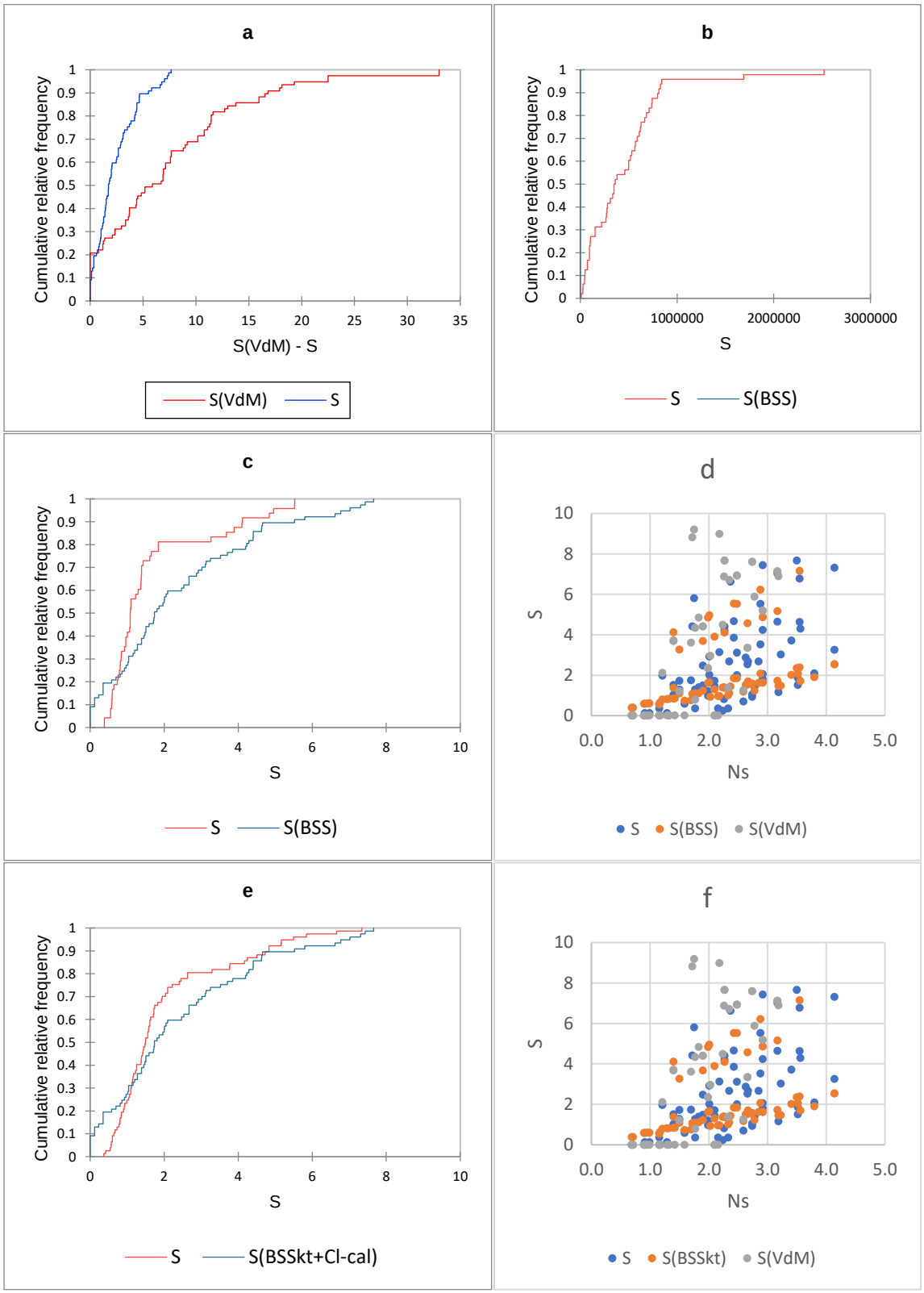

Figure 4.4. Cumulative damage for VdM (a), BSS (b) and BSS-calibrated (c). Measured and predicted damage (S) for BSS-calibrated and VdM versus Ns (d). Cumulative damage for S-BSSkt-calibrated (e). Measured and predicted damage (S) for BSSkt-calibrated and VdM predictions versus Ns (f).

Table 4.3. Parameter estimates for BSS model pre and post-calibration for damage progression experiment.

	Cl	r
Previously calibrated values	0.29	0.05
Original values	0.35	1.00
BSS Calibrated values	-0.20	3944
BSSkt Calibrated values	-0.20	3945
BSSkt Calibrated values with Torum model for Cl	-0.285 to 0.080	3867
BSSkt Calibrated values with Torum model for Cl with parameters calibrated	-1.0 to -0.57	4.3

4.4.3 Effects of Coefficient of Lift

BSSkt-Cl (Torum) model with lift coefficient varying with KC from Torum (1994) (Equation 4.2) predicted damage (Figure 4.5b) not similar to data ($p<0.003$) (Figure 4.5a). Torum's (1994) data and the derived relationship between lift and KC number proved beneficial and resulted in bias (RMSE) of -0.23 (1.67). Coefficient of lift varied between -0.285 and 0.080 (average of -0.105) and suggested that lift can be positive under lower KC numbers and negative under more cyclical wave conditions (higher KC number), but primarily negative (Table 4.3). Lift predominantly acts as a stabilizing force in LCS rather than a destabilizing force. This method and its findings have not been seen in the literature and represent a possible innovation. Stability and the resulting damage vary significantly with KC and lift conditions.

BSSkt-Cl model with a modified lift coefficient equation (Equation 4.25) predictions was similar to the data ($p= 0.153$). Bias (and correlation) was also considerably reduced (increased) to 1.67 (0.6) (Figure 4.5c and d). Lift coefficient varied between -1.0 to -0.57 (with an average of -0.78) and suggested that lift is predominantly a stabilizing force (-ive) rather than a destabilizing force (Table 4.3). The reduction coefficient changed considerably to 4.3 and suggested justification of the continuous damage model proposed by Van Rijn. Interestingly, the maximum predicted damage (6.54) is similar to measured damage (7.7). In contrast, the previous model based on Torum (1994) predicted damage >9. This suggests

an improvement with this approach with a variable Cl of ~-0.78 (i.e. dependent on KC). Further research is necessary to understand this component better.

Equation 4.25. Calibrated coefficient of lift from KC number.

$$C_L = 0.0039.K_C - 1.14 \sim -0.78$$

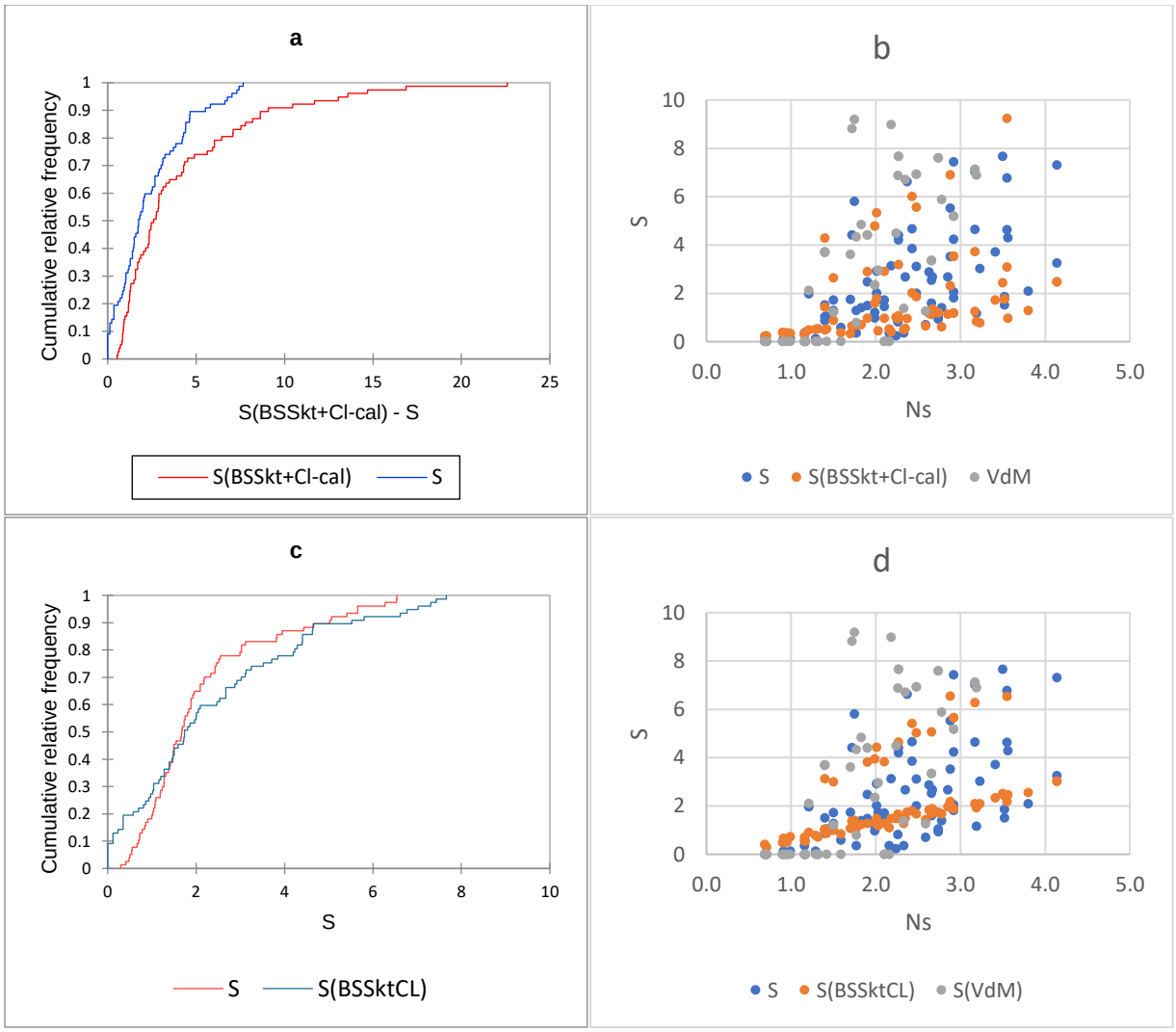

Figure 4.5 Cumulative damage for S-BSSkt with Coefficient of lift sub-model from Torum (1994) (a) and calibrated BSSkt and VdM predictions versus Ns (b). Cumulative damage for S-BSSkt with calibrated Coefficient of lift sub-model (c) and calibrated BSSkt and VdM predictions versus Ns (d).

4.4.4 Effects of blocking on VdM

Block effects for Re are significant and were informed by the Variance and Means analysis. VdM can predict similar damages for Re<40,000 (RMSE = 3.2), but not for Re>40,000 (Figure 4.6a and b). In several instances VdM either over predicted or predicted no damage (Figure 4.6c). It is noted that BSSkt with Torum parameters performed better with lower bais and RMSE than VdM model. Further development of the VdM model is required to cover a wider and higher range of Re that is possible in design conditions. Predicted damages are predominantly higher and suggest that that the model is likely to result in conservative results.

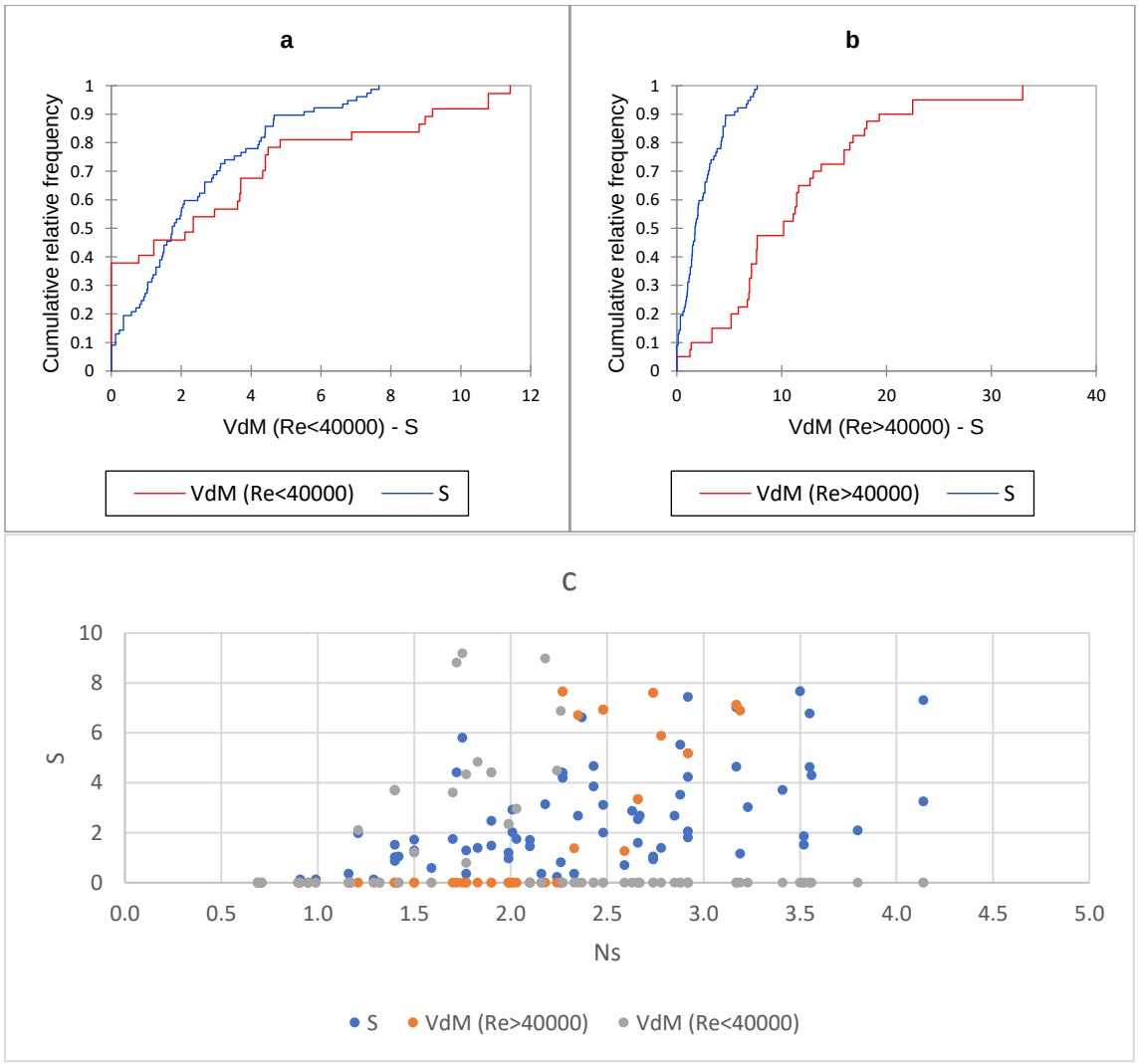

Figure 4.6 Cumulative damage for S-VdM for Re<40,000 (a) and Re>40,000 (b) and VdM predictions versus Ns (c).

4.5 Summary

Two analytical models were developed based on Morrison friction (MF) and Bed shear stress (BSS) for the armor unit at the seaward crest of LCS. The seaward crest unit is considered because of insight from laboratory studies that show that the forces are maximized (Losada et al., 2005 and Garcia et al., 2004). The combination of restoring moments from submerged weight and friction and disturbing moments from lift, drag and shear stress were considered. Inertial forces were neglected. The BSS was based on bed shear stresses explained by the Shield parameter (BSS) with an adjusted r factor to account for protrusion and increased mobility in waves and currents. The second class of models (MFkt and BSSkt) was developed that accounts for removing the wave energy transmitted past the crest of the structures. The performance of the MF and BSS models was explored by utilizing parameter values from the literature and the available flume damage data. Additionally, the Van der Meer and Daemen (1994) wave transmission estimates were used to explore the MFkt and BSSkt models with wave energy removal.

Initiation of damage is difficult to predict reliability with the models investigated. This is despite calibration and model development. MF, BSS and VdM are not able to predict damage reliability. Inferring when damage is initiated from "progressive damage" modeling is recommended.

BSSkt calibrated model was able to predict damage similar to the data, whereas VdM could not. Removal of wave energy transmitted over the crest is beneficial in the model development process. Additionally, the lift was determined to be a stabilizing factor and deserves further investigation. A lift coefficient model based on Torum's data produced better results. Further improvement was realized with calibration that suggested that lift is a stabilizing force with a -ive Coefficient of lift. The proposed model could predict damage at significant levels when transmitted wave energy is removed and when the lift is considered. Further research is needed into the lift coefficient.

Significant block effects were determined for VdM, wherein VdM can predict similar damages for Re<40,000, but not for Re>40,000. Further development of VdM is required.

The proposed initial BSS_{kt} model for damage, S is as follows:

Equation 4.26. Stability number for BSS_{kt} model with transmitted wave energy removed.

$$S = \left[\frac{1 - \frac{N_s}{2.\kappa.\sqrt{\left(1 - {K_t}^2\right)}}\left(C_L.\left(1 + Sin(\alpha)\right)^2\right)}{\left(1 + Sin(\alpha)\right).r.\left(\frac{Sin(\phi + \alpha)}{Sin(\phi)}\right)}\right]^{3/2} .\frac{13.N_w.T_m.(g.\Delta)^{\frac{1}{2}}}{D^{\frac{1}{2}}}$$

Several insights can be inferred from the proposed model. Namely:

1. Damage is directly proportional to Nw and Tm. In other words, longer durations and periods are more damaging.
2. Damage is exponentially proportional to Ns, providing the lift coefficient is negative. This latter point deserves exploration.
3. Damage is inversely proportional to the square of Kt and the square root of D_{50}. In other words, deeper LCS and larger stones are more stable

5 EXPERIMENT AND MODEL DEVELOPMENT

5.1 Method

5.1.1 Approach

Physical experiments were designed to focus on: i) maximize (minimize) collection of variables that had more (less) effect on the dependent variable and ii) enhanced replication, randomization and blocking. Treatments and blocks of importance were identified from variance and multiple means analysis of existing and proposed model variables. Likewise, less important variables were also identified. Replication and randomization in the experiments were balanced by ensuring that: i) not less than 30% of the independent variable samples were replicated for more important variables, ii) that the range of treatments and blocks of importance were sampled near uniformly over a wider range.

The range of treatments and blocks of importance was informed from the practical application of the dependent variable (damage, S) as S<10 and the multiple means analysis to identify the range for blocks of importance. The range for the independent variables on the dependent variables was estimated to minimize clustering and check randomization. This was done by i) wave transformation models to estimate conditions for important blocks, and ii) projecting damages from the calibrated damage model. Experimental conditions were then defined.

5.1.2 Material: density, porosity and gradation

The specific density of the crushed quarry stones used to construct the LCS test was determined. Four samples of each stone class were tested for specific density (Table 8.6 and Figure 8.1). Samples of masses between 1.20 and 2.50 kg were weighed in air (M_a) and in water (M_w) and used to determine the specific density (Equation 5.1). A median specific density of 2422 kg/m^3 was determined.

Equation 5.1. Specific density of armor stones from weight in air and water

$$\rho_a = \frac{M_a}{M_a - M_w}, \text{where } \Delta = \rho_a - 1$$

Porosity (P) of the packed stones was used to determine the damage in the formula to estimate the damage and was therefore determined for each class of stones. Porosity is a function of sphericity and angularity, and the stone could, in general, be described as having medium sphericity and angular. Porosity was estimated from six samples for each of the two classes of stones by determining stones and water's weight to fill the pores of a known volume of stones that were hand tapered in a cylinder. Stone A (B) porosity was determined to be 0.431 (0.472) (Figure 8.2 and Table 8.8). A test of similarity of the central tendency of both samples' porosity at the 95% confidence reveals that there is sufficient evidence indicating that the porosity of the two classes of stones was equal. Therefore, it is implausible that the mean of the porosity of the two samples is not equal. The median of both stone classes of 0.464 was used.

Equation 5.2. The porosity of armor stones

$$P = \frac{M_w}{V_a}$$

Three sizes or classes of armor stones were available: i) yellow, ii) green, and iii) red. Two sizes were selected, with one in each half (300mm) of the flume's width. Gradation surveys (see Figure 8.3 and Table 8.9) on each class of stones were conducted to verify that the sampling was representative. Dn50 (M50) for the yellow, green and red stone classes were determined to be 13, 18 and 23 mm (5, 15 and 29 grams) with D_{85}:D_{15} of 1.2 to 1.6 respectively and could be described as well sorted. Green and Red stones were eventually used to build the seaward, crest and front slope, with the largest stones in each range used to build the toes.

5.1.3 Test Section and damage measurement

A pair of smaller (18mm) and larger (29mm) stone sizes test sections were built adjoining in the flume, similar to Garcia and Kobayashi (2015). The geometric requirement for slope and homogenous section were hand-packed, and the slopes checked with a template of the various hc/h required. See Figure 5.1. A data extraction window with a buffer of 1 stone diameter was used to minimize the effects of limited or differential interlocking from both the flume glass wall and adjoining stone sizes. This approach is consistent with other physical model studies (Ranasinghe et al., 2009). Edge or wall effects were believed to be minimized.

Damage was measured by firstly determining the average erosion cross-section area and then equating to the damage number S. The traditional method of applying the Broderick formula was considered but not used. This would have entailed counting displaced stones and applying the modified formulae (Equation 2.11), where A_e is the area of erosion, N is the number of stones moved, n is porosity, and Y is the counting width zone. Photographs were taken after each test interval and subjected to digital terrain modeling using Pix4D. The errors in erosion measurements were estimated to be less than 1mm (Figure 5.2). The greater accuracy and applicability of E_{D50} (Equation 2.13) was contemplated to be more useful to future studies and was preferentially used. The method entailed:

1. Defining location and height of eight control points
2. Creation of pre-test surface
    a. Scanning of test sections with eight control points
    b. Processing of scan to define 3-dimensional surface using Pix-4d
3. Running of test waves
    a. Estimating time of run from Tm and running waves

   b. Draining tank below test sections with controls in view above water
4. Creation of post-test surface
   a. Scanning of test sections with eight control points
   b. Processing of scan to define 3-dimensional surface
5. Determining erosion of surface between tests
   a. Extracting surface for of the two stone sizes by removing D_{n50} stone size from side walls of the flume and adjoining stone size cross-section (see sample rectangle in Figure 5.1)
   b. Determine V_e by subtracting post-test surface from pre-test surface, using ArcGis tool, to find erosion surface.
   c. Determine $A_{\text{erosion c-x average}}$ by V_e divide by $W_{c\text{-}x}$ and by extension E_{D50} and S.

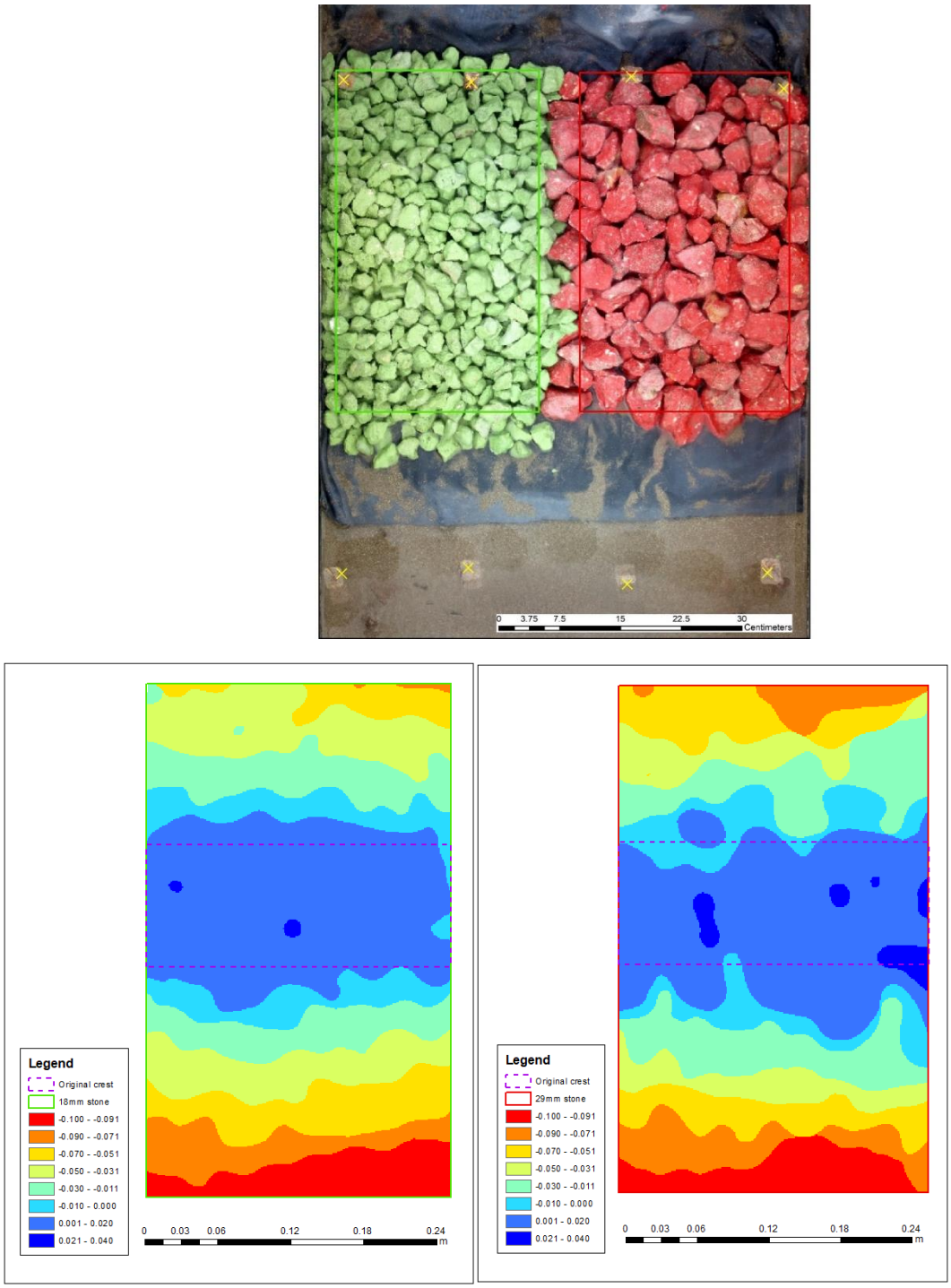

Figure 5.1. Example of flume test section for 18mm (green) and 29mm (red) section (top) showing photo-controls (yellow X). Note sample areas (green and red rectangle used to extract data. Digital terrain model before (bottom left) and after (bottom right) test, showing the approximate location of the crest (dashed lines) with seaward direction to the bottom of the page.

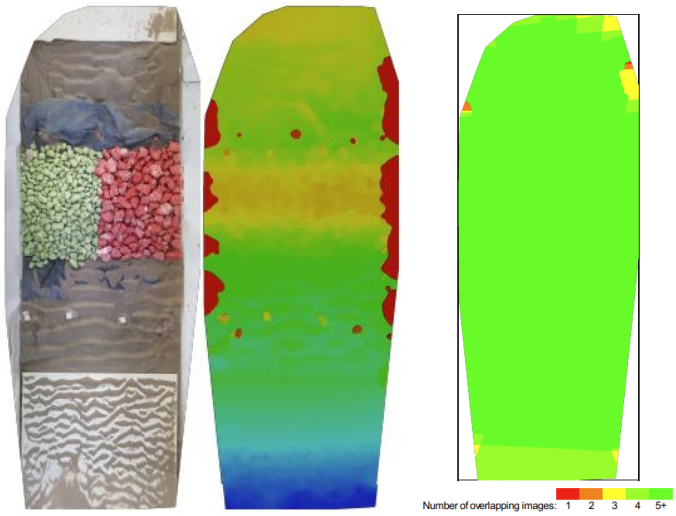

Geolocation Details

Ground Control Points

GCP Name	Accuracy XY/Z [m]	Error X [m]	Error Y [m]	Error Z [m]	Projection Error [pixel]	Verified/Marked
1 (3D)	0.020/ 0.020	-0.002	-0.000	0.001	1.516	10 / 10
2 (3D)	0.020/ 0.020	0.001	-0.000	-0.001	1.124	11 / 11
3 (3D)	0.020/ 0.020	0.001	-0.000	-0.000	0.788	9 / 9
5 (3D)	0.020/ 0.020	0.000	0.001	0.000	1.305	8 / 8
6 (3D)	0.020/ 0.020	0.000	-0.000	-0.001	1.498	11 / 11
7 (3D)	0.020/ 0.020	0.000	-0.002	0.001	1.905	9 / 9
8 (3D)	0.020/ 0.020	-0.001	0.001	0.000	1.738	6 / 6
Mean [m]		0.000000	0.000000	-0.000000		
Sigma [m]		0.000922	0.000836	0.000935		
RMS Error [m]		0.000922	0.000836	0.000935		

Localisation accuracy per GCP and mean errors in the three coordinate directions. The last column counts the number of calibrated images where the GCP has been automatically verified vs. manually marked.

Figure 5.2. Sample orthomosaic, preliminary Digital terrain model and overlapping images (top) and error report for GCP (bottom.)

5.1.4 Reynolds Criterion

A Re criterion relating to homogenous and near homogenous LCS of not less than 10,000 was used throughout the experiments. The criterion was used to guide the minimum wave sizes for the stone classes (Table 5.1). All the experiments were determined to be non-viscous and scalable for wave heights greater than 0.03 meters.

Table 5.1. Estimated Reynold's Number (Kinematic viscosity, v @ 25C = 9.0 x 10^{-7}) for wave heights and yellow, green and red stone sizes. Blue shaded areas are acceptable with Re >10,000.

	Yellow	Green	Red
Hs (m)	D_{50} = 13 mm	D_{50} = 18 mm	D_{50} = 29 mm
0.01	4585	6351	10092
0.02	6484	8981	14273
0.03	7941	11000	17480
0.04	9169	12701	20185
0.05	10251	14201	22567
0.06	11230	15556	24721
0.07	12130	16802	26702
0.08	12967	17962	28545
0.09	13754	19052	30277
0.1	14498	20083	31915
0.11	15205	21063	33472
0.12	15882	21999	34961

5.1.5 Wave spectrum, gauge and machine

The Brettschneider spectrum generator was used to generate three different deep-water waves throughout the experiments to duplicate the combined effects of fresh seas and fully developed seas. An array of two resistance-type wave gauges were used to measure waves at the deep water and the structures' toe. Waves were recorded for 30 minutes after the start of each series and analyzed with zero-crossing analysis (ZCA) spreadsheets.

Wave measurements in the wave flume were done with an Ocean Sensors System Teflon coated staff measuring staff or probes that measure the water's conductivity between the end and water line. Gauge linear correction factors were determined through a calibration process of incrementally lifting and sinking the gauge over known distances and comparing the readings over five intervals. The correction factors were determined and used throughout the experiments.

A piston-type generator controlled by a spectrum generator was used to generate depth-limited and shallow water wave conditions. Target deep-water and structure toe wave heights and periods were pre-

determined, and wave time series were measured and subjected to time series analysis. The water level time series were measured (over a 136 seconds duration with measurements at 0.0333-second intervals ~4,080 measurements) and analyzed to define the measured waves and to ensure repeatability of the predictable wave heights at both the deep-water and structure toe depth locations. The objective was to ensure three distinctly different wave series in deep and shallow-water and depth-limited or shallow water conditions over the series of tests.

5.1.6 Flume and Cross section geometry

An Omey ® flume 9.0 meters long x 0.6 meters wide and 0.6 meters deep was used for the experiments (Figure 5.3). There was a wave attenuator at the end of the flume to reduce the reflected waves. A series of tests with a cross-section crest width of 0.10 meter (~4 or more stone widths), side-slopes of 1:1.5 and 1:2.0, constant water depth (h) of 0.10 meter and h_c/h from 1.2 to 0.5 were examined. Gaps in the filtered and pooled damage and stability data were filled with the physical model data collection program.

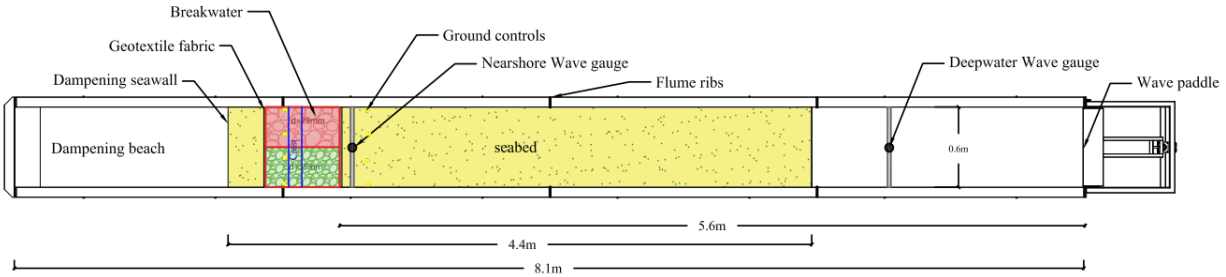

Wave Flume Plan Layout

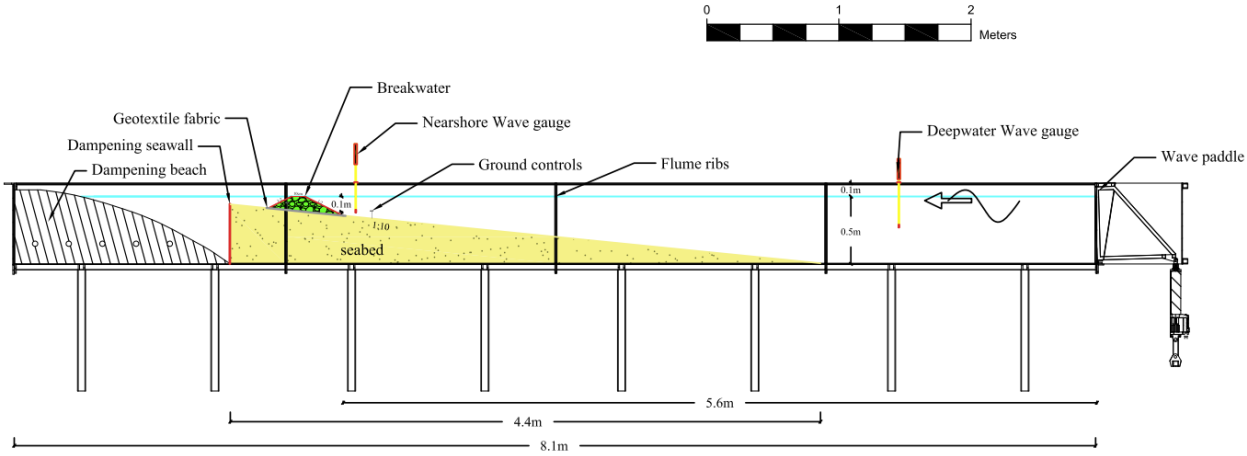

Wave Flume Cross-Section

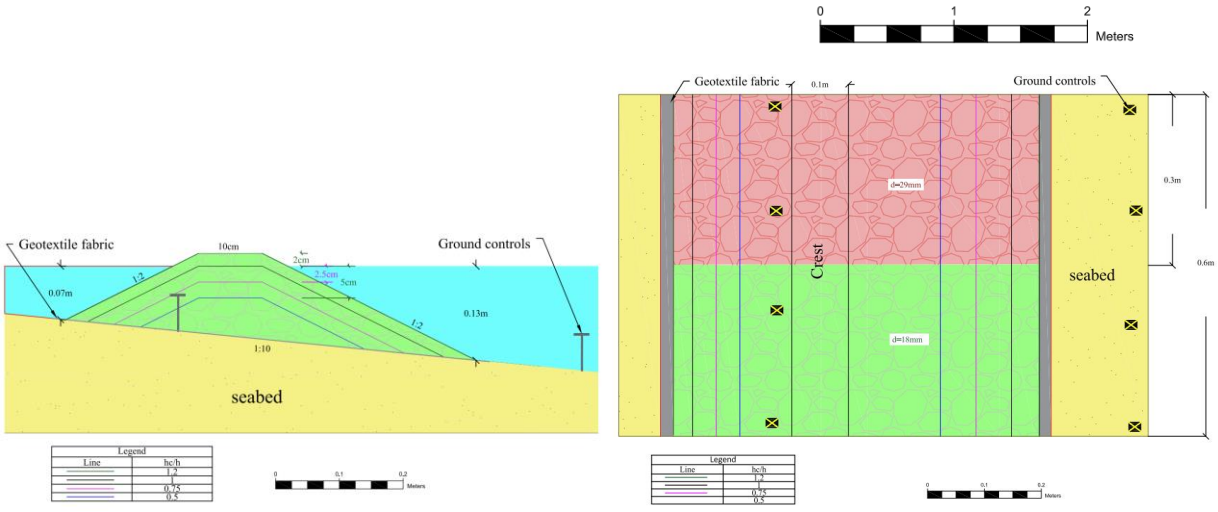

Figure 5.3. Plan and profile of flume set up (top) and cross-section and plan of test section (bottom)

5.2 Experimental Design

Replication, randomization for most variables, and blocking were achieved in the experimental data collection program's design. Expected values were derived using target wave conditions, wave transformation analysis and BSSkt and VdM (Equation 5.3) models to achieve dependent variable S<8. Replication with varying Cot α (@100%), randomization and blocking (Re and KC) were achieved in the design of the program. The caveat is the Re number that will not exceed 40,000. This was because of the limitations of the wave flume. Flume stone size required to achieve measurable damage and desirable Ns and KC variations were determined to be 18 and 29mm. The data collection plan is summarized in Table 5.2 and shown in the appendices in Table 8.5.

Equation 5.3. Stability of LCS from Van der Meer and Daemen (1994)

$$S = 10.e^{ln\left(\frac{h_c}{h}\right)+0.14.Ns*} - 21$$

Table 5.2. Data collection program expected dependent and independent variable frequencies for D_{50} 13mm (C-X 1) and D_{50} 18mm (C-X 2).

		D50 (mm)	18	D50 (mm)	29
Variable	Categories	Counts	Frequencies %	Counts	Frequencies %
Kt	High Kt>0.45	40	65%	40	65%
	Low Kt<0.45	22	35%	22	35%
Ns	Ns<4	62	100%	62	100%
	NS>4	0	0%	0	0%
Hs	Hs<0.1	62	100%	62	100%
	H=0.1	0	0%	0	0%
	Hs>0.1	0	0%	0	0%
cot a	Cot a = 1.5	31	100%	31	100%
Nw	Nw<=1500	18	29%	18	29%
	1500<Nw<7500	18	29%	18	29%
	Nw>=7500	26	42%	26	42%
Tm	Tm<2.083	22	35%	22	35%
	Tm>2.083	40	65%	40	65%
Re	10,000<Re<40,000	62	100%	62	100%
	Re>40000	0	0%	0	0%
KC	Kc<70	0	0%	22	35%
	70<Kc<110	22	35%	22	35%
	Kc>110	40	65%	18	29%
S	S<2	40	65%	56	90%
	2<S<4	20	32%	6	10%
	S>4	2	3%	0	0%

5.3 Calibration of Waves

5.3.1 Water levels

Both wave gauges were calibrated to determine the central tendency and dispersion of the readings versus movements. A median of 0.101 and dispersion of 0.007 (~+/-7%) was determined for the pooled sample that was used throughout the experiments for the wave gauges (Table 8.10and Figure 5.4).

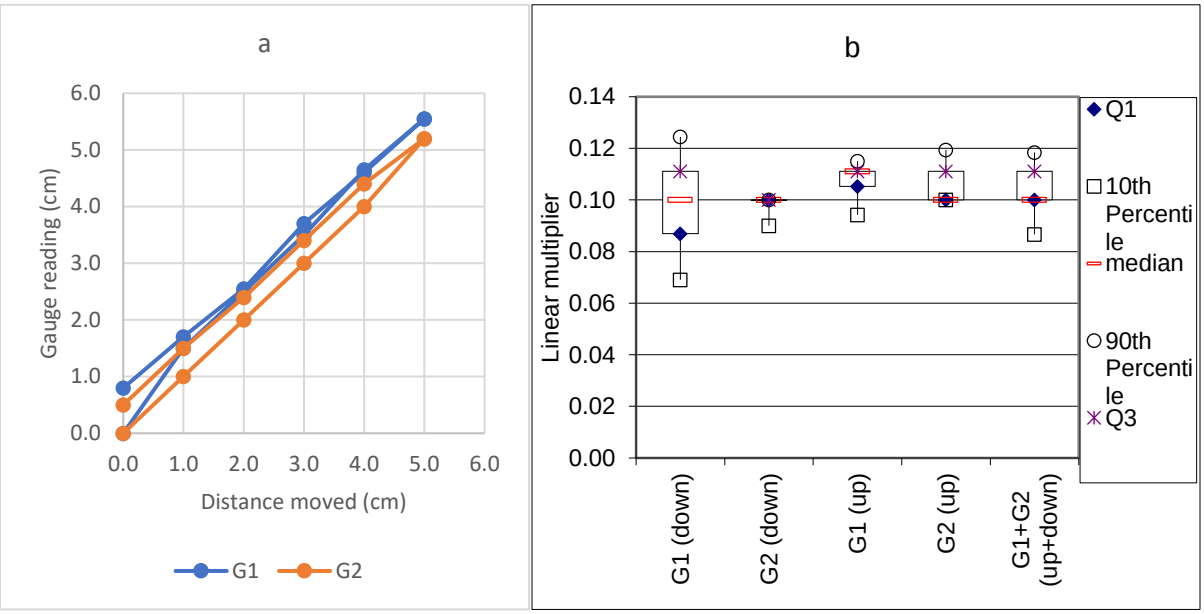

Figure 5.4. Linear wave gauges 1 and 2 readings (a) and conversion factors for gauges up and down and pooled sample (b)

5.3.2 Time-domain analysis

5.3.2.1 Deep-water conditions

Three unique deep-water wave conditions were explored (Table 5.3) herein. Deep-water waves measured at G1 ((H_{1o}, H_{2o} and H_{3o}) for the three-wave series investigated (W1, W2 and W3) were determined not to be similar at the 5% level and satisfied transitional or shallow water conditions (h/Lo>0.5) (Table 5.4). The wave heights ranged from 0.043 to 0.071 meters (Figure 5.5 and Figure 5.6). These waves were used throughout the experiments.

Table 5.3. Gauge wave heights and periods for input wave conditions W1, W2, and W3 and peak period (Tp) used in experiments and measured deep water (Hso and Tpo) and nearshore wave heights and periods (Hsi and Tpi) at the toe of the structure.

Wave	Requested		Measured			
	Hso (m)	Tpo (sec)	Hso (m)	Tpo (sec)	His (m)	Tpi (sec)
W1	0.131	1.7	0.071	1.67	0.074	1.63
W2	0.075	2.5	0.044	2.56	0.052	2.17
W3	0.068	3.5	0.043	3.57	0.055	3.60

Table 5.4. Wave analysis of deep and shallow-water waves used in flume model

Input	W1	W2	W3
Deep-water depth, ho (m)	0.5	0.5	0.5
Hso (m)	0.071	0.044	0.043
Tmo (sec)	1.39	2.13	2.98
Tpo (sec)	1.67	2.56	3.57
Slope, m	10%	10%	10%
Shallow-water depth, h (m)	0.1	0.1	0.1
Hs (m)			
Tm (sec)	2.88	5.11	14.05
Tp (sec)	0.17	0.10	0.04
Deep-water analysis	T	T	SW
Lo (m)	0.0246	0.0086	0.0031
h/L			
Wave type	0.074	0.052	0.055
sop	1.36	1.81	3.00
Shallow-water analysis	1.63	2.17	3.60
Lm (m)	1.30	1.75	2.95
Lp (m)	1.56	2.10	3.54
C (m/s)	0.95	0.97	0.98
h/L	0.08	0.06	0.03
Breaking criteria, Hb/h	0.79	0.79	0.79
Hb (m)	0.06	0.04	0.04
ξbp	0.47	0.69	0.91
Breaking conditions (h/L<0.05)	Breaking	Breaking	Breaking
Breaker type	plunging	plunging	plunging
Wave type (DW-deep-water, T-Transitional, SW-Shallow-water)	T	T	SW

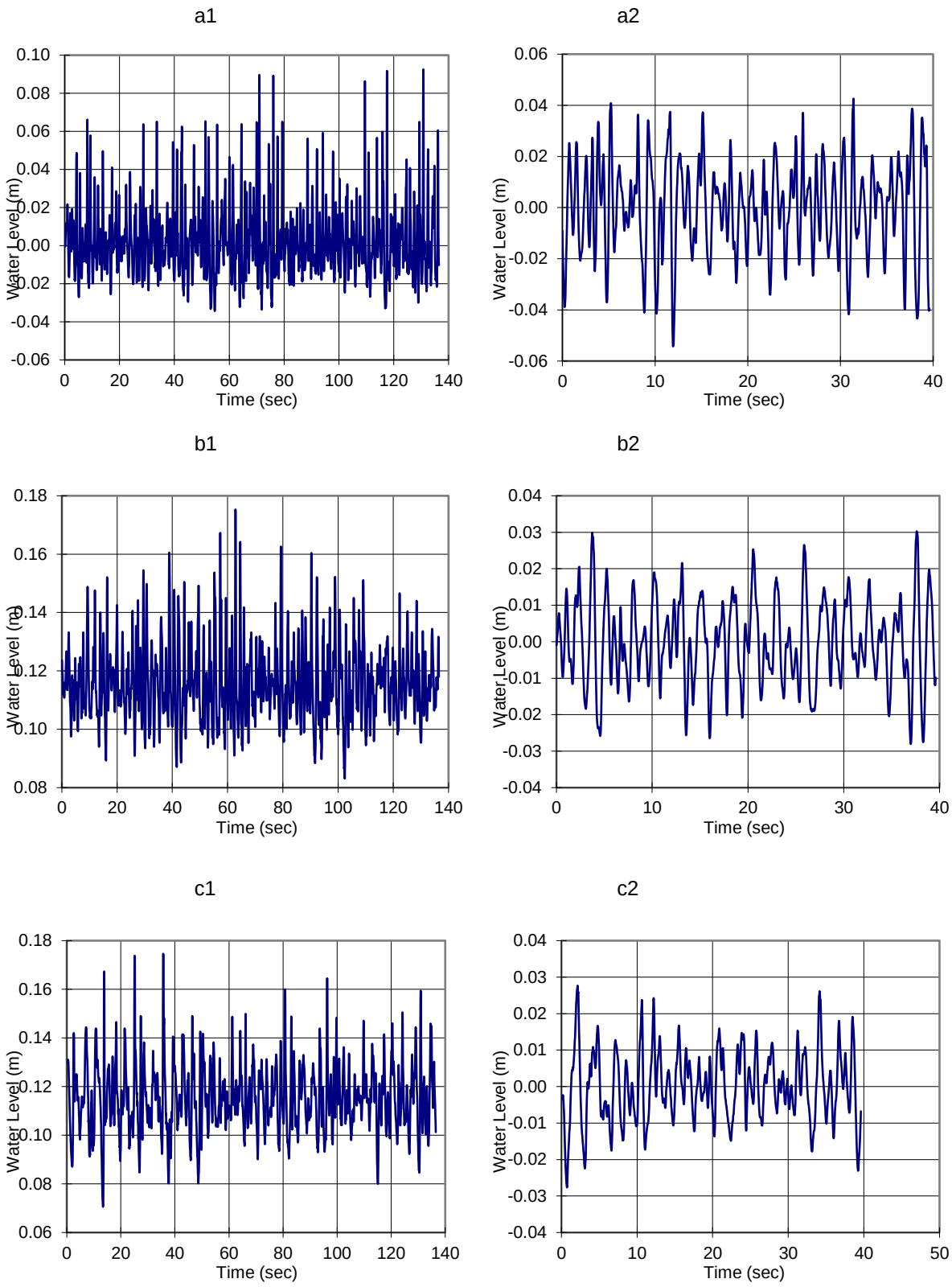

Figure 5.5 Deep-water wave water surface (eta) for W1, W2 and W3 (a, b and c), respectively

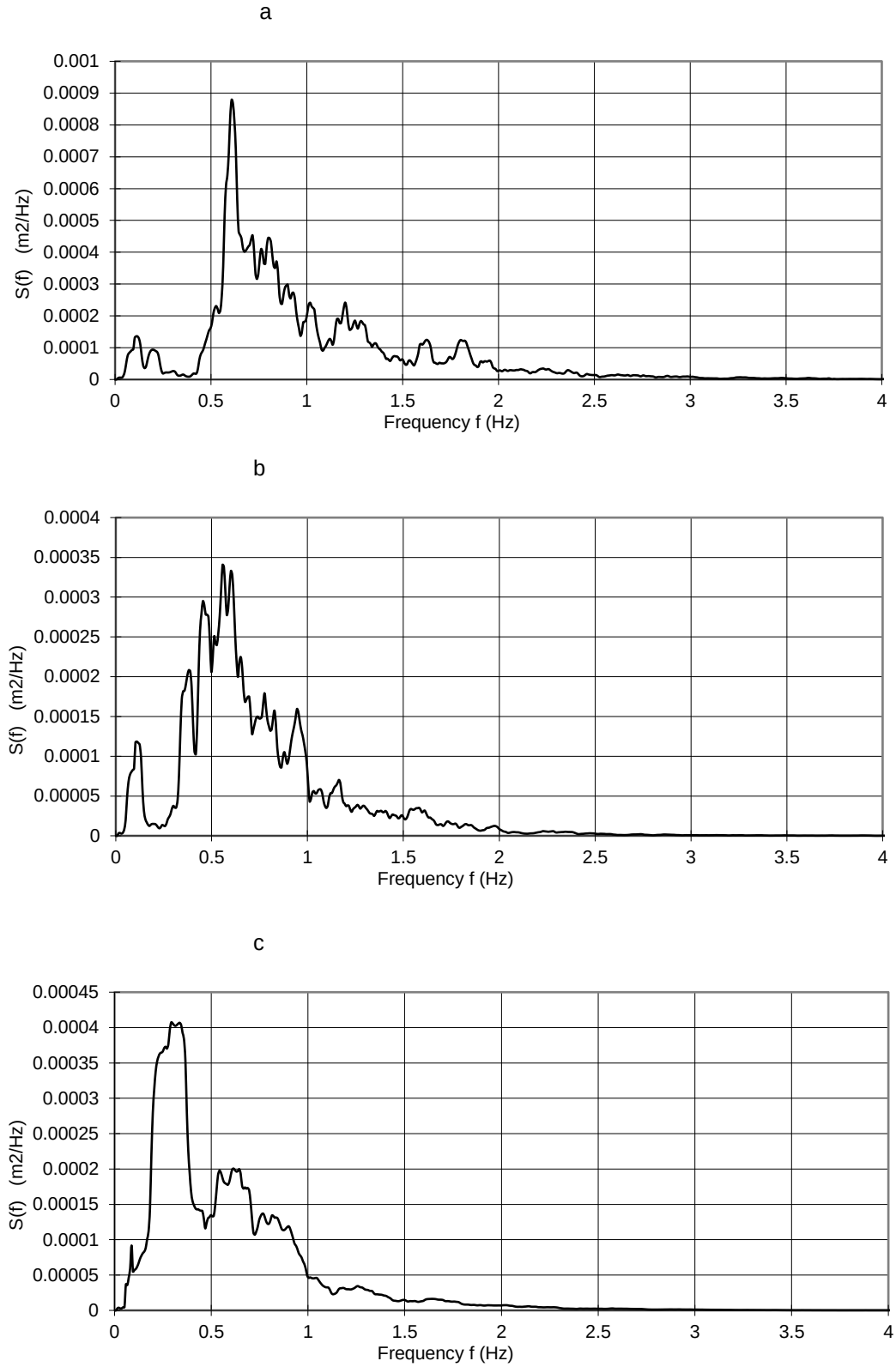

Figure 5.6 Deep-water wave spectrums for W1, W2 and W3 (a, b and c), respectively

5.3.2.2 Depth-limited and shallow water conditions

Three unique nearshore depth-limited wave conditions were explored herein. Nearshore waves (measured at G2) were determined to be different at the 5% level and depth limited. Transitional and shallow water depth limited wave conditions with h/L ratios of 0.16 were determined for all three nearshore waves, resulting from W1, W2 and W3 conditions (Table 5.4). H_s exceeded the breaking criterion (H_s>Hb), with wave heights of 0.09, 0.0616 and 0.052 meters in 0.1 meters of water depth, respectively (Figure 5.7 and Figure 5.8). The nearshore waves were determined to be depth-limited waves.

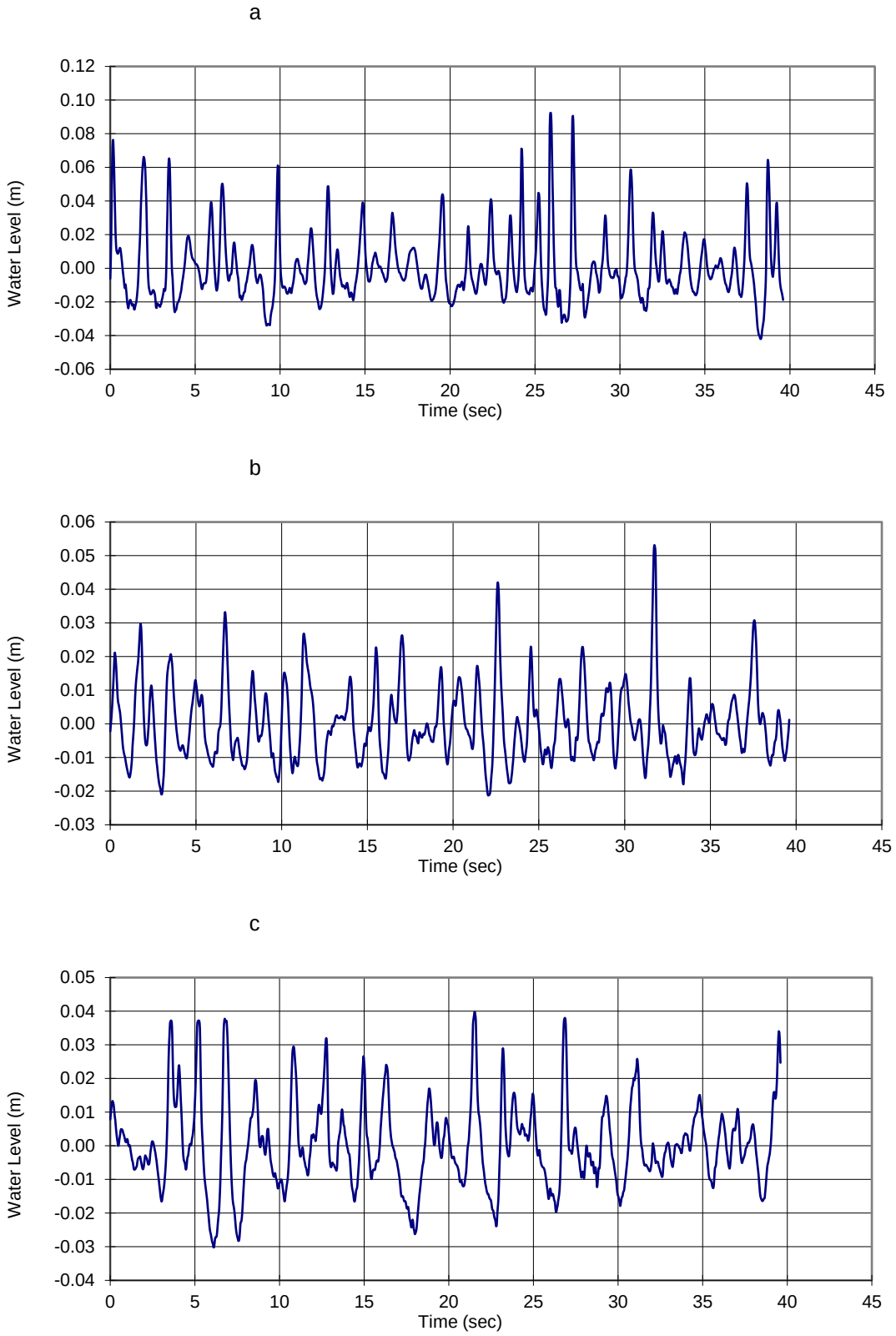

Figure 5.7 Shallow-water wave water surface (eta) for W1, W2 and W3 (a, b and c), respectively

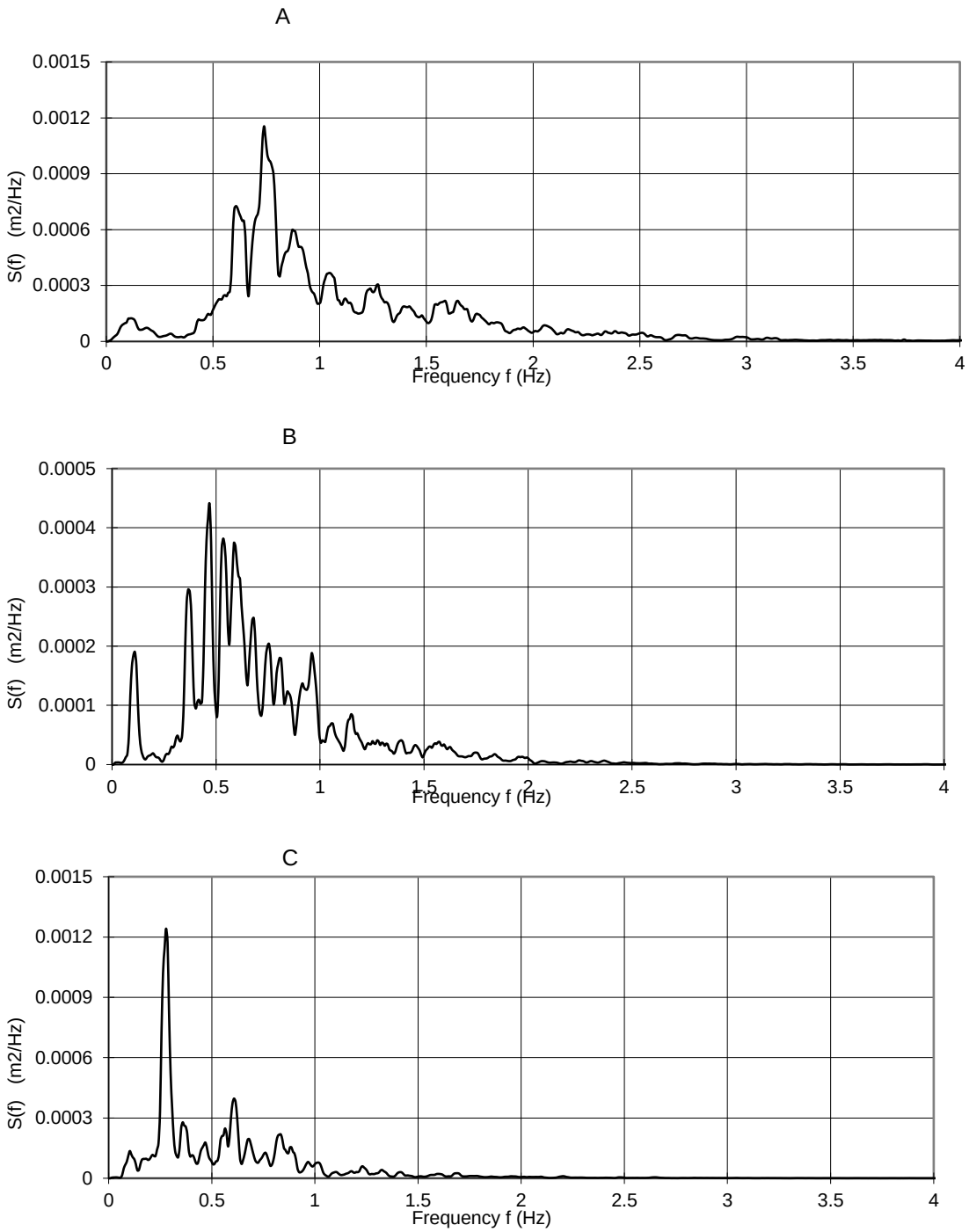

Figure 5.8. Shallow-water wave spectrums for W1, W2 and W3 (a, b and c) respectively

5.4 Analysis and Results

5.4.1 Erosion Patterns

Erosion and deposition generally occurred on the LCS crest and seaward slope and were maximized for higher hc/h and Nw and smaller Dn50. Scale model cross-sections and crests were generally built to the intended elevations and extent to within 1 cm of the design surfaces. Initial structure surface, erosion patterns and estimated damage are shown in 8.5 and summarized as follows, with a sample of the plots shown in Table 5.5:

a) Erosion is initiated at the seaward-crest intersect and progresses both along the crest and seaward slope. Erosion depths of 2 to 3 cm were noted in this area for the smaller stone size model at the seaward-crest intersect and near-zero towards the rear.
b) Erosion was remarkedly focused on the crest throughout the experiments. Smaller (larger) stone sizes having erosion depths of 8 to 9 (2 to 3) cm after 25,000 waves. This translated to damages of 37 (and 6). This highlights the need to focus on the stability of units at or near the seaward crest. Erosion depths declined to near zero from the crest-seaward slope intersect to the structures' toe for both stone sizes. This underlines the need to focus on armor units at the crest-seaward slope intersect and seaward slope and the importance of down-rushing conditions.
c) Deposition occurs on both the seaward and leeward sides and primarily at the toe of the structure with deposition depth of 2 to 3 (1 to 2) cm. Again, this points to a need to consider both up rush and down rush conditions in the model development, focusing on the down rush that erodes the seaward slope.
d) Damage progresses with an increasing number of waves. Erosion depths for the smaller (larger) stone size of 1.5 (1) cm at 1,500 waves increased to 8 to 9 (2 to 3) cm after 24,000 waves. This underlines the importance of considering damage progression in LCS.
e) Increased submergence (hc/h = 0.75) decreased erosion for the smaller (and larger) stone models to 3 (less than 1) cm. Erosion was again focused on the seaward slope and crest intersect and with reduced measured damage of 7 (and 1) from the comparable emergent scenario.

Overall, a pattern of damage focused on the seaward slope-crest intersect, damage progress with the number of waves and reduced damaged with submergence was determined. These findings were considered in the model development process.

Table 5.5. Surface and erosion plots with damage measurements for Hs= 12 and 7.5 cm, Tp 1.7 and 2.5 seconds, Cot α = 1.5 and 2.0 and hc/h 1.2 and 0.75.

Test series family: Series 3 Hs = 120mm, Tp =1.7s , hc/h = 1.2, Cotα = 1.5		
Nw	Green stones Dn50 = 18mm	Red stones Dn50 = 29mm
0	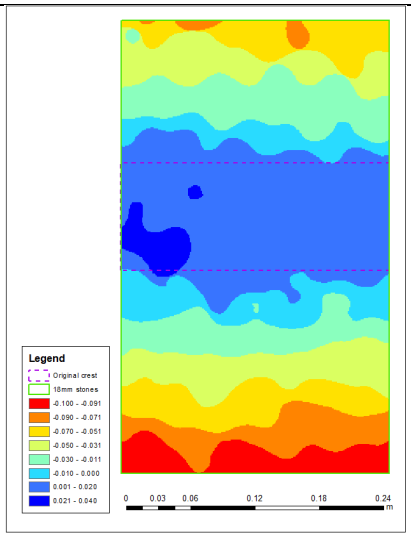	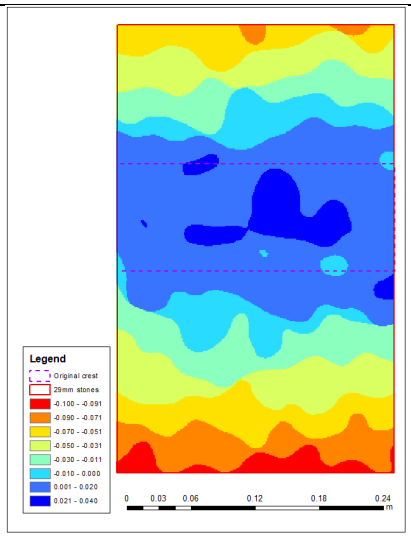
1500	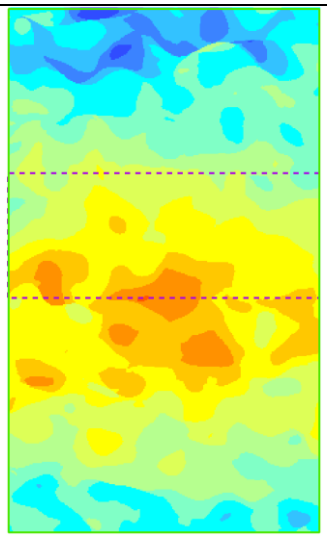 S = 16.92	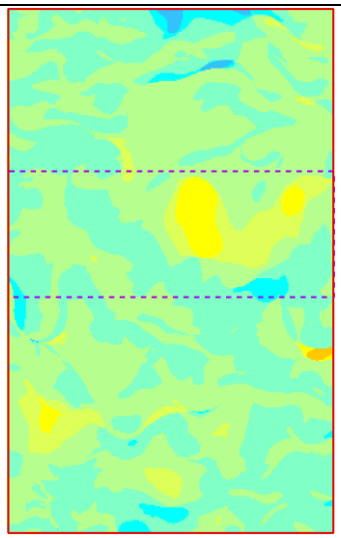 S = 2.10

24000	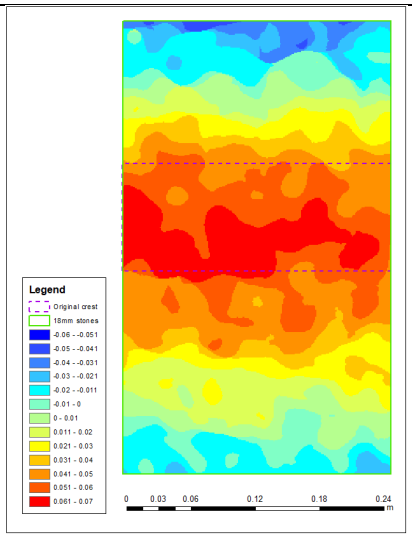 S = 37.72	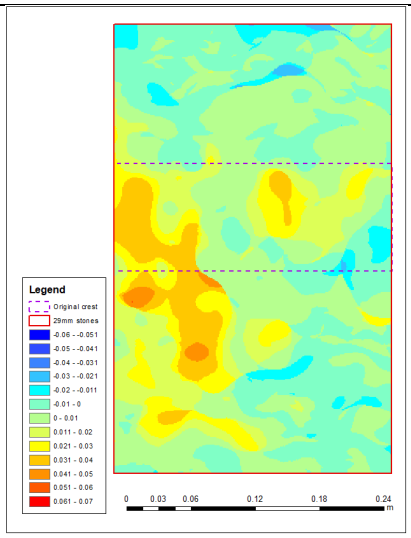 S = 6.48
Test series family: Series 16 Hs = 75mm, Tp =2.5s , hc/h = 0.75, Cotα = 2		
Nw	Green stones Dn50 = 18mm	Red stones Dn50 = 29mm
0	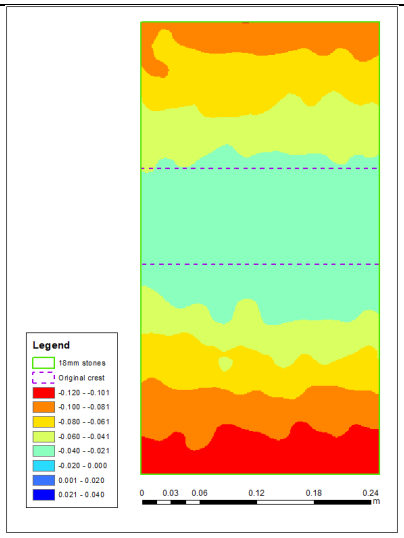	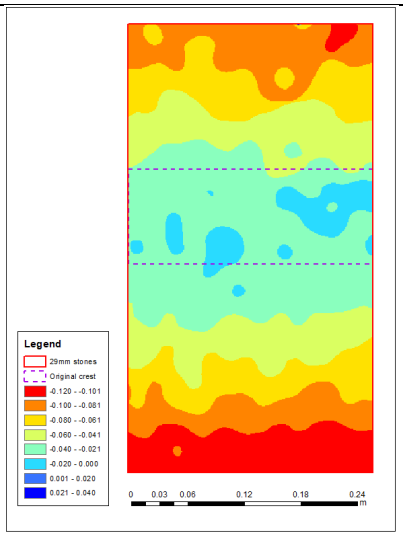

24000	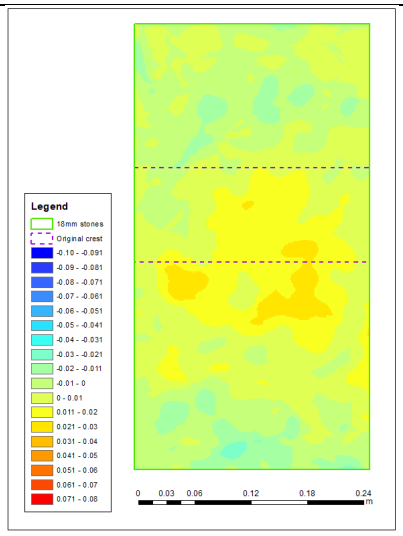 S = 7.28	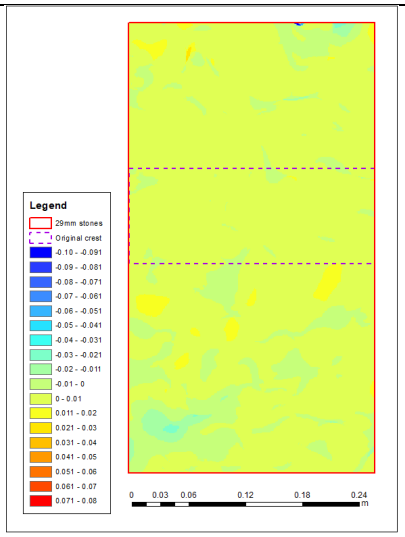 S = 1.15

5.4.2 Effects

5.4.2.1 Stability number

Damage generally increased with stability number across all hc/h considered (Figure 5.9). Damage was also more significant for increased emergence and suggests the importance of considering this variable in model development.

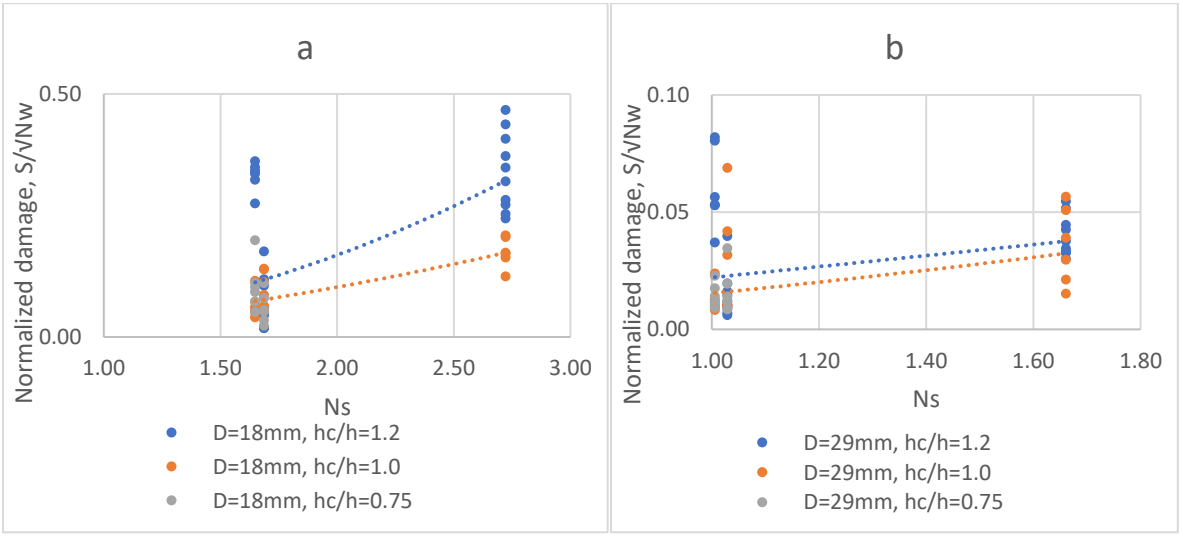

Figure 5.9. Effects of stability number on normalized damage for D=18mm(a) and 29mm(b)

5.4.2.2 *Wave characteristics*

Damage was minimized for the steepness of ~3.5 for both stone sizes (Figure 5.10a) Kramer et al., (2002) made a similar observation. Damage also increased with the number of waves for both stone sizes at significant levels and underlines the importance of considering damage progression (Figure 5.10b).

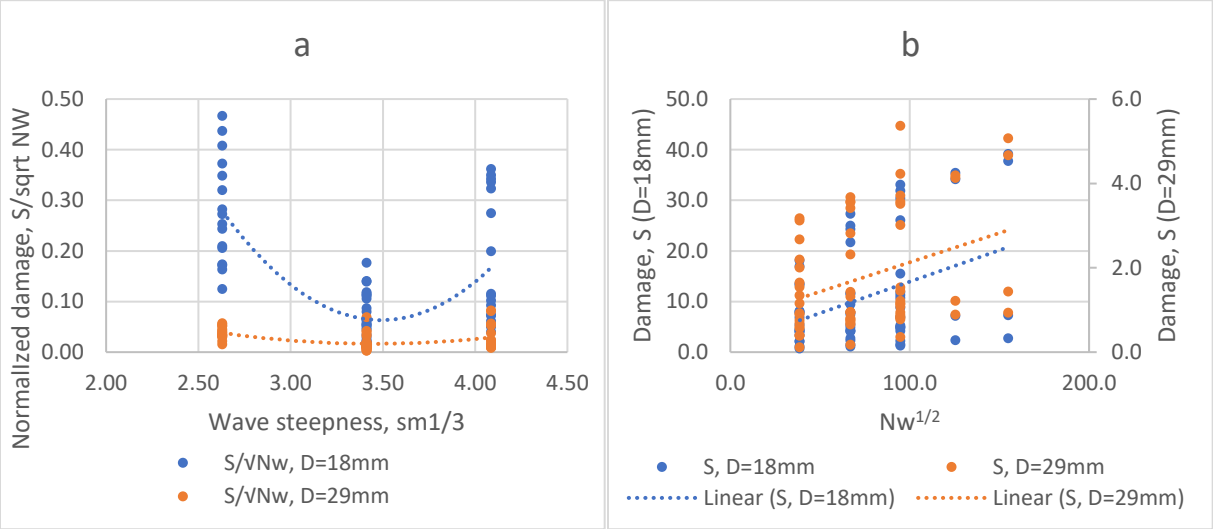

Figure 5.10 Effects of wave steepness (a) and Duration(b)

5.4.2.3 *Geometry*

Damage for Cot α = 1.5 and 2.0 was similar at the 5% level for both stone sizes (Figure 5.11a and b). While the data suggests increased stability for Cot α = 2.0, these are not at significant levels. The determination of similarity at the 5% level allows for an estimate of data error for each stone size of RMSE = 3.2 (1.5) for Dn50=18mm (29mm). Analysis of the bias in differential damages suggests that the differences are normally distributed at significant levels with a mean of 0.0 and inter-quantile range of 4.1 (1.05) for Dn=19 (29) mm (Figure 5.11c and d). The performance of the model can be compared to this error in data.

5.4.2.4 *Wall effects and stone size intersections*

Erosion (and, by extension, damage) was not perturbed in the areas adjoining at either the walls or intersections of the two stone sizes. Inspection of the erosion plots (see Appendices) suggested three potentially anomalous series from the 18-test series that were classified and assessed as follows:

1. Wall effects anomaly:
    a. Series 15, Hs = 120mm, Tp =1.7s , hc/h = 1, Cotα = 2 Dn50 = 18mm with damage of 15.48, possible perturbation (localized damage ~10) is greater than data error range, but less than estimated average damage for series.
2. Stone size intersection anomaly:
    a. Series 1, Hs = 68mm, Tp =3.5s , hc/h = 1.2, Cotα = 1.5 Dn50 = 29mm with damage of 4.49, possible perturbation (localized damage ~0.4) is less than data error range, but less than estimated average damage for series.
    b. Series 10, Hs = 68mm, Tp =3.5s , hc/h = 1.2, Cotα = 2 Dn50 = 29mm with damage of 4.27, possible perturbation (localized damage ~2) is greater than data error range, but less than estimated average damage for series.

Localized wall and stone size intersection effects possibly occurred in less than 20% of the series but unlikely to have affected the average damage estimates.

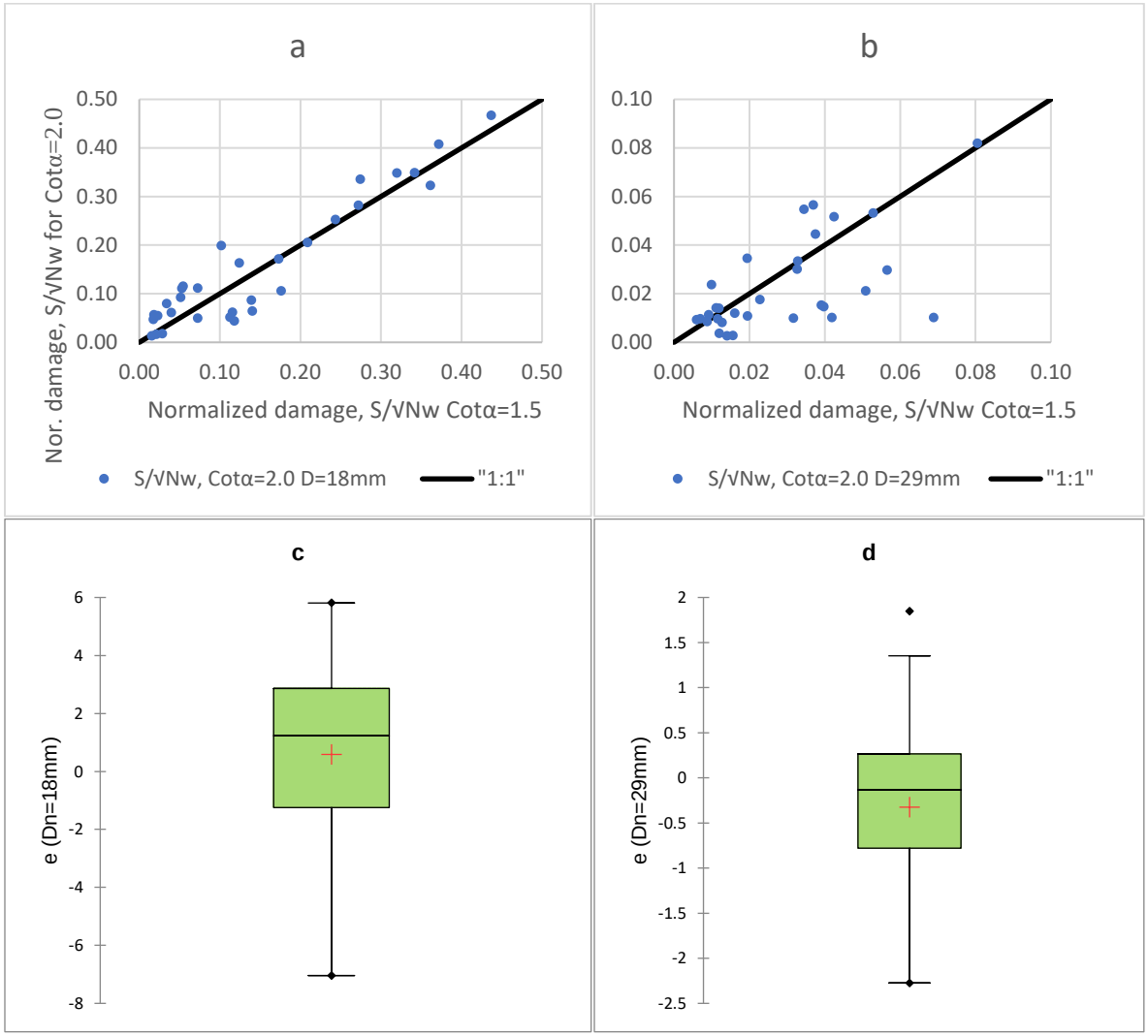

Figure 5.11. Effects of structure slope for D=18mm (a) and D=29mm (b) and error analysis $S_{cot\alpha = 2.0}$ - $S_{cot\alpha = 1.5}$ for Dn=18mm (c) and 29mm (d)

5.5 Model Development: Testing, improvements and validation

5.5.1 Testing and recalibration

Both BSSkt and VdM with previously calibrated parameters failed to predict damage at significant levels. A considerably higher predicted damage was noted. Further calibration to minimize errors (with r=32,044) improved the prediction for the larger stone sizes to provide predictions similar to the data at significant levels (p=0.131). A general trend of under-predicted damage of the smaller stone sizes by a factor of ~½ was observed and comparable damage for the larger stone sizes (Figure 5.12 c and d). BSSkt model could predict damage at significant levels for one of the two test stone sizes (Figure 5.12 e and f). Further investigations were carried out to see if the model's performance would improve using the VdM data for calibration and data collected herein for validation. The r (shear stress reduction parameter) increased, and higher Re conditions were present (Table 5.6). It was determined that the model could not predict damage to similar levels at significant levels and consistently over-predicted damages. It was concluded that the form of the proposed model needed improvement to capture the underlining processes for a range of stone sizes.

Table 5.6. Model parameters (Cl and r) and variables (Kc and Re) for calibrated and recalibrated BSSkt model on ODU data (top two rows) and VdM data (bottom two rows).

		Model parameters			
		Cl	r	Kc	Re
Calibration on ODU data	Minimum	-0.96	32,048	46	12767
	Maximum	-0.48		168	26892
Calibration on VdM data	Minimum	-0.23	169,000	66	33220
	Maximum	-0.02	169,000	128	56024

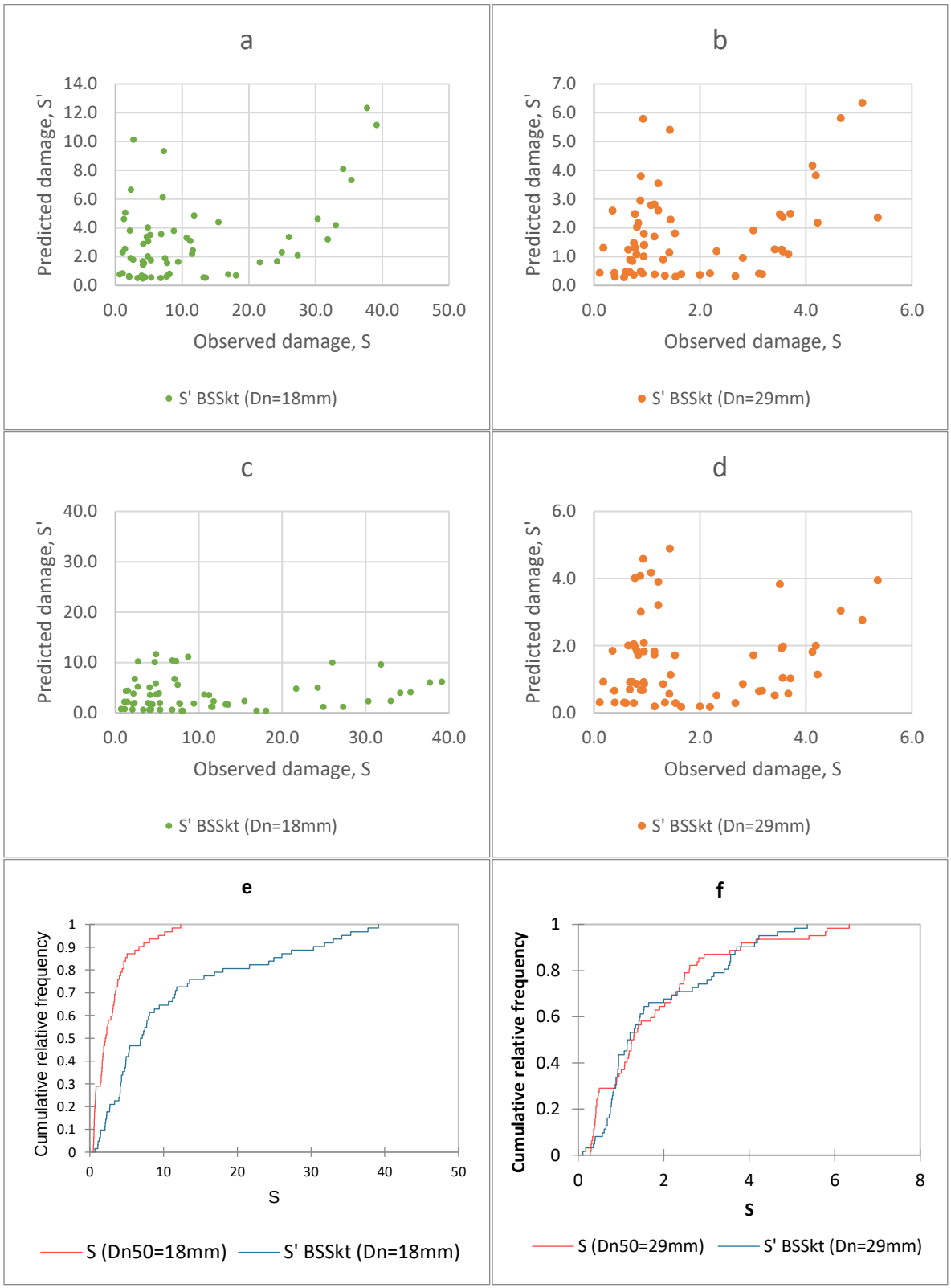

Figure 5.12. Predicted damage for initially calibrated model for smaller (a) and larger (b) stone sizes and same for recalibrated model (c and d), with the corresponding cumulative frequency distribution of observed and predicted damage (e and f).

5.5.2 Improvements: calibration and validation

Experimental data and further literature review inform several improvements to approach and model in Equation 4.24 that were implemented as follows:

1. Experimental data gathered herein (ODU) and AU and DELFT (VdM) are collated and partitioned ½ and ½ into calibration and validation datasets (Figure 5.13a and b) and determined not to be similar at the 5% level (Figure 5.13c and d). This approach is justified for three reasons: i) the determination that Cot = 1.5 and 2.0 were similar, implied that the data collected here was 100% replication and therefore could be split, ii) the determination that Ns/(hc/h) for the two partitioned datasets were different confirmed that both the driving forces for the calibration and validation datasets were different and should therefore be unique in their results of damage and iii) the use of a wider set of imposed forces in calibration (represented in the two datasets) would allow for better calibration. The calibration and validation datasets represent the full range of hc/h, S and N_S.
2. Erosion is predominantly on the seaward slope, and deposition also occurs on the seaward slope. Therefore, down-slope, internal friction stability factor (K_α=Sin(ϕ-α)/Sinϕ) (van Rijn, 2019) is utilized instead of the previously used up slope stability factor (K_α=Sin(ϕ+α)/Sinϕ) in Equation 4.18.
3. An alternate scheme of estimating maximum wave-induced velocity in the water column ($\left(\frac{u_{crest}}{u_{max}}\right)^2 \sim Cosh^2\{k.(z+h)\}$) in shallow water replaces the estimate of transmitted wave energy ($\frac{1}{\sqrt{(1-K_t{}^2)}}$) in Equation 4.21 and Equation 4.23.
4. Shear stress-induced instability ($+D.\Delta.\theta.\left(1+Sin(\alpha)\right)$) down slope (acting in the direction of gravity) is utilized instead of opposing gravity ($-D.\Delta.\theta.\left(1+Sin(\alpha)\right)$.
5. The usual lift coefficient constraints (see section 4.1.2 and Equation 4.2) were relaxed by allowing tuning coefficients for the Torum lift coefficient equation in Equation 5.4. This would allow for the simultaneous accounting of drag effects that are also considered by the same variables. Therefore, the same empirical coefficients are determined herein (Van Rijn, 1993, page 4.1).

Equation 5.4. The proposed equation for coefficient of lift from Torum (1994) data.

$$C_L = K_{cl1}(-0.00333.K_C + 0.2) + K_{cl2}$$

6. Shear stress-induced flow (synonymous to damage) varies with relative stones size, Re and protrusion/gradation. Contemplating the observations of Vithana (2013) and van Rijn (2019), the following factors were applied to the shear stress reduction factor, r:
    a. Critical shear stress reduces (increases) with relative depth (inverse of relative stone size) h/D_{n50} $K_{h/Dn50} = \ln(k_1.h/D_{n50})$
    b. Critical shear stress influence (friction factor, f_w) increases (reduces) with increasing Re (Vithana, 2013 figure 5.14). Therefore $K_{Re} = Re^{k2}$. An upper limit on the Re was imposed in line with the Moody Diagram that suggests friction factor does not increase past very high turbulence (Re >20,000 to 60,000).
    c. Critical shear stress increases with protrusion synonymous with D85:D15 ratio, wherein lower D85:D15 has a higher relative protrusion (p/D) (Vithana, 2013 figures 2.8, 6.5, 6.17 and 8.3). Therefore $K_{D85:D15} = (D_{85}:D_{15})^{k3}$. This assumption requires verification.

The improved form of the equation was subjected to calibration and validation.

Equation 5.5. Improved form of BSSkt

$$S = \left[\frac{1 + \frac{N_s.Cosh^2\{k.(z+h)\}}{2.\kappa}\left(C_L.\left(1+Sin(\alpha)\right)^2\right)}{\left(1+Sin(\alpha)\right).\left(r.K_{h/DN50}.K_{Re}.K_{D85:D15}\right).\left(\frac{Sin(\phi-\alpha)}{Sin(\phi)}\right)}\right]^{3/2}.\frac{13.{N_w}^{k_{nw}}.T_m.(g.\Delta)^{\frac{1}{2}}}{D^{\frac{1}{2}}}$$

The improved BSSkt model provides damage predictions that are similar to the calibration and validation data at significant levels with p=0.18 and 0.24, respectively (Figure 5.14 a and b) and RMSE= 2.8. BSSkt predicted initiation of damage in equal proportions to the data (p=0.883) for S= 2.0, but not for S=0.5 and 1.0, and again supports inferring initiation of damage from damage progression models. Interestingly, r was determined to be 0.09 and in line with Van Rijn's (2019) suggested values. It was further determined that VdM model predictions were not similar to the calibration or validation datasets at significant levels and had RMSE=3.85 (Figure 5.14 c and d). The relative performance of both models is relatively close except and cluster of points in the dataset around S=0 to 10 (Figure 5.14 e). Recalling the determination of RMSE = 3.2 and 1.5 in data error (in section 5.4.2.3), data errors are estimated to account for ~80 to 100% of the predictions' errors. Further assessment of the residuals (Figure 5.15 a and b) suggests non-stationarity at significant levels ($p<0.05$) with a mean error of 1.1 (-7.0) for S<10 (>10). BSSkt is therefore likely to over (under) predict damage for S<10 (S>10) by S ~ 1.1 (-7.0) and will therefore be conservative for the typical design range and best applied for S<10.

BSSkt model parameter estimates (Table 5.7) suggest:

1. Importance of: i) relative stone size to water depth, ii) turbulence, and iii) stone gradation, contrary to the findings of Burger (1995).
2. A non-linear increase of damage with the number of waves ($Nw^{0.29}$) was determined, similar to Melby (1999). There is confidence in this prediction because of the long durations (Nw = 24,000) used in the experiments.

Table 5.7. Key model parameters (Cl, r, k_1, k_2 and k_3) and variables (Kc and Re) for improved BSSkt model.

	Model parameters							
	Cl	r	Kc	Re	k_1 (k.h/D)	k_2 (Re^k)	k_3 ($D85:D15^k$)	k (Nw^k)
Minimum	0.70		46	12767				
Average	0.87	0.09			5.38	0.89	0.68	0.29
Maximum	0.97		168	19085				

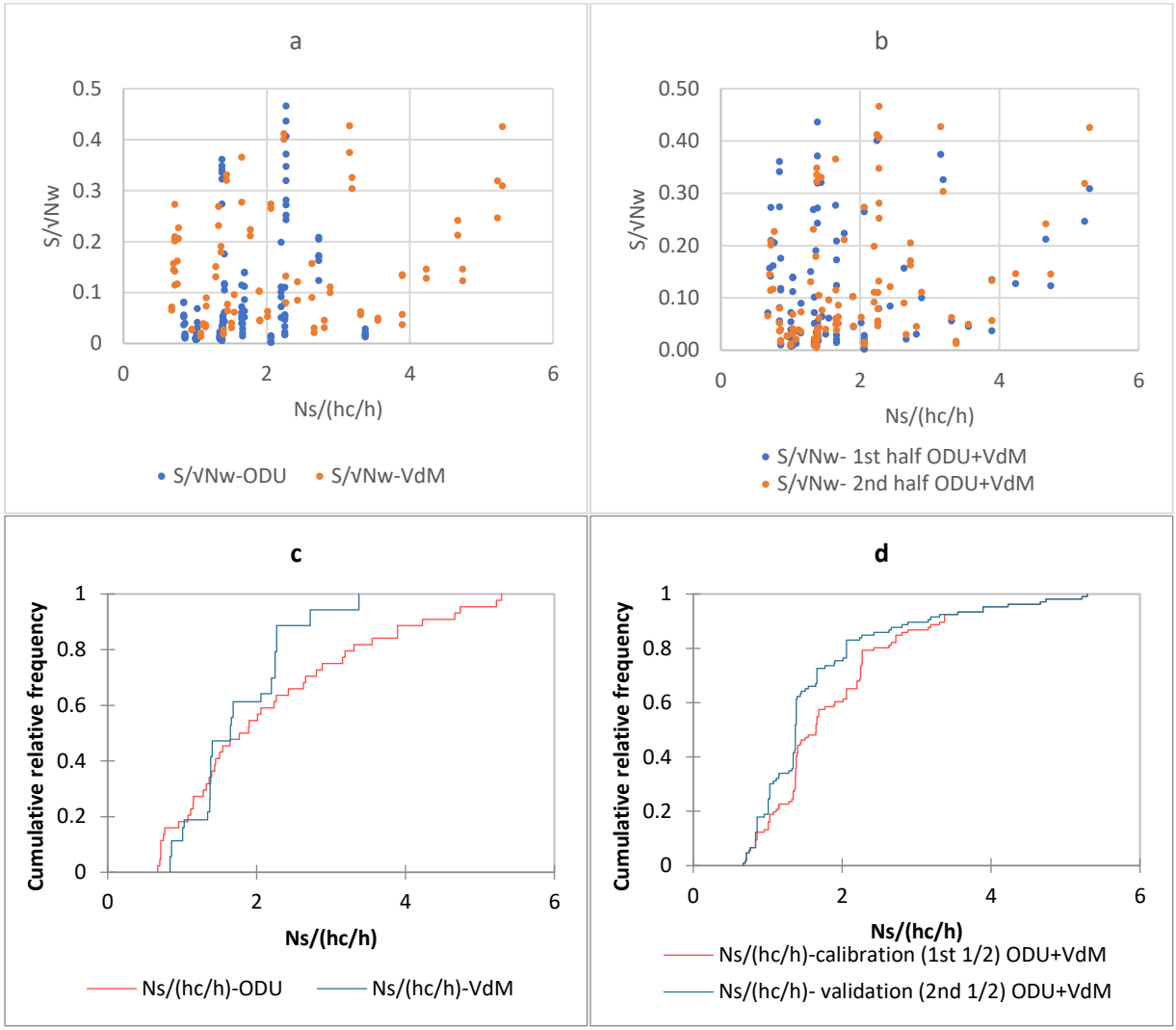

Figure 5.13. Initial calibration (validation) datasets from ODU (VdM) data (a) and mixture of datasets using in improvements using 50% ODU+VdM in each (b). Cumulative frequency of Ns for same (c and d).

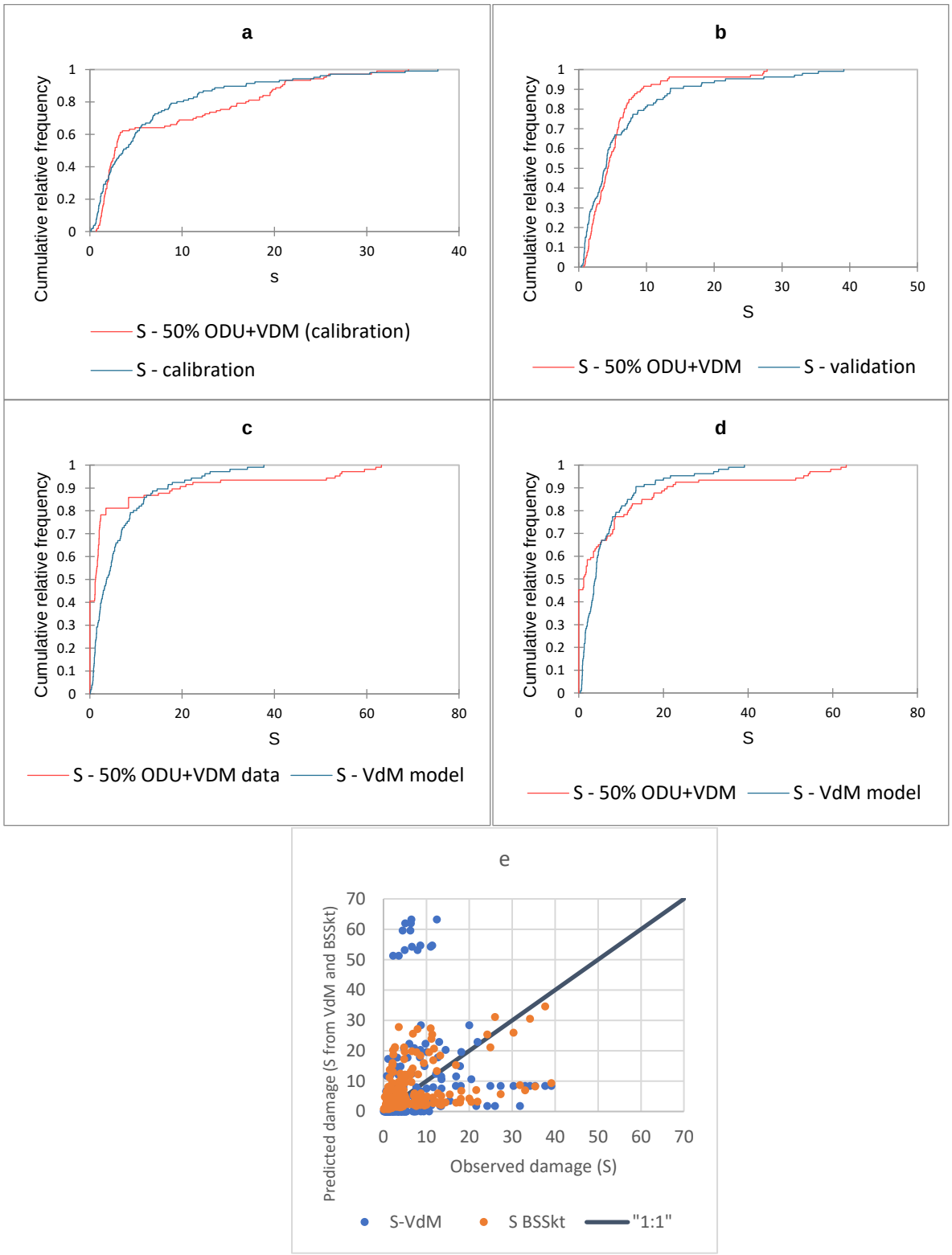

Figure 5.14. Cumulative distribution of damage (S) from BSSkt predictions from calibration (a) and validation (b). Comparison to VdM performance on calibration dataset (c) and validation dataset (d). Predicted damage from BSSkt and VdM on both calibration and validation datasets (e)

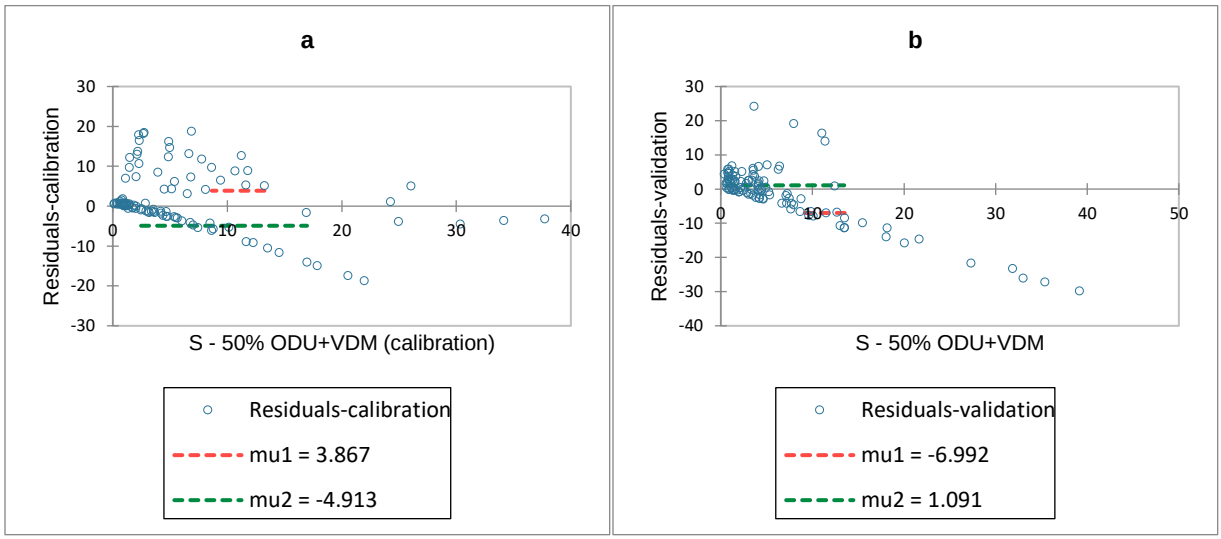

Figure 5.15. Assessment of residuals (model - data) from BSSkt calibration (a) and validation (b).

5.6 Application

5.6.1 Comparison

BSSkt generally predicted smaller (larger) damage than VdM with a limited (extended) number of waves. Emergent (hc/h = 1.2) and partially submerged (hc/h =1.0) conditions, with wave limited (Nw=1,500) and extended design life (Nw = 15,500) were explored for BSSkt and the VdM (Table 5.8). The limited number of waves scenario was explored in keeping with most experimental studies in the literature, and the extended number of waves scenario was explored because of the socio-economic circumstance in the Latin-American and Caribbean countries were in structures are likely to have limited maintenance over their design life (40 to 60 years) and experience 3 to 5 hurricane events (~14,000 to 16,000 waves). The usual requirements of 3,000 or 7,500 is believed to be too short. There were general trends wherein BSSkt had: i) comparable responses to geometric and wave properties variations and ii) more response to material property variations. The following was noted:

a) BSSkt (3.12) generally predicted less damage than VdM (7.5) for the emergent crest and a limited number of waves scenario.

b) BSSkt (6.6) predicted more extensive damage than VdM (2.0) at the end of the design life and underlines the importance of considering damage progression in the design process.

BSSkt and VdM predictions in the application mode are not similar at the 5% limit (Figure 5.18). BSSkt generally provided marginally lower damage predictions than VdM for S<3.4 but higher predictions when damage progression is explored. The models are providing unique predictions.

Table 5.8. Design predictions for emergent hc/h=1.2(1.0) and limited (extended) number of waves Nw=1500 (15,000) conditions from BSSkt and VdM models

Input				Output	
Wave properties		**Material properties**		**Damage**	
Hi (m)	1.5	Dn50 (m)	0.49	S BSS_{kt}	3.44 **(6.8)**
Tm (sec)	8.0	D85:D15	1.25	S VdM	6.45 **(6.45)**
Nw	1,500 (15,000)	ϕ (rad)	0.70		
Steepness, $sm^{-1/3}$	2.85	ϕ (degrees)	40.00	Ns	2.09
Iribarren num., ξ	5.44	Δ	1.47	Ns*	5.95
Geometry				Kt	0.38
Cot α	1.5				
hc (m)	2.4 (2.0)				
h (m)	2				
hc/h	1.2 (1.0)				

Observations of the predictions of each model and their trends are summarized as follows:

1. Geometry:
    a. hc/h (Figure 5.16a): More damage was predicted by VdM (0 to 6) for increased emergence (hc/h = 1.0 to 1.2) than BSSkt (3.0 to 3.4). No further damage was predicted by VdM for submergence less than 0.9. BSSkt was less responsive than VdM to crest submergence. There is support for both models with the flume data for BSSkt hc/h <1 and VdM steep increase in damage for hc/h > 1.
    b. h, water depth (Figure 5.16b): More damage was predicted by VdM (0 to 12) for increased water depth (h = 1.6 to 3) than BSSkt (3.5 to 4.7). There is support for both models with measured damage moderating between both BSSkt and VdM.
    c. Structure slope, Cot α (Figure 5.16c): BSSkt damage predictions decreased considerably from 10 to 1.0 for slopes of 1.25 to 1.5 and suggested avoiding slopes steeper than 1.5 in the design process. VdM does not directly consider structure slope, and therefore, no response was observed other than predicted damage of 2.0.

BSSkt was more responsive than VdM to variations in Cot α. The effect of this variable deserves further investigation. Notwithstanding, a slope flatter than 1.5 (probably 2.0) should be considered in designs until this variable is better understood

2. Material:
    a. Nominal diameter, D_{n50} (Figure 5.17d): VdM determined higher damage (of 30) for Dn50 less than 0.3m in comparison to BSSkt (6.6). Both VdM and BSSkt had comparable damage predictions (~4.0) for larger stone sizes (>0.44m). This significant variation in damage predictions for potentially undersized stones might have an implication for damage progression considerations. There is support for both models measured damage.
    b. Gradation, D85:D15 (Figure 5.16e): BSSkt predicted decreased stability (~3) with narrower gradations (D85:D15 < 1.5) and greater damage than VdM (2). Increased stability with wider gradation might be due to the sheltering effects of larger stones and the smoother surface that results in less friction and bed shear stress and is contrary to Burger (1995). BSSkt had more response to this variable than VdM. There is support for BSSkt with measured damage.
    c. Internal friction angle, Φ (Figure 5.16f): BSSkt predicting reduced damage (10 to 2, a factor of 5) from smooth rounded armors to angular rough armor. The VdM does not directly consider this parameter. This prediction offered insight into potentially important design considerations.
    d. Specific density, Δ (Figure 5.17g): BSSkt predicted marginal increase in stability (3.1 to 2.7) for Δ 1.37 to 1.72 in comparison to VdM (3.5 to ~0). VdM is more responsive to specific density changes.
3. Wave
    a. The number of waves, Nw (Figure 5.17**h): BSSkt predicted increased damage (3.0 to 7.5) from 1,500 to 15,000 waves and approximated a ¼ power function. This parameter is not considered directly in VdM model. The results underline the importance of considering damage progression in the design process and that structure design for damage of 2.0 can experience more significant damage in its design life.** There is support for BSSkt with measured damage.
    b. Wave height, Hs (Figure 5.17i): BSSkt predicted more significant damage across the range of Hs investigated. Damage predictions from VdM increased considerably (0.0 to 2.5) for increased wave heights (1.0 to 1.8) versus BSSkt that had a muted response (2.2

to 3.0) for the same range. There is support for both models with measured damage, but the early prediction of damage provides support for BSSkt.

c. Wave period, Tm (Figure 5.17j): Vdm damage predictions were more responsive (0.2 to 5.7) than BSSkt (2.5 to 4.1) to increased wave period from 6 to 13 seconds. The models were comparable around a period of 6 to 7 seconds. Both models have a similar response pattern. There is no support for both models with measured damage.
d. Wave type, ξ (Figure 5.17j and k): Considerably more significant damage is predicted by VdM (3 to 7.6) than BSSkt (0.1 to 0.3) for spilling ($\xi<0.4$) to plunging waves ($0.4<\xi<2.0$) respectively. A trend of increased damage by BSSkt (0.3 to 4) and VdM (7.6 to 12.9) for surging and collapsing waves ($\xi>2.0$) was predicted. It is this type of wave that is believed to be of greater design importance.

A test of similarity of the predictions of BSSkt versus VdM confirmed that the models' predictions are not similar and therefore are providing unique predictions ($p = .0001$) using the KS test (Figure 5.18).

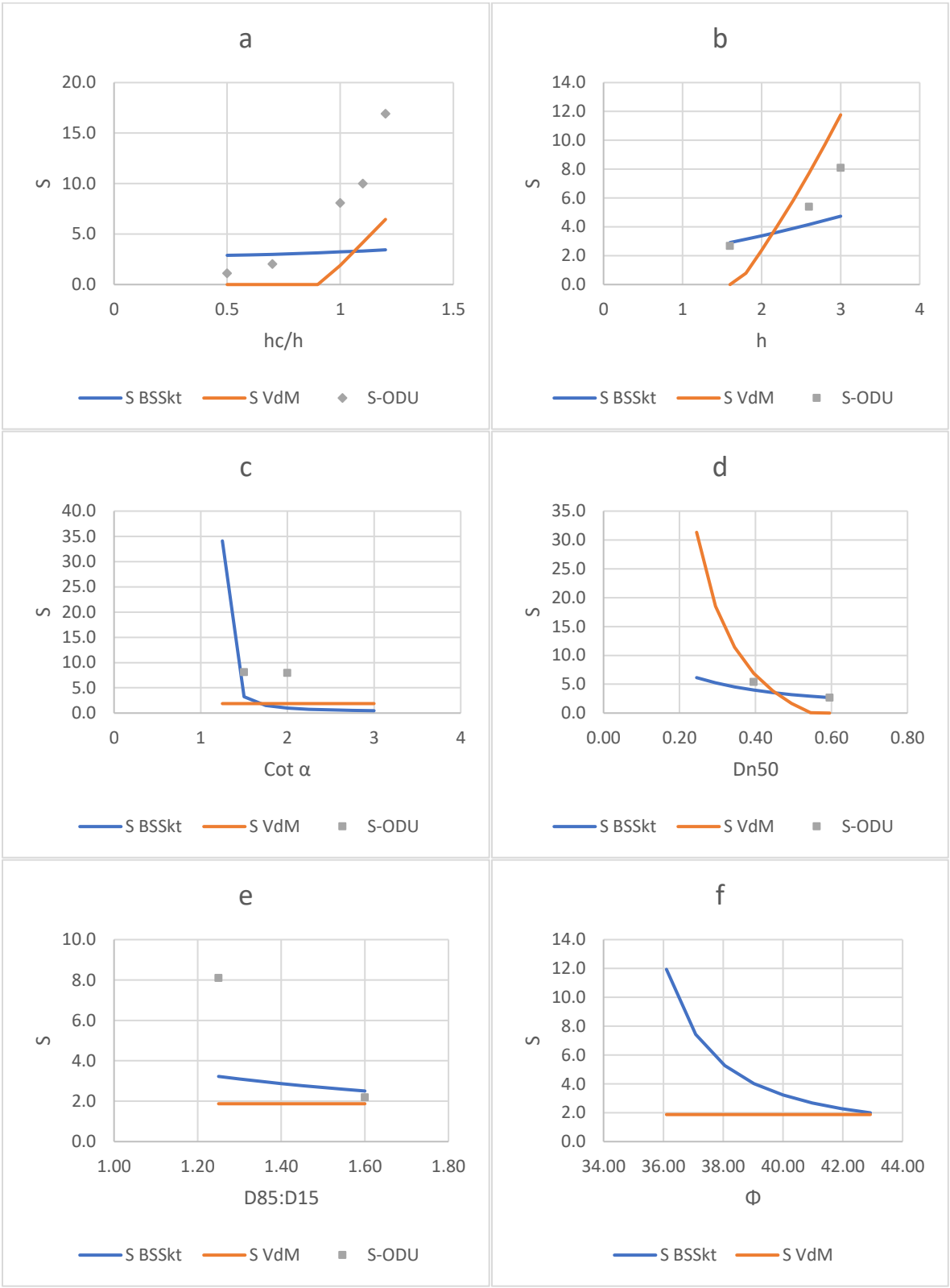

Figure 5.16. Predicted damage, S for variations in geometric, material and wave properties, with ODU model test data

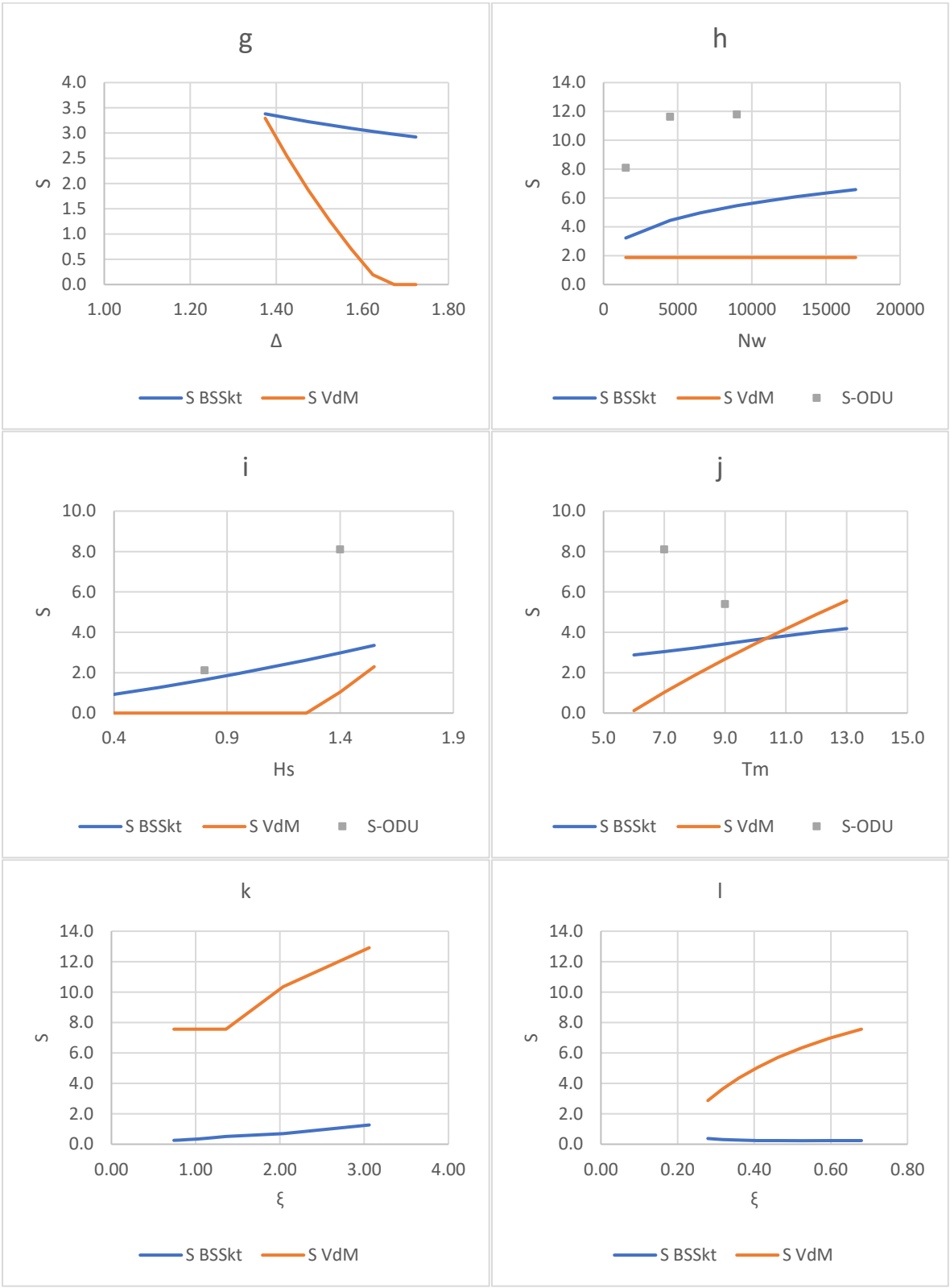

Figure 5.17. Predicted damage, S for variations in geometric, material and wave properties, with ODU model test data

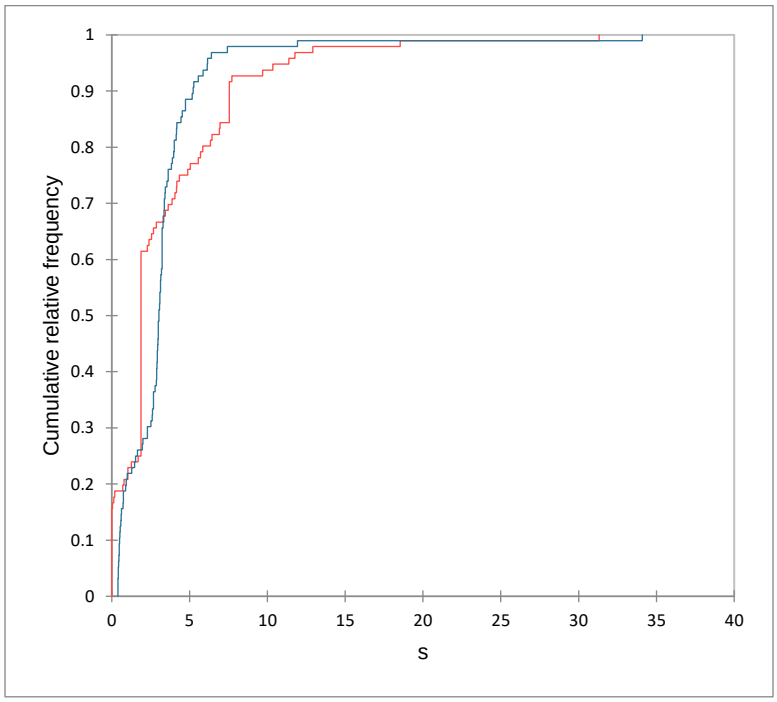

Figure 5.18. Cumulative distribution of damage (S) from BSSkt and VdM predictions from the application mode

5.6.2 "Rule of thumb"

A climate-resilient "Rule of Thumb" was determined. A comparison was then made to two other models to determine the greatest damage as a result of the following conditions (Kramer 2006, Burcharth et al., 2006 and Pilarczyk, 2003 in Taviera-Pinto, 2005):

1. In *a posteriori* damage progression is considered from an acceptable level (S_{3000} = 2.0) to damage at end of life = 50 years ($S_{15,500}$ < 4.0) and global Sea Level Rise (SLR) of 8mm per year on average. This concept has been explored by other *a priori* (Graauw, 2014)
2. Least favorable depth limited wave conditions with no storm surge and Tm = 6.0 to 9.0 seconds in 1 to 3 meters of water with hc/h = 1.0 at start of project life
3. Graded armor stone with D_{85}:D_{15} = 1.8, moderately dense Δ = 1.5, rough angular stones Φ = 40.0◦ with Cot α = 2.0 and homogenous (no core) structure.

Damage predictions by the "Rule of thumb" (Equation 5.6) suggest long-term damage S<4 (Figure 5.19a) at the end of the design life with SLR. The "Rule of Thumb" (RoT) D_{n50} predictions are greater (lesser) than the Kramer and Burcharth (Pilarczyk) model. A more robust RoT with long-term resilience (S<2) in Figure 5.19b predicts larger stone sizes than Kramer and Burcharth model.

Equation 5.6. "Rule of Thumb" for the stability of LCS (S<2, Nw = 3000, future climate with SLR)

$$D_{n50} = 0.15 \times h + 0.08$$

Equation 5.7. "Rule of Thumb" for stability of LCS (S<2, Nw = 15,500, future climate with SLR)

$$D_{n50} = 0.2 \times h + 0.3$$

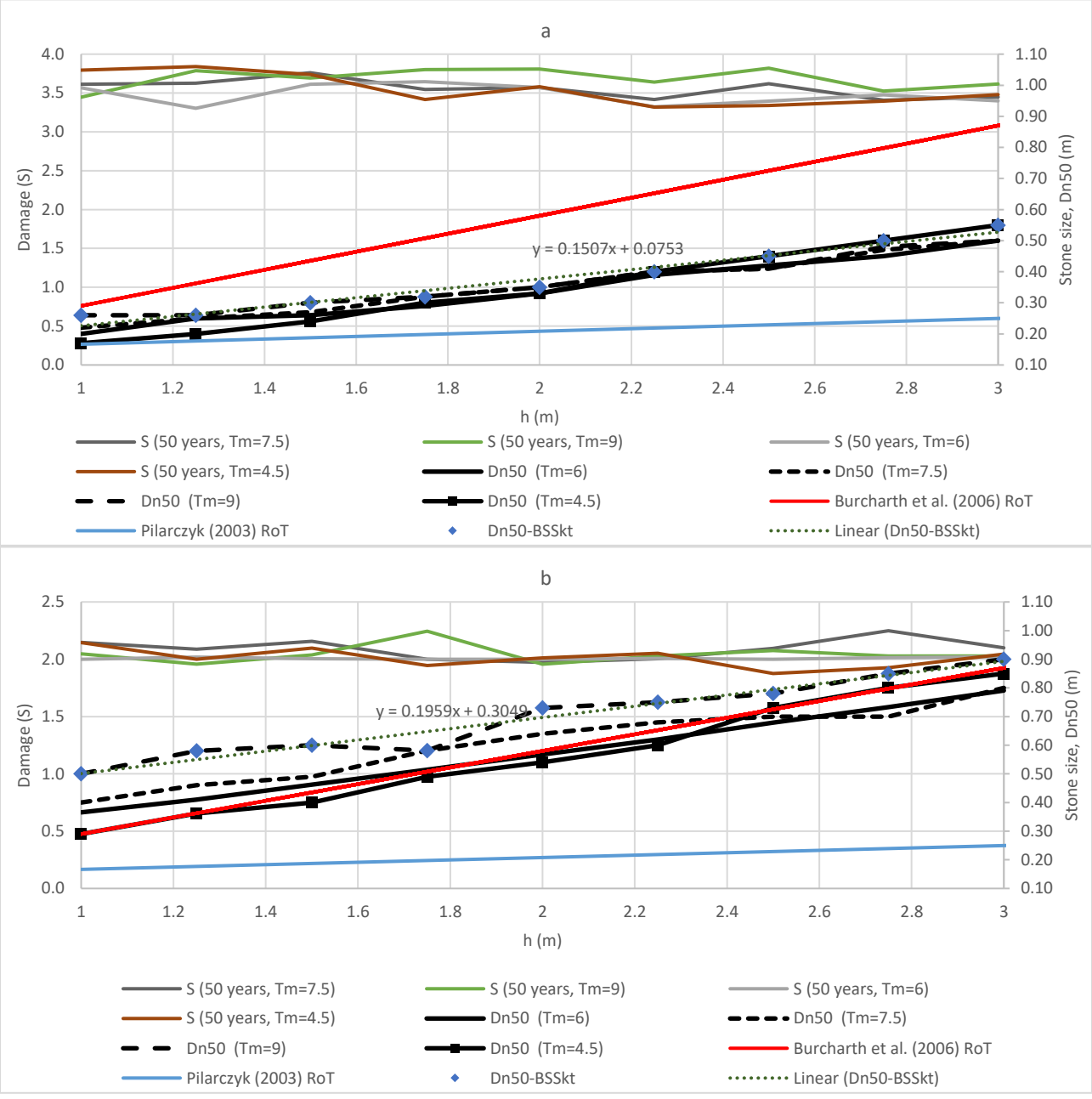

Figure 5.19. Predicted stability of LCS for S<2 at Nw= 3,000, and S<4 for Nw to 15,500 (a) and S<2 at Nw = 15,500 (b).

5.7 Summary

The existing LCS dataset (77 points) was extended by 124 points and covered a range of conditions. Damage generally increased with stability number, emergence and number of waves. Conversely, the damage was minimized for a steepness of ~3.5 for both stone sizes. No difference in damage for structure slope steepness in the range of Cot α = 1.5 to 2.0 was observed. Interestingly, this is a point previously suggested in the PCA analysis. Assessment of the bias suggests data error in the order of S = 1.05 to 4.1 and the model's performance can be compared to this component of error. Observations underlined the importance of relative crest elevation (hc/h), damage progression, wave steepness, or corresponding wave period.

Erosion and deposition plots of the scale model tests confirmed the vulnerability of the seaward slope-crest intersect. Additionally, the scale model test erosion plots suggest: i) initiation of damage at the seaward-crest intersect that progresses both along the crest and seaward slope, ii) decreasing erosion to the toe of LCS, iii) damage progression with the number of waves, iv) decreased damage with increased submergence.

The initial BSSkt and VdM models over predicted damage and required further recalibration. Recalibration only resulted in similar predictions for the larger stone sizes, and the model was concluded to need improvement to capture both stabilizing and destabilizing processes. Several improvements were implemented, including i) inclusion of additional experimental data from Van der Meer, ii) changes in the model formulation to account for the predominantly seaward slope erosion, iii) an alternate scheme of estimating maximum wave-induced velocities, iv) relaxation of lift coefficient range and v) several factors to account for shear stress reduction due to relative depth, stone size, Re and gradation. The improved BSSkt model provided damage predictions and initiation of damage similar to the data at significant levels and provided further insights into the damage progression being non-linear. BSS_{kt} model provides better damage predictions (RMSE = 2.8) than the VdM formulae (RMSE = 3.95) and similar initiation of damage predictions to Kramer's model (refer to section 3.3.1).

In the application mode, marginally lower damage is generally predicted by the BSSkt model than VdM. The model offers the possibility of exploring other design considerations not considered by VdM, including structure slope (Cot α), gradation (D_{85}:D_{15}), damage progression (N_w) and internal friction (Φ). Slopes of Cot α = 2.0 and greater should be considered until this variable is better understood. These should be further investigated with additional experimental data. A simplified Rule of Thumb was determined that is climate-resilient to Sea Level Rise.

6 CONCLUSIONS AND FUTURE RESEARCH

The following was summarized, concluded and recommended for future research

1. The literature points to increasing understanding of the stability of LCS, albeit as it relates to initiation of damage. The shear stress-induced erosion using Shield's formulation has been shown in the literature to offer a pathway to better understanding damage progression (van Rijn 2019). We have not seen the co-joint formulation with wave-induced forces, and this framework was explored herein.
2. Existing LCS data were retrieved and screened (from 737 to 94 data points) and used to test the Kramer and Van der Meer and Daemen stability models. Generally, the Kramer and VdM models are skillful in predicting initiation of damage. Both Kramer and VdM models can predict the initiation of damage for S = 1.0 and 2.0 in equal proportions to the data at significant levels.
3. Two analytical models (MF and BSS) and two variations of each (MF_{kt} and BSS_{kt}) that remove transmitted wave energy were developed herein. Initiation of damage remained difficult to predict consistently at significant levels for all models (MF, BSS and VdM). It is recommended that damage initiation be inferred from progressive progression models.
4. The removal of transmitted wave energy in the calibrated BSS_{kt} model was beneficial and resulted in predictions similar to the data, with lower bias (and RMSE) than VdM model. Further research on the role of the lift coefficient is required. Block effects were determined for VdM, wherein VdM can predict similar damages for Re<40,000. This limitation of the VdM model requires further investigation.
5. A scale model testing programme was successfully undertaken that added 124 new data points to the body of knowledge on LCS. Interestingly, while familiar trends were observed, there were points of note, including i) there was no difference in damage for Cot α = 1.5 versus 2.0, ii) damage is minimized with decrease relative crest height hc/h, iii) erosion and deposition plots of the scale model tests confirmed the vulnerability of the seaward slope and crest intersect iv) damage progressed with the number of waves up to the 25,000-wave series explored herein. The low to the moderate influence of structure slope was observed in the pairwise comparison of the means in the factorial analysis.
6. Previously calibrated BSS_{kt} and VdM models failed to predict damage similar to the new data, recalibration results in similar predictions for the larger stone sizes. Implementing several improvements helped derive an LCS model that predicted damage similar to the data with smaller RMSE (2.8) than VdM model (3.95) and provided several insights. Namely: i) model formulation to account for seaward slope erosion is key ii) both drag and lift (pressure-induced forces) might

be at play in the destabilizing of units, iii) Shield's stress-related forces might be a function of relative depth and stone size, Re and gradation and iv) damage progression is likely to be non-linear. The seaward slope importance is underlined in Burcharth et al. (2014). The most feasible climate change adaption approach is likely to reinforce the seaward slopes with an additional layer of armor. Assessment of the residuals confirms that BSS_{kt} is likely to be conservative and best applied S<10. Further research is required on the role of lift and the factors that affect shear stress. Data error (S = 1.05 to 4.1) is significant in comparison to the RMSE (2.8 to 3.95) and suggests the need for more duplication in physical scale models to better understand the central tendency and replication of damage predictions. The final form of the model is:

Equation 6.1. An improved form of BSS_{kt} for LCS

$$S = \left[\frac{1 + \frac{N_s.Cosh^2\{k.(z+h)\}}{2.\kappa}\left(C_L.\left(1+Sin(\alpha)\right)^2\right)}{\left(1+Sin(\alpha)\right).\left(r.K_{h/DN50}.K_{Re}.K_{D85:D15}\right).\left(\frac{Sin(\phi-\alpha)}{Sin(\phi)}\right)}\right]^{3/2}.\frac{13.{N_w}^{0.29}.T_m.(g.\Delta)^{\frac{1}{2}}}{D^{\frac{1}{2}}}$$

Where:

- C_l = -0.0023 x K_c+1.08
- r = 0.088
- $K_{h/Dn50}$ = ln(5.38 x h/D_{n50})
- $K_{Re} = Re^{0.89}$, $R_{e\ max}$ = 19,084
- $K_{D85:D15} = (D_{85}:D_{15})^{0.68}$

7. In the application mode, BSSkt predicts marginally lower (higher) damage than VdM for a limited (extended) number of waves and allows for exploring the influence of Structure slope (Cot α), gradation (D_{85}:D_{15}), Damage progression (Nw) and angle of repose (Φ). These should be further investigated with additional experimental data with variations in i) both rounded and angular stones to vary Φ, ii) D_{85}:D_{15} ratio = 1.25 to 3, iii) steep to flatter structures with Cot α = 1.5 to 3. Slopes of Cot α = 2.0 and greater should be considered in the design until this variable is better understood.
8. A "Rule of Thumb" is proposed to be climate resilient to SLR and provide smaller stone sizes predictions compared to Burcharth (2006).

Equation 6.2. Climate resilient "Rule of Thumb" for the stability of LCS (S<2, N_W=3,000)

$$D_{n50} = 0.16 \times h + 0.07$$

Or an alternative that is more robust at the end of the design life:

Equation 6.3. Climate resilient "Rule of Thumb" for the stability of LCS ($S<2$, $N_W=15{,}500$)

$$D_{n50} = 0.2 \times h + 0.3$$

7 REFERENCES

Agrawal, Amit, Srikumar Ramalingam, Yuichi Taguchi, and Visesh Chari (2012). "A theory of multi-layer flat refractive geometry." In 2012 IEEE Conference on Computer Vision and Pattern Recognition, pp. 3346-3353. IEEE.

Ahrens, John P (1989) "Stability of reef breakwaters." Journal of Waterway, Port, Coastal, and Ocean Engineering 115.2: 221-234.

Attal, M., & Lavé, J. (2009). Pebble abrasion during fluvial transport: Experimental results and implications for the evolution of the sediment load along rivers. Journal of Geophysical Research: Earth Surface, 114(F4).

Asai, Takeshi, Takao Akatsuka, and Steve Haake (1998). "The physics of football." Physics World 11, no. 6: 25.

Burcharth, H. F., Andersen, T. L., & Lara, J. L. (2014). Upgrade of coastal defence structures against increased loadings caused by climate change: A first methodological approach. Coastal Engineering, 87, 112-121.

Burcharth, Hans F., Morten Kramer, Alberto Lamberti, and Barbara Zanuttigh (2006). "Structural stability of detached low crested breakwaters." Coastal Engineering 53, no. 4: 381-394.

Burcharth, H. F., and S. A. Hughes (2002). "Coastal Engineering Manual, Part VI-Chapter VI-5-2 Fundamentals of Design." US Army Corps of Engineers.

Burger, G. (1995). "Stability of low-crested breakwaters. Stability of front, crest and rear. Influence of rock shape and gradation." PhD diss., MSc. thesis Delft University of Technology and Delft Hydraulics Report.

Burnham, Kenneth P., and David R. Anderson (2004). "Multimodel inference: understanding AIC and BIC in model selection." Sociological methods & research 33, no. 2: 261-304.

Campos, Álvaro, Rafael Molina-Sanchez, and Carmen Castillo (2020). "Damage in Rubble Mound Breakwaters. Part II: Review of the Definition, Parameterization, and Measurement of Damage." Journal of Marine Science and Engineering 8.5: 306.

Coastal Engineering Research Center (CERC) (US) (1984). Shore Protection Manual. Department of the Army, Waterways Experiment Station, Corps of Engineers, Coastal Engineering Research Center,

Dai, Yin Ben, and A. M. Kamel (1969). Scale Effect Tests for Rubble-Mound Breakwaters: Hydraulic Model Investigation. Vol. 69. No. 2. US Army Corps of Engineers, Waterways Experiment Station [Hydraulics Laboratory].

de Almeida, Ermano, Marcel RA van Gent, and Bas Hofland (2019). "Damage characterization of rock slopes." Journal of Marine Science and Engineering 7, no. 1: 10.

Farhadzadeh, Ali, Nobuhisa Kobayashi, and J. A. Melby (2009). "Wave overtopping and damage progression on rubble mound structures." Research Rep. No. CACR-09-05, Center for Applied Coastal research, Univ. of Delaware, Newark, Del.

Froehlich, David C (2011). "Mass angle of repose of open-graded rock riprap." Journal of irrigation and drainage engineering 137, no. 7: 454-461.

Garcia, N., J. L. Lara, and I. J. Losada. "2-D numerical analysis of near-field flow at low-crested permeable breakwaters." Coastal Engineering 51, no. 10 (2004): 991-1020.

Garcia, R., & Kobayashi, N. (2014). Damage variations on low-crested breakwaters. COASTAL ENGINEERING, 2. Downloaded March 2021 from: https://journals.tdl.org/icce/index.php/icce/article/download/7077/pdf_402/0

Garde, R. J., and S. Sethuraman (1969). "Variation of the drag coefficient of a sphere rolling along a boundary." La Houille Blanche 7: 727-732.

Givler, Lindley David (1986). "An investigation of the stability of submerged homogeneous rubble-mound structures under wave attack.".

Graauw, Arthur de (2014). "The long-term failure of rubble mound breakwaters." Méditerranée. Revue géographique des pays méditerranéens/Journal of Mediterranean geography.

Hald, Tue, and H. F. Burcharth (2001). "An alternative stability equation for rock armoured rubble mound breakwaters." In Coastal Engineering 2000, pp. 1921-1934.

Hofland, B., Gent, M. V., Raaijmakers, T., & Liefhebber, F. (2013). Damage evaluation using the damage depth. In Coastal Structures 2011: (In 2 Volumes) (pp. 812-823).

Hofland, Bas, Paulo Rosa-Santos, Francisco Taveira-Pinto, Ermano de Almeida, Rute Lemos, Ana Mendonça, and Conceição Juana Fortes (2018). "Measuring damage in physical model tests of rubble mounds." In Coasts, Marine Structures and Breakwaters 2017: Realising the Potential, pp. 929-940. ICE Publishing.

Hughes, Steven A (1993). Physical models and laboratory techniques in coastal engineering. Vol. 7. World Scientific.

Jensen, O. J., & Klinting, P. (1983). Evaluation of scale effects in hydraulic models by analysis of laminar and turbulent flows. Coastal Engineering, 7(4), 319-329.

Kramer, Morten, and Hans F. Burcharth (2002). "Environmental Design of Low Crested Coastal Defence Structures: DELOS D31 Wave Basin Experiment Final Form-3D Stability Tests at AAU."

Kramer, Morten (2005). Structural stability of low-crested breakwaters. Diss. Aalborg University, Department of Civil Engineering, Water & Soil.

Kobayashi, Nobuhisa, and Ashwini K. Otta (1987). "Hydraulic stability analysis of armor units." Journal of waterway, port, coastal, and ocean engineering 113, no. 2: 171-186.

Kobayashi, Nobuhisa (2009). "Hydraulic Response And Armor Layer Stability On Coastal Structures." , Center for Applied Coastal research, Univ. of Delaware, Newark, Del.

Kobayashi, Nobuhisa, Haoyu Zhao, Beatriz Pozueta, and Jeffrey A. Melby (2004). "Virtual performance of rubble mound structures." In Coastal Structures 2003, pp. 1-13.

Kramer, Morten, Zanuttigh, B., Van der Meer, J. W., Vidal, C., & Gironella, F. X. (2005). "Laboratory experiments on low-crested breakwaters." Coastal Engineering 52.10-11: 867-885.

Kramer, Morten, and Hans F. Burcharth. "Environmental Design of Low Crested Coastal Defence Structures: DELOS D31 Wave Basin Experiment Final Form-3D Stability Tests at AAU." (2002).

Jensen, O. Juul and P. Klinting (1983). "Evaluation of scale effects in hydraulic models by analysis of laminar and turbulent flows." Coastal engineering 7, no. 4: 319-329.

Jensen, Bjarne, Erik Damgaard Christensen, and B. Mutlu Sumer (2014). "Pressure-induced forces and shear stresses on rubble mound breakwater armor layers in regular waves." Coastal Engineering 91: 60-75.

Losada, I. J., Lara, J. L., Christensen, E. D., & Garcia, N. (2005). “Modeling of velocity and turbulence fields around and within low-crested rubble-mound breakwaters”. Coastal Engineering, 52(10-11). 887-913.

Martín, Francisco, Cynthia Martínez, Pedro Lomónaco and Cesar Vidal (2003). "A new procedure for the scaling of core material in rubble mound breakwater model tests." Coastal Engineering 2002: Solving Coastal Conundrums. 1594-1606.

Melby, Jeffrey A (1999). "Damage Progression on breakwaters." PhD Dissertation, University of Delaware

Melby, Jeffrey A., and Nobuhisa Kobayashi (1997). "Incipient motion of breakwater armor units." In Coastal Engineering 1996, pp. 1803-1815.

Melby, Jeffrey A., and Nobuhisa Kobayashi (1998). "Progression and variability of damage on rubble mound breakwaters." Journal of waterway, port, coastal, and ocean engineering 124.6: 286-294.

Merli, Davide (2009). "Stability of wide-graded rubble mounds." Downloaded from https://core.ac.uk/download/pdf/46667692.pdf

Mizutani, N., K. Iwata, T. M. Rufin Jr, and K. Kurata (1993). "Laboratory investigation on the stability of a spherical armor unit of a submerged breakwater." In Coastal Engineering 1992, pp. 1400-1413.

Neves, Ana, F. Gomes, and F. Pinto (2016). "Advanced experimenting on wave interaction with low-crested breakwaters." The International Journal of Multiphysics 4, no. 3.

Norton, P. A., and P. Holmes (1993). "Armor displacements on reshaping breakwaters." In Coastal Engineering 1992, pp. 1448-1460.

Pilarczyk, K. W. (2003). Design of low-crested (submerged) structures: An overview. In 6th COPEDEC (Int. Conf. on Coastal and Port Engng. in Develop. Countries), Sri. Downloaded March 2021 from: https://repository.tudelft.nl/islandora/object/uuid:49609414-c7ef-4e8d-a8b8-52c41a852ed7

Panizzo, Andrea, and Riccardo Briganti (2007). "Analysis of wave transmission behind low-crested breakwaters using neural networks." Coastal Engineering 54.9: 643-656.

Porter, Kate, Richard Simons, and John Harris(2014). "Comparison of three techniques for scour depth measurement: photogrammetry, echosounder profiling and a calibrated pile." Coastal Engineering Proceedings 34: 64-64.

Powell, Keith Andrew, and W. Allsop (1985). "Low-crest breakwaters, hydraulic performance and stability." Hydraulic Research Wallingford.

Raftery, Adrian E (1999). "Bayes factors and BIC: Comment on “A critique of the Bayesian information criterion for model selection”." Sociological Methods & Research 27, no. 3: 411-427.

Ranasinghe, D. P. L., T. Pemasiri, K. Raveenthiran, M. Young, C. W. Seo, and M. Mendis (2009). "Hydraulic Stability of Tetrapod Toe Apron on Coreloc Armor Breakwater: A 2d Physical Model Study." In International Conference in Ocean Engineering, ICOE.

Sammis, Charles G., David A. Lockner, and Ze’ev Reches (2011). "The role of adsorbed water on the friction of a layer of submicron particles." Pure and applied geophysics 168, no. 12: 2325-2334.

Shimada, Atsuyuki, Toshimi Fujimoto, Syozo Saito, Tsutomu Sakakiyama, and Hiromaru Hirakuchi (1987). "Scale effects on stability and wave reflection regarding armor units." In Coastal Engineering 1986, pp. 2238-2252.

Sila, Dharma IGB (2004). "A study of transmission, reflection and stability of low-crested rubble mound breakwaters under wave action.": 1838-1838.

Taveira-Pinto, F (2005). "Analysis of submerged breakwaters stability design." WIT Transactions on the Built Environment 78.

Thompson, D. M., and R. M. Shuttler (1975). "Riprap design for wind-wave attack, a laboratory study in random waves." Wallingford report EX707 for CIRIA.

Tirindelli, Matteo, and Alberto Lamberti (2004). "Wave action on rubble mound breakwaters: the problem of scale effects." Delos report D52.

Todd, D., J. Sutherland, N. Crossouard, R. Rankine, T. Rigden, and R. J. S. Whitehouse (2016). "Comparison between methods for creating DEMs of physical models." Coastlab16.

Tørum, Alf (1994). "Wave-induced forces on armor unit on berm breakwaters." Journal of waterway, port, coastal, and ocean engineering 120, no. 3: 251-268.

Van der Meer, J. W., and K. W. Pilarczyk (1985). "Stability of rubble mound slopes under random wave attack." Coastal Engineering 1984. 2620-2634.

Van der Meer, Jentsje W (1988). "Rock slopes and gravel beaches under wave attack.". PhD Dissertation. Technische Universiteit Delft (The Netherlands).

Van der Meer, Jentsje W., and Krystian W. Pilarczyk (1991). "Stability of low-crested and reef breakwaters." Coastal Engineering 1990. 1375-1388.

van der Meer, Jentsje W., and Ivar FR Daemen (1994). "Stability and wave transmission at low-crested rubble-mound structures." Journal of waterway, port, coastal, and ocean engineering 120, no. 1: 1-19.

Van der Meer, Jentsje W (1995). "Conceptual design of rubble mound breakwaters." Advances In Coastal and Ocean Engineering: (Volume 1). 221-315.

Van der Meer, Jentsje W., van Gent, M. R., Pozueta, B., Verhaeghe, H., Steendam, G. J., & Medina, J. R. (2005). "Applications of a neural network to predict wave overtopping at coastal structures." ICE, Coastlines, Structures and Breakwaters, London: 259-268.

Van der Meer, Jentsje (2011). "Design aspects of breakwaters and sea defences." In th 5 SCACR 2011 International Short Conference on Applied Coastal Research, p. 3.

Van Gent, M. R. A. (1995). "Porous flow through rubble-mound material." Journal of waterway, port, coastal, and ocean engineering 121, no. 3: 176-181.

Van Gent, M. R. A., Plate, S. E., Berendsen, E., Spaan, G. B. H., Van Der Meer, J. W., & d'Angremond, K. (1999) "Single-layer rubble mound breakwaters." Proc. Coastal Structures. Vol. 99.

Van Gent, Marcel RA, Alfons J. Smale, and Coen Kuiper (2004). "Stability of rock slopes with shallow foreshores." In Coastal Structures 2003, pp. 100-112.

Van Rijn, Leo C (1993). Principles of sediment transport in rivers, estuaries and coastal seas. Vol. 1006. Amsterdam: Aqua publications,

van Rijn, L. C. (2019). "Critical movement of large rocks in currents and waves." International Journal of Sediment Research 34, no. 4: 387-398.

Vidal, C., Losada, I. J., & Martin, F. L. (1999). Stability of near-bed rubble-mound structures. In *Coastal Engineering 1998* (pp. 1730-1743). Vidal, C., Losada, I. J., & Martin, F. L. (1999). Stability of near-bed rubble-mound structures. In Coastal Engineering 1998 (pp. 1730-1743).

Vidal, C., R. Medina, and F. L. Martín (2000). "A methodology to assess the armor unit stability of lowcrested and submerged rubble-mound breakwaters." In Proceedings of the Coastal Structures, vol. 99, pp. 721-725.

Vidal Pascual, César, Fernando López Mera, and Íñigo Losada Rodríguez (2009). "Stability Analysis of Low Crested and Submerged Rubble Mound Breakwaters: Relationship Between Flow Characteristics and Measured Damage and Stability Formulae for Low Crested and Submerged Breakwaters." Coastal Structures 2007: (In 2 Volumes). 939-950.

Vithana, Hela Perakum Viduragomi (2013). "The effect of stone protrusion on the incipient motion of rock armor under the action of regular waves." PhD diss., UCL (University College London),

Wolters, G., M. van Gent, W. Allsop, L. Hamm, and D. Mühlestein (2007). "Guidelines for physical model testing of breakwaters. Rubble mound breakwaters." Report prepared for Hydralab III, Coasts, marine structures and breakwaters: Adapting to change: Proceedings of the 9th international conference organised by the Institution of Civil Engineers and held in Edinburgh on 16 to 18 September 2009. Thomas Telford Ltd, 2010..

Zhang, Shaoxiong, Youhua Chen, and Bin Zhang (2015). "A study on incipient sediment motion and the stability conditions of rubble." Engineering Letters 23, no. 1: 49-54.

8 APPENDICES

8.1 Existing Stability-damage data

Table 8.1. AU and DEFLT datasets after screening for hc/h<=1.2 and removing outliers (AC).

Source	S	hc/h	Hs	Δ	Dn50	Sop	Sm	Nw	P	H2%	ξom	(Sm)^-1/3	Som	Ns	Ns*	ln(Ns)	ln(Ns*)
AU	0.12	1.20	0.05	1.65	0.0325	0.0195	0.035	1000	0.6	0.07	0.41	3.06	0.03	0.91	3.40	-0.09	1.22
AU	1.97	1.20	0.07	1.65	0.0325	0.0173	0.036	1000	0.6	0.09	0.34	3.03	0.03	1.21	4.68	0.19	1.54
AU	4.41	1.20	0.09	1.65	0.0325	0.0184	0.043	1000	0.6	0.13	0.29	2.86	0.03	1.72	6.50	0.54	1.87
AU	8.71	1.20	0.12	1.65	0.0325	0.0192	0.049	1000	0.6	0.17	0.26	2.73	0.03	2.24	8.35	0.81	2.12
AU	0.00	1.20	0.04	1.65	0.0325	0.0293	0.044	1000	0.6	0.05	0.59	2.82	0.04	0.69	2.24	-0.37	0.81
AU	0.00	1.20	0.06	1.65	0.0325	0.0328	0.054	1000	0.6	0.09	0.48	2.64	0.05	1.16	3.61	0.15	1.28
AU	1.74	1.20	0.09	1.65	0.0325	0.0361	0.065	1000	0.6	0.13	0.41	2.49	0.05	1.70	5.13	0.53	1.64
AU	3.13	1.20	0.12	1.65	0.0325	0.0372	0.072	1000	0.6	0.16	0.37	2.40	0.05	2.18	6.54	0.78	1.88
AU	0.00	1.00	0.05	1.65	0.0325	0.0203	0.034	1000	0.6	0.07	0.41	3.07	0.03	0.95	3.49	-0.05	1.25
AU	1.04	1.00	0.08	1.65	0.0325	0.0203	0.039	1000	0.6	0.11	0.34	2.94	0.03	1.42	5.20	0.35	1.65
AU	1.28	1.00	0.10	1.65	0.0325	0.0190	0.041	1000	0.6	0.13	0.29	2.90	0.03	1.77	6.64	0.57	1.89
AU	4.41	1.00	0.12	1.65	0.0325	0.0194	0.046	1000	0.6	0.17	0.26	2.79	0.03	2.26	8.40	0.81	2.13
AU	0.00	1.00	0.04	1.65	0.0325	0.0300	0.045	1000	0.6	0.05	0.59	2.82	0.04	0.71	2.28	-0.34	0.82
AU	0.35	1.00	0.06	1.65	0.0325	0.0328	0.052	1000	0.6	0.09	0.48	2.68	0.05	1.16	3.61	0.15	1.28
AU	0.58	1.00	0.09	1.65	0.0325	0.0338	0.057	1000	0.6	0.12	0.41	2.59	0.05	1.59	4.90	0.46	1.59
AU	1.74	1.00	0.11	1.65	0.0325	0.0346	0.063	1000	0.6	0.15	0.37	2.51	0.05	2.03	6.24	0.71	1.83
AU	2.67	1.00	0.13	1.65	0.0325	0.0336	0.065	1000	0.6	0.18	0.34	2.49	0.05	2.35	7.28	0.85	1.99
AU	0.00	0.86	0.07	1.65	0.0325	0.0189	0.035	1000	0.6	0.10	0.34	3.06	0.03	1.32	4.97	0.28	1.60
AU	0.35	0.86	0.10	1.65	0.0325	0.0190	0.039	1000	0.6	0.13	0.29	2.96	0.03	1.77	6.64	0.57	1.89
AU	0.81	0.86	0.12	1.65	0.0325	0.0194	0.043	1000	0.6	0.17	0.26	2.85	0.03	2.26	8.40	0.81	2.13
AU	2.67	0.86	0.14	1.65	0.0325	0.0191	0.046	1000	0.6	0.20	0.24	2.80	0.03	2.67	9.98	0.98	2.30

Table 8.2. (continued)

Source	S	hc/h	Hs	Δ	Dn50	Sop	Sm	Nw	P	H2%	ξom	(Sm)^-1/3	Som	Ns	Ns*	ln(Ns)	ln(Ns*)
AU	9.63	0.86	0.21	1.65	0.0325	0.0238	0.061	1000	0.6	0.29	0.22	2.54	0.03	3.90	13.54	1.36	2.61
AU	0.00	0.86	0.06	1.65	0.0325	0.0250	0.041	1000	0.6	0.09	0.41	2.90	0.04	1.17	4.02	0.16	1.39
AU	0.35	0.86	0.13	1.65	0.0325	0.0397	0.069	1000	0.6	0.18	0.37	2.44	0.06	2.33	6.83	0.85	1.92
AU	1.39	0.86	0.15	1.65	0.0325	0.0397	0.073	1000	0.6	0.21	0.34	2.39	0.06	2.78	8.14	1.02	2.10
AU	3.02	0.86	0.17	1.65	0.0325	0.0397	0.077	1000	0.6	0.24	0.32	2.35	0.06	3.23	9.45	1.17	2.25
AU	4.29	0.86	0.19	1.65	0.0325	0.0382	0.078	1000	0.6	0.27	0.29	2.34	0.06	3.56	10.58	1.27	2.36
AU	0.93	0.75	0.15	1.65	0.0325	0.0235	0.050	1000	0.6	0.21	0.26	2.72	0.03	2.74	9.56	1.01	2.26
AU	1.51	0.75	0.19	1.65	0.0325	0.0252	0.057	1000	0.6	0.26	0.24	2.60	0.04	3.52	12.01	1.26	2.49
AU	3.25	0.75	0.22	1.65	0.0325	0.0253	0.061	1000	0.6	0.31	0.22	2.54	0.04	4.14	14.10	1.42	2.65
AU	0.35	0.75	0.12	1.65	0.0325	0.0368	0.062	1000	0.6	0.16	0.37	2.53	0.05	2.16	6.50	0.77	1.87
AU	0.70	0.75	0.14	1.65	0.0325	0.0371	0.065	1000	0.6	0.19	0.34	2.49	0.05	2.59	7.77	0.95	2.05
AU	1.16	0.75	0.17	1.65	0.0325	0.0393	0.072	1000	0.6	0.24	0.32	2.40	0.06	3.19	9.38	1.16	2.24
AU	1.86	0.75	0.19	1.65	0.0325	0.0378	0.073	1000	0.6	0.26	0.29	2.39	0.05	3.52	10.50	1.26	2.35
AU	2.09	0.75	0.20	1.65	0.0325	0.0362	0.073	1000	0.6	0.29	0.28	2.39	0.05	3.80	11.50	1.34	2.44
AU	0.12	1.20	0.05	1.65	0.0325	0.0210	0.038	1000	0.6	0.07	0.41	2.98	0.03	0.99	3.58	-0.01	1.28
AU	1.51	1.20	0.08	1.65	0.0325	0.0200	0.041	1000	0.6	0.11	0.34	2.89	0.03	1.40	5.15	0.34	1.64
AU	5.80	1.20	0.09	1.65	0.0325	0.0188	0.044	1000	0.6	0.13	0.29	2.84	0.03	1.75	6.59	0.56	1.89
AU	9.05	1.20	0.12	1.65	0.0325	0.0186	0.048	1000	0.6	0.16	0.26	2.76	0.03	2.16	8.17	0.77	2.10
AU	0.00	1.00	0.05	1.65	0.0325	0.0191	0.032	1000	0.6	0.07	0.41	3.14	0.03	0.90	3.35	-0.11	1.21
AU	0.12	1.00	0.07	1.65	0.0325	0.0184	0.036	1000	0.6	0.10	0.34	3.04	0.03	1.29	4.87	0.25	1.58
AU	1.39	1.00	0.10	1.65	0.0325	0.0196	0.042	1000	0.6	0.14	0.29	2.87	0.03	1.83	6.78	0.60	1.91
AU	6.62	1.00	0.13	1.65	0.0325	0.0203	0.048	1000	0.6	0.18	0.26	2.75	0.03	2.37	8.68	0.86	2.16
AU	0.23	0.86	0.12	1.65	0.0325	0.0240	0.049	1000	0.6	0.17	0.29	2.74	0.03	2.24	7.76	0.81	2.05
AU	2.67	0.86	0.15	1.65	0.0325	0.0245	0.054	1000	0.6	0.21	0.26	2.64	0.04	2.85	9.82	1.05	2.28

Table 8.3. (continued)

Source	S	hc/h	Hs	Δ	Dn50	Sop	Sm	Nw	P	H2%	ξom	(Sm)^-1/3	Som	Ns	Ns*	ln(Ns)	ln(Ns*)
AU	8.01	0.86	0.18	1.65	0.0325	0.0246	0.059	1000	0.6	0.26	0.24	2.57	0.04	3.43	11.80	1.23	2.47
AU	1.04	0.75	0.15	1.65	0.0325	0.0235	0.050	1000	0.6	0.21	0.26	2.72	0.03	2.74	9.56	1.01	2.26
AU	3.71	0.75	0.18	1.65	0.0325	0.0244	0.055	1000	0.6	0.26	0.24	2.62	0.04	3.41	11.76	1.23	2.46
AU	7.31	0.75	0.22	1.65	0.0325	0.0253	0.061	1000	0.6	0.31	0.22	2.54	0.04	4.14	14.10	1.42	2.65
DEFLT	1.48	1.00	0.11	1.604	0.0344	0.0175	0.034	1000	0.5	0.15	3.28	3.08	0.02	1.90	6.66	0.64	1.90
DEFLT	4.20	1.00	0.13	1.604	0.0344	0.0208	0.041	1000	0.5	0.18	3.02	2.91	0.03	2.27	7.52	0.82	2.02
DEFLT	2.87	1.00	0.15	1.604	0.0344	0.0237	0.047	1000	0.5	0.20	2.82	2.77	0.03	2.63	8.33	0.97	2.12
DEFLT	13.53	1.00	0.17	1.604	0.0344	0.0290	0.056	1000	0.5	0.24	2.58	2.61	0.04	3.15	9.41	1.15	2.24
DEFLT	1.28	1.00	0.08	1.604	0.0344	0.0138	0.027	1000	0.5	0.12	3.69	3.33	0.02	1.50	5.70	0.41	1.74
DEFLT	3.85	1.00	0.13	1.604	0.0344	0.0131	0.032	1000	0.5	0.19	3.77	3.14	0.02	2.43	9.34	0.89	2.23
DEFLT	3.52	1.00	0.16	1.604	0.0344	0.0155	0.038	1000	0.5	0.22	3.48	2.97	0.02	2.88	10.50	1.06	2.35
DEFLT	16.91	1.00	0.20	1.604	0.0344	0.0192	0.048	1000	0.5	0.27	3.09	2.75	0.03	3.55	11.96	1.27	2.48
DEFLT	2.01	1.00	0.11	1.604	0.0344	0.0108	0.027	1000	0.5	0.16	4.16	3.35	0.01	2.01	8.26	0.70	2.11
DEFLT	0.86	1.00	0.08	1.604	0.0344	0.0077	0.019	1000	0.5	0.11	4.98	3.77	0.01	1.40	6.46	0.33	1.86
DEFLT	9.62	1.00	0.18	1.604	0.0344	0.0172	0.043	1000	0.5	0.25	3.29	2.86	0.02	3.19	11.20	1.16	2.42
DEFLT	1.59	0.75	0.15	1.604	0.0344	0.0245	0.047	1000	0.5	0.21	2.80	2.76	0.03	2.66	8.41	0.98	2.13
DEFLT	4.64	0.75	0.18	1.604	0.0344	0.0298	0.056	1000	0.5	0.25	2.57	2.61	0.04	3.17	9.44	1.15	2.25
DEFLT	4.63	0.75	0.20	1.604	0.0344	0.0327	0.063	1000	0.5	0.27	2.43	2.51	0.04	3.55	10.18	1.27	2.32
DEFLT	10.10	0.75	0.22	1.604	0.0344	0.0360	0.069	1000	0.5	0.30	2.34	2.44	0.05	3.91	10.95	1.36	2.39
DEFLT	1.45	0.75	0.12	1.604	0.0344	0.0197	0.038	1000	0.5	0.16	3.12	2.97	0.03	2.10	7.12	0.74	1.96
DEFLT	1.81	0.75	0.16	1.604	0.0344	0.0263	0.052	1000	0.5	0.23	2.68	2.68	0.03	2.92	8.93	1.07	2.19
DEFLT	7.66	0.75	0.19	1.604	0.0344	0.0193	0.047	1000	0.5	0.27	3.10	2.76	0.03	3.50	11.80	1.25	2.47
DEFLT	4.23	0.75	0.16	1.604	0.0344	0.0157	0.040	1000	0.5	0.23	3.39	2.94	0.02	2.92	10.46	1.07	2.35
DEFLT	2.00	0.75	0.14	1.604	0.0344	0.0134	0.034	1000	0.5	0.19	3.68	3.10	0.02	2.48	9.39	0.91	2.24

Table 8.4. (continued)

Source	S	hc/h	Hs	Δ	Dn50	Sop	Sm	Nw	P	H2%	ξom	(Sm)^-1/3	Som	Ns	Ns*	ln(Ns)	ln(Ns*)
DEFLT	0.97	0.75	0.11	1.604	0.0344	0.0108	0.027	1000	0.5	0.15	4.11	3.33	0.01	1.99	8.11	0.69	2.09
DEFLT	13.47	0.75	0.22	1.604	0.0344	0.0207	0.054	1000	0.5	0.31	2.88	2.64	0.03	3.97	12.76	1.38	2.55
DEFLT	2.47	1.00	0.11	1.604	0.0344	0.0175	0.034	3000	0.5	0.15	3.28	3.08	0.02	1.90	6.66	0.64	1.90
DEFLT	4.40	1.00	0.13	1.604	0.0344	0.0208	0.041	3000	0.5	0.18	3.02	2.91	0.03	2.27	7.52	0.82	2.02
DEFLT	8.63	1.00	0.15	1.604	0.0344	0.0237	0.047	3000	0.5	0.20	2.82	2.77	0.03	2.63	8.33	0.97	2.12
DEFLT	20.54	1.00	0.17	1.604	0.0344	0.0290	0.056	3000	0.5	0.24	2.58	2.61	0.04	3.15	9.41	1.15	2.24
DEFLT	1.72	1.00	0.08	1.604	0.0344	0.0138	0.027	3000	0.5	0.12	3.69	3.33	0.02	1.50	5.70	0.41	1.74
DEFLT	4.66	1.00	0.13	1.604	0.0344	0.0131	0.032	3000	0.5	0.19	3.77	3.14	0.02	2.43	9.34	0.89	2.23
DEFLT	5.52	1.00	0.16	1.604	0.0344	0.0155	0.038	3000	0.5	0.22	3.48	2.97	0.02	2.88	10.50	1.06	2.35
DEFLT	46.38	1.00	0.20	1.604	0.0344	0.0192	0.048	3000	0.5	0.27	3.09	2.75	0.03	3.55	11.96	1.27	2.48
DEFLT	2.92	1.00	0.11	1.604	0.0344	0.0108	0.027	3000	0.5	0.16	4.16	3.35	0.01	2.01	8.26	0.70	2.11
DEFLT	1.02	1.00	0.08	1.604	0.0344	0.0077	0.019	3000	0.5	0.11	4.98	3.77	0.01	1.40	6.46	0.33	1.86
DEFLT	17.87	1.00	0.18	1.604	0.0344	0.0172	0.043	3000	0.5	0.25	3.29	2.86	0.02	3.19	11.20	1.16	2.42
DEFLT	2.53	0.75	0.15	1.604	0.0344	0.0245	0.047	3000	0.5	0.21	2.80	2.76	0.03	2.66	8.41	0.98	2.13
DEFLT	7.02	0.75	0.18	1.604	0.0344	0.0298	0.056	3000	0.5	0.25	2.57	2.61	0.04	3.17	9.44	1.15	2.25
DEFLT	6.77	0.75	0.20	1.604	0.0344	0.0327	0.063	3000	0.5	0.27	2.43	2.51	0.04	3.55	10.18	1.27	2.32
DEFLT	13.54	0.75	0.22	1.604	0.0344	0.0360	0.069	3000	0.5	0.30	2.34	2.44	0.05	3.91	10.95	1.36	2.39
DEFLT	1.71	0.75	0.12	1.604	0.0344	0.0197	0.038	3000	0.5	0.16	3.12	2.97	0.03	2.10	7.12	0.74	1.96
DEFLT	2.05	0.75	0.16	1.604	0.0344	0.0263	0.052	3000	0.5	0.23	2.68	2.68	0.03	2.92	8.93	1.07	2.19
DEFLT	11.66	0.75	0.19	1.604	0.0344	0.0193	0.047	3000	0.5	0.27	3.10	2.76	0.03	3.50	11.80	1.25	2.47
DEFLT	7.43	0.75	0.16	1.604	0.0344	0.0157	0.040	3000	0.5	0.23	3.39	2.94	0.02	2.92	10.46	1.07	2.35
DEFLT	3.11	0.75	0.14	1.604	0.0344	0.0134	0.034	3000	0.5	0.19	3.68	3.10	0.02	2.48	9.39	0.91	2.24
DEFLT	1.20	0.75	0.11	1.604	0.0344	0.0108	0.027	3000	0.5	0.15	4.11	3.33	0.01	1.99	8.11	0.69	2.09
DEFLT	16.96	0.75	0.22	1.604	0.0344	0.0207	0.054	3000	0.5	0.31	2.88	2.64	0.03	3.97	12.76	1.38	2.55

8.2 Data collection program and damage measurements

Table 8.5. Data collection program design and damage measurements (in bold)

Series	Exper. family #	hc/h	Nw	Hs (m)	Tm (sec)	L (m)	Cot α	S for CX1 (Dn50 =18mm)	Ns	Ns*	Exper. family. #	S for CX2 (Dn50 =29mm)	Ns	Ns*	hc (m)	h (m)
1	1.00	1.2	1500	0.05	2.92	0.92	1.5	**13.2**	1.65	4.58	2.00	**3.1**	1.006	2.794	0.12	0.1
	1.01	1.2	4500	0.05	2.92	0.92	1.5	**24.3**	1.65	4.58	2.01	**3.5**	1.006	2.794	0.12	0.1
	1.02	1.2	9000	0.05	2.92	0.92	1.5	**26.0**	1.65	4.58	2.02	**3.5**	1.006	2.794	0.12	0.1
2	1.03	1.2	1500	0.06	2.08	0.92	1.5	**6.8**	1.69	4.65	2.03	**1.5**	1.029	2.837	0.12	0.1
	1.04	1.2	4500	0.06	2.08	0.92	1.5	**7.8**	1.69	4.65	2.04	**1.3**	1.029	2.837	0.12	0.1
	1.05	1.2	9000	0.06	2.08	0.92	1.5	**11.2**	1.69	4.65	2.05	**1.5**	1.029	2.837	0.12	0.1
3	1.06	1.2	1500	0.07	1.44	0.92	1.5	**16.9**	2.72	6.40	2.06	**1.6**	1.661	3.903	0.12	0.1
	1.07	1.2	4500	0.07	1.44	0.92	1.5	**25.0**	2.72	6.40	2.07	**2.3**	1.661	3.903	0.12	0.1
	1.08	1.2	9000	0.07	1.44	0.92	1.5	**30.3**	2.72	6.40	2.08	**3.6**	1.661	3.903	0.12	0.1
	1.09	1.2	15750	0.07	1.44	0.92	1.5	**34.2**	2.72	6.40	2.09	**4.1**	1.661	3.903	0.12	0.1
	1.10	1.2	24000	0.07	1.44	0.92	1.5	**37.7**	2.72	6.40	2.1	**5.1**	1.661	3.903	0.12	0.1
4	1.11	1	1500	0.05	2.92	0.92	1.5	**2.1**	1.65	4.58	2.11	**0.4**	1.006	2.794	0.1	0.1
	1.12	1	4500	0.05	2.92	0.92	1.5	**2.7**	1.65	4.58	2.12	**0.8**	1.006	2.794	0.1	0.1
	1.13	1	9000	0.05	2.92	0.92	1.5	**6.9**	1.65	4.58	2.13	**1.2**	1.006	2.794	0.1	0.1
5	1.14	1	1500	0.06	2.08	0.92	1.5	**5.4**	1.69	4.65	2.14	**2.7**	1.029	2.837	0.1	0.1
	1.15	1	4500	0.06	2.08	0.92	1.5	**9.4**	1.69	4.65	2.15	**2.8**	1.029	2.837	0.1	0.1
	1.16	1	9000	0.06	2.08	0.92	1.5	**10.7**	1.69	4.65	2.16	**3.0**	1.029	2.837	0.1	0.1
6	1.17	1	1500	0.07	1.44	0.92	1.5	**8.1**	2.72	6.40	2.17	**2.2**	1.661	3.903	0.1	0.1
	1.18	1	4500	0.07	1.44	0.92	1.5	**11.6**	2.72	6.40	2.18	**3.4**	1.661	3.903	0.1	0.1
	1.19	1	9000	0.07	1.44	0.92	1.5	**11.8**	2.72	6.40	2.19	**3.7**	1.661	3.903	0.1	0.1

Table 8.5 (continued)

7	1.20	0.75	1500	0.06	2.08	0.92	1.5	**2.0**	1.69	4.65	2.2	**0.8**	1.029	2.837	0.075	0.1
	1.21	0.75	4500	0.06	2.08	0.92	1.5	**2.3**	1.69	4.65	2.21	**0.8**	1.029	2.837	0.075	0.1
	1.22	0.75	9000	0.06	2.08	0.92	1.5	**2.2**	1.69	4.65	2.22	**0.8**	1.029	2.837	0.075	0.1
	1.23	0.75	15750	0.06	2.08	0.92	1.5	**2.3**	1.69	4.65	2.23	**0.9**	1.029	2.837	0.075	0.1
	1.24	0.75	24000	0.06	2.08	0.92	1.5	**2.7**	1.69	4.65	2.24	**0.9**	1.029	2.837	0.075	0.1
8	1.25	0.75	1500	0.05	2.92	0.92	1.5	**3.9**	1.65	4.58	2.25	**0.9**	1.006	2.794	0.075	0.1
	1.26	0.75	4500	0.05	2.92	0.92	1.5	**4.9**	1.65	4.58	2.26	**0.8**	1.006	2.794	0.075	0.1
	1.27	0.75	9000	0.05	2.92	0.92	1.5	**4.9**	1.65	4.58	2.27	**0.9**	1.006	2.794	0.075	0.1
9	1.28	0.50	1500	0.07	1.44	0.92	1.5	**1.1**	1.69	4.65	2.28	**0.6**	1.029	2.837	0.05	0.1
	1.29	0.50	4500	0.07	1.44	0.92	1.5	**1.5**	1.69	4.65	2.29	**0.9**	1.029	2.837	0.05	0.1
	1.30	0.50	9000	0.07	1.44	0.92	1.5	**1.5**	1.69	4.65	2.3	**1.1**	1.029	2.837	0.05	0.1
10	1.31	1.20	1500	0.05	2.92	0.92	2	**13.5**	1.65	4.58	2.31	**3.2**	1.006	2.794	0.12	0.1
	1.32	1.20	4500	0.05	2.92	0.92	2	**21.7**	1.65	4.58	2.32	**3.6**	1.006	2.794	0.12	0.1
	1.33	1.20	9000	0.05	2.92	0.92	2	**31.8**	1.65	4.58	2.33	**5.4**	1.006	2.794	0.12	0.1
11	1.34	1.20	1500	0.06	2.08	0.92	2	**4.1**	1.69	4.65	2.34	**0.6**	1.029	2.837	0.12	0.1
	1.35	1.20	4500	0.06	2.08	0.92	2	**4.1**	1.69	4.65	2.35	**0.7**	1.029	2.837	0.12	0.1
	1.36	1.20	9000	0.06	2.08	0.92	2	**4.2**	1.69	4.65	2.36	**1.1**	1.029	2.837	0.12	0.1
12	1.37	1.20	1500	0.07	1.44	0.92	2	**18.1**	2.72	6.40	2.37	**2.0**	1.661	3.903	0.12	0.1
	1.38	1.20	4500	0.07	1.44	0.92	2	**27.3**	2.72	6.40	2.38	**3.7**	1.661	3.903	0.12	0.1
	1.39	1.20	9000	0.07	1.44	0.92	2	**33.0**	2.72	6.40	2.39	**4.2**	1.661	3.903	0.12	0.1
	1.40	1.20	15750	0.07	1.44	0.92	2	**35.4**	2.72	6.40	2.4	**4.2**	1.661	3.903	0.12	0.1
	1.41	1.20	24000	0.07	1.44	0.92	2	**39.1**	2.72	6.40	2.41	**4.7**	1.661	3.903	0.12	0.1

Table 8.5 (continued)

13	1.42	1	1500	0.05	2.92	0.92	2	**4.5**	1.65	4.58	2.42	**0.9**	1.006	2.794	0.1	0.1
	1.43	1	4500	0.05	2.92	0.92	2	**4.1**	1.65	4.58	2.43	**0.6**	1.006	2.794	0.1	0.1
	1.44	1	9000	0.05	2.92	0.92	2	**4.7**	1.65	4.58	2.44	**0.8**	1.006	2.794	0.1	0.1
14	1.45	1	1500	0.06	2.08	0.92	2	**3.3**	1.69	4.65	2.45	**0.4**	1.029	2.837	0.1	0.1
	1.46	1	4500	0.06	2.08	0.92	2	**4.3**	1.69	4.65	2.46	**0.7**	1.029	2.837	0.1	0.1
	1.47	1	9000	0.06	2.08	0.92	2	**4.9**	1.69	4.65	2.47	**0.9**	1.029	2.837	0.1	0.1
15	1.48	1	1500	0.07	1.44	0.92	2	**8.0**	2.72	6.40	2.48	**1.1**	1.661	3.903	0.1	0.1
	1.49	1	4500	0.07	1.44	0.92	2	**11.5**	2.72	6.40	2.49	**1.4**	1.661	3.903	0.1	0.1
	1.50	1	9000	0.07	1.44	0.92	2	**15.5**	2.72	6.40	2.5	**1.4**	1.661	3.903	0.1	0.1
16	1.51	0.75	1500	0.06	2.08	0.92	2	**4.3**	1.69	4.65	2.51	**1.3**	1.029	2.837	0.075	0.1
	1.52	0.75	4500	0.06	2.08	0.92	2	**5.3**	1.69	4.65	2.52	**0.9**	1.029	2.837	0.075	0.1
	1.53	0.75	9000	0.06	2.08	0.92	2	**5.2**	1.69	4.65	2.53	**0.8**	1.029	2.837	0.075	0.1
	1.54	0.75	15750	0.06	2.08	0.92	2	**7.1**	1.69	4.65	2.54	**1.2**	1.029	2.837	0.075	0.1
	1.55	0.75	24000	0.06	2.08	0.92	2	**7.3**	1.69	4.65	2.55	**1.4**	1.029	2.837	0.075	0.1
17	1.56	0.75	1500	0.05	2.92	0.92	2	**7.7**	1.65	4.58	2.56	**0.7**	1.006	2.794	0.075	0.1
	1.57	0.75	4500	0.05	2.92	0.92	2	**7.5**	1.65	4.58	2.57	**0.9**	1.006	2.794	0.075	0.1
	1.58	0.75	9000	0.05	2.92	0.92	2	**8.8**	1.65	4.58	2.58	**1.1**	1.006	2.794	0.075	0.1
18	1.59	0.5	1500	0.07	1.44	0.92	2	**0.7**	1.69	4.65	2.59	**0.1**	1.029	2.837	0.05	0.1
	1.60	0.5	4500	0.07	1.44	0.92	2	**1.1**	1.69	4.65	2.6	**0.2**	1.029	2.837	0.05	0.1
	1.61	0.5	9000	0.07	1.44	0.92	2	**1.3**	1.69	4.65	2.61	**0.4**	1.029	2.837	0.05	0.1

8.3 Stone characteristics data

8.3.1 Density

Table 8.6. IQR of specific density of Stone A (green) and Stone B (red).

Parameters	Stone A (Green)	Stone B (Red)
Q1	2.294	2.428
10th Percentile	2.269	2.420
median	2.383	2.461
90th Percentile	2.533	2.494
Q3	2.485	2.490

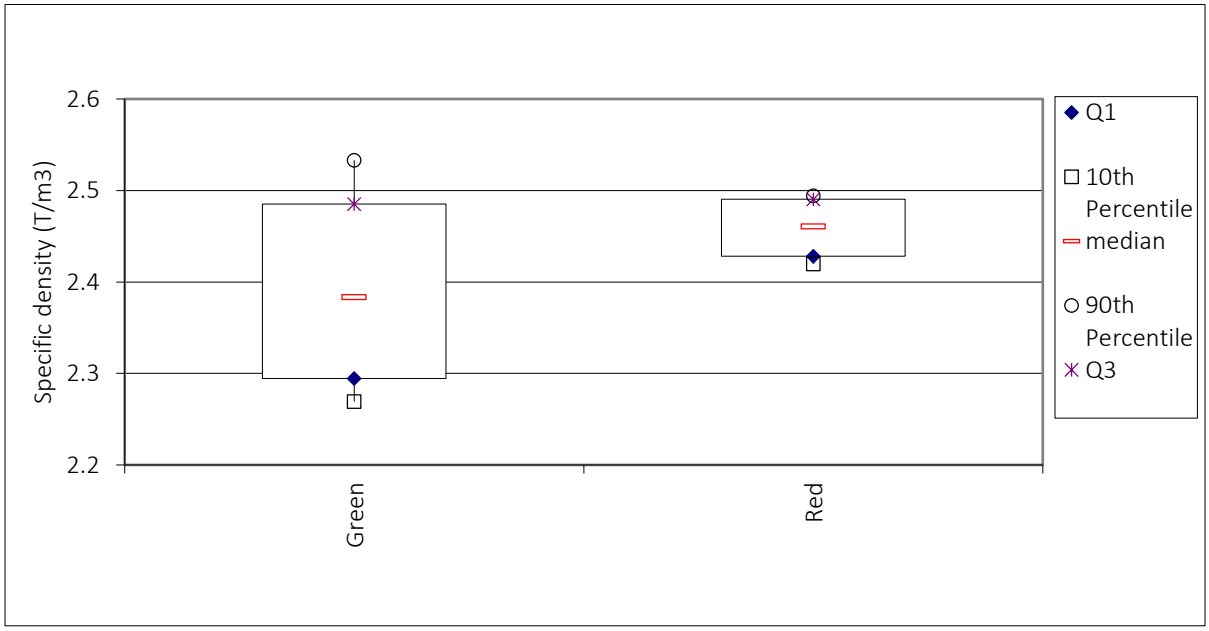

Figure 8.1. Specific density box-whiskers plot of 4 tests for red and green stones.

8.3.2 Porosity

Table 8.7. Porosity of Stone A and B from 6 measurements

Class A (green)				Class B (red)			
Ma (g)	Va (ml)	Mw (g)	P	Ma (g)	Va (ml)	Mw (g)	P
1334.5	1000.0	574	0.57	1334.5	1000.0	506	0.51
2761.3	2000.0	968	0.48	2761.3	2000.0	934	0.47
4295.2	3000.0	1382	0.46	4188.2	3000.0	1355	0.45
1334.5	1000.0	387	0.39	1334.5	1000.0	537	0.54
2761.3	2000.0	772	0.39	2761.3	2000.0	953	0.48
4104.2	3000.0	1206	0.40	4271.8	3000.0	1372	0.46

Table 8.8. IQR of porosity of Stone A and B

Parameters	Stone A (green)	Stone B (red)	A+B (green+red)
Q1	0.391	0.460	0.439
10th Percentile	0.386	0.452	0.386
median	0.431	0.472	0.464
90th Percentile	0.574	0.537	0.574
Q3	0.478	0.499	0.490

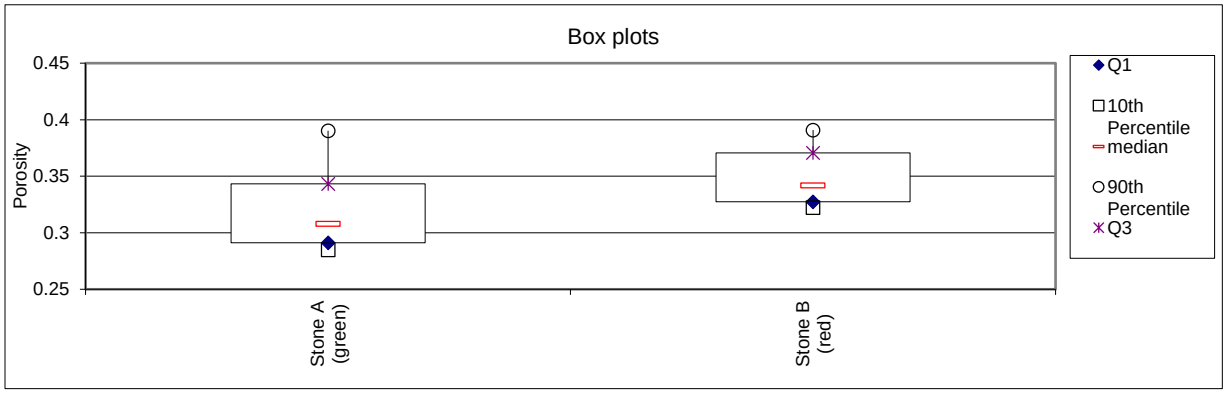

Figure 8.2. Porosity box-whiskers plot of Stone A (green) and B (red).

8.3.3 Gradation

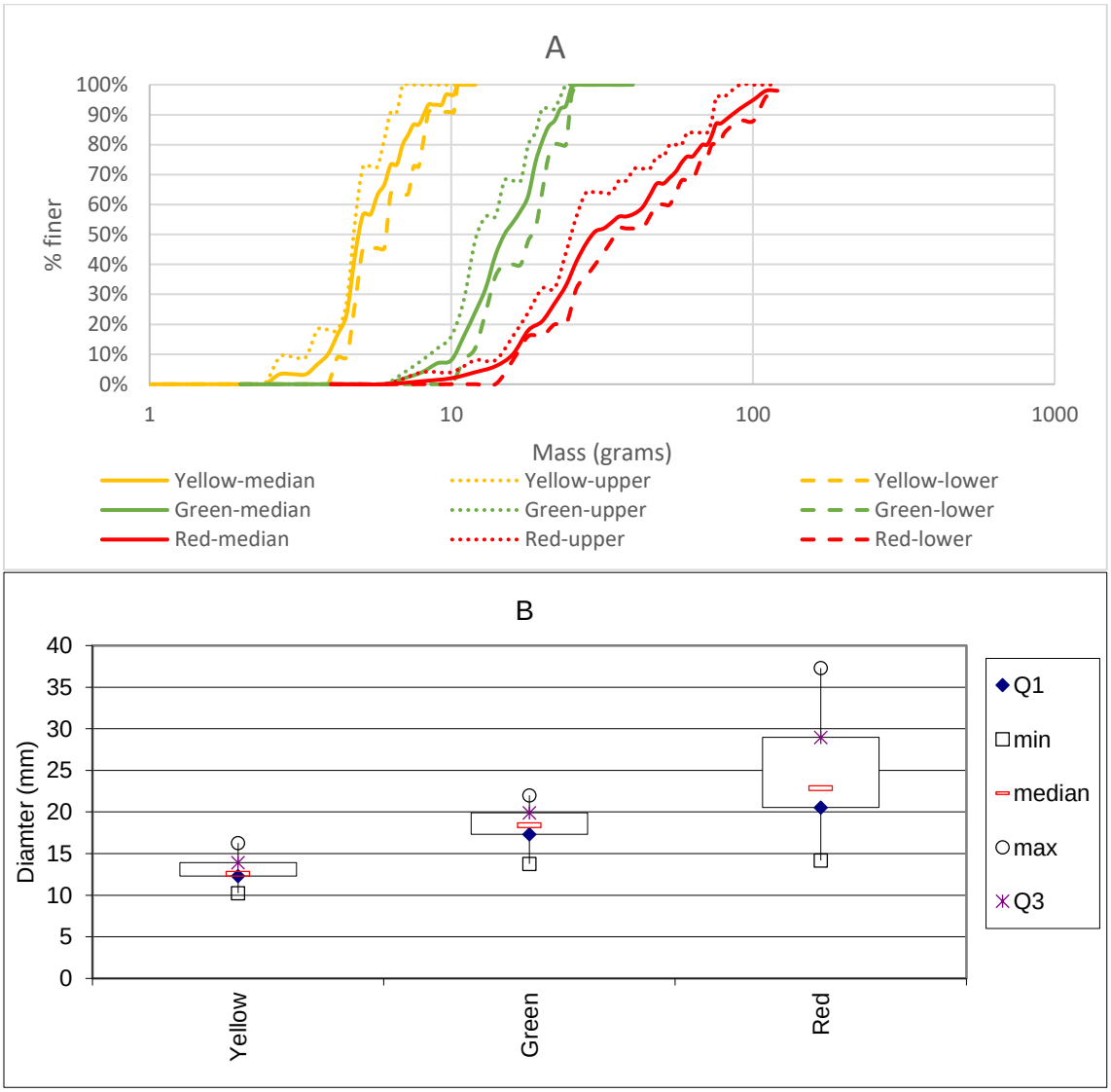

Figure 8.3. Gradation (% finer mass, grams) of yellow, green and red stones (a) and box-whiskers plot of diameters (b).

Table 8.9. Summary of yellow, green and red stones mass (grams) and diameters (mm).

	Yellow	Green	Red
M_{15}	4.2	11.0	17.8
M_{50}	4.8	15.1	28.9
M_{85}	7.1	20.7	73.9
M_{85}:M_{15}	1.7	1.9	4.2
D_{15}	12.0	16.6	19.5
D_{50}	**12.6**	**18.4**	**22.9**
D_{85}	14.3	20.4	31.3
D_{85}:D_{15}	1.2	1.2	1.6

8.4 Wave Gauge Calibration

Table 8.10. Linear wave gauge readings for G1 and G2 for up down and up directions

Reading	G1 (down)	G2 (down)	G1 (up)	G2 (up)
1	0.05714	0.1	0.10526	0.125
2	0.13333	0.1	0.11111	0.1
3	0.1	0.1	0.08696	0.1
4	0.08696	0.1	0.11765	0.11111
5	0.11111	0.08333	0.11111	0.1

Table 8.11. Box-whiskers analysis of gauges 1 and 2

Parameters	G1 (down)	G2 (down)	G1 (up)	G2 (up)	G1+G2 (up+down)
Q1	0.087	0.100	0.105	0.100	0.100
10th Percentile	0.069	0.090	0.094	0.100	0.087
median	0.100	0.100	0.111	0.100	0.100
90th Percentile	0.124	0.100	0.115	0.119	0.118
Q3	0.111	0.100	0.111	0.111	0.111

8.5 Surface, erosion and damage data

<table>
<tr><td colspan="3">Test series family: Series 1

Hs = 68mm, Tp =3.5s , hc/h = 1.2, Cotα = 1.5</td></tr>
<tr><td>Nw</td><td>Green stones Dn50 = 18mm</td><td>Red stones Dn50 = 29mm</td></tr>
<tr><td>0</td><td> 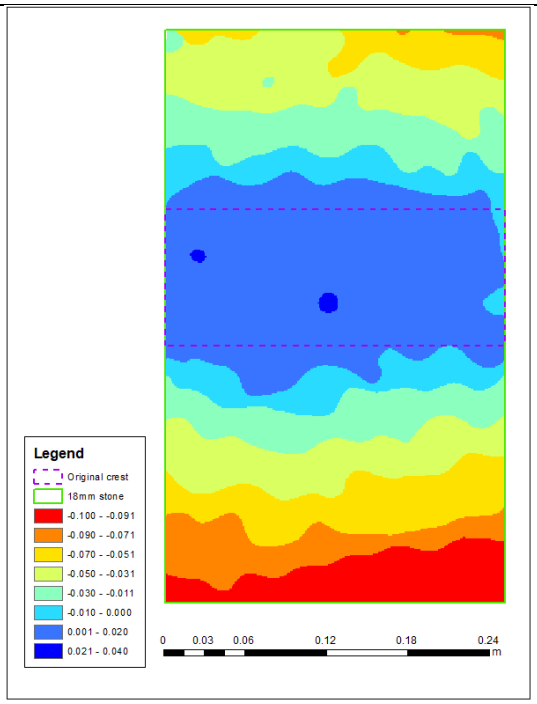
</td><td> 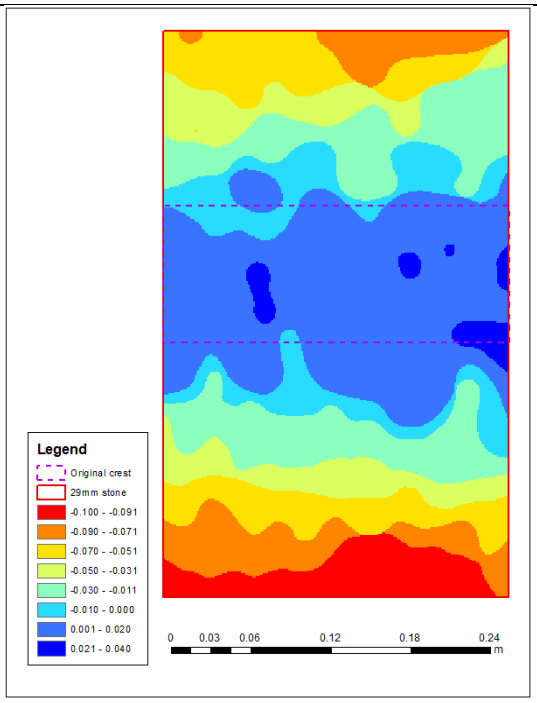
</td></tr>
<tr><td>1500</td><td> 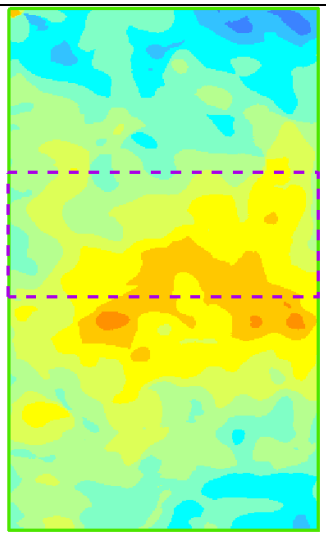
S = 13.24</td><td> 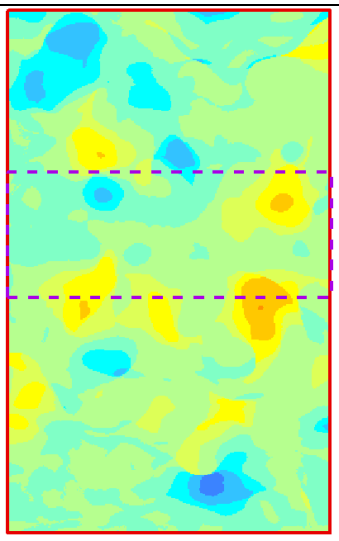
S = 3.99</td></tr>
</table>

4500	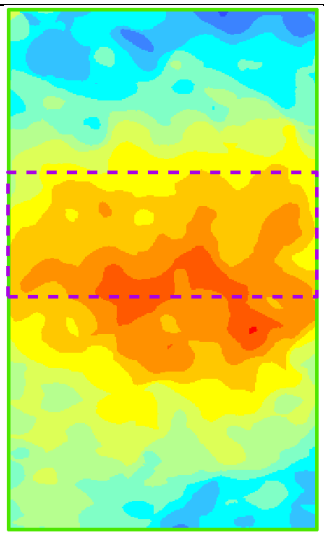 S = 24.26	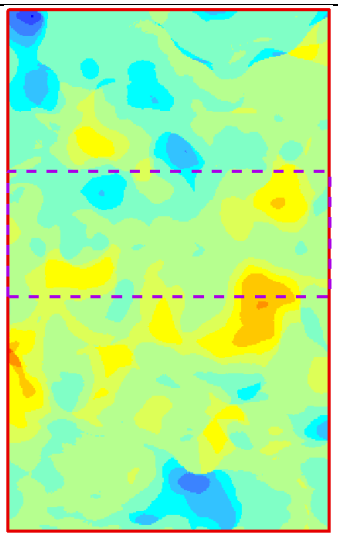 S = 4.53
9000	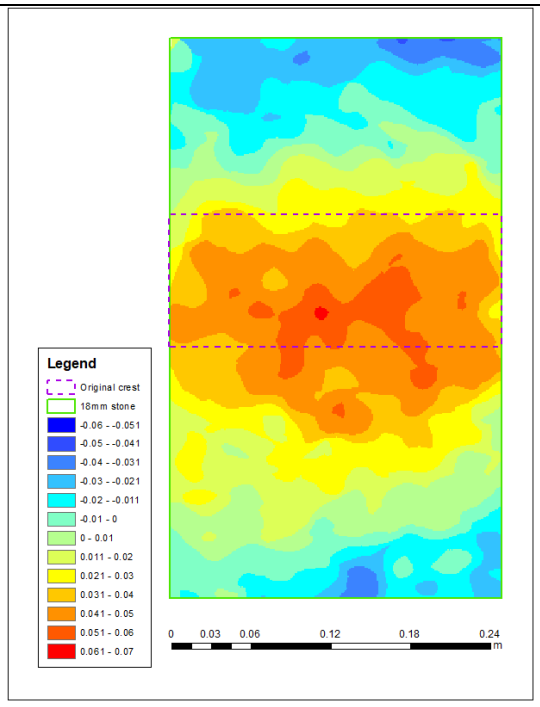 S = 26.04	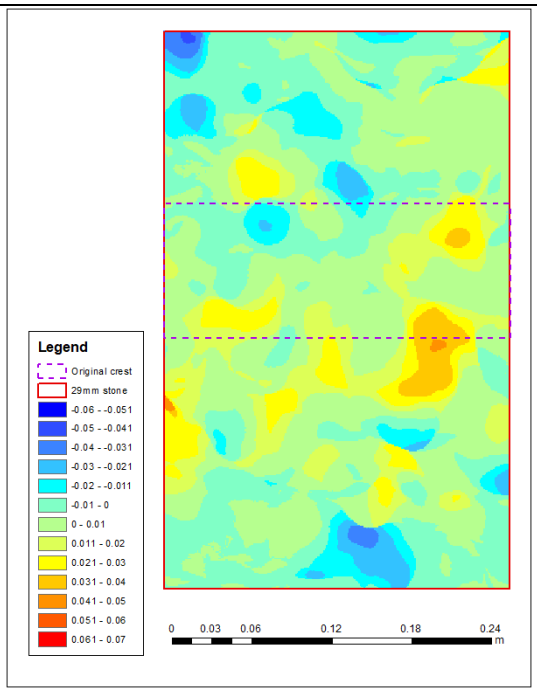 S = 4.49

<table>
<tr><td colspan="3">Test series family: Series 2

Hs = 75mm, Tp =2.5s , hc/h = 1.2, Cotα = 1.5</td></tr>
<tr><td>Nw</td><td>Green stones Dn50 = 18mm</td><td>Red stones Dn50 = 29mm</td></tr>
<tr><td>0</td><td> 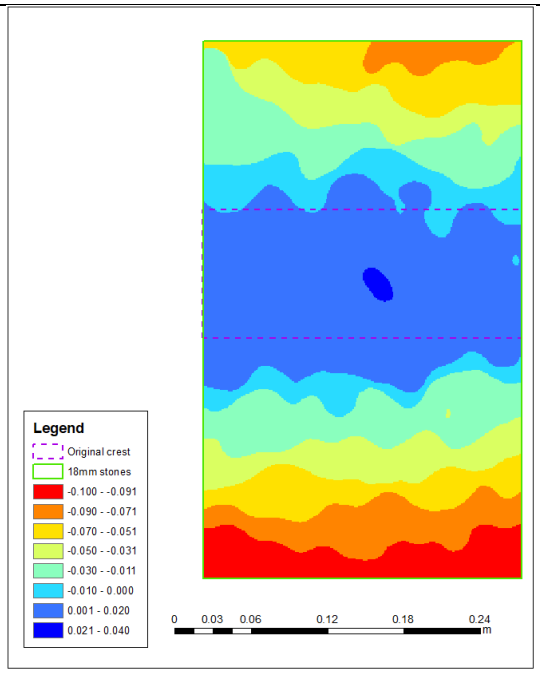
</td><td> 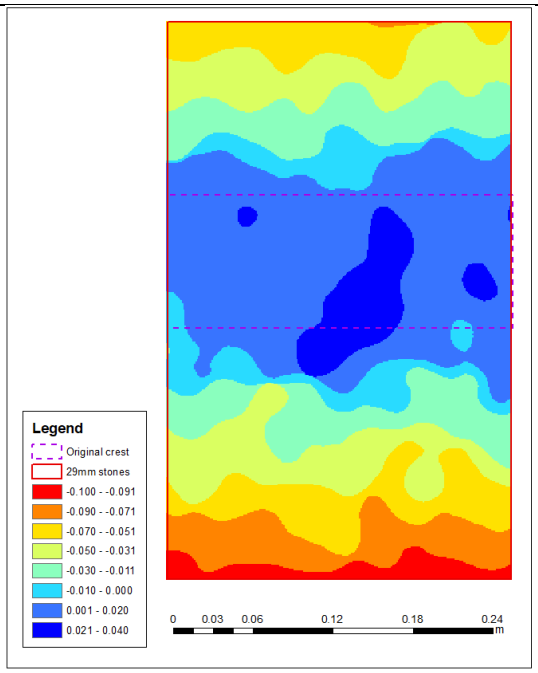
</td></tr>
<tr><td>1500</td><td> 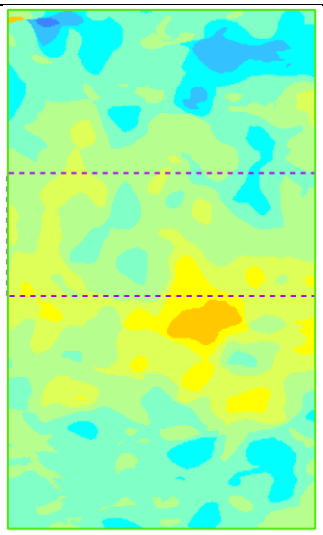
S = 6.82</td><td> 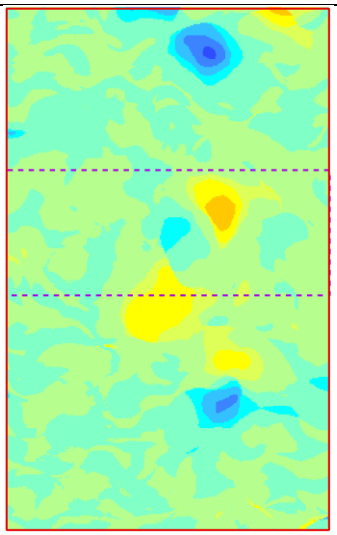
S = 1.97</td></tr>
</table>

4500	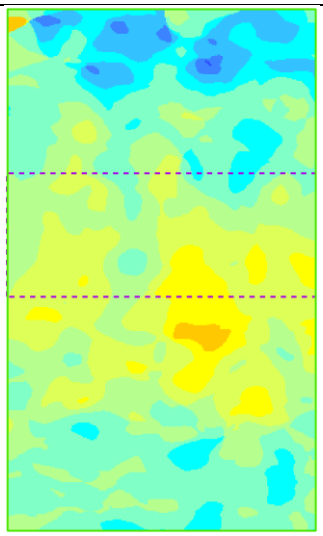 S = 7.76	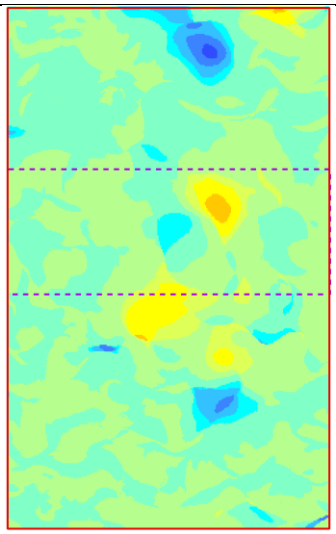 S = 1.67
9000	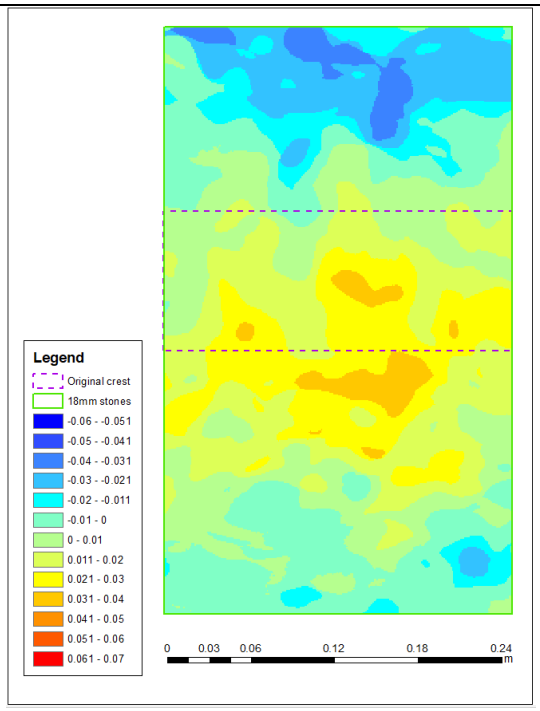 S = 11.22	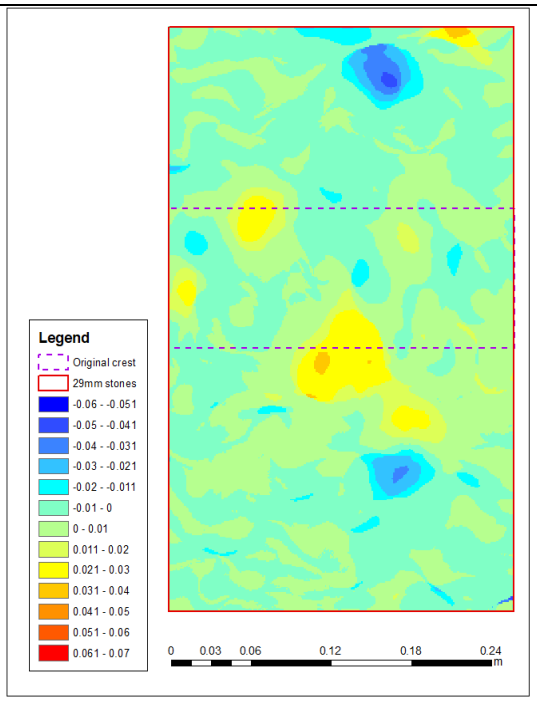 S = 1.96

Test series family: Series 3 Hs = 120mm, Tp =1.7s , hc/h = 1.2, Cotα = 1.5		
Nw	Green stones Dn50 = 18mm	Red stones Dn50 = 29mm
0	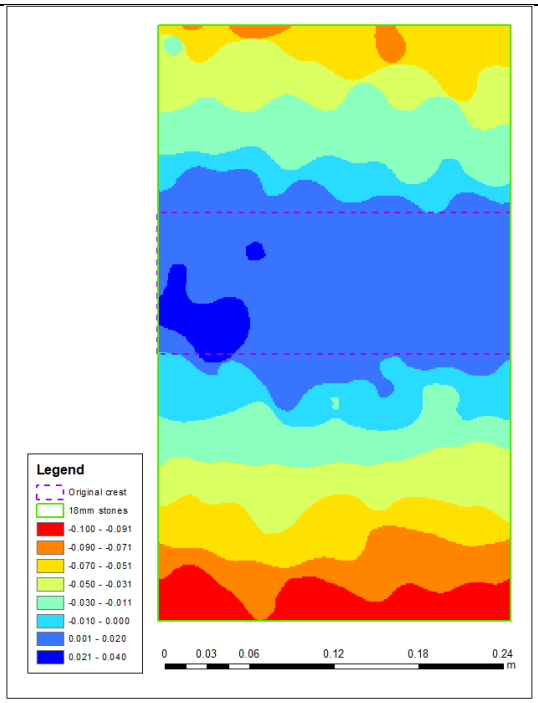	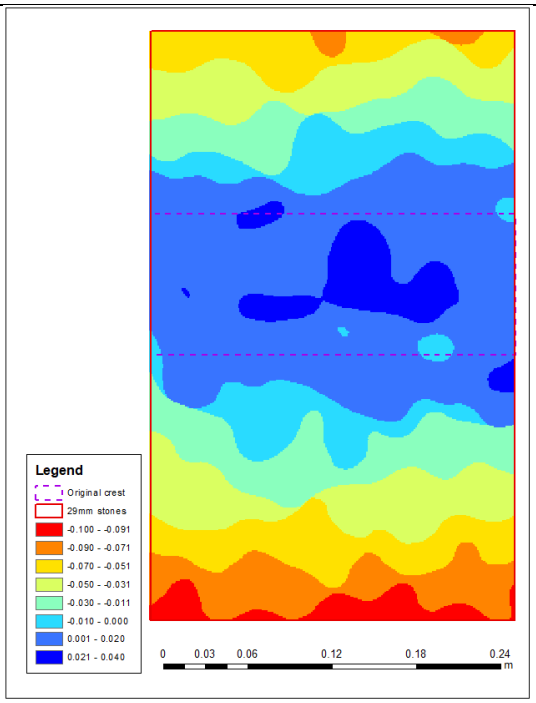
1500	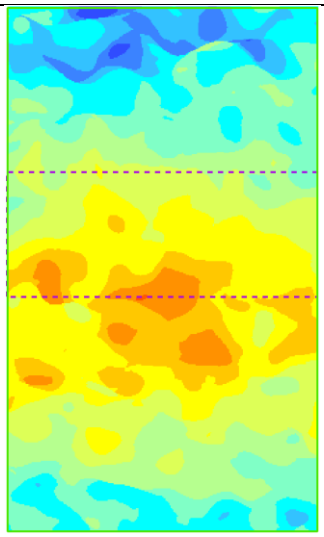 S = 16.92	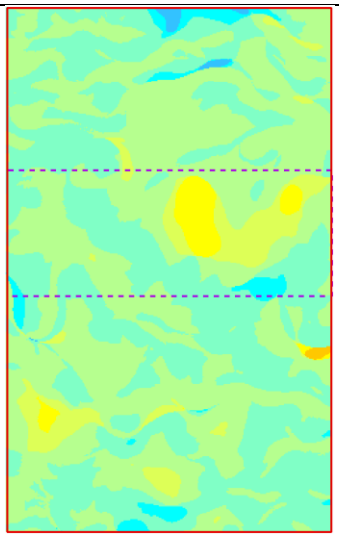 S = 2.10

4500	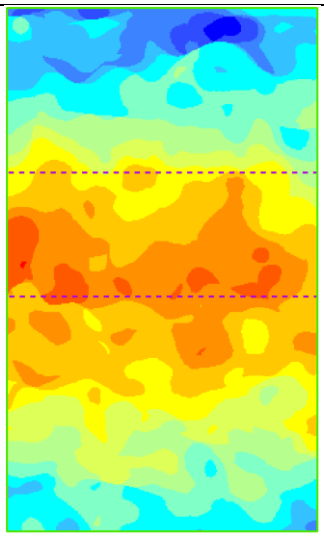 S = 24.96	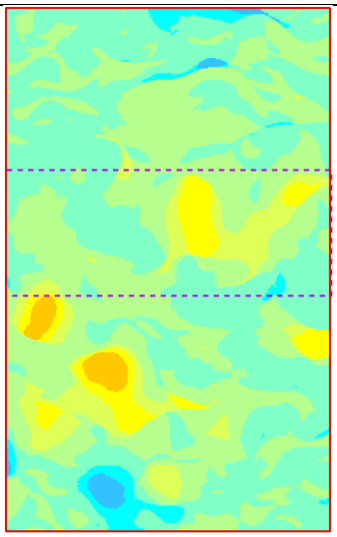 S = 2.96
9000	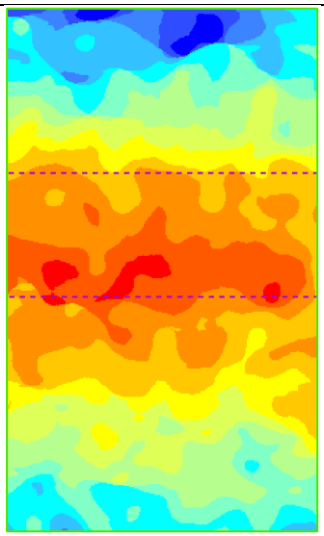 S = 30.34	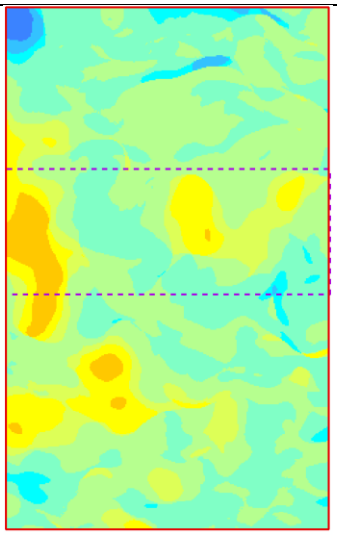 S = 4.56

15750	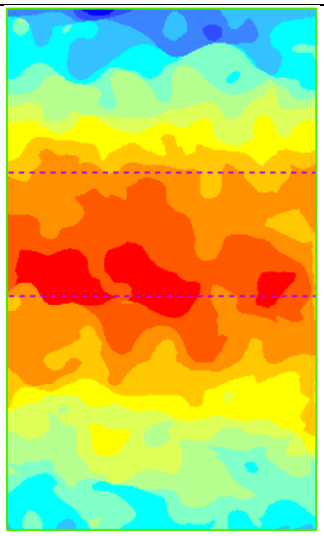 S = 34.16	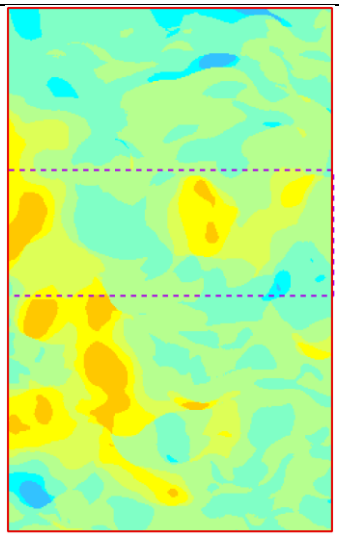 S = 5.27
24000	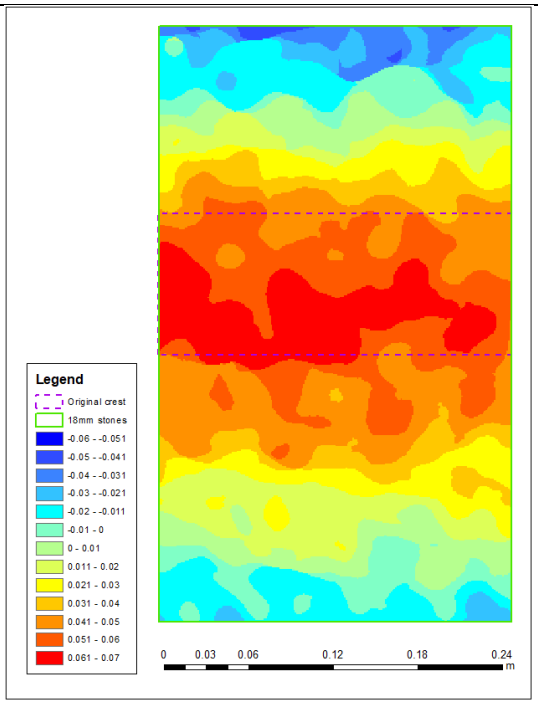 S = 37.72	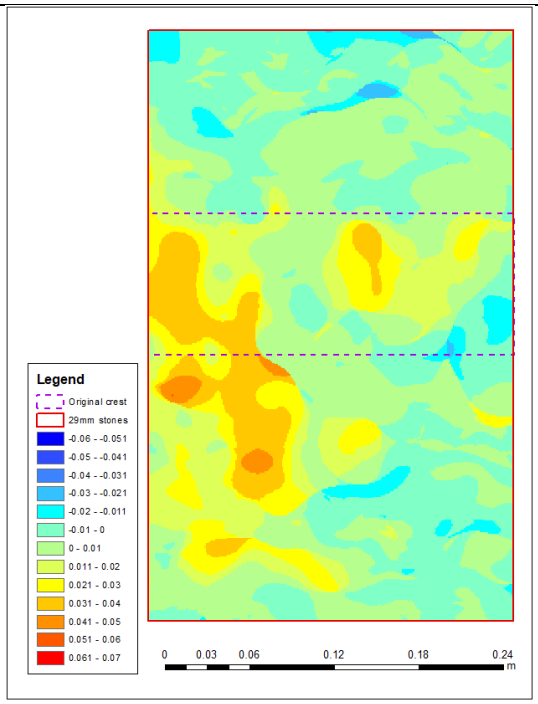 S = 6.48

<table>
<tr><td colspan="3">Test series family: Series 4

Hs = 68mm, Tp =3.5s , hc/h = 1, Cotα = 1.5</td></tr>
<tr><td>Nw</td><td>Green stones Dn50 = 18mm</td><td>Red stones Dn50 = 29mm</td></tr>
<tr><td>0</td><td> 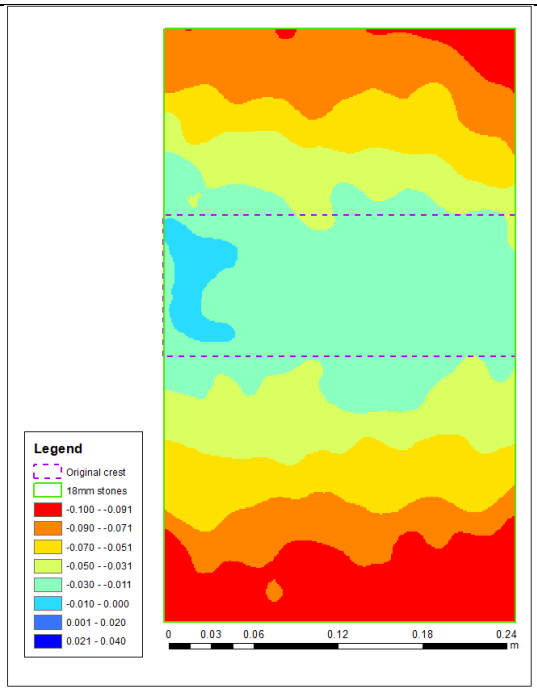
</td><td> 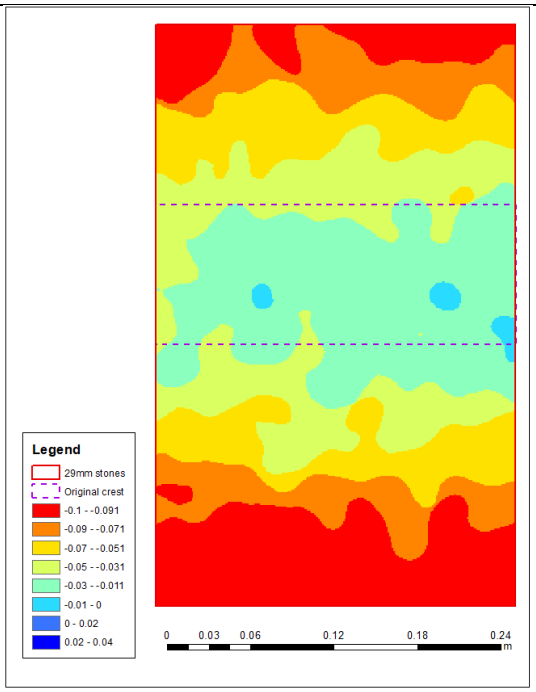
</td></tr>
<tr><td>1500</td><td> 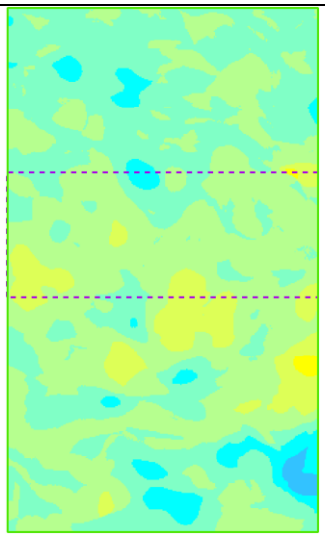
S = 2.11</td><td> 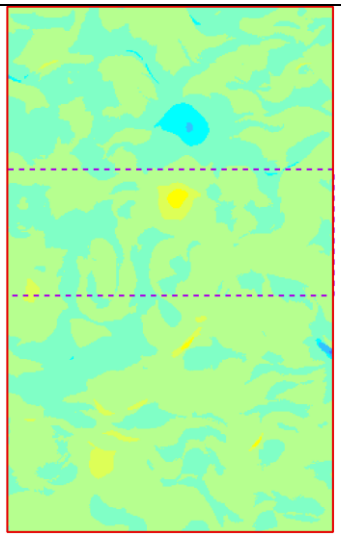
S = 0.49</td></tr>
</table>

4500	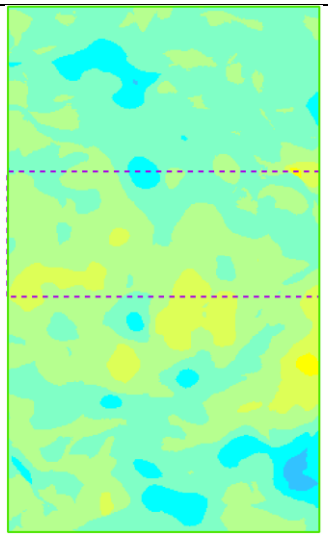 S = 2.69	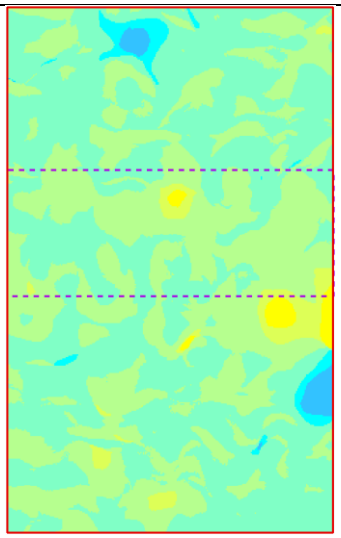 S = 1.00
9000	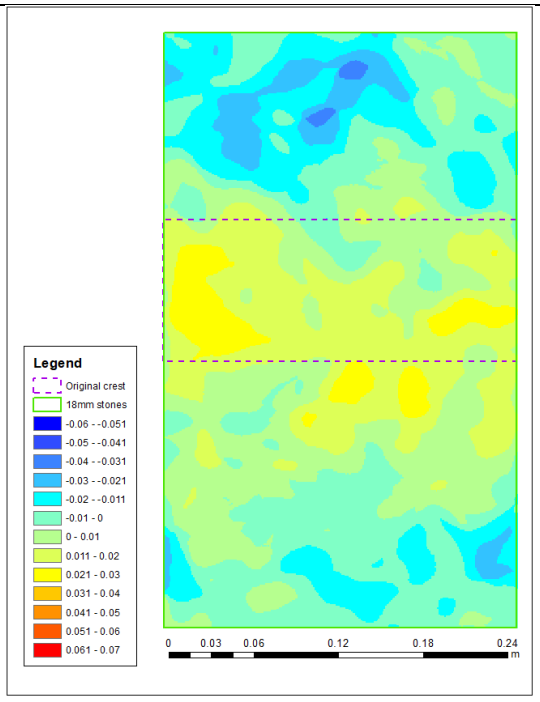 S = 6.87	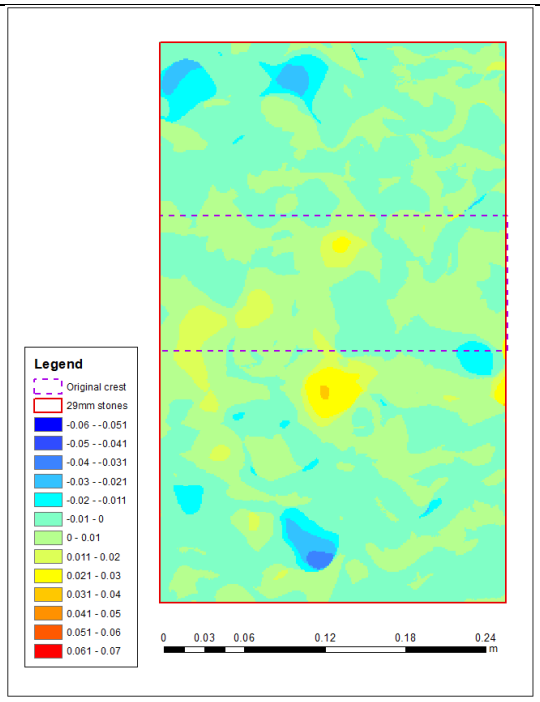 S = 1.55

Test series family: Series 5 Hs = 75mm, Tp =2.5s , hc/h = 1, Cotα = 1.5		
Nw	Green stones Dn50 = 18mm	Red stones Dn50 = 29mm
0	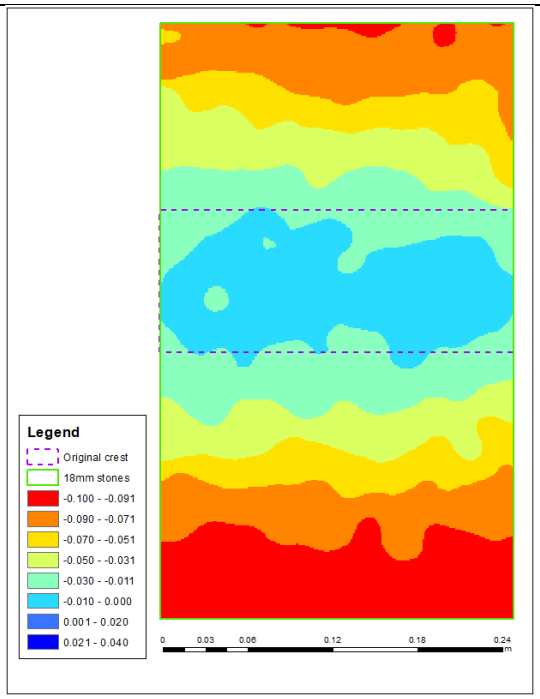	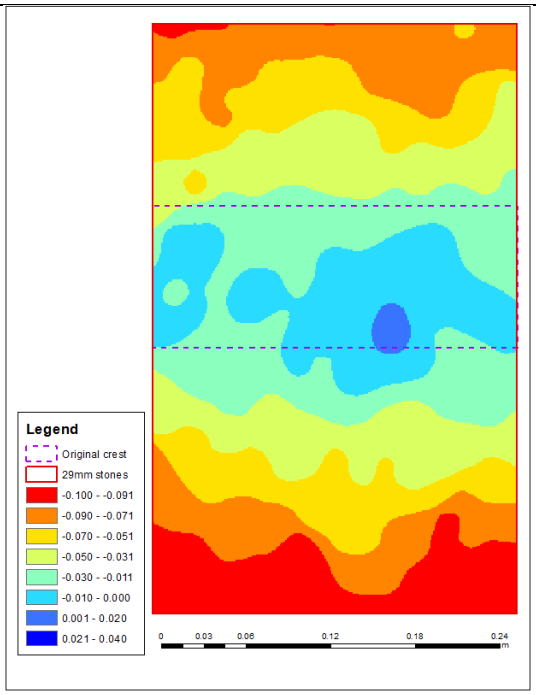
1500	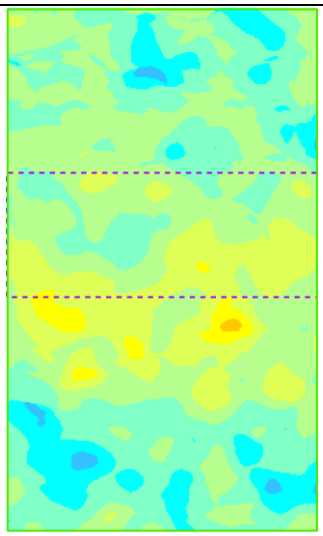 S = 5.39	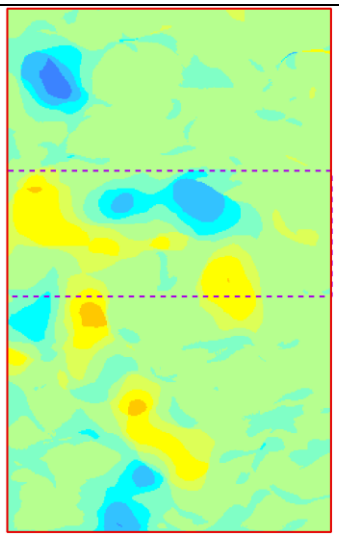 S = 3.41

4500	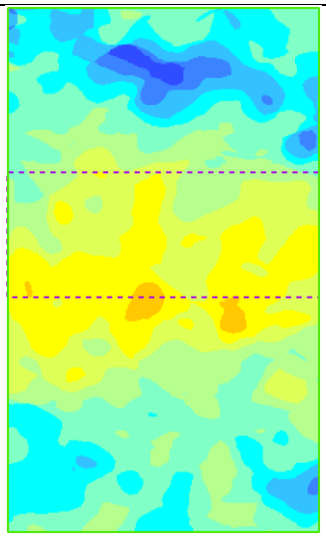 S = 9.42	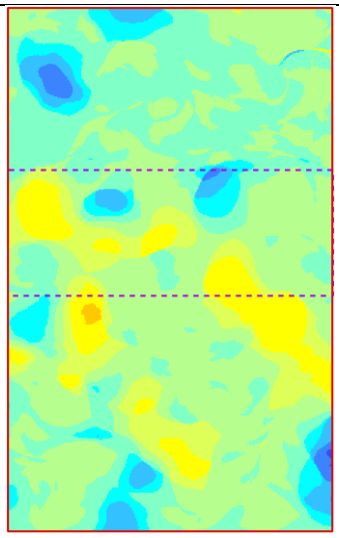 S = 3.59
9000	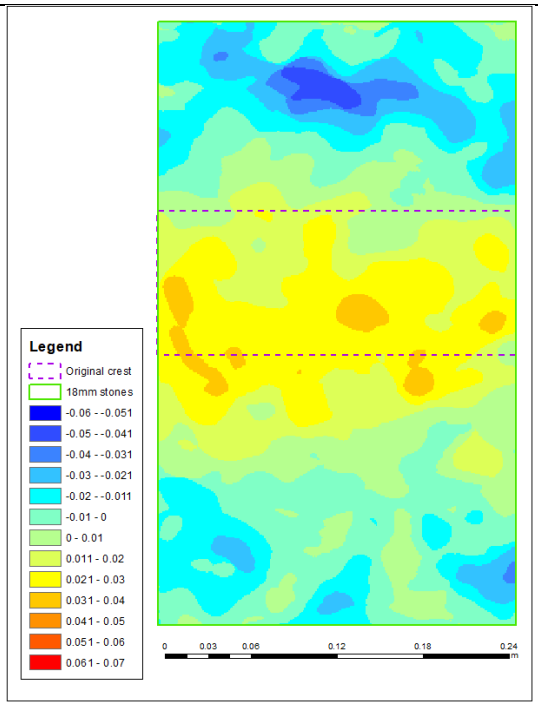 S = 10.68	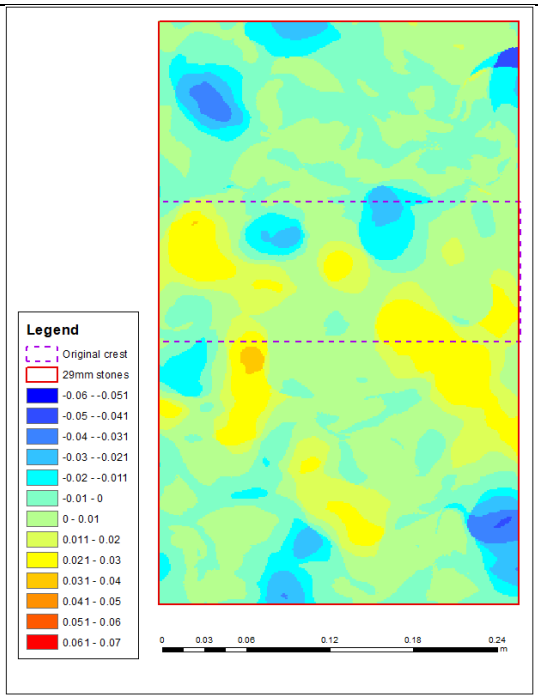 S = 3.85

<table>
<tr><td colspan="3">Test series family: Series 6

Hs = 120mm, Tp =1.7s , hc/h = 1, Cotα = 1.5</td></tr>
<tr><td>Nw</td><td>Green stones Dn50 = 18mm</td><td>Red stones Dn50 = 29mm</td></tr>
<tr><td>0</td><td> 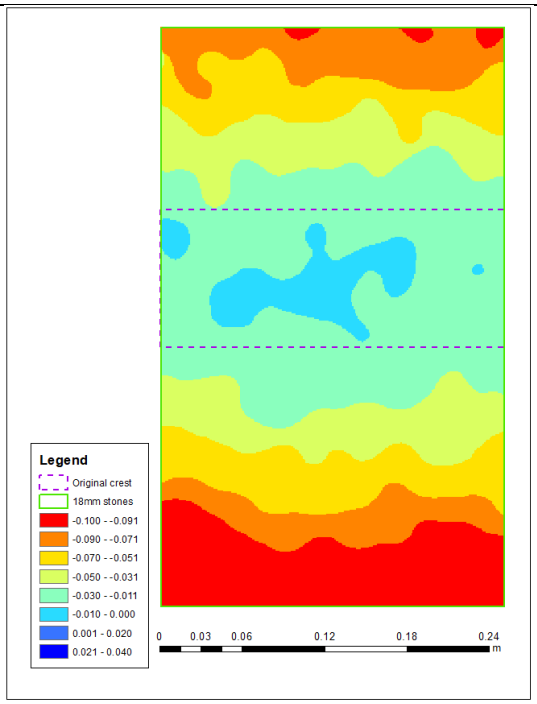
</td><td> 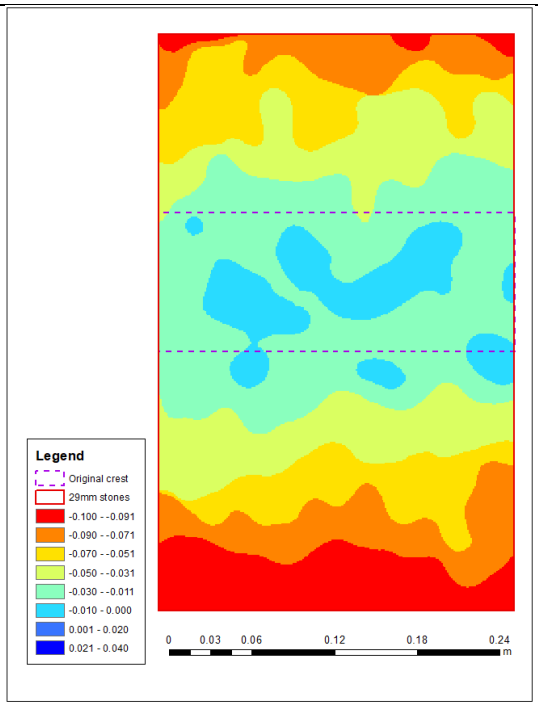
</td></tr>
<tr><td>1500</td><td> 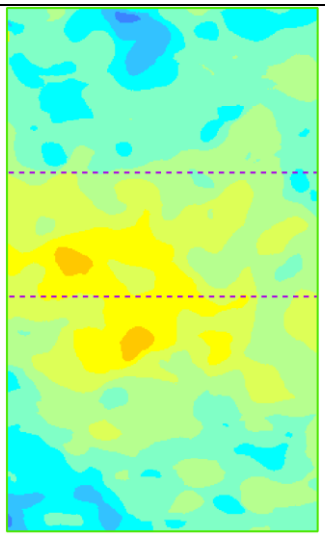
S = 8.10</td><td> 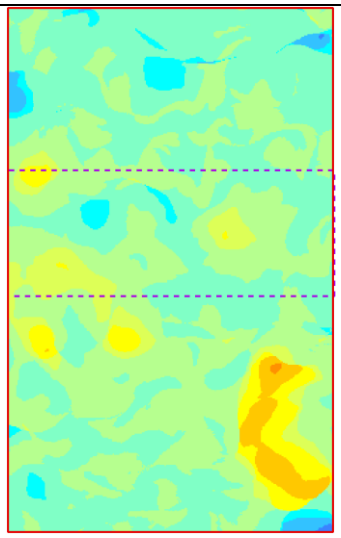
S = 2.80</td></tr>
</table>

4500	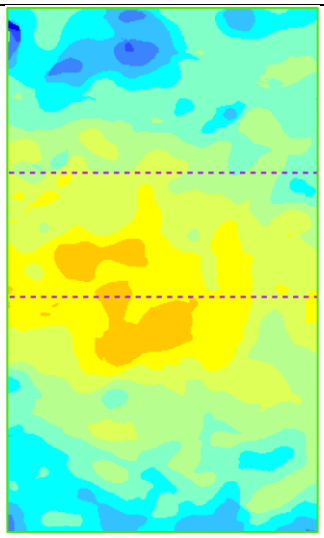 S = 11.63	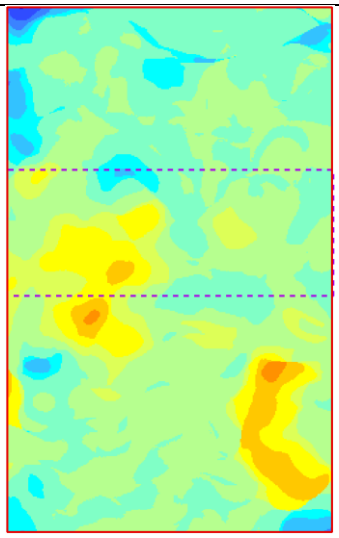 S = 4.36
9000	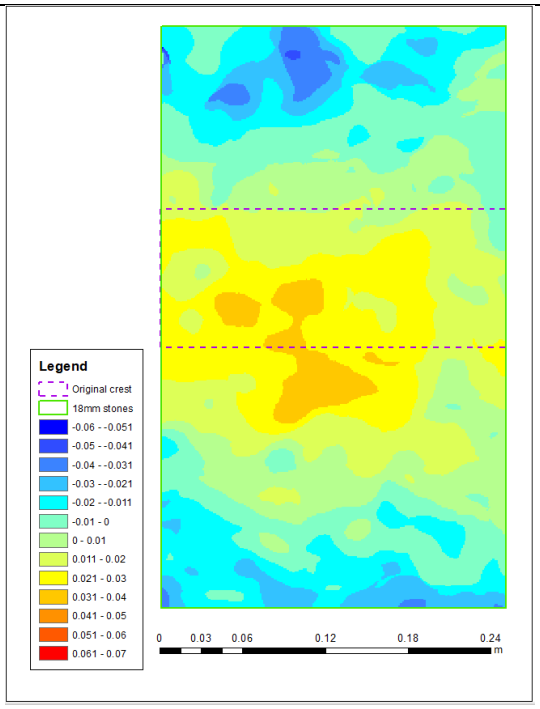 S = 11.80	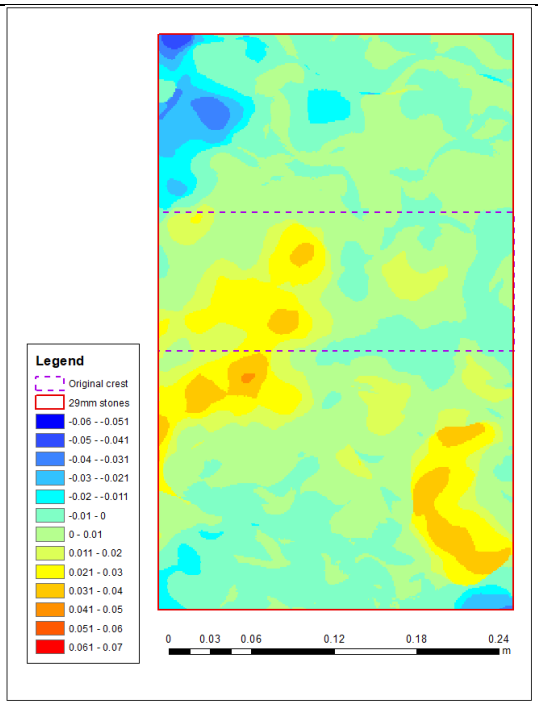 S = 4.74

Test series family: Series 7 Hs = 75mm, Tp =2.5s , hc/h = 0.75, Cotα = 1.5		
Nw	Green stones Dn50 = 18mm	Red stones Dn50 = 29mm
0	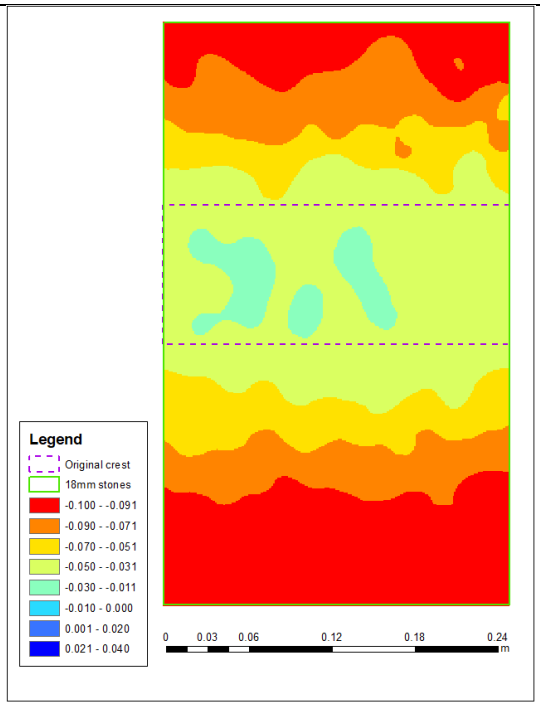	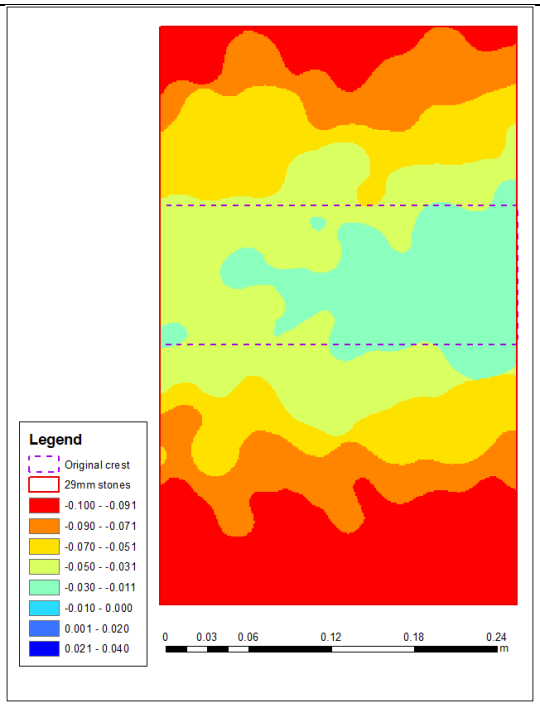
1500	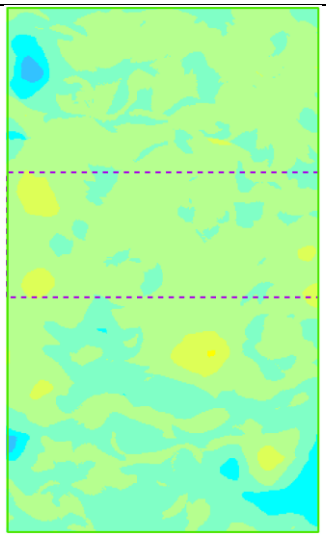 S = 2.05	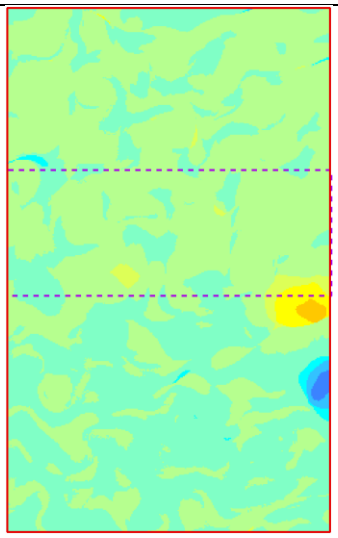 S = 0.96

4500	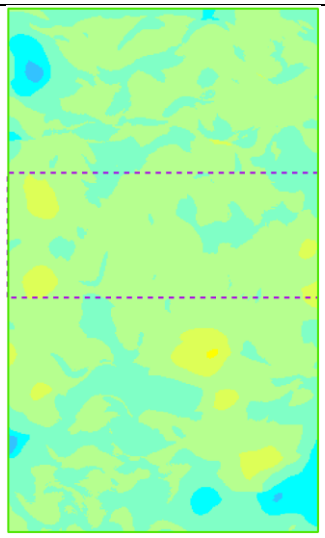 S = 2.28	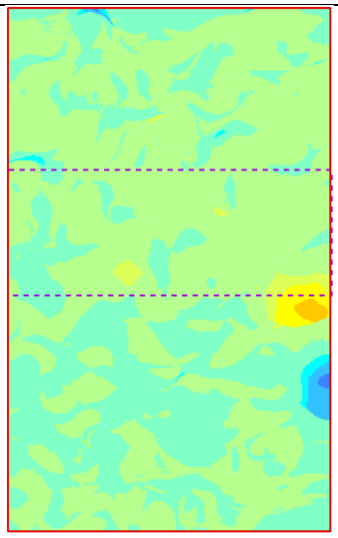 S = 1.03
9000	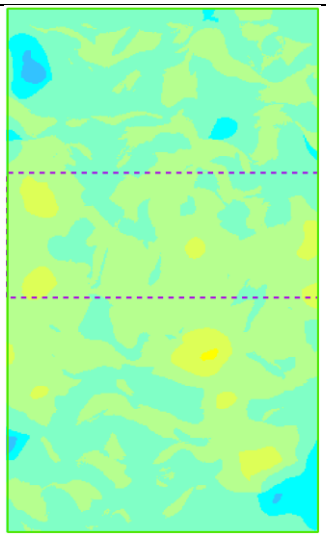 S = 2.18	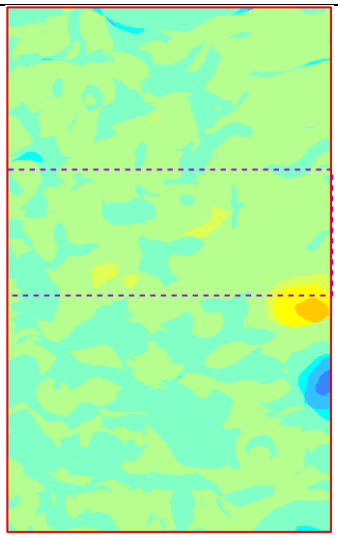 S = 1.07

15750	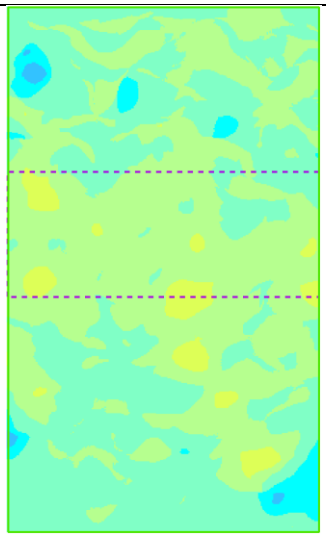 S = 2.32	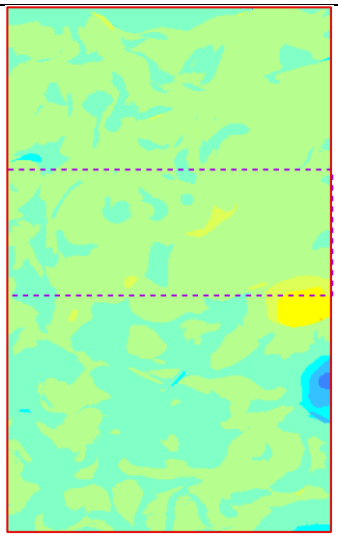 S = 1.13
24000	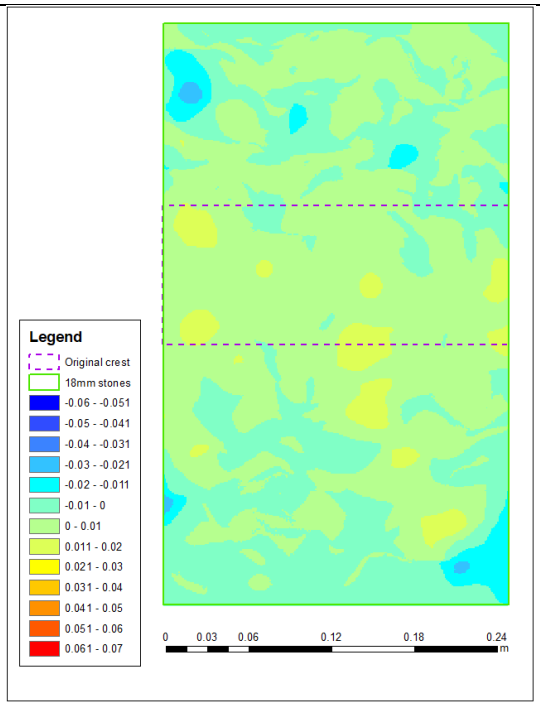 S = 2.73	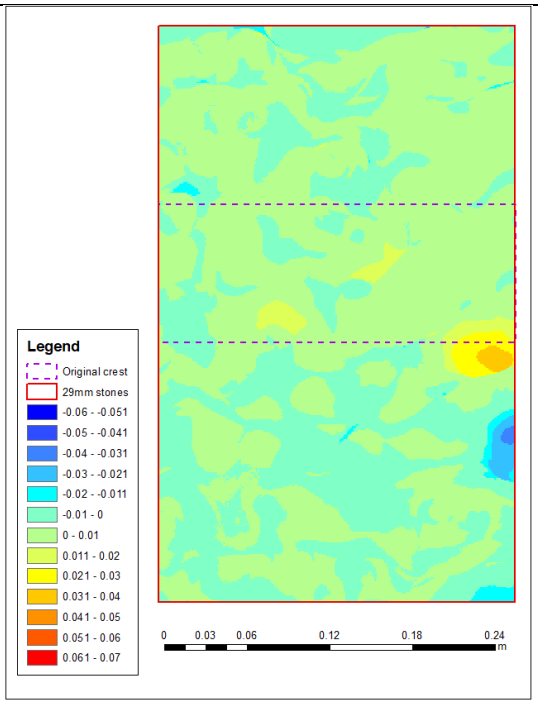 S = 1.19

Test series family: Series 8

Hs = 68mm, Tp =3.5s , hc/h = 0.75, Cotα = 1.5

Nw	Green stones Dn50 = 18mm	Red stones Dn50 = 29mm
0	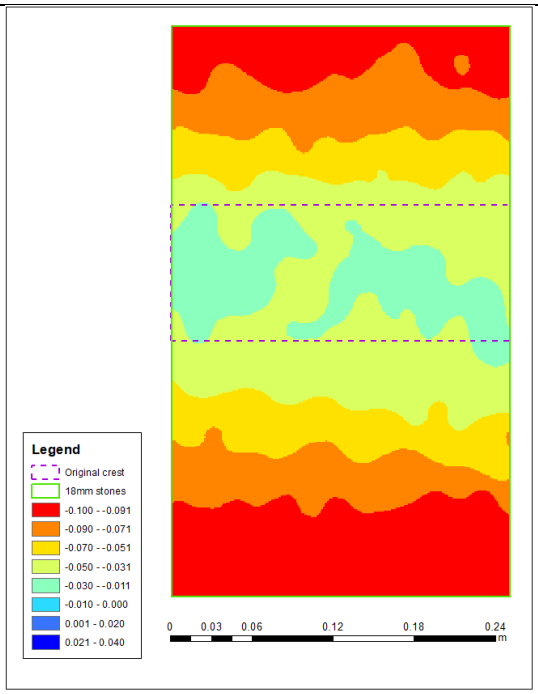	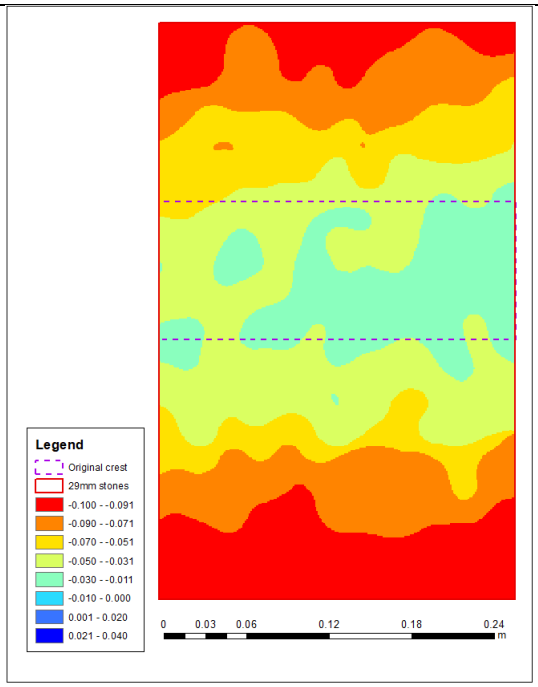
1500	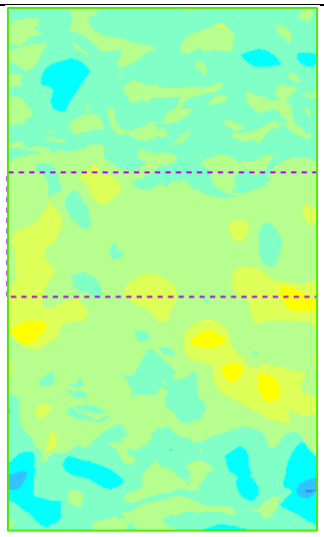 S = 3.94	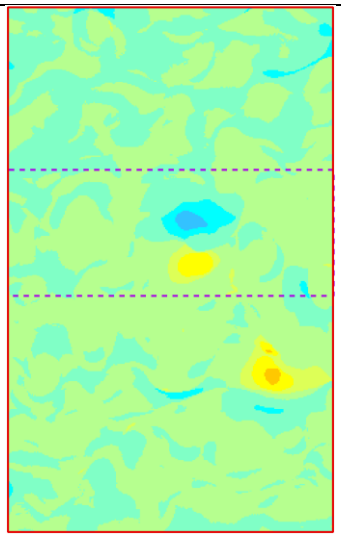 S = 1.13

4500	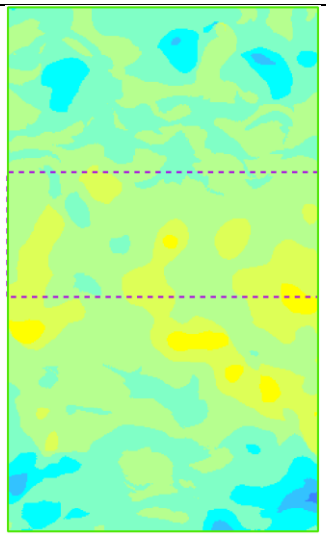 S = 4.87	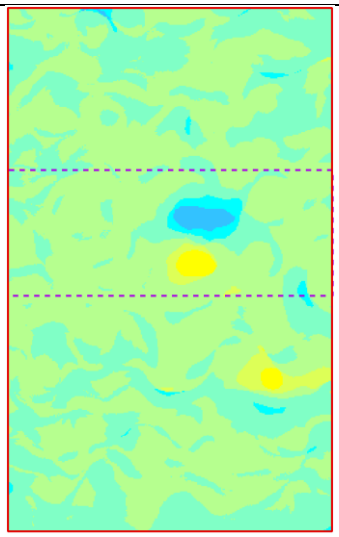 S = 0.97
9000	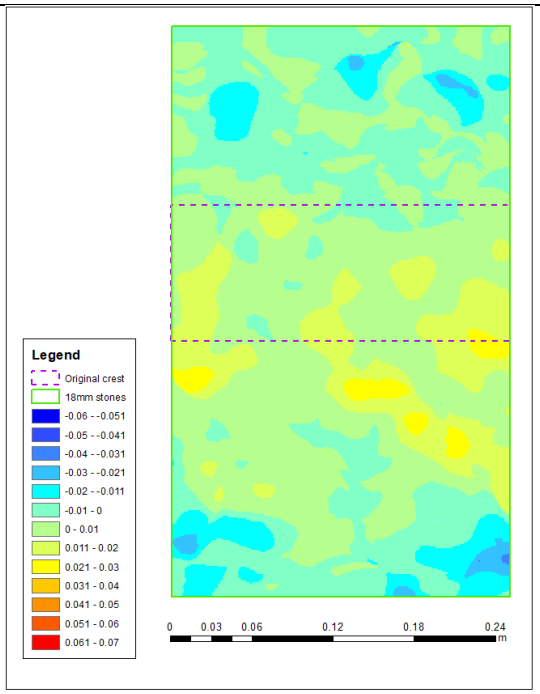 S = 4.89	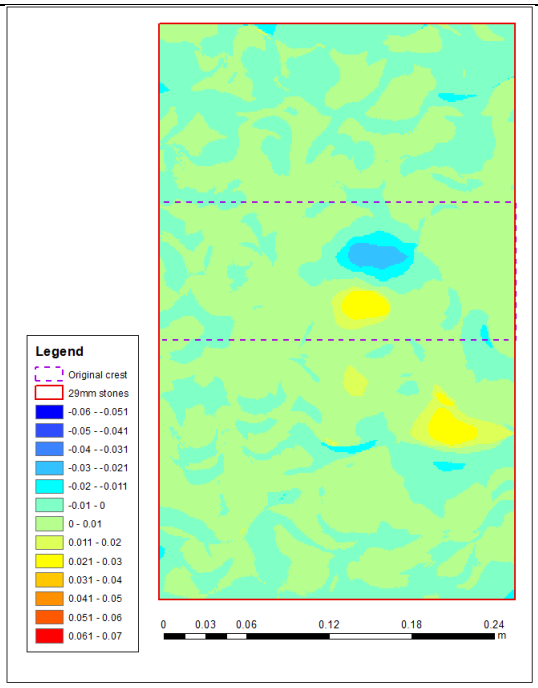 S = 1.12

<table>
<tr><td colspan="3">Test series family: Series 9

Hs = 75mm, Tp =2.5s , hc/h = 0.5, Cotα = 1.5</td></tr>
<tr><td>Nw</td><td>Green stones Dn50 = 18mm</td><td>Red stones Dn50 = 29mm</td></tr>
<tr><td>0</td><td> 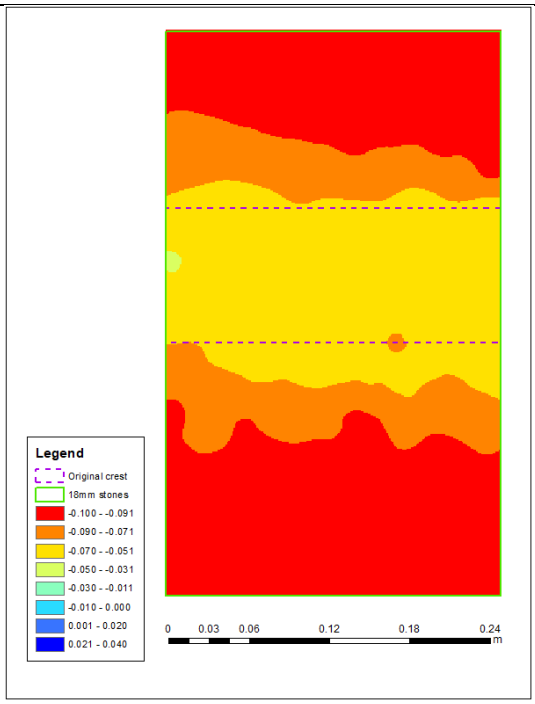
</td><td> 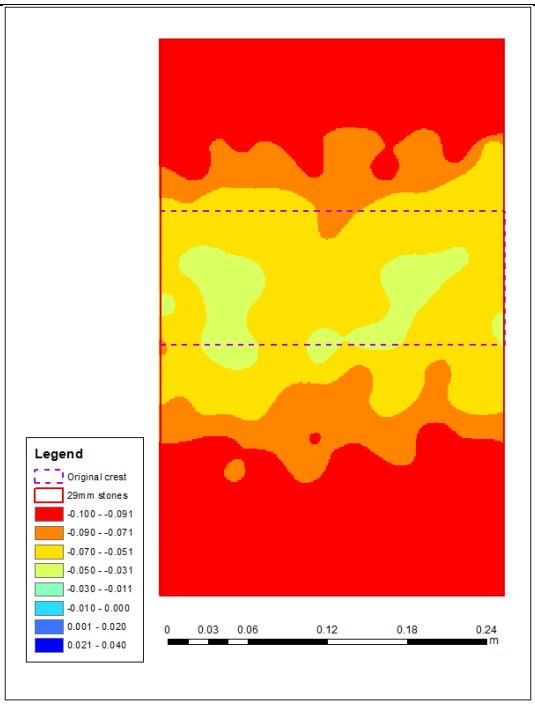
</td></tr>
<tr><td>1500</td><td> 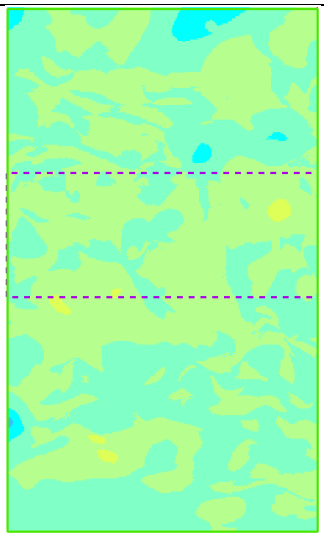
S = 1.12</td><td> 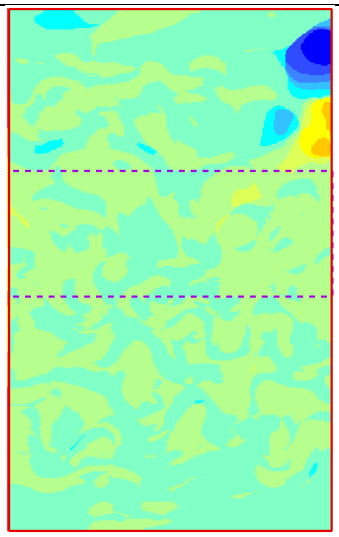
S = 0.77</td></tr>
</table>

4500	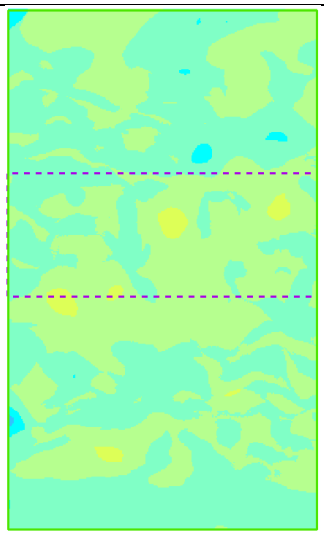 S = 1.45	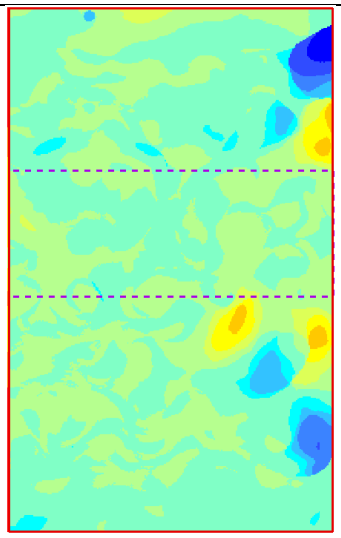 S = 1.21
9000	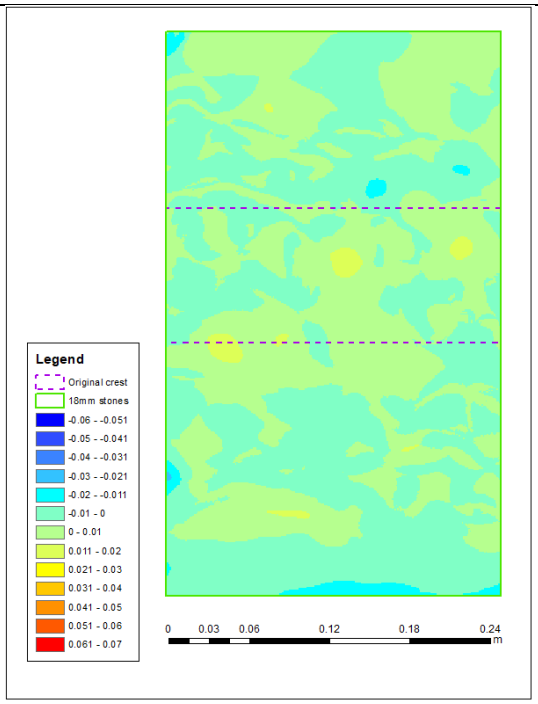 S = 1.48	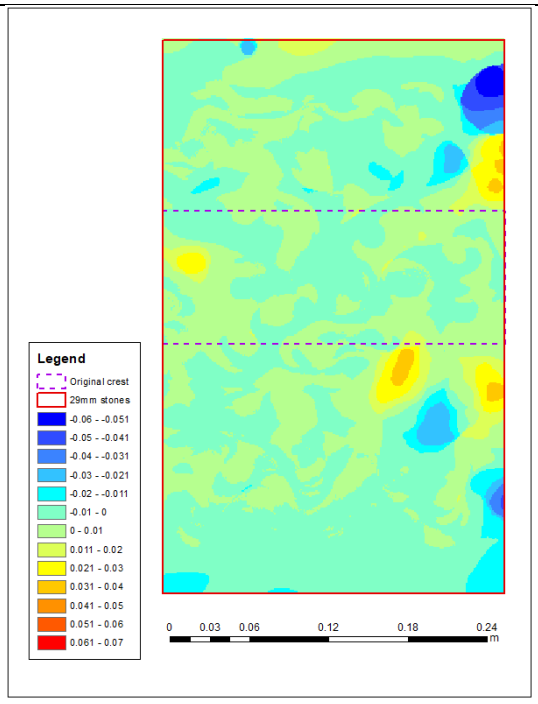 S = 1.46

Test series family: Series 10 Hs = 68mm, Tp =3.5s , hc/h = 1.2, Cotα = 2		
Nw	Green stones Dn50 = 18mm	Red stones Dn50 = 29mm
0	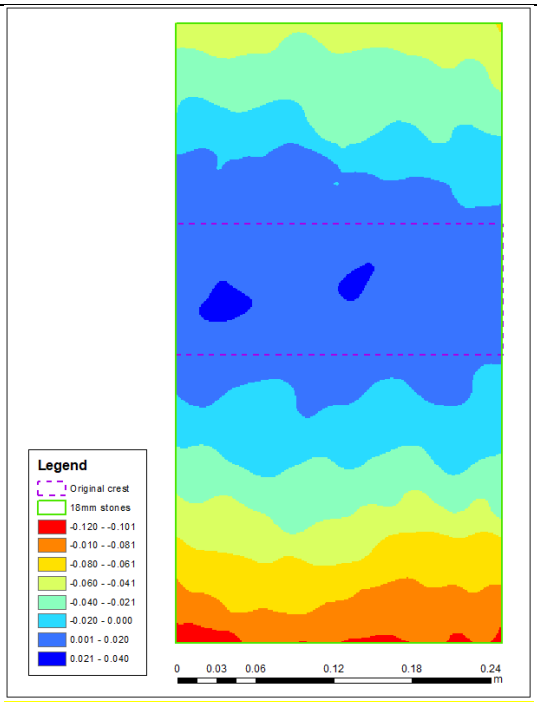	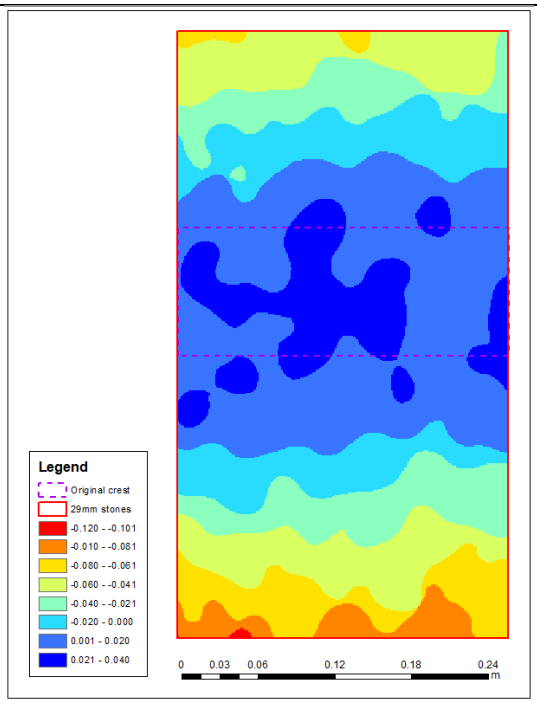
1500	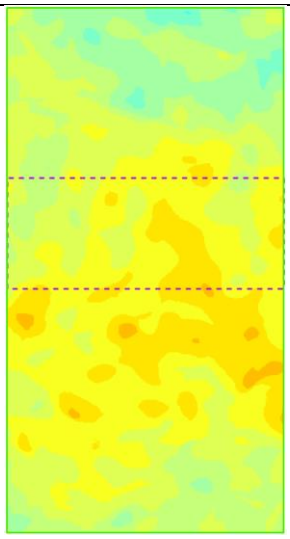 S =13.46	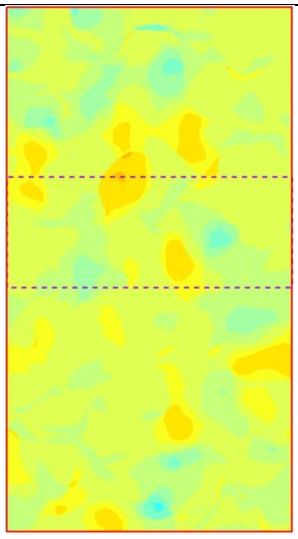 S = 2.52

4500	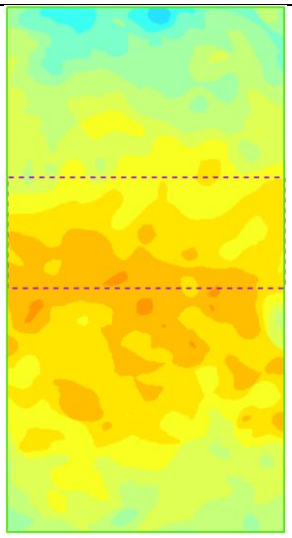 S = 21.67	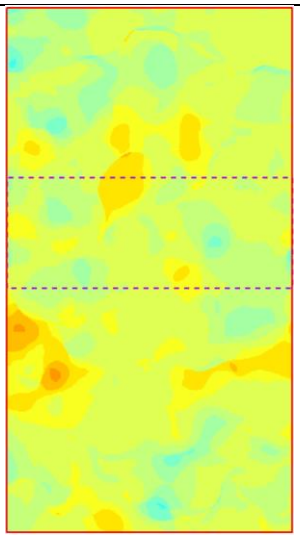 S = 2.84
9000	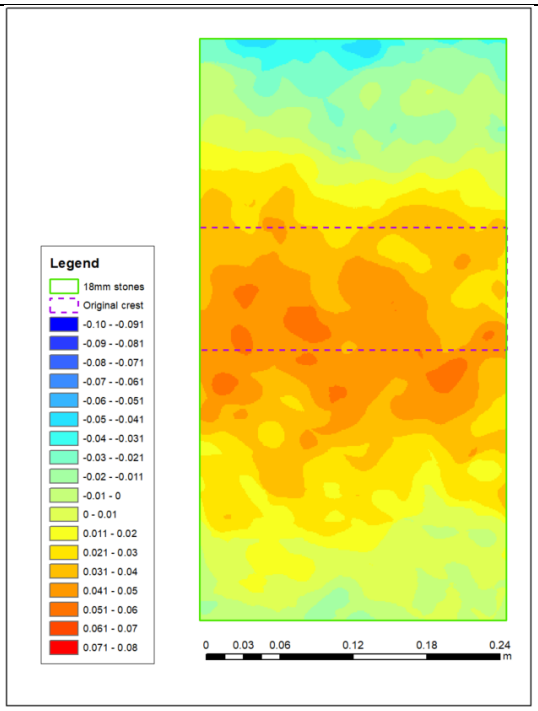 S = 31.74	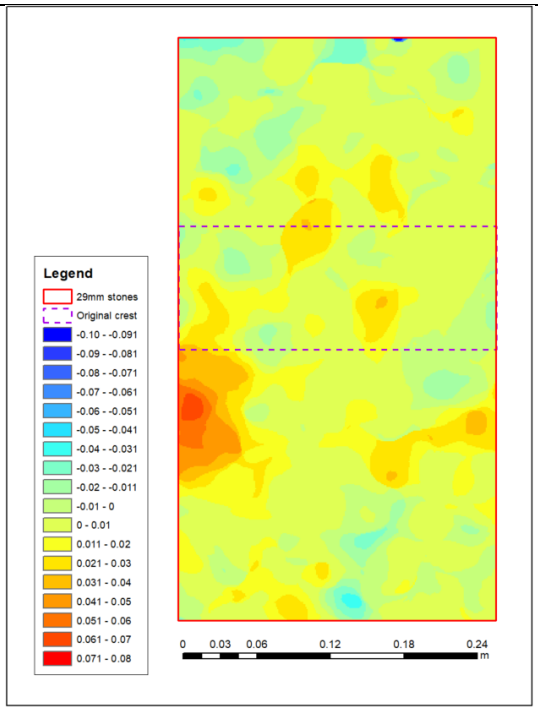 S = 4.27

Test series family: Series 11 Hs = 75mm, Tp =2.5s , hc/h = 1.2, Cotα = 2		
Nw	Green stones Dn50 = 18mm	Red stones Dn50 = 29mm
0	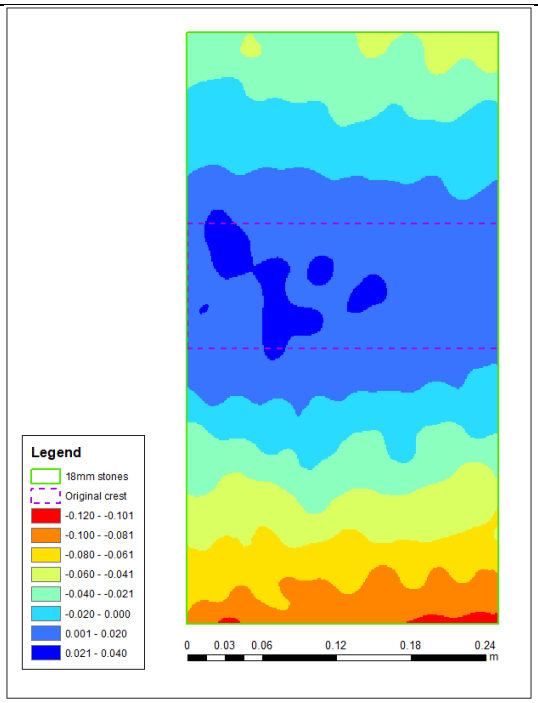	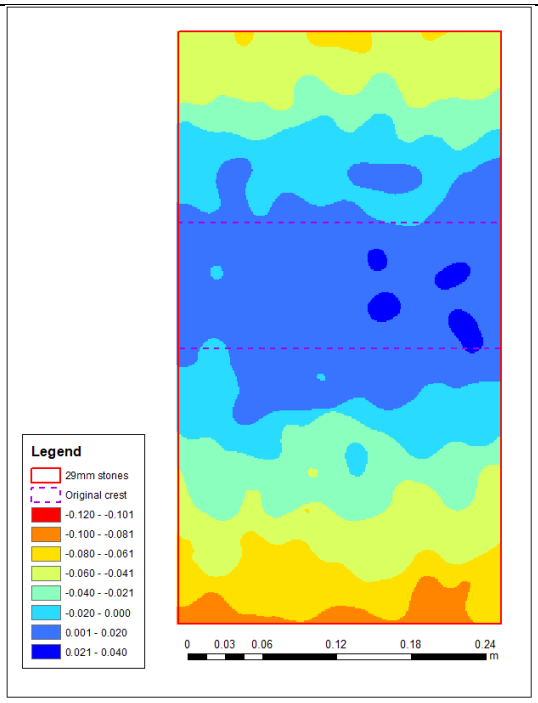
1500	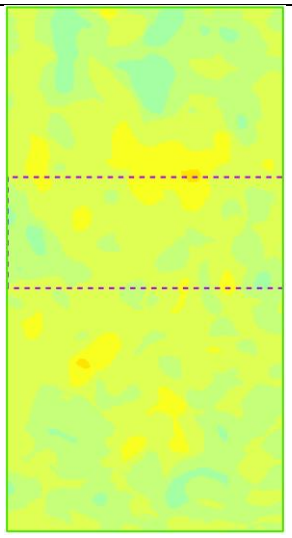 S = 4.04	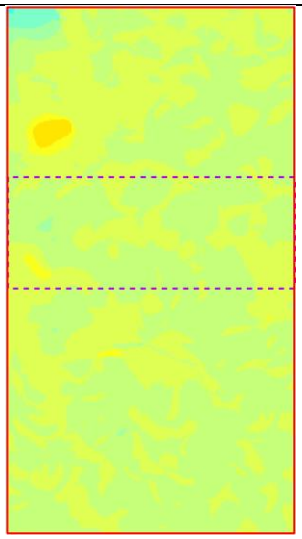 S = 0.44

4500	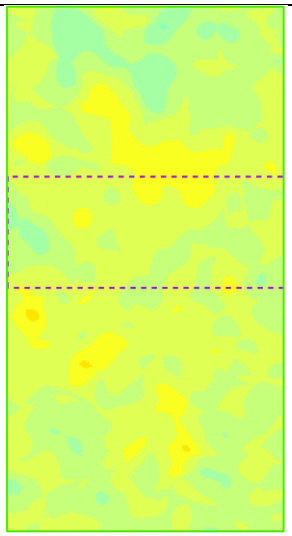 S = 4.09	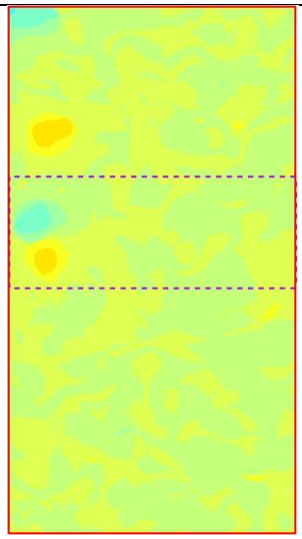 S = 0.56
9000	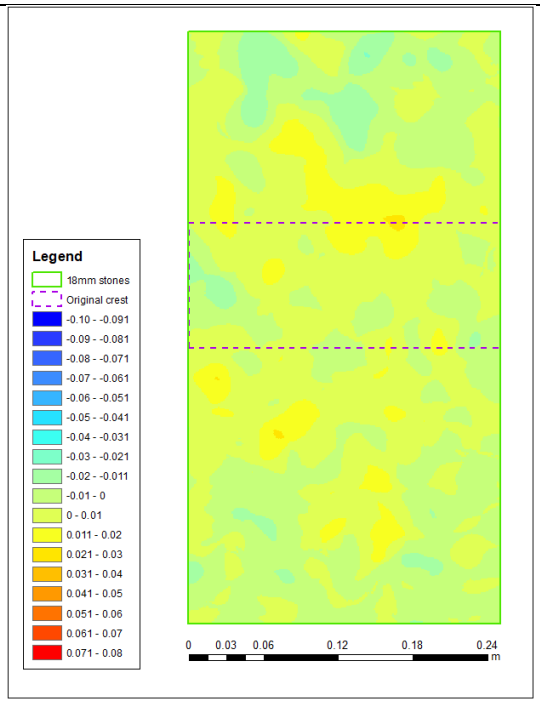 S = 4.13	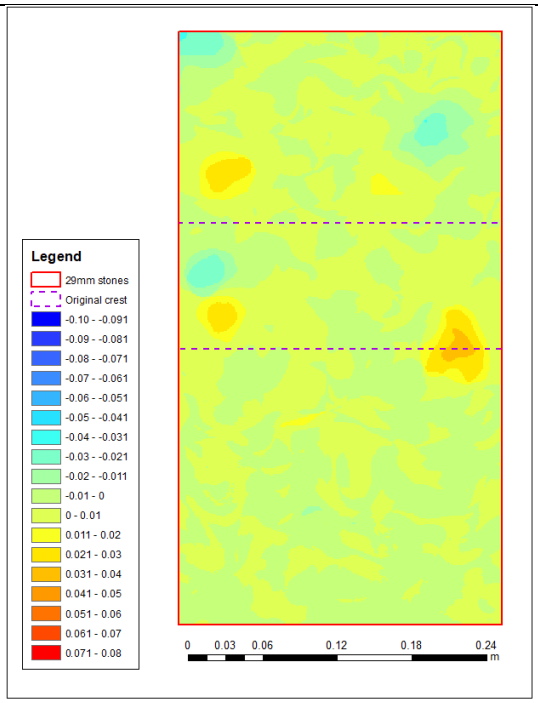 S = 0.91

Test series family: Series 12

Hs = 120mm, Tp =1.7s , hc/h = 1.2, Cotα = 2

Nw	Green stones Dn50 = 18mm	Red stones Dn50 = 29mm
0	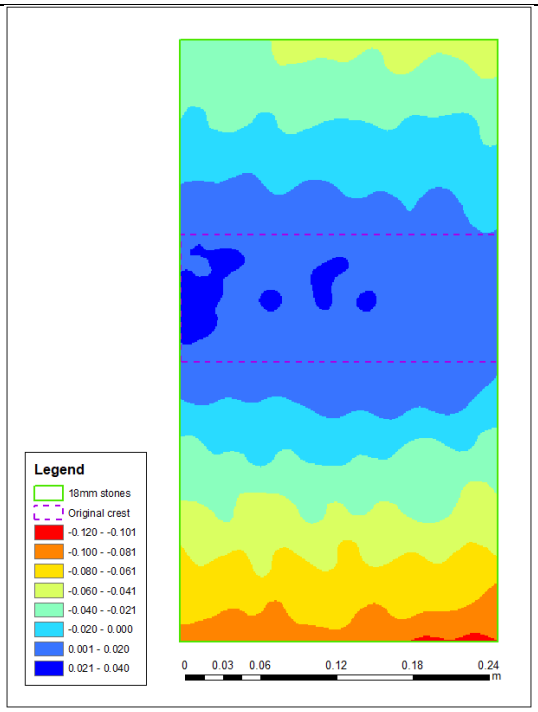	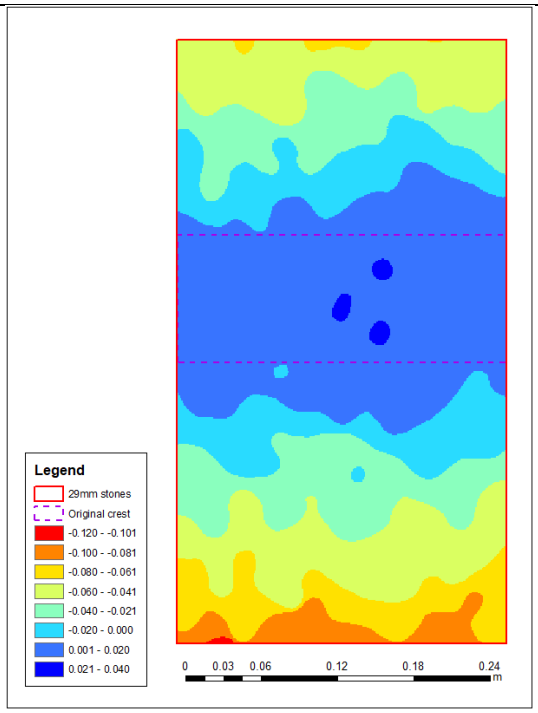
1500	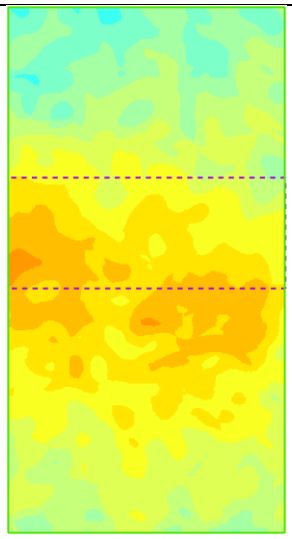 S = 18.12	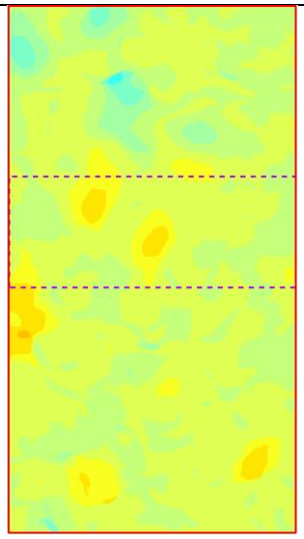 S = 1.60

4500	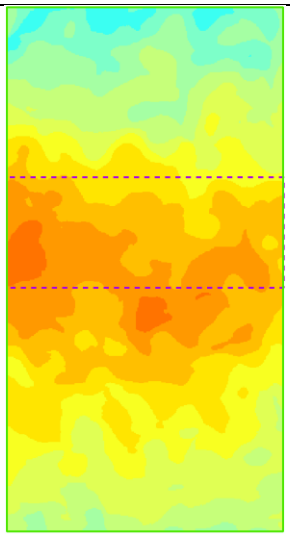 S = 27.39	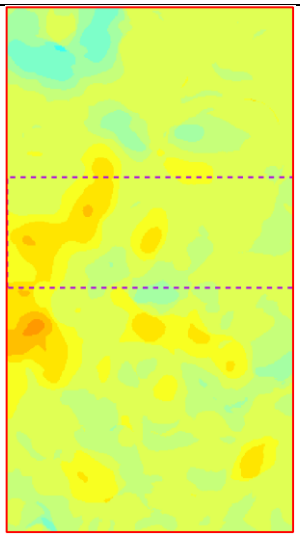 S = 2.93
9000	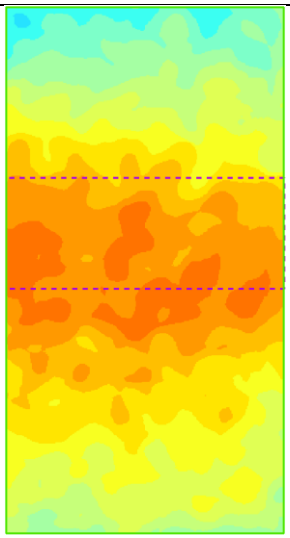 S = 33.09	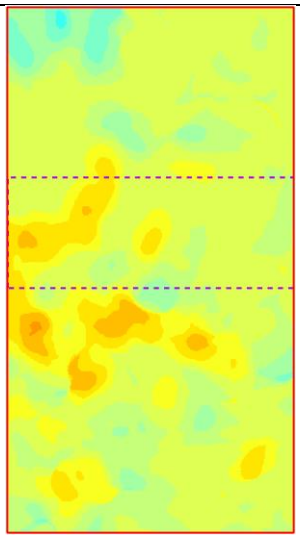 S = 3.38

15750	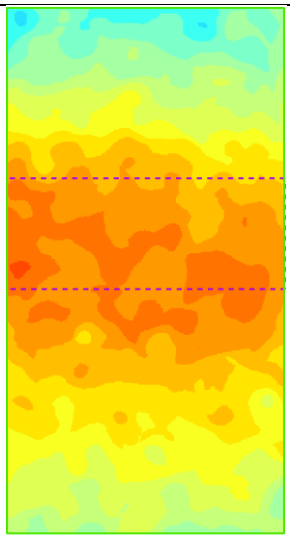 S = 35.43	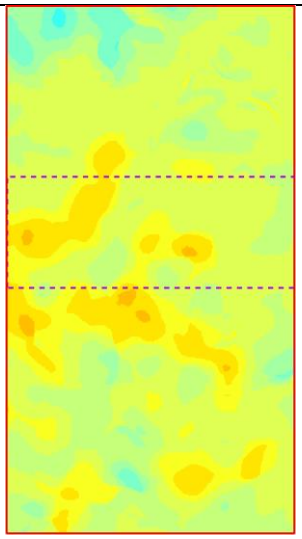 S = 3.35
24000	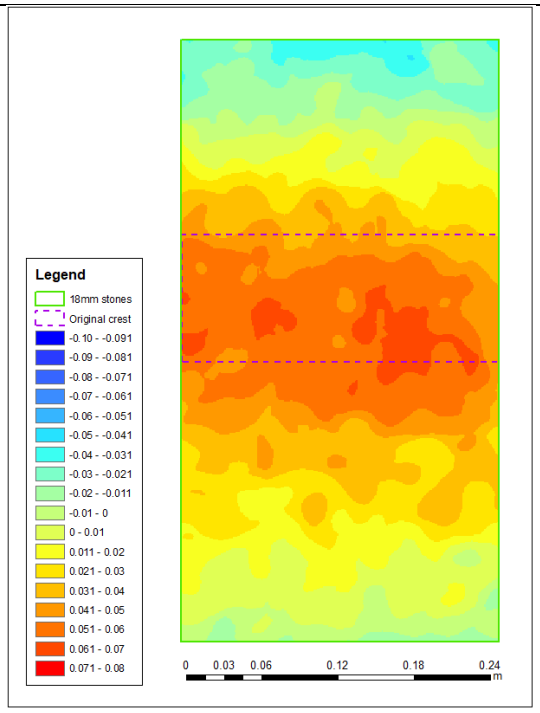 S = 39.30	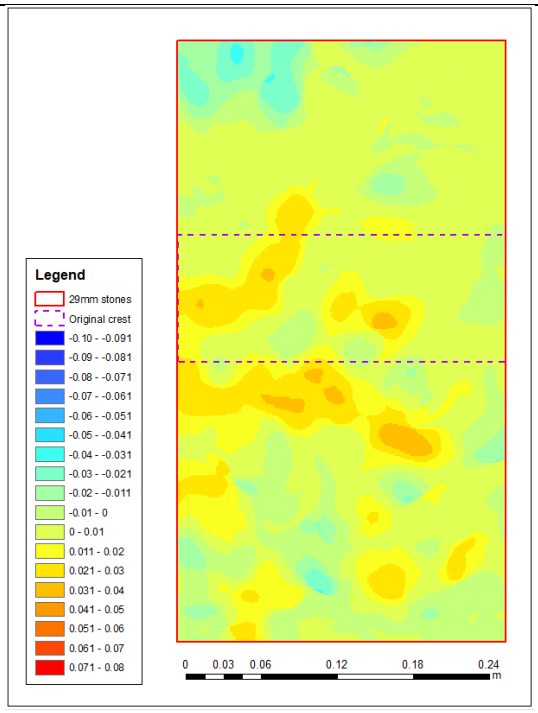 S = 3.72

<table>
<tr><td colspan="3">Test series family: Series 13

Hs = 68mm, Tp =3.5s , hc/h = 1, Cotα = 2</td></tr>
<tr><td>Nw</td><td>Green stones Dn50 = 18mm</td><td>Red stones Dn50 = 29mm</td></tr>
<tr><td>0</td><td> 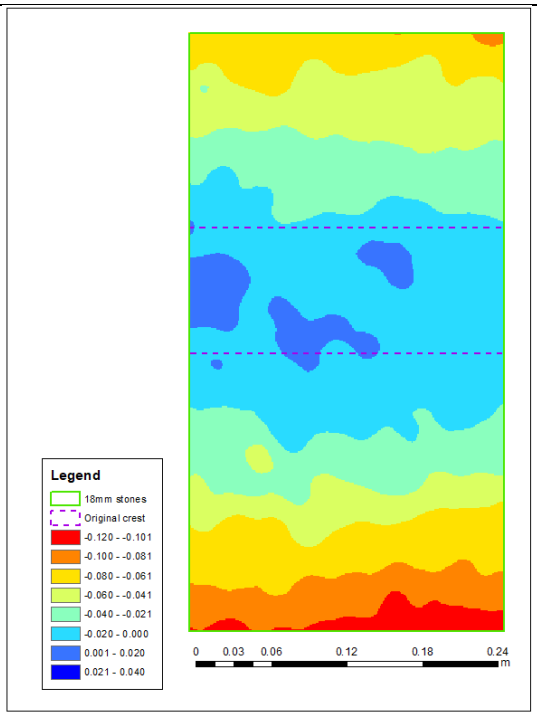
</td><td> 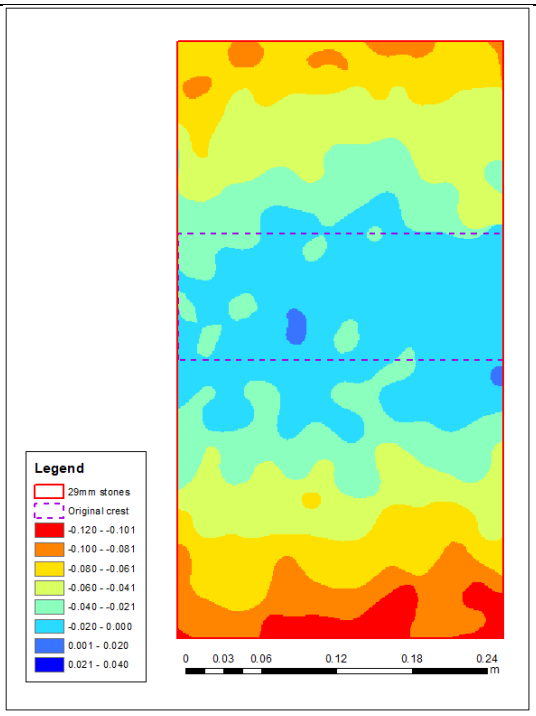
</td></tr>
<tr><td>1500</td><td> 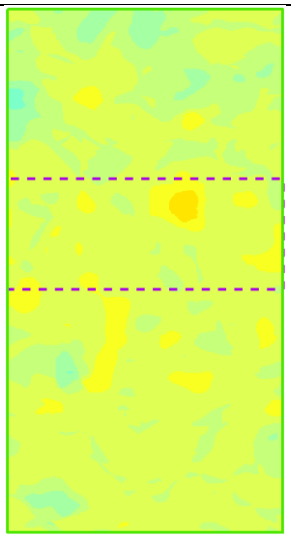
S = 4.46</td><td> 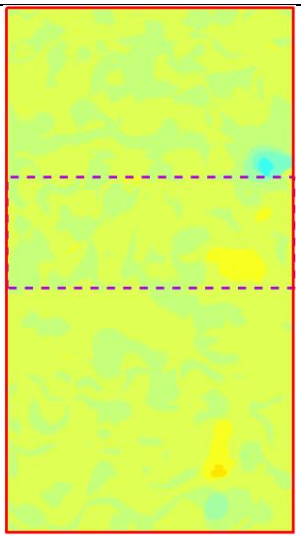
S = 0.74</td></tr>
</table>

4500	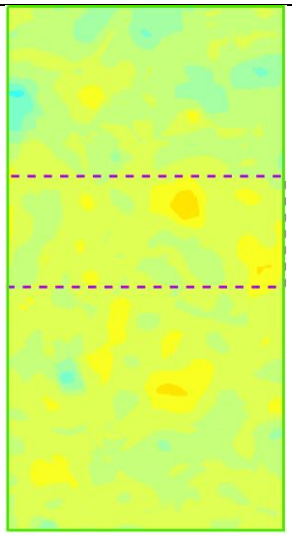 S = 4.11	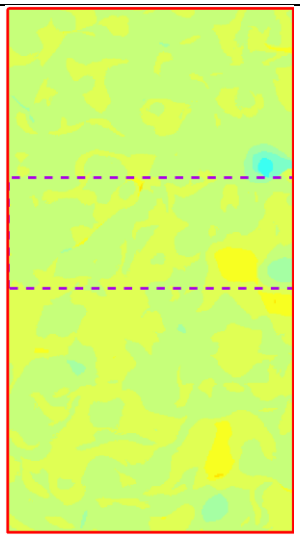 S = 0.52
9000	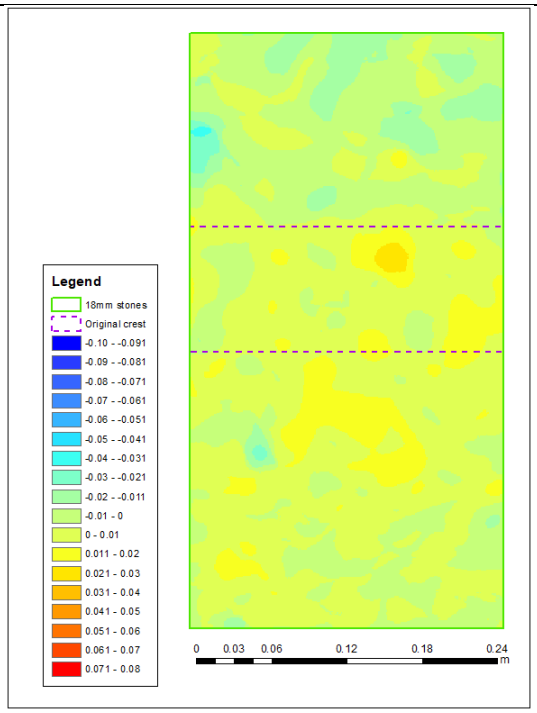 S = 4.73	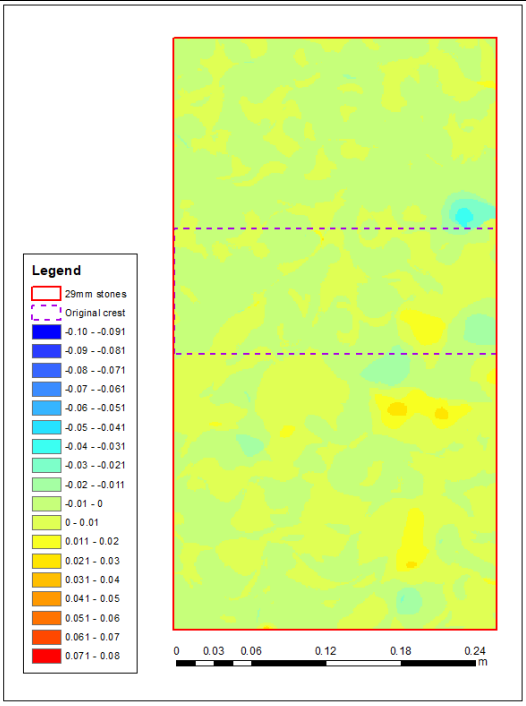 S = 0.62

Test series family: Series 14 Hs = 75mm, Tp =2.5s , hc/h = 1, Cotα = 2		
Nw	Green stones Dn50 = 18mm	Red stones Dn50 = 29mm
0	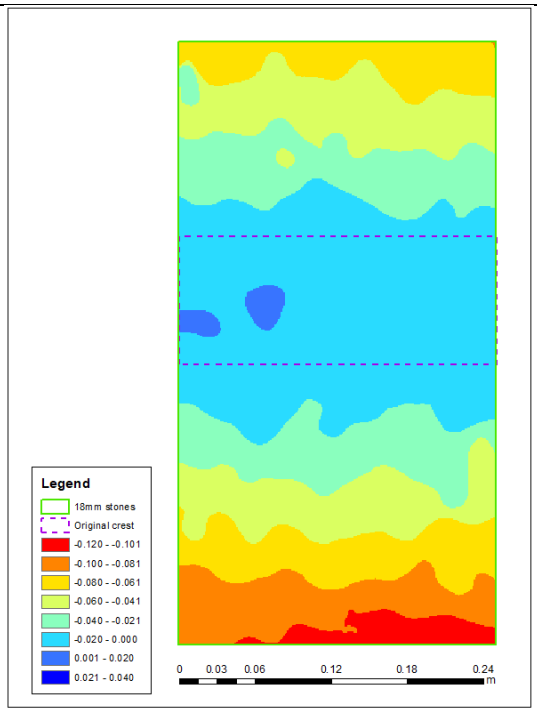	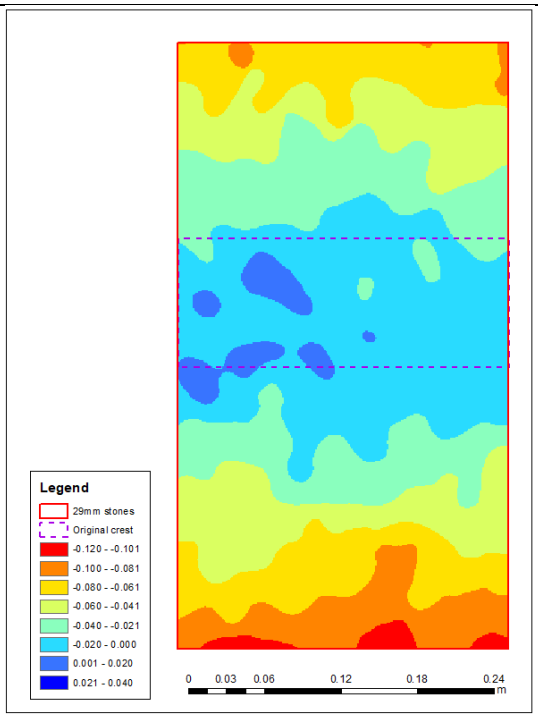
1500	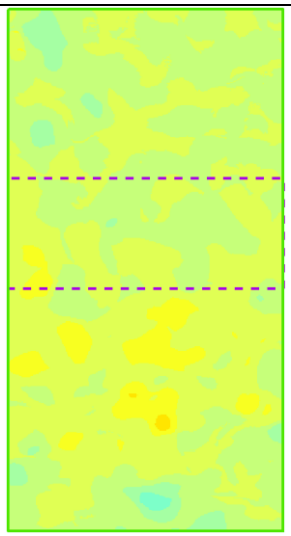 S = 3.35	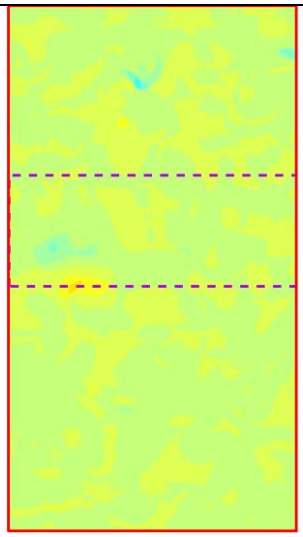 S = 0.32

4500	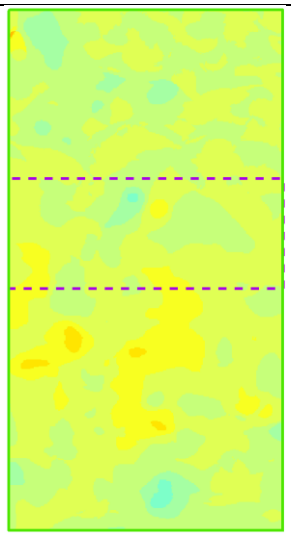 S = 4.31	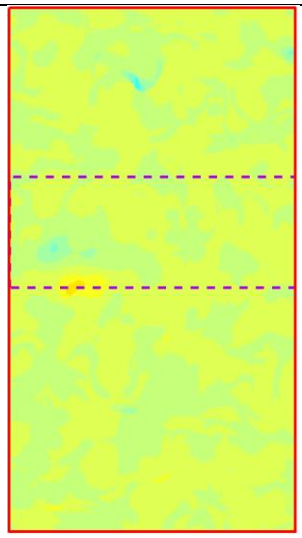 S = 0.55
9000	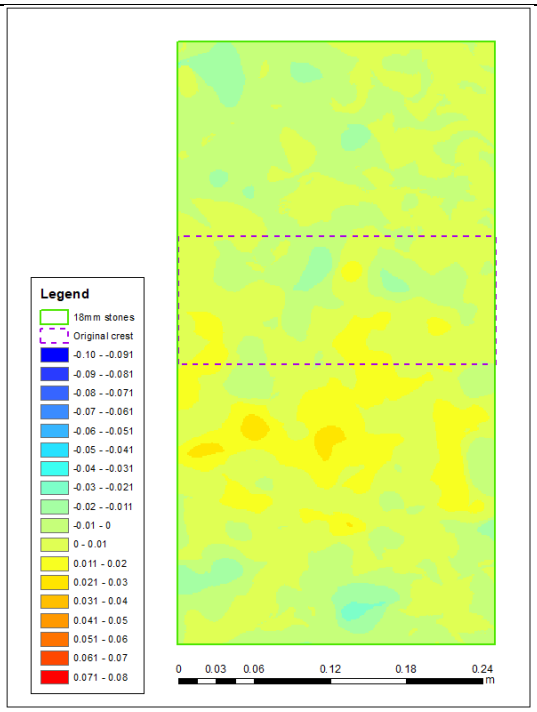 S = 4.91	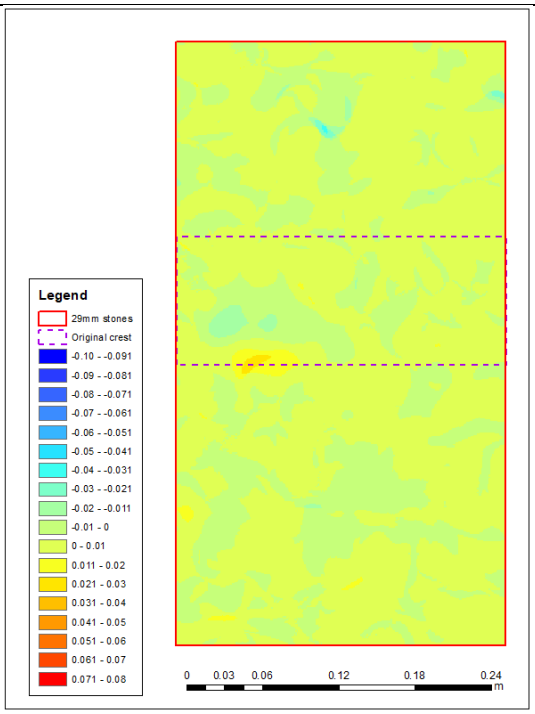 S = 0.76

Test series family: Series 15 Hs = 120mm, Tp =1.7s , hc/h = 1, Cotα = 2		
Nw	Green stones Dn50 = 18mm	Red stones Dn50 = 29mm
0	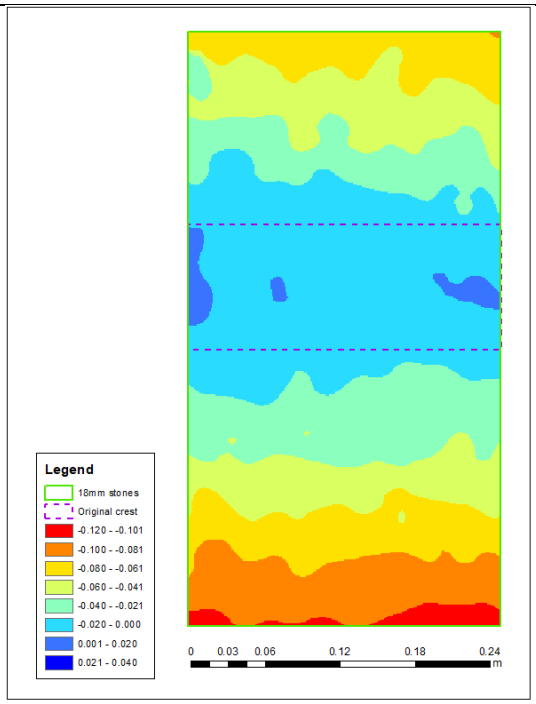	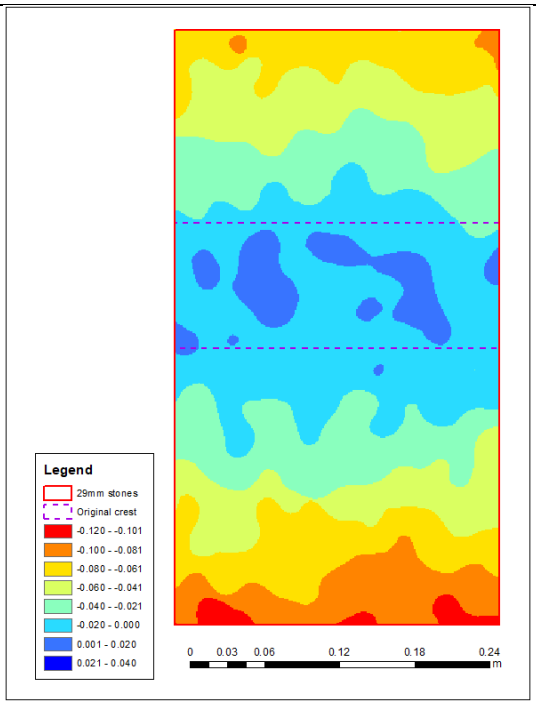
1500	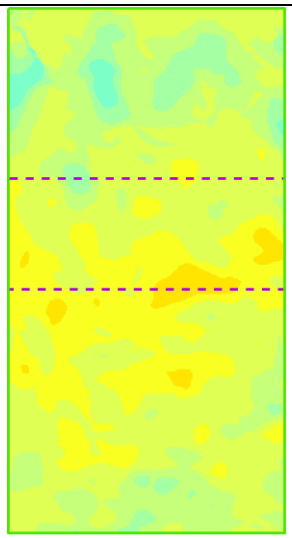 S = 7.96	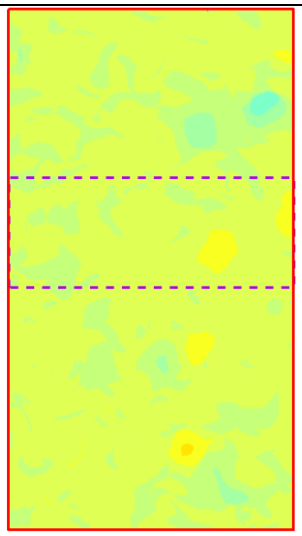 S = 0.92

4500	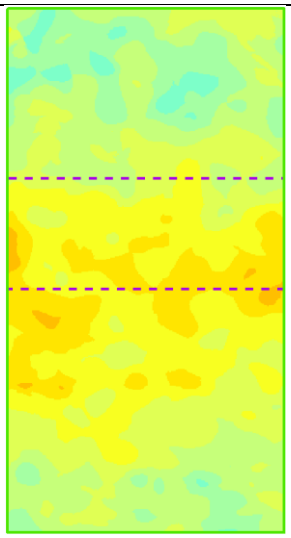 S = 11.51	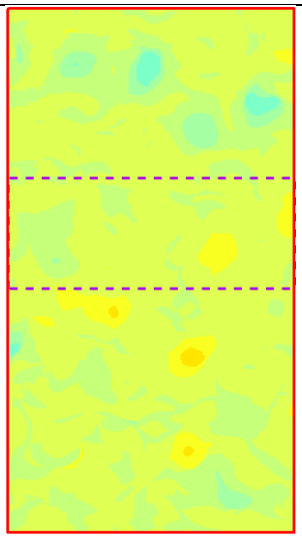 S = 1.14
9000	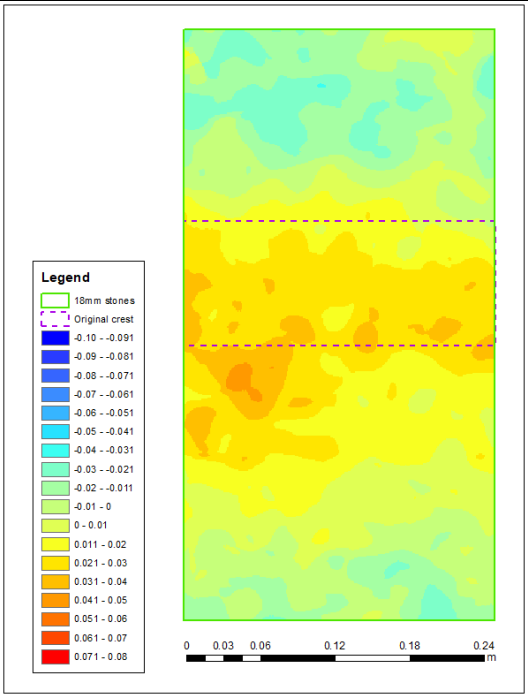 S = 15.48	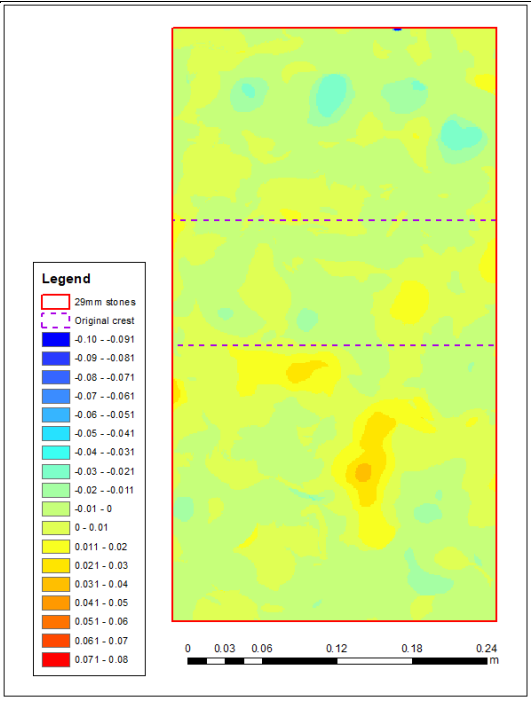 S = 1.16

Test series family: Series 16 Hs = 75mm, Tp =2.5s , hc/h = 0.75, Cotα = 2		
Nw	Green stones Dn50 = 18mm	Red stones Dn50 = 29mm
0	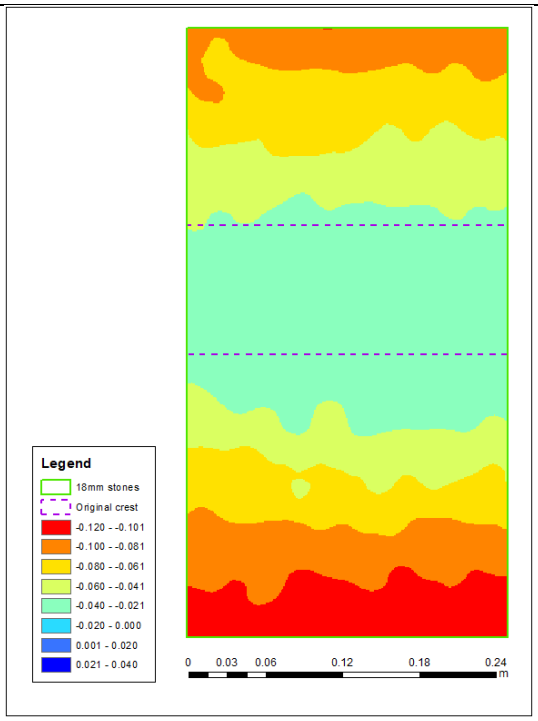	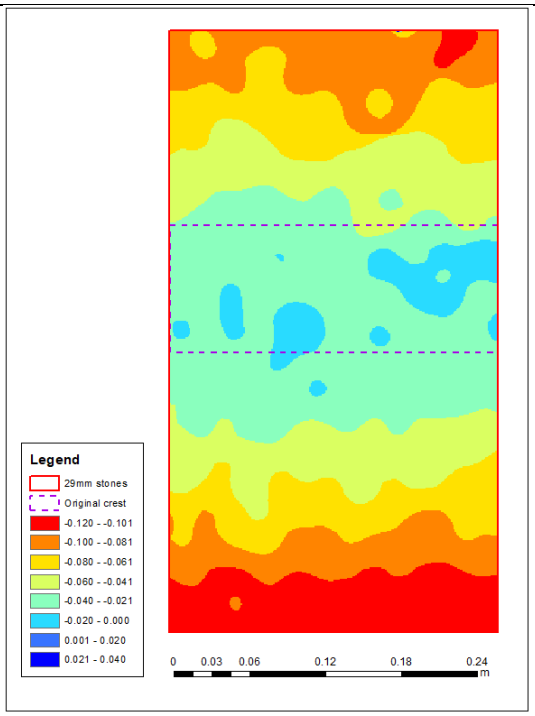
1500	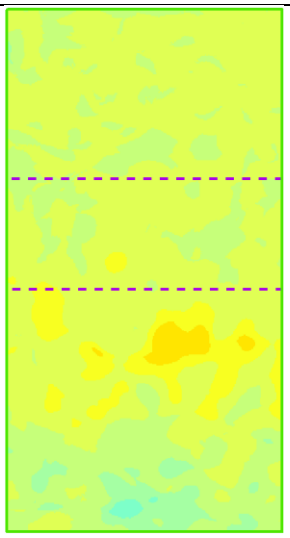 S = 4.30	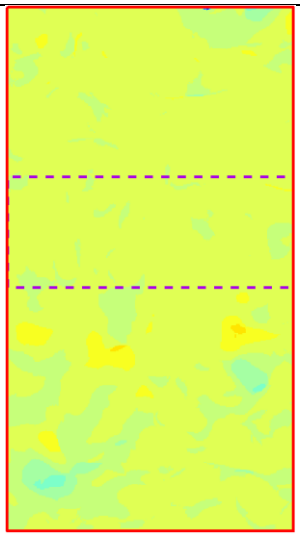 S = 1.08

4500	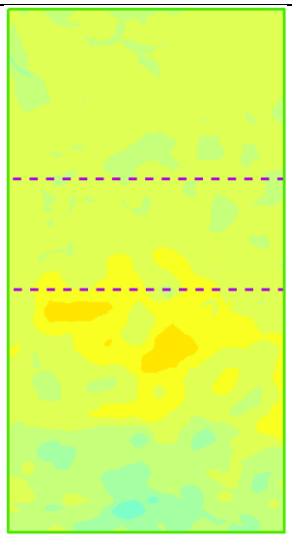 S = 5.34	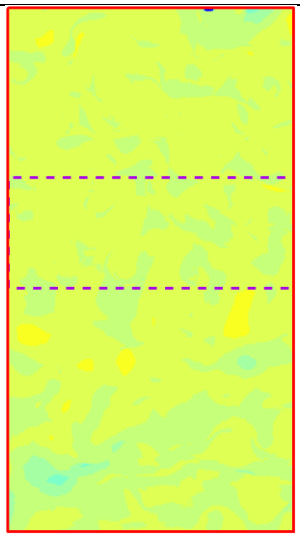 S = 0.76
9000	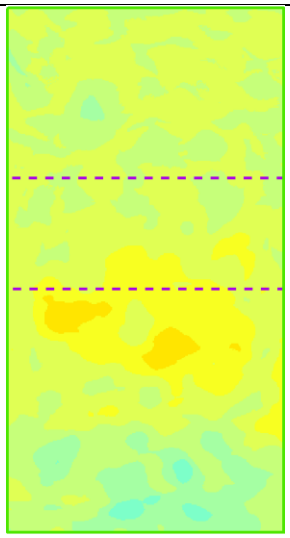 S = 5.23	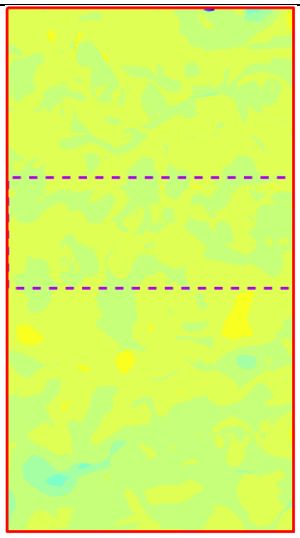 S = 0.65

15750	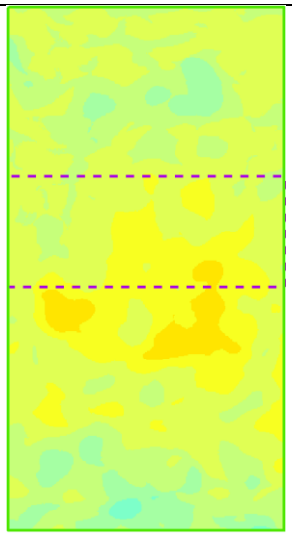 S = 7.12	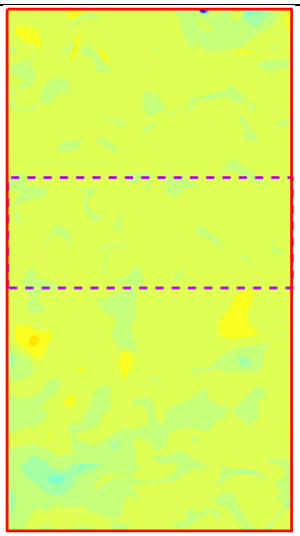 S = 0.98
24000	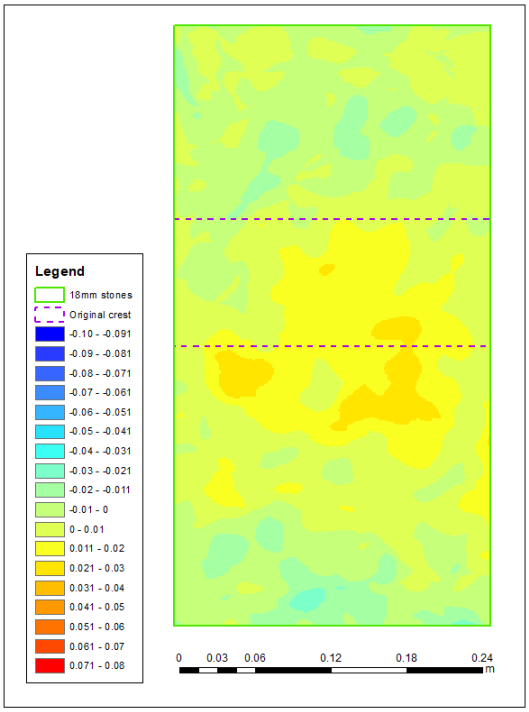 S = 7.28	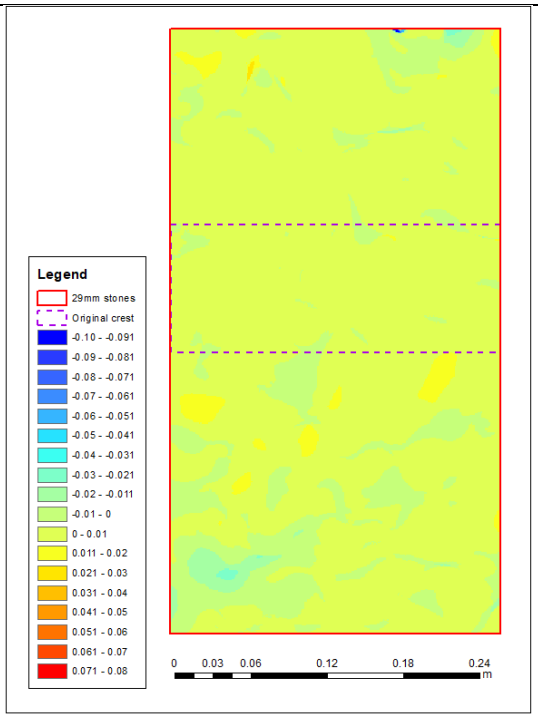 S = 1.15

Test series family: Series 17 Hs = 68mm, Tp =3.5s , hc/h = 0.75, Cotα = 2		
Nw	Green stones Dn50 = 18mm	Red stones Dn50 = 29mm
0	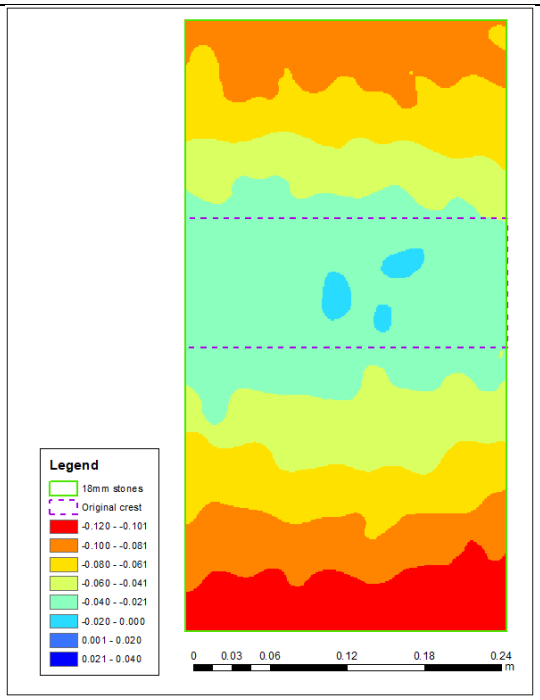	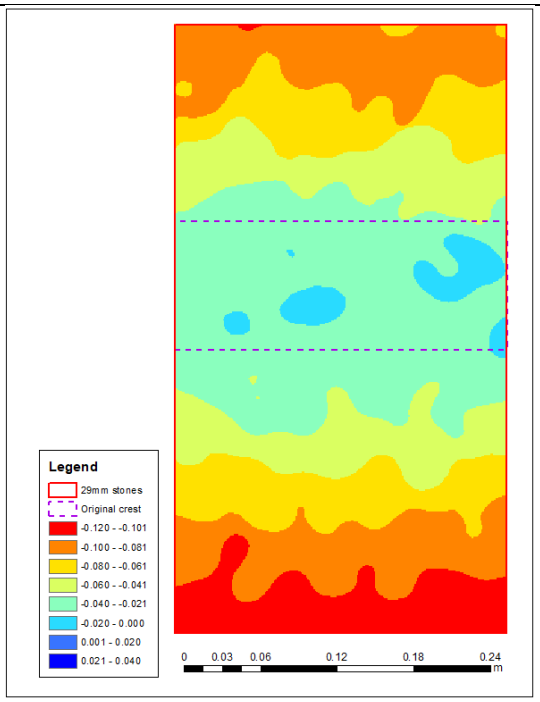
1500	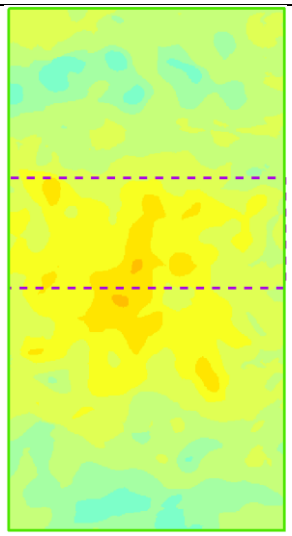 S = 7.71	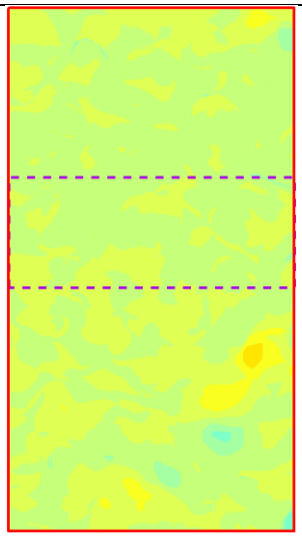 S = 0.55

4500	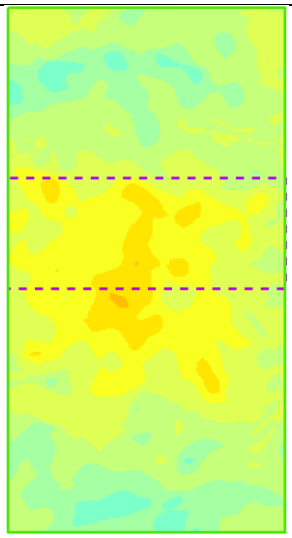 S = 7.47	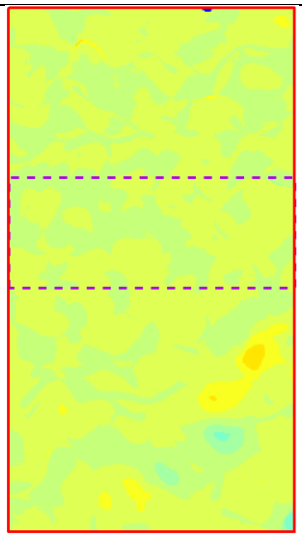 S = 0.76
9000	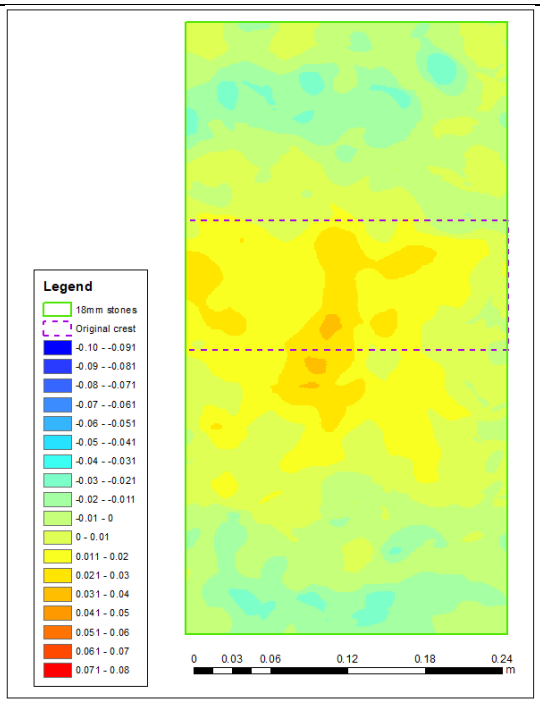 S = 8.75	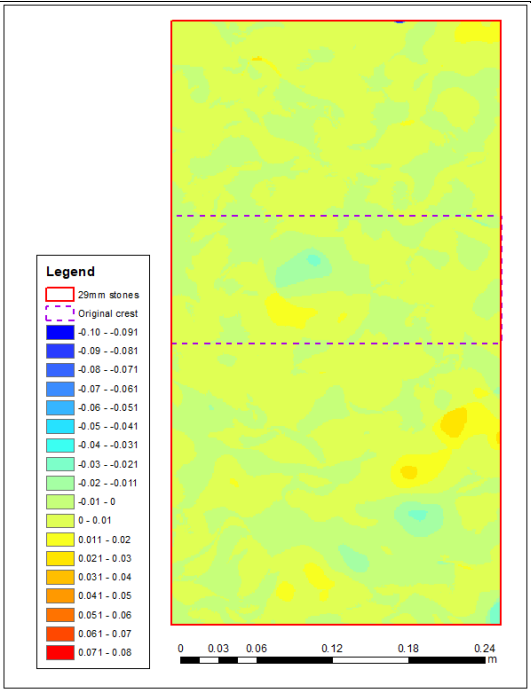 S = 0.87

Test series family: Series 18 Hs = 75mm, Tp =2.5s , hc/h = 0.5, Cotα = 2		
Nw	Green stones Dn50 = 18mm	Red stones Dn50 = 29mm
0	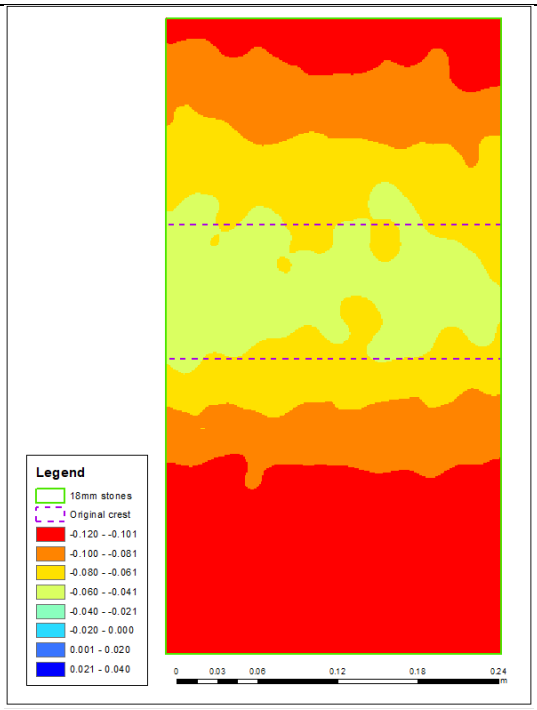	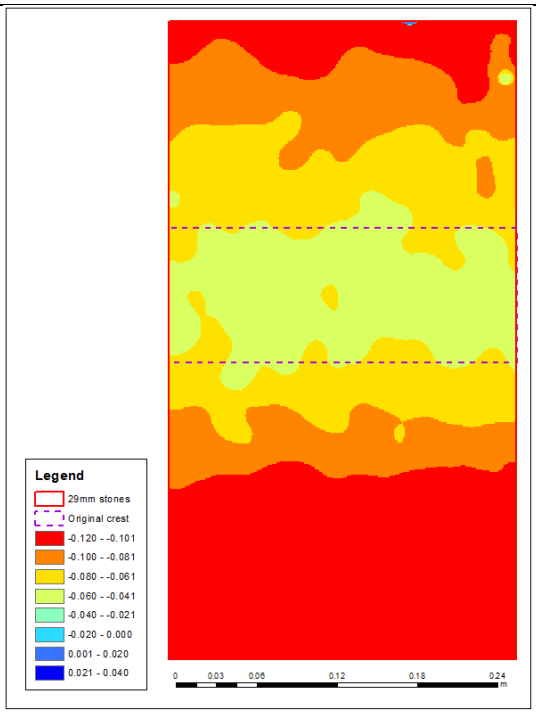
1500	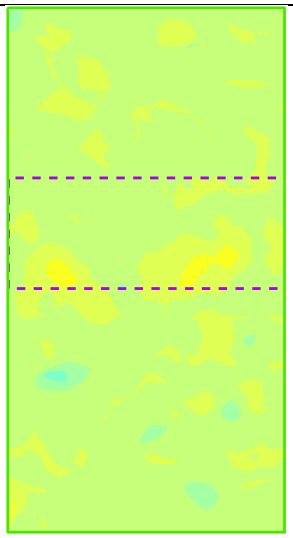 S = 0.68	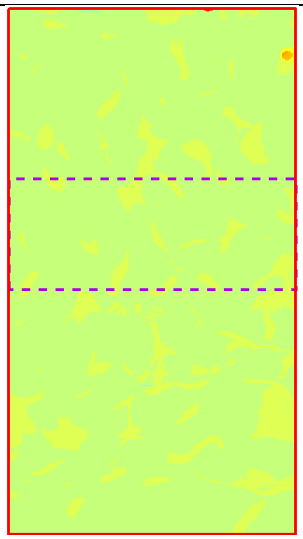 S = 0.09

4500	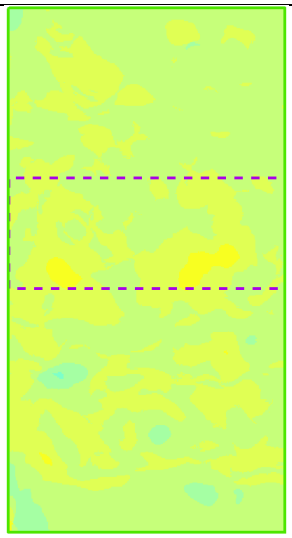 S = 1.10	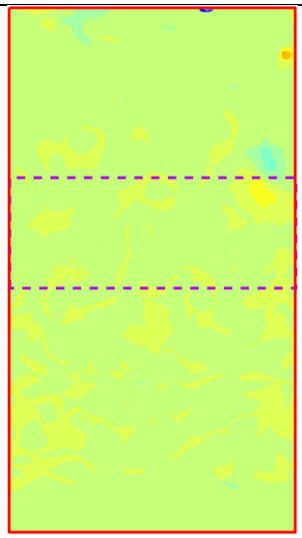 S = 0.14
9000	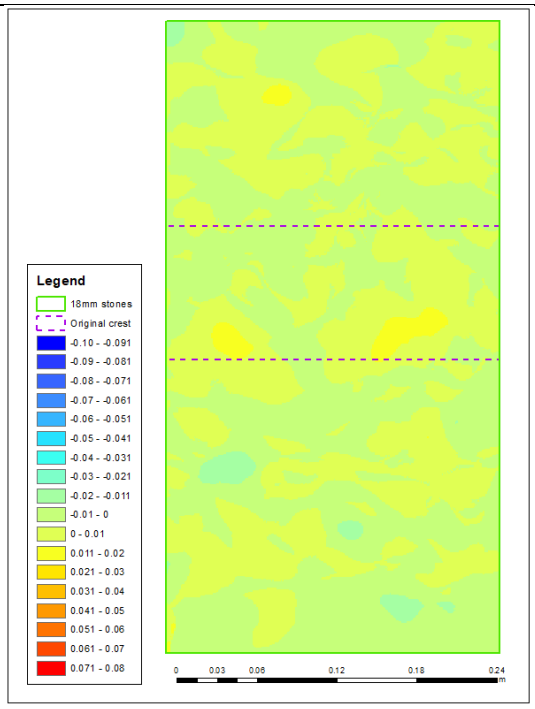 S = 1.29	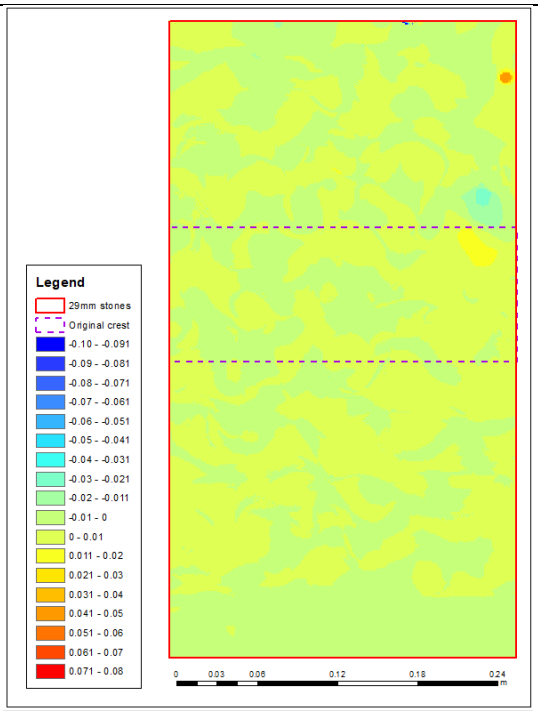 S = 0.28

9 VITA

Christopher P. Burgess Tel.: 8763994236

Old Dominion University Email: cburgess@ceacsolutions.com

Department of Civil & Environmental Engineering

135 Kaufman Hall, Norfolk, VA 23529

Educational Background:

Ph.D. in Physics at the University of the West Indies-Mona. Research interests: extreme rainfall and climate change. Dissertation: Extreme precipitation in Jamaica: past, present and future trends (2016).

MSc in Environmental Engineering at Department of Civil and Environmental Engineering, Imperial College of Science, Technology and Medicine, London. Dissertation: A Genetic Algorithm for Waste Stabilization Ponds (1998).

BSc in Civil Engineering at Department of Civil Engineering, University of the West Indies-St. Augustine. Dissertation: A Coastal Hydrodynamic Model for Kingston Harbour, Jamaica (1994).

Professional Experience and Membership:

Registered Professional Engineer (since 2001) - Professional Engineers Registration Board of Jamaica.

Publications:

Burgess, Christopher, et al. (2018). "Estimating damages from climate-related natural disasters for the Caribbean at 1.5 C & 2 C global warming above pre-ind. levels." Reg. Env. Change 18, no. 8: 2297-2312.

Burgess, Christopher, et al. (2015). "A macro-scale flood risk model for Jamaica with impact of climate variability." Natural Hazards 78, no. 1: 231-256.

Burgess, Christopher P., et al. (2015). "Frequency analysis, infilling and trends for extreme precipitation for Jamaica (1895–2100)." Journal of Hydrology: Regional Studies 3: 424-443.

Carby, B., C P Burgess, et al. (2012). "Vulnerability of Jamaica's infrastructure to the impact of climate change." Poster session presented at the 37th annual natural hazards workshop, Bloomfield, CO.

Wilson, Matthew, A Mandal, M Taylor, C P Burgess, et al. (2014). "Flood Risk and Climate Change in Negril, Jamaica" In WCRP Conference for Latin America and the Caribbean, pp. 17-21.

Derek Gay and Christopher Burgess (1994). "Hydrodynamic modeling of Kingston Harbour with a Finite Element model" in Caribbean Water and Wastewater Association Annual Conference journal.